

**An Investigation of the Doppler Signal Power Method
For Detecting Changes in the Size of the Middle Cerebral Artery**

Thesis submitted for the degree of
Doctor of Philosophy
at the University of Leicester

by

Stephanie Deverson
Division of Medical Physics
University of Leicester

September 2000

UMI Number: U140223

All rights reserved

INFORMATION TO ALL USERS

The quality of this reproduction is dependent upon the quality of the copy submitted.

In the unlikely event that the author did not send a complete manuscript and there are missing pages, these will be noted. Also, if material had to be removed, a note will indicate the deletion.



UMI U140223

Published by ProQuest LLC 2013. Copyright in the Dissertation held by the Author.
Microform Edition © ProQuest LLC.

All rights reserved. This work is protected against
unauthorized copying under Title 17, United States Code.



ProQuest LLC
789 East Eisenhower Parkway
P.O. Box 1346
Ann Arbor, MI 48106-1346

**An Investigation of the Doppler Signal Power Method
for Detecting Changes in the Size of the Middle Cerebral Artery**

Stephanie Deverson

Abstract

The Transcranial Doppler ultrasound technique is widely used for detecting velocity changes in the middle cerebral artery. However, flow changes inferred from velocity alone may be subject to error if the cross-sectional area of the vessel changes during a recording. One potentially ideal method for measuring changes in middle cerebral artery size is the Doppler signal power method. This is based on the theory that the power of a Doppler signal is proportional to the volume of blood from which the signal originates. In practice a number of factors other than vessel size influence signal power and hence may invalidate the technique. This thesis documents an investigation of the feasibility of using the Doppler signal power to measure changes in middle cerebral artery size. The main factors influencing signal power were considered. In-vitro recordings from a wall-less flow phantom showed a non-proportional relationship between power and channel size. This was deduced to be caused primarily by non-uniform insonation and high pass filtering. Following from these results, non-uniform insonation was identified as the main source of error for in-vivo recordings. An investigation of the effects of temporal bone on beam shape showed that beam shape across the middle cerebral artery is likely to be highly distorted and vary unpredictably between individuals. Theoretical modeling was used to predict the errors caused by beam shape in power changes detected from the middle cerebral artery, and demonstrated a variable error magnitude dependent on beam shape, vessel size, vessel position and beam angle. A novel technique for correcting the Doppler power spectrum for the effects of beam shape was proposed, and performed well when tested with theoretical and in-vitro spectra. Finally, an initial investigation of the correction technique using in-vivo spectra provided important information regarding future investigations of the in-vivo use of the Doppler power method.

PUBLICATIONS

Deverson S, Evans DH, Bouch DC (2000) The effects of temporal bone on transcranial Doppler ultrasound beam shape. Ultrasound Med Biol 26: 239-244

Deverson S, Evans DH (2000) The effects of beam shape on the ability to predict changes in vessel size from Doppler signal power. Ultrasound Med Biol 26: 245-253

Deverson S, Evans DH (2000) Using Doppler signal power to detect changes in vessel size: a feasibility study using a wall-less flow phantom. Ultrasound Med Biol 26:593-602.

ACKNOWLEDGEMENTS

Special thanks go to my supervisor, Professor David H. Evans, for his advice, support and encouragement.

I am also grateful to everyone in the Medical Physics department at The Leicester Royal Infirmary, in particular the volunteers who took part in the CO₂ reactivity study, and the following members of staff who directly and indirectly assisted with the research in this thesis:

Mr. Stephen Bentley, Mr. Glen Bush, Mrs. Tina Craig, Dr. Joanne Garnham, Dr. John Gittins, Mr. Harry Hall, Mr. Peter Mahony, Mr. Marco von Kruger, Dr. Julia Smith.

Thanks also go to Dr. Paul Hayes in the Department of Surgery, Dr. Clive Bouch in the Department of Pathology, and finally to Dr. Craig Foster.

CONTENTS

CHAPTER 1

Introduction: Measuring Changes in Cerebral Blood Flow	1
1.1 Cerebral Blood Flow	1
1.1.2 The Accuracy of TCD Velocity as a Measure of Blood Flow in the MCA	1
1.1.3 Changes in the Size of the MCA	3
1.1.4 Detecting Changes in MCA Size	5
1.1.5 The Doppler Signal Power Method	6
1.1.6 Validation and Use of the Doppler Signal Power Method	7
1.2 Summary and Aims	9

CHAPTER 2

The Doppler Power Spectrum	10
2.1 Introduction	10
2.2 The Origin of the Doppler Power Spectrum	10
2.3 Factors affecting the Doppler Power Spectrum	11
2.3.1 Transducer Frequency	11
2.3.2 Spectral Broadening	11
2.3.3 Spectral Noise	12
2.3.4 High Pass Filtering	12
2.3.5 Non-Uniform Insonation	12
2.3.6 Attenuation	13
2.3.7 Transducer Position	14
2.3.8 Scatterer Concentration and Flow Conditions	14
2.4 Conclusions	14

CHAPTER 3

An In-vitro Investigation of the Doppler Power Method	15
3.1 Introduction	15
3.2 Factors affecting the In-Vitro Doppler Power Spectrum	15
3.3 Method and Materials	16
3.3.1 Flow Phantom Construction	16
3.3.2 Recordings	17
3.3.3 Signal Power Corrections	18
3.4 Results	19
3.5 Discussion	20
3.6 Conclusions	23

CHAPTER 4	
The In-Vivo Doppler Power Spectrum	24
4.1 Introduction	24
4.2 Factors Affecting the In-Vivo Doppler Power Spectrum	24
4.2.1 High Pass Filtering	24
4.2.2 Non-Uniform Insonation	26
4.2.3 Attenuation	26
4.2.4 Transducer Position	27
4.2.5 Flow Conditions	27
4.2.6 Blood Composition	28
4.3 Conclusions	28
CHAPTER 5	
The Effects of Temporal Bone on TCD Beam Shape	29
5.1 Introduction	29
5.2 Methods and Materials	30
5.3 Results	31
5.4 Discussion	31
5.5 Conclusions	33
CHAPTER 6	
The Effects of Beam Shape on the Ability to Predict Changes in Vessel Size Using the Doppler Power Method	34
6.1 Introduction	34
6.2 Method	34
6.2.1 Beam Intensity Recordings	35
6.2.2 Calculation of the Theoretical Signal Power Received From a Vessel	35
6.2.3 Calculation of Power Change Arising From a Change in Vessel Size	36
6.3 Results	37
6.4 Discussion	38
6.5 Conclusions	41
CHAPTER 7	
Correcting the Doppler Signal Power For the Effects of Beam Shape and Filtering	43
7.1 Introduction	43
7.2 Modelling the Doppler Power Spectrum	43
7.2.1 Non-Uniform Insonation	44
7.2.2 High Pass Filtering	45
7.3 Testing the Doppler Power Spectrum Model	46

7.3.1 Steady Flow	47
7.3.2 Pulsatile Flow	47
7.4 The Ensemble Mean Spectrum Correction Method	48
7.4.1 Derivation of the Ensemble Mean Spectrum	48
7.4.2 Testing the Ensemble Mean Spectrum	49
7.4.3 Theoretical Background to the Ensemble Mean Spectrum Correction	49
7.4.4 Correcting the Ensemble Mean Spectrum	56
7.5 Testing the Ensemble Mean Spectrum Correction Method	57
7.5.1 MCA Pulsatile Flow	57
7.5.2 Flow Phantom Signals	60
7.6 Conclusions	60
CHAPTER 8	
Application of the Ensemble Mean Spectrum Correction to In-Vivo Doppler Signals	62
8.1 Introduction	62
8.2 Adapting the Ensemble Mean Spectrum Correction for Use With In-Vivo Signals	63
8.3 The Carbon Dioxide (CO ₂) Reactivity Test	64
8.3.1 Method and Subjects	65
8.3.2 Analysis of Doppler Signal Power	65
8.3.3 Results	66
8.6 Discussion	67
8.7 Conclusions	72
CHAPTER 9	
Summary and Future Work	74
9.1 Introduction	74
9.2 Summary of Research	74
9.3 Future Work	77
REFERENCES	79

CHAPTER 1

Introduction: Measuring Changes in Cerebral Blood Flow

1.1 Cerebral Blood Flow

The brain needs a consistent, regulated blood supply for the delivery of oxygen and glucose and the removal of the waste products of metabolism. Although the total volume of blood reaching the brain remains relatively constant, there are continuous variations in localised flow arising in response to differences in metabolic rate. In addition, regional cerebral blood flow may be affected by parameters such as blood gases, body temperature and blood haematocrit.

The ability of the brain to alter blood flow in response to the above factors can be affected either locally or globally by imbalances in the chemical mechanisms determining flow changes, and also by drugs, or medical conditions such as stroke or tumours. In order to ascertain whether the regulation of the blood supply is normal or abnormal under such conditions and hence evaluate the possibility of damage to the brain, an accurate method is required for the measurement of changes in cerebral blood flow (CBF). One technique that is widely used in this context is Transcranial Doppler (TCD) ultrasound, which estimates relative changes in blood flow volume from blood flow velocity measurements.

Compared to alternative methods that are currently available for measuring cerebral blood flow, for example radioactive tracer techniques and Electromagnetic (EM) flowmetry, TCD is ideal for investigating blood flow in the large cerebral arteries as it is safe, reliable, reproducible, non-invasive and inexpensive, and allows real-time monitoring of changes in blood flow velocity. However, it is limited by the fact that changes in the blood flow volume in a cerebral vessel are only estimated from the flow velocity. The Doppler signal is generated by the backscatter of ultrasound from the red blood cells in a vessel; because the cells are moving, the frequency of the backscattered signal is shifted relative to the frequency of the original signal. The size of the frequency shift is proportional to the velocity of the red blood cells, but is not related to the volume of blood contained in the vessel. Consequently, any change in velocity that is accompanied by a compensatory change in vessel area could be falsely interpreted as a change in flow volume. In order to overcome this limitation, TCD flow velocity measurements are generally related to the blood flow volume by assuming that the vessel cross section remains constant throughout the recordings. If this is the case, then the blood velocity is proportional to the flow volume and changes in velocity can be directly related to changes in flow.

Because TCD recordings from humans are most commonly taken from the middle cerebral artery (MCA), the work covered by this thesis will concentrate on this specific vessel.

1.1.2 The Accuracy of TCD Velocity as a Measure of Blood Flow in the MCA

A number of authors have carried out research to assess the accuracy of the TCD technique for predicting relative changes in blood flow volume in the MCA, and studies of both animals and humans have been published. However, the relevance of results obtained from animals to the human cerebral

circulation is disputable. The assessment of the cerebral autoregulation dynamics of humans by Aaslid et al. (1991) led to the suggestion that the intact human cerebral circulation in the absence of pharmacological influences does not function as predicted from pial vessel observations in animals. In addition, Giller et al. (1993) stated that because animal vessels are much smaller than those in humans, they may be more prone to diameter changes as pressure or resistance varies, and hence results observed from animals may not apply to human vessels. Owing to the questionable relevance of animal studies, only research relating to the human case will be reviewed in this chapter.

Several studies have verified the accuracy of the TCD technique under specific circumstances by demonstrating that blood flow velocity changes in the MCA reflect actual changes in blood flow volume. Bishop et al. (1986) recorded changes in CBF using Xe-133 clearance recordings and compared the results to TCD recordings of flow velocity during hypercapnia in patients with cerebrovascular disease. The authors observed that changes in MCA velocity correlated reliably with changes in CBF, but that the absolute velocity value was not an accurate indicator of CBF. Lindegaard et al. (1987) used EM flowmetry to measure blood flow in the internal carotid artery (ICA) of patients undergoing carotid endarterectomy (CEA), and compared this to TCD blood flow velocity recordings from the MCA. A linear relationship between flow and velocity was reported for decreasing values of blood pressure. However, the authors were careful to state that the assumption of a linear relationship should not be extrapolated to situations other than those with the same conditions as their measurements. Dahl et al. (1992a) used single-photon emission computed tomography (SPECT) to measure regional CBF before and after acetazolamide administration in patients with suspected cerebrovascular disease, and found that there was a significant positive correlation ($r=0.63$) between the absolute increase in CBF and the percentage increase in MCA velocity. The same group also investigated the relationship between CBF and velocity in resting healthy subjects (Dahl et al. 1992b), and found the same positive correlation between the two parameters. Newell et al. (1994) measured flow in the ICA using the EM flowmetry technique and compared the results to Doppler recordings of maximum blood flow velocity from patients undergoing CEA or aneurysm surgery. Results showed that changes in maximum velocity accurately reflected changes in ICA flow during dynamic autoregulation testing. Larsen et al. (1994) used SPECT to measure the baseline global cerebral blood flow, and compared the results to those obtained for blood flow velocity in the MCA during changes in cerebral perfusion pressure in normal subjects. The authors concluded that changes in cerebral blood flow can be reliably evaluated by TCD during changes in cerebral perfusion pressure in normal subjects, but only if the vessel diameter does not change. Muller et al. (1995) invoked changes in CBF and MCA velocity in patients with carotid artery disease by using breath-holding and acetazolamide administration as vasodilatory stimuli. Changes in CBF measured with xenon-enhanced computed tomography were found to correlate with TCD velocities for both stimuli. Kofke et al. (1995) investigated the effect of balloon test occlusion of the ICA on CBF, and found that MCA velocities reflected changes in CBF under these conditions. Finally, Van der Linden et al. (1991) compared thermodilution-estimated CBF with MCA velocity to show that TCD velocity measurements are valid as an estimate of changes in volume flow during cardiac operations.

The evidence presented above suggests that TCD flow velocity measurements can potentially

provide an accurate prediction of changes in MCA volume flow. However, it is important to note that these results are only valid for the specific circumstances under which the investigations took place, and may not extrapolate to other situations where cerebral vessel sizes do not remain constant during recordings. In support of this, other research has shown that the TCD technique may not always provide an accurate prediction of volume flow changes.

Hartmann et al. (1991) studied both normal volunteers and patients with cerebrovascular disorders during normocapnia and hypocapnia, and concluded that changes in CBF measured using Xe-133 clearance correlated poorly with MCA velocity. Meixensberger et al. (1992) used Xe-133 clearance to measure cerebral blood flow in patients who had suffered subarachnoid haemorrhage, in order to find if a correlation existed between TCD and CBF. Their results led to the conclusion that determination of blood velocity does not seem to be a precise marker for cerebral blood flow in every case, and suggested that TCD examinations should be supplemented by measurements of blood flow if there is any doubt as to their clinical value. Madsen et al. (1993) used the Kety-Schmidt technique to record global average levels of CBF during rest and dynamic exercise, and demonstrated that the exercise-induced increase in mean MCA velocity was not a proportional reflection of the increase in CBF. Weyland et al. (1994) investigated the reliability of TCD velocities as an index of CBF during cardiac surgery, and in contrast to Van der Linden et al. (1991) concluded that individual responses of MCA velocity do not reliably predict percentage changes in CBF during hypothermic cardiopulmonary bypass. This contradictory conclusion is supported by the findings of Nuttall et al. (1996) and Grocott et al. (1998). Clark et al. (1996) utilised the Xe-133 clearance technique in healthy volunteers to obtain recordings of CBF over a wide range of arterial pCO₂ levels, and found that percentage changes in MCA velocity were significantly smaller than those for CBF at increased pCO₂ levels, and larger than CBF changes for reduced pCO₂. Demolis et al. (1996) also used Xe-133 clearance, to assess CBF changes due to administration of acetazolamide, and concluded that changes in MCA velocity did not satisfactorily model changes in CBF for patients with cerebrovascular disease. Finally, the results obtained by Brauer et al. (1998) for patients with a variety of types of intracranial pathology indicated that the relationship between changes in velocity and changes in CBF may depend on the underlying patient diagnosis, with the correlation between the two parameters depending on the intracranial pathology.

1.1.3 Changes in the Size of the MCA

Although changes in MCA blood velocity have been shown to be related to changes in volume flow in certain circumstances, the accuracy of the TCD technique depends in all cases on the diameter of the vessel remaining constant during recordings. The availability of evidence showing that the TCD technique is sometimes inaccurate leads to the speculation that MCA size changes may occur under some conditions.

A number of animal and human studies have been carried out to investigate the ability of the MCA to change in size in response to various stimuli; once again, only the human studies have been reviewed in this chapter due to the uncertainty of the relevance of animal studies to the human case.

Direct evidence for size changes in the adult human MCA has been presented by several authors.

Huber and Handa (1967) investigated the effects of contrast material, hypercapnia, hyperventilation, hypertonic glucose and papaverine on the diameter of the cerebral arteries by using angiography to visualise the vessels. Their measurements showed that the degree of dilation arising from increased arterial pCO₂ and pO₂ was dependent on the size of the vessel. Arteries larger than 2.5mm diameter showed no change in size, but for arteries below this size the dilation increased with decreasing vessel diameter. The MCA most commonly fell within the size range 1.5-2.5mm, and vessels in this size group showed changes in diameter of up to approximately 8% under the influence of some stimuli. Giller et al. (1993) made direct visual measurements of cerebral artery diameters during craniotomy on adult patients, and observed that the mean change in diameter was less than 4% for the large cerebral arteries (carotid, middle cerebral and vertebral), but as large as 29% for the smaller arteries (anterior cerebral, M2 segment of the MCA).

In addition to these direct observations of changes in the diameter of the MCA, other research has provided results that the authors have concluded to be indicative of size changes. Dahl et al. (1989) used SPECT and TCD to measure CBF and MCA velocity respectively during nitroglycerin administration, and concluded that the observed reduction in velocity without a concurrent change in flow was due to MCA vasodilation. Similarly, Brooks et al. (1989) investigated the effects of orthostatic hypotension on patients with autonomic failure and observed a decrease in velocity but not in CBF which was again assumed to be caused by an increase in the MCA size. Clark et al. (1996) concluded that the poor relationship between CBF and MCA velocity at high and low levels of pCO₂ in healthy subjects was consistent with MCA dilation occurring under these conditions. Finally, Valdueza et al. (1999) used TCD velocities recorded from the MCA and the sphenoparietal sinus to predict an MCA diameter increase of $9.5 \pm 7\%$ during variations in end-tidal CO₂.

As well as adult evidence, changes in cerebral arterial diameter have also been inferred from data recorded from infants. Drayton and Skidmore (1987) measured the blood flow in the aorta of pre-term and full term infants, using M-mode ultrasound to calculate the cross sectional area of the vessel, and compared the values to those of blood flow velocity obtained from TCD measurements in the MCA. They discovered that velocities increased with time after birth while blood flow remained constant, and concluded that the MCA must have progressively constricted, implying that the major intracranial arteries in infants are vasoactive.

The available evidence suggests that the human MCA is capable of changing diameter in response to various stimuli. However, the lack of comprehensive investigation means that there is uncertainty regarding the precise conditions for which MCA size changes will occur. This uncertainty is accentuated by additional research which has shown that size changes do not occur in all cases. Van der Linden et al. (1992) monitored MCA diameter in children undergoing cardiac surgery, using ultrasound echoes obtained simultaneously from opposite vessel walls, and found that the mean diameter did not change despite wide variations in blood pressure and nasopharyngeal temperature. Another study of children by Bissonnette et al. (1992) examined the MCA during cerebral angiography and used measurements from radiographic film to demonstrate that the diameter did not change for different levels of pCO₂. Newell et al. (1994) compared EM measurements of flow in the ICA to TCD measurements of flow velocity in the adult MCA during changes in blood pressure, and

concluded from the correlation between the values that MCA diameter changes do not occur. Valdueza et al. (1997) used magnetic resonance imaging (MRI) to study the effect of hyperventilation on MCA diameter in healthy volunteers, and found that vessel size remained practically unchanged for this stimulus. Djurberg et al. (1999) investigated the quantitative effects of CO₂ on cerebral arterial diameters, and found that angiographic measurements revealed no significant size changes in arteries of diameter 0.57mm and above. Finally, Schreiber et al. (1999) measured MCA size changes during and after administration of acetazolamide using high resolution MRI, and found that no changes in diameter of greater than 4% occurred.

1.1.4 Detecting Changes in MCA Size

The evidence presented above suggests that the MCA is capable of changing in size under certain conditions. In addition, TCD estimates of relative flow changes in the MCA based on the measurement of velocity alone do not appear to be accurate for all cases, suggesting that vessel size changes might have occurred during recordings. In view of these facts, it must be assumed that the MCA is potentially vasoactive, and therefore estimation of blood flow made exclusively from TCD flow velocity values should be treated with caution. TCD velocities may provide useful approximations under steady state conditions in situations for which changes in vessel calibre are relatively small, but measurements could be subject to error in conditions of rapidly changing blood flows and blood pressures.

Due to the major advantages that TCD offers over other methods of measuring cerebral blood flow, the technique cannot be discarded solely on the basis of possible inaccuracy in some circumstances. An obvious solution would be to create a more robust measurement of blood flow by incorporating TCD recordings of blood velocity with measurements of cerebral vessel size, but few ideal techniques are currently available for this purpose. Existing methods which might potentially allow in-vivo measurement of changes in the diameters of blood vessels are radiation based imaging methods, magnetic resonance imaging, ultrasound imaging and the Doppler signal power technique.

Radiation based methods involve either the injection of microspheres labelled with various radioactive isotopes or the inhalation of a radioactive gas such as Xe-133. In both cases the tracer enters the bloodstream and can be detected in the cerebral vessels a short time after administration. Such techniques are generally unsuitable for routine monitoring purposes owing to the risk introduced to the patient by the radiation dose, and the fact that their accuracy for visualising and measuring the size of vessels is limited by the sensitivity and resolution of the imaging equipment. In addition, the amount of time required to acquire an image means that there is a limit to the speed at which size changes can be detected, making the techniques unsuitable for real-time detection of changes in volume flow.

MRI of cerebral vessels offers the advantage of improved image resolution and does not involve radiation. However, negative aspects are that it is expensive, time consuming to implement and may be uncomfortable for the patient due to the noise and confined space. It is also subject to an image acquisition time delay similar to that described for the radiation-based techniques. While MRI may offer a fairly accurate means for measuring vessel sizes under specific circumstances, for example to

study the effects of drugs, it is still not ideal for routine patient monitoring or for situations where a greater degree of access to the patient is required during monitoring.

Ultrasound methods are more suitable for routine monitoring as the equipment is generally compact and portable compared to other imaging techniques. In addition, there is no evidence available to suggest any risk to the patient, and the discomfort is minimal. B-mode ultrasound can be used to image vessels, but the resolution and sensitivity of equipment and the required post-processing of signals prevent the visualisation of vessels and vessel diameter changes below a certain size, and make accurate measurements of larger vessels difficult. A-mode ultrasound uses the time separation of ultrasound echoes and estimates of the speed of the ultrasound in different media to calculate the distance between reflecting surfaces (i.e. the vessel walls), but the technique requires a perpendicular beam-vessel angle and the accuracy is limited by frequency-dependent attenuation and non-linear propagation of the ultrasound pulses as they travel through the body. M-mode traces provide a means of viewing changes in the separation of reflecting surfaces in real time, but measurement accuracy is again limited by a combination of the factors affecting the B-mode and A-mode techniques. Furthermore, all of the above ultrasound imaging techniques are unsuitable for the case of the cerebral vessels, due to the presence of bone in the beam path causing significant attenuation and distortion of the beam.

It is evident that none of the above methods are ideal for accurately measuring changes in vessel diameter simultaneously to Doppler recordings of blood velocity, especially in the case of the cerebral circulation where the vessels are of the order of a few millimetres in size and are shielded by the skull. However, there is currently one further method which could potentially overcome the stated problems. The Doppler signal power technique utilises the power of the Doppler signal received from cerebral vessels during blood velocity monitoring, and offers the advantages of ultrasound with the added benefit that it requires no additional equipment. Furthermore, it potentially provides a real-time evaluation of changes in vessel size, and is not constrained by the resolution inaccuracies that affect imaging methods.

1.1.5 The Doppler Signal Power Method

The theory behind the Doppler signal power method is based on assumptions made by Arts and Roelvros (1972) in their derivation of an equation for calculating instantaneous blood flow. The authors state that if a theoretical blood vessel is insonated with uniform intensity and each red blood cell in the insonated volume contributes an equal amount to the total power, then the total power of the Doppler signal will be equal to the sum of the powers reflected from each of the cells in the insonated volume. In practice, the relationship between the number of red blood cells and the backscattered power is only linear for low red blood cell concentrations (Mo et al. 1994, Shung et al. 1984). However, if red cell concentration remains constant then the total Doppler signal power should be proportional to the volume of blood within the sample volume. Any contraction or dilation of a vessel will be accompanied by an equivalent change in blood volume, and should therefore produce a change in signal power that is theoretically proportional to the change in vessel size that has occurred. Variations in tissue morphology and vessel sizes between individuals mean that it is not feasible to use

the signal power to quantify the absolute size of a vessel. However, it should be possible to relate changes in the received power to changes in the cross-sectional area of a vessel.

Although the relationship between signal power and vessel size appears straightforward, there are a number of factors other than blood volume that may affect the total power received from in-vivo cerebral vessels (Evans 1992) and hence potentially alter the theoretical linear proportionality between power changes and vessel size changes. These include non-uniform insonation of the blood vessel, attenuation of the signal, intrinsic spectral broadening, electronic filtering, blood haematocrit and flow conditions. The specific effects of each factor on the Doppler signal power will be discussed in more detail in the next chapter.

1.1.6 Validation and Use of the Doppler Signal Power Method

Despite the currently questionable accuracy of using the Doppler power to assess size changes in in-vivo vessels, the technique has already been used in several published investigations of CBF. At the present time only limited research has been carried out to specifically investigate the validity of assuming a proportional relationship between changes in the power of the Doppler signal received from cerebral vessels and changes in the vessel cross sectional area. Hatab et al. (1997) used a flow phantom constructed from silicon tubes in water to investigate the relationship between power and tube size, and showed that the two parameters were proportional over a range of flow velocities. However, the influence on the signal power of factors other than vessel size were considered only briefly by the authors, as was the relevance of their findings to the in-vivo case.

Other authors have used flow phantoms to investigate the use of flow indices derived from the Doppler signal spectrum as a measure of volume flow. Saini et al. (1983) generated Doppler signals using human blood in vinyl tubes of internal diameters 1mm, 2.5mm and 5mm, and compared the mean frequency value derived from the spectral zeroth and first moments with velocity measurements and flow volume values. Results showed that the mean frequency flow index did not provide a measure of the absolute flow rate, but gave a more accurate indication of relative flow changes than standard velocity measurements. Discussion was not extended to the relationship between signal power and vessel size changes. Harer et al. (1995) recorded Doppler signals from a single flow phantom vessel, and looked at changes in a signal power based flow index with variations in flow velocity and pulsatility index. Changes in the signal intensity and hence the flow index with both of these variables led the authors to conclude that the Doppler signal power method might not provide accurate quantification of cerebral artery diameter changes.

Despite the lack of thorough investigation into the validity of using the Doppler signal power method in-vivo, the technique has already been used as a supplement to Doppler blood velocity recordings in a number of publications. Aaslid (1987) used a flow value based on the first moment of the spectral power to investigate the effects of visual stimulus on flow in the posterior cerebral artery, the MCA and the superior cerebellar artery. The observed differences between changes in velocity and power were small, and this was assumed to eliminate the possibility that any vessel area changes had occurred during the recordings. Further work by the same group investigated the changes in velocity and signal power for step decreases in blood pressure during normocapnia, hypocapnia and

hypercapnia (Aaslid et al. 1989, 1991), and for carotid compression during normocapnia and hypocapnia (Aaslid 1991). The small changes in power observed in all cases were assumed to be representative of insignificant changes in the MCA size, and therefore to validate the relationship between velocity and flow for these circumstances. Muller et al. (1991) investigated the response of the volume flow in the middle cerebral artery of human subjects to orthostasis (tilting), using signal power to quantitatively assess the relative changes in the calibre of the vessel. The results of the investigation showed that there were a large range of velocity and power responses, which in most cases were indicative of MCA dilation. Another study by Muller (1994) also used the Doppler signal power to demonstrate the occurrence of MCA dilation due to subjects moving from a sitting to a standing position. Schregel et al. (1994) used power to determine changes in vessel area and volume flow in the MCA during Isoflurane inhalation. Both parameters showed increases after administration of the gas, again suggesting vessel dilation. Poulin et al. (1996a, 1996b) investigated changes in Doppler power during hypercapnia, hypoxia and a combination of the two stimuli; little variation was observed in the former study, although an increase in power of approximately 4% was seen for the combined stimuli in the latter. The authors concluded that the calibre of the larger cerebral vessels does not change significantly when cerebral blood flow is moderately increased. Giller et al. (1998) compared MCA velocity and a flow index derived from signal power during periodic fluctuations in velocity, and found that the velocity values did not reliably reflect putative flow changes under these circumstances. The authors concluded that this was due to changes in the size of the MCA occurring in phase with changes in velocity and flow. Finally, Mahajan et al. (1998) looked at the signal power received from the MCA for carotid compression during normocapnia, hypocapnia and hypercapnia, and observed that the power was unchanged from the baseline value for all tests, suggesting that the MCA size remained constant.

All of the investigations described above used measurements of the Doppler signal power to draw conclusions about changes in cerebral vessel size and flow. However, in all cases it was assumed that changes in the backscattered power were proportional to changes in the vessel diameter. Some additional basic factors were also taken into consideration, for example the effect of transducer movements during recordings; this was discussed by most of the authors, with the consensus being that the transducer position must remain stationary in order to prevent variations in the beam path properties or the transducer coupling to the head causing spurious changes in power. Schregel et al. (1994) observed that the increase in signal power seen in their investigation was unlikely to be due to any inadvertent displacement of the probe, as it was fixed in position and not touched during recordings. This assumption was supported by the fact that the signal power was maximised prior to recordings so that any change in the position of the probe was most likely to cause a decrease in the recorded signal power due to movement of the insonation volume away from the centre of the vessel. Muller et al. (1991) acknowledged that the power could be considerably affected by local differences in the attenuation of bone, and also by movements of the transducer causing changes in the quality of the coupling to the skin surface, and assumed that by positioning and coupling the probe with care so as to receive a Doppler signal of maximum power, any increase in power not due to a change in vessel diameter could only be caused by a displacement of the vessel with respect to the skull. Aaslid (1987,

1989, 1991) also noted that errors may be introduced due to movement of the probe during recordings, and in addition observed the problems involved in measuring signal power unless the signal to noise ratio is very high.

1.2 Summary and Aims

Information regarding the supply of blood to the brain is important for identifying variations in CBF caused by disease, drugs or other physiological stimuli. The TCD technique is widely used for detecting flow changes in the MCA due to the many advantages that it offers over other available methods of measuring CBF. However, TCD is limited by the fact that it measures only blood velocity and not the true flow volume, and hence TCD measurements of flow changes inferred from velocity alone may be subject to error if the MCA undergoes size changes during recordings. Evidence is available to show that the MCA is capable of changing in size, and this might be a cause of the inaccuracies that have been observed in some TCD measurements of flow.

In order to improve TCD accuracy a method is required for measuring the scale of MCA size changes simultaneously to TCD velocity measurements. One possible option is the Doppler signal power technique, which depends on the assumption that the power of the Doppler signal is proportional to the volume of blood from which the signal originated. However, this assumption may not be valid in practice due to the fact that factors other than vessel size influence the Doppler power spectrum. The lack of depth with which the Doppler signal power technique has been investigated means that the conclusions drawn by authors who have previously utilised this method cannot be accepted with total confidence. In order to validate the technique for use in-vivo, all factors that could potentially affect the Doppler signal power spectrum must first be considered in much greater detail.

The aim of the work in this thesis is to investigate the validity of using the Doppler signal power as a method for measuring changes in MCA size. Chapter 2 describes the origin of the Doppler signal power spectrum, and discusses the various factors that may affect the spectrum and hence distort the theoretical proportionality between power and vessel size. An in-vitro flow phantom investigation of the relationship between power and vessel size is detailed in chapter 3, with discussion of the reasons for the deviation of this relationship from the theoretical one. Chapter 4 applies the conclusions drawn from the in-vitro experiments to the use of the power method for detecting size changes in the MCA, and identifies additional factors which might affect the results obtained in the in-vivo case. An investigation of the potential beam shape distortion caused by the presence of the skull during MCA signal power recordings is described in chapter 5; the results are then used in chapter 6 to theoretically model the errors arising due to beam shape in the signal power changes detected for specified changes in vessel size. Chapter 7 reviews the predicted distorting influences on the relationship between power and vessel size for MCA signals, and introduces a novel method of correction for these factors that potentially provides a more robust estimation of MCA size changes from changes in signal power. Finally, chapter 8 applies this correction method to signals recorded from healthy volunteers undergoing CO₂ reactivity tests, and analyses the responses of the MCA size and volume flow to this stimulus.

CHAPTER 2

The Doppler Power Spectrum

2.1 Introduction

The theoretical basis of the Doppler power method is the assumption that the total spectral power of a Doppler signal received from a vessel is proportional to the volume of blood from which the signal originated, and hence that any changes in the cross-sectional area of the insonated vessel will produce proportional changes in the magnitude of the signal power. However, in practice it may not be accurate to assume this proportionality owing to the influence on signal power of a number of factors other than vessel size.

In order to identify these potential sources of inaccuracy, this chapter describes the origin of the Doppler power spectrum, and discusses the factors that influence its shape and magnitude. Because the Doppler power method requires the insonation of the entire vessel lumen, discussion will be restricted to continuous wave (CW) and long-gate pulsed wave (PW) TCD, which both produce similar spectra.

2.2 The Origin of the Doppler Power Spectrum

The basic components of human blood are plasma, erythrocytes (red blood cells), leukocytes (white blood cells) and platelets. The backscatter of ultrasound waves from blood is thought to be mostly caused by the erythrocytes, as despite being smaller than leukocytes and of a similar size to platelets, they have a much greater concentration than both, occupying approximately 45% of the blood volume compared to 0.8% and 0.2% for leukocytes and platelets respectively. The movement of the red cells as blood flows through a vessel gives rise to the Doppler effect of a change in the frequency of the backscattered signal relative to that of the original signal. The magnitude and direction of the frequency shift are respectively dependent on the velocity of the cells and the direction of the blood flow relative to the transducer.

The relationship between frequency shift and velocity is given by the well-known Doppler equation:

$$f_d = \frac{2f_i v \cos \theta}{c} \quad [2.1]$$

where f_i is the original frequency of the ultrasound transmitted by the transducer, f_d is the magnitude of the frequency shift arising due to backscatter from a moving red blood cell, v is the speed of the red blood cell, c is the speed of sound in the medium and θ is the angle between the ultrasound beam and the direction of motion of the cell. Information regarding the direction of blood flow is obtained via electronic post-processing of the received signal.

Because the red blood cells in a vessel move at a range of different velocities, there is a corresponding range of Doppler frequency shifts at any point in time, and the resulting signal spectrum therefore has components at each of these frequencies. The magnitude of each component depends in the first instance on the volume of red blood cells travelling at the relevant velocity, and the spectral shape is therefore initially determined by the velocity profile of the flow in a vessel. For parabolic

velocity profiles such as those assumed under steady flow conditions in the MCA, the blood velocity is at a maximum in the centre of the vessel and decreases to zero velocity at the vessel walls. Theoretically, the Doppler signal spectrum resulting from parabolic flow is rectangular in shape because an equal volume of blood is travelling at each velocity. Consequently, the total spectral power is proportional to the total blood volume in the insonated portion of the vessel. This theory forms the basis of the Doppler power method.

2.3 Factors affecting the Doppler Power Spectrum

The shape and magnitude of the Doppler power spectrum is in fact affected by several factors other than the velocity profile in a vessel and the volume of red blood cells travelling at each velocity. The origin of each of these factors and their potential to affect the relationship between signal power and vessel size is discussed below

2.3.1 Transducer Frequency

The size of red blood cells (largest dimension approximately $7.2\mu\text{m}$) is small compared to the wavelength of ultrasound typically used to obtain Doppler signals (1-0.1mm in blood, corresponding to a frequency range of 1-10MHz). Despite the fact that the red blood cell concentration is too high for blood to be treated as a random distribution of scatterers, it has been shown that the signal power backscattered from blood is proportional to the fourth power of the transducer frequency (Shung et al. 1976) as would be expected for the case of Rayleigh scattering from individual particles with dimensions much smaller than the incident wavelength. In addition to affecting the power of the signal backscattered from the red blood cells, the transducer frequency also influences the attenuation of the signal that occurs during its passage to and return from a blood vessel; this will be discussed in more detail in section 2.3.6.

Although the magnitude of the signal power received from a blood vessel is dependent on the frequency of the transmitted ultrasound beam, the relationship between signal power and vessel size will not be affected by this mechanism unless a change in transducer frequency is introduced during a TCD recording.

2.3.2 Spectral Broadening

The power spectrum of a Doppler signal will be affected by intrinsic spectral broadening, a process which occurs due the finite transit time of the erythrocytes across the width of the ultrasound beam causing a range of angles to be subtended between each blood cell and the beam axis. This results in the signal received from each erythrocyte containing a range of frequencies rather than a single frequency corresponding to its velocity, and hence causes a broadening of the final signal spectrum. The amount of broadening is proportional to the tangent of the beam-vessel angle, and therefore is more pronounced for larger angles.

While intrinsic spectral broadening may affect the shape of the spectrum, it should not in theory alter the magnitude of the total power in the spectrum. In practice, changes in the distribution of power

within the spectrum may cause variation in the proportion falling below the high pass filter cut-off frequency, and hence the total power value may be affected indirectly. However, provided that the sample length, the angle of insonation and the filter cut-off frequency do not change during a recording, the effects of spectral broadening should remain approximately constant for all vessel sizes and the relationship between signal power and vessel size should not be affected by this factor.

2.3.3 Spectral Noise

Constructive and destructive interference of the wavefronts backscattered from red blood cells cause both spatial and temporal fluctuations in the intensity of the received signal, giving rise to the noise-like character of Doppler signals. This produces inherent variations in the power of the spectral components at different frequencies. In addition, the fact that the Fourier transform only provides an estimate of the signal power at each frequency means that additional noise is introduced to the spectra.

The effects of spectral noise on the total power can be reduced by applying spectral averaging techniques, for example by deriving the mean of the power values calculated from a number of consecutive beats. This also has the advantage of minimising any additional spurious temporal fluctuations in signal power that may arise from other sources such as variation in red blood cell concentration.

2.3.4 High Pass Filtering

High pass filtering is employed in all Doppler equipment in order to remove the low frequency noise components in the signal which arise due to slow moving objects in the path of the beam, for example vessel wall movements. However, in addition to removing low frequency noise, filtering also removes the signal components originating from the red blood cells travelling at low velocities close to the vessel walls.

Elimination of the low frequency portion of the Doppler spectrum should theoretically not affect the relationship between signal power and vessel size changes, provided that the filter cut-off frequency remains constant and the velocity does not change. However, variations in flow velocity will result in different percentages of the signal spectrum being removed by the filter; the significance of this for the power-vessel size proportionality will depend on the relative sizes of the filter frequency and the flow velocity, with lower filter cut-offs and higher flow velocities reducing the error.

2.3.5 Non-Uniform Insonation

Non-uniform insonation of a vessel will occur if it falls within a region of the beam that contains significant spatial variations in intensity. Non-uniform insonation is likely to occur for all but the smallest vessels, as ultrasound beams inherently contain axial and lateral variations in intensity which are characteristic of the sensitivities of the transmitting and receiving crystals of the transducer and their relative positions and orientations. CW and long-gate PW Doppler ultrasound beams exhibit large variations in intensity in the near field (Fresnel zone) and a gradual decrease in intensity in the far field (Fraunhofer zone), plus a decrease in intensity perpendicular to the beam axis.

In addition to inherent spatial variations in beam intensity, the shape of the beam across a vessel is dependent on the physical characteristics of the media through which it passes, with the potential for focusing and refraction arising at the various tissue interfaces in the beam path. Further distortion to the beam shape may also be caused by non-uniform attenuation of the incident beam if there are lateral or axial variations in the properties of the tissues in the beam path; the effects of attenuation are discussed in more detail in section 2.3.6.

Proportionality between the total power of the Doppler signal and the volume of blood from which it was backscattered can only be assumed if the intensity of the incident beam remains uniform across the insonated vessel. Intensity variations across a vessel cause unequal weighting of the signal components originating from different positions, and hence distortion in the power spectrum of the received signal (Cobbold et al. 1983). Because it is unlikely that the relative insonation pattern will remain the same for different vessel sizes, the nature of the spectral distortion may vary, meaning that the relationship between signal power and blood volume may not be proportional for any changes in vessel size that occur.

2.3.6 Attenuation

Attenuation of ultrasound signals is caused during the passage of the sound waves through the materials that lie between the transducer and a vessel, and will therefore affect both the incident beam and the backscattered Doppler signal. Signal power is reduced due to a combination of the effects of absorption, reflection, refraction, scattering, non-linear propagation and beam divergence.

The major cause of attenuation in most human tissues is absorption, which transfers some of the acoustic energy of the ultrasound beam into heat. Reduction of the signal power also occurs due to reflection of the beam at the boundaries between media with different acoustic impedances. Further attenuation arises from divergence of the ultrasound beam, which causes the total beam energy to be spread across a larger cross-sectional area, hence reducing the energy in the region of the beam that is incident on a vessel. Signal intensity may also be reduced by scattering of the ultrasound waves occurring at small localised discontinuities in the acoustic properties of a medium. The most obvious site for this is the red blood cells that give rise to the Doppler signal, but scattering also takes place in the tissues lying in the signal path, as discontinuities may be present within even supposedly homogeneous tissues.

Because attenuation increases with frequency, the higher frequency components of a signal will be attenuated more than the lower ones. However, this effect is likely to have a negligible influence on the magnitude of the signal power components due to the relatively small range of Doppler shift frequencies produced by the blood in the MCA.

The incident beam intensity and the Doppler signals originating from different positions in a vessel will both undergo attenuation by an amount that is dependent on the length of the signal path and the material of which it is composed. If the materials in the beam path are homogeneous, then attenuation will not significantly affect beam shape, and the magnitude of the spectral components of the Doppler signal will be reduced by an approximately equal amount (discounting any frequency-

dependent attenuation effects). Consequently, the effects of attenuation on the signal spectra will be similar for all vessel sizes, and therefore should not adversely affect the relationship between power and vessel size. However, if non-uniform attenuation of the incident beam and the backscattered Doppler signal takes place due to spatial and lateral variations in the materials in the beam path, then uneven weighting of the power spectrum may produce errors in the power-vessel size proportionality assumption.

2.3.7 Transducer Position

As explained previously, the signal power received from a vessel is affected by inherent spatial variations in beam intensity and by the attenuating properties of the materials in the beam path. The combined effects of these factors vary according to the location of a vessel in the beam. Vessel location is determined by the position of the transducer relative to the vessel, and hence any changes in transducer position can potentially affect the shape of the Doppler signal spectrum and consequently alter the total spectral power.

2.3.8 Scatterer Concentration and Flow Conditions

The backscattered signal power is dependent on the distribution of the scatterers in a vessel and is therefore affected by both the flow conditions and scatterer concentration (Shung 1976, Angelsen 1980, Shung et al. 1984, Shung et al. 1992, Cloutier & Shung 1993, Bascom & Cobbold 1996). For the former, increased backscatter may arise at very low shear rates due to scatterers clumping together, or at very high shear rates if laminar flow breaks down and becomes turbulent.

Variations in flow conditions not accompanied by a compensatory vessel size change could potentially produce fluctuations in backscattered power that might be misinterpreted as a change in vessel calibre. Alternatively, any changes in flow conditions occurring simultaneously to a vessel dilation or contraction may affect the magnitude of the power change and consequently influence the relationship between power and vessel size.

Variations in the percentage volume of scatterers in a vessel may also cause changes in the power of the backscattered signal, with the relationship between the two parameters depending on the nature of both the fluid and the scatterers. In order to guarantee that significant fluctuations in power do not arise from this source, either scatterer concentration should be monitored or Doppler power recordings should be restricted to those cases for which the scatterer concentration can be reasonably assumed to remain approximately constant.

2.4 Conclusions

The theory presented in this chapter has illustrated that the power spectrum of a Doppler signal may be affected by factors other than blood volume. The relative importance of these factors with respect to their influence on the theoretical proportionality between signal power and vessel size changes will depend on the specific conditions for which a Doppler power recording is made. This will be discussed in further detail in chapters 3 and 4 for the in-vitro and in-vivo cases respectively.

CHAPTER 3

An In-vitro Investigation of the Doppler Power Method

3.1 Introduction

Despite the likelihood of factors other than blood volume influencing the relationship between the Doppler signal power and vessel size, only one reported study (Hatab et al. 1997) has attempted to directly validate the assumed in-vivo proportionality between the two parameters. This investigation made in-vitro measurements using a flow phantom constructed from different sizes of rubber tubing in a water bath, and showed a linear relationship between tube cross-sectional area and the Doppler signal power. However, the influence on the power spectrum of factors other than vessel size were considered only briefly by the authors. The effects of high pass filtering on the received signal power were examined theoretically, and solely on this basis determined to be insignificant for the flow velocities used in the study. No discussion was included regarding the possible effects of beam shape on the power spectra, a factor which could be particularly relevant due to the use of bovine femoral bone samples to provide attenuation of the ultrasound beam. Refraction of the beam at the bone and tubing interfaces, intrinsic spectral broadening and preferential attenuation of higher frequency signal components were all assumed to have no effect on the signal power, but justification for these assumptions was not included. Finally, no details were given regarding the positioning of the transducer for different tubes.

The lack of detailed research into the accuracy of the Doppler power method suggests that a more thorough in-vitro study is required in order to provide a robust assessment of the relationship between signal power and vessel size, and to subsequently allow a detailed analysis of the factors that are likely to be important for the in-vivo case.

3.2 Factors affecting the In-Vitro Doppler Power Spectrum

Chapter 2 discussed the influences of various different factors on the signal power received from a vessel. However, not all of these factors are relevant for the in-vitro case. Transducer frequency, scatterer concentration and flow conditions can all be disregarded provided respectively that the transducer frequency is not altered, that precautions are taken to ensure a stable concentration of scattering particles, and that the flow phantom is designed to allow the development of parabolic flow before the point of insonation. The use of an approximately homogeneous material between the transducer and the vessel means that attenuation can be considered to be uniform, although the effects of path length still need to be considered, and spectral broadening can also be assumed to remain constant if the beam vessel angle does not change. Finally, the influence of spectral noise can be minimised by optimising the signal-to-noise ratio (SNR) of the recorded Doppler signals and by averaging power values over time.

The remaining factors which are therefore most likely to affect signal power are non-uniform insonation, high pass filtering and transducer position, and these need to be considered carefully when making in-vitro recordings of Doppler signal power.

3.3 Method and Materials

3.3.1 Flow Phantom Construction

A disadvantage of the water and tubing flow phantom used by Hatab et al. (1997) is that distortion of the Doppler signal power spectrum may arise due to the impedance mismatch between the tube material and water (Thompson et al. 1990). A wall-less flow phantom design (Rickey et al. 1995) was therefore chosen to overcome this potential source of error and hence model the in-vivo case more closely.

The wall-less flow phantom was constructed from a tissue-mimicking material (TMM) developed to have physical properties close to those of soft tissue (Teirlinck et al. 1998). The design of the phantom (figure 3.1) was based on that described by Rickey et al. (1995). The TMM was cast around rods of external diameters 2mm, 3mm and 4mm threaded through close-fitting inlet and outlet pipes; removal of the rods after the TMM had set produced channels with internal diameters identical to the rod size. The channel sizes used in the investigation were chosen to cover the likely range of sizes of the adult MCA, based on recordings by van der Zwan et al. (1993). The TMM was set with the container at an angle of 45 degrees to the horizontal, producing channels at a 45 degree angle to the phantom surface. Although the 45 degree beam-vessel angle used in the phantom is not the same as the zero degree angle usually assumed for insonation of the MCA, the fact that the latter can vary by up to ± 30 degrees (Martin et al. 1993, Martin et al. 1995) suggests that the flow phantom configuration is not unreasonable as a model of the in-vivo case. Seals were included around the inlet and outlet tubes to prevent leakage when the TMM was under flow pressure.

The blood-mimicking fluid (BMF) used in the phantom was an orgasol-based mixture with properties analogous to human blood (Ramnarine et al. 1998, Teirlinck et al. 1998, Ramnarine et al. 1999). A calculation of inlet length using a theoretical mean velocity of 50.0cm s^{-1} and the maximum BMF kinematic viscosity value of $3.85 \times 10^{-6}\text{m}^2\text{s}^{-1}$ (derived from BMF data given by Ramnarine et al. 1998) gave a value of approximately 6.2cm for the largest channel size. An inlet length of approximately 10.0cm was therefore used for each channel to ensure that the flow profile had stabilised before the point of insonation. Owing to the tendency of the TMM to split if subjected to high pressures, flow velocities were kept fairly low relative to those found in-vivo. The time-averaged peak velocity calculated for each channel using the maximum frequency envelope of the Doppler signal was between $15\text{--}46\text{cm s}^{-1}$, whereas the time-averaged peak velocity for the MCA is $62 \pm 12\text{cm s}^{-1}$ (Evans et al. 1989).

Forward pulsatile flow in the phantom channels was generated using a simple flow circuit (figure 3.2) consisting of a reservoir, a peristaltic roller pump and a damping chamber. The damping chamber was included to prevent reverse flow occurring in the circuit, and consisted of a piece of elastic tubing of diameter 1.0cm and length 15.0cm. In order to reduce the incidence of high intensity noise in the Doppler signal due to the presence of air bubbles and particle clumps in the BMF, the fluid was filtered several times using a 38 micron sieve (Endecotts Ltd., London, UK) and placed in a vacuum chamber prior to recordings. The same batch of BMF was used for all recordings to ensure that particle concentration remained constant between channel sizes, and the liquid in the reservoir was

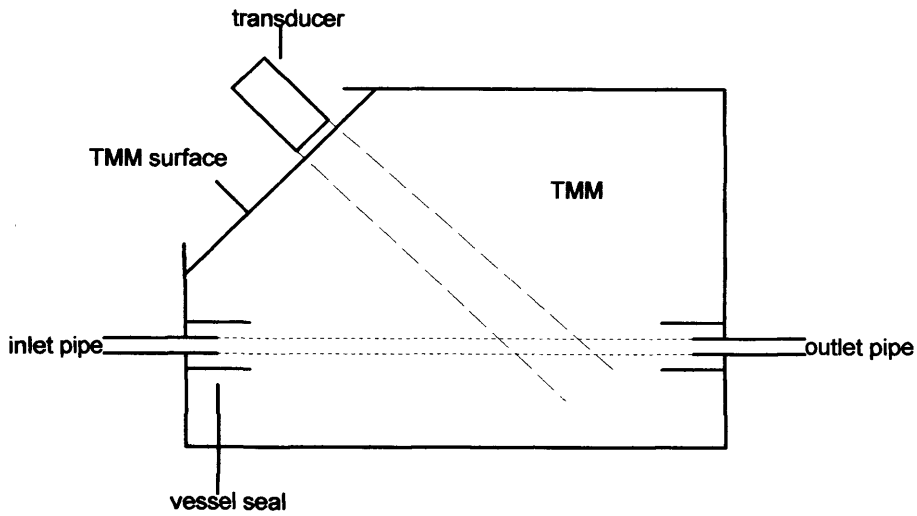


Figure 3.1 Schematic drawing of the wall-less flow phantom design, illustrating the 45 degree angle between the beam axis and the flow phantom channels.

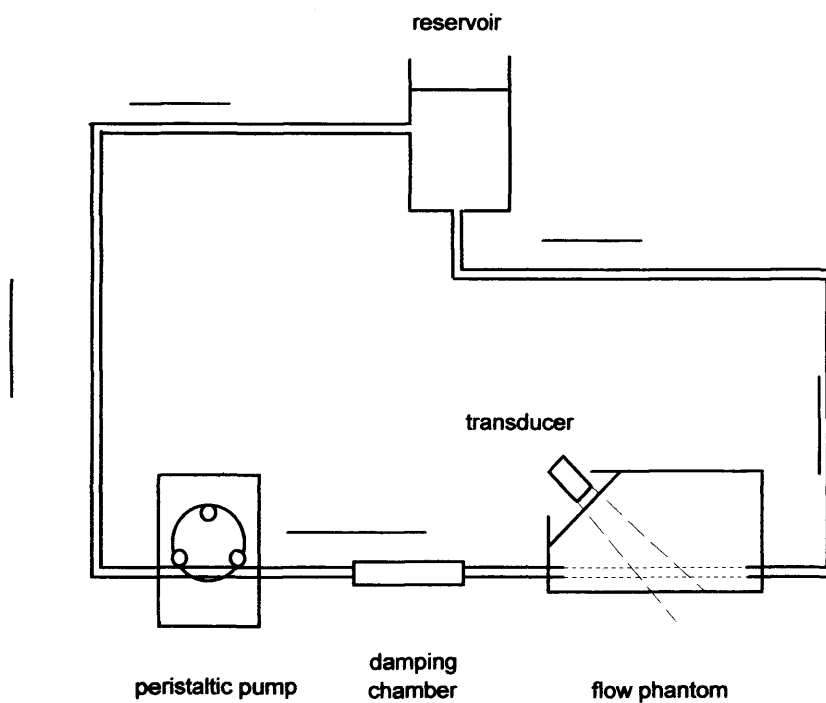


Figure 3.2 Flow system utilising a peristaltic pump to produce pulsatile flow and a damping chamber to eliminate reverse flow components.

gently stirred before each recording to evenly distribute the orgasol particles throughout the BMF. To allow the flow to stabilise, the BMF was pumped through the circuit for at least one minute before recordings were started.

Doppler signals were recorded from the flow phantom to DAT tape (SONY Digital Audio Tape recorder TCD-D10) using a 2MHz pulsed wave transducer in conjunction with a commercial TCD system (Scimed PCDop842, Bristol, UK). Recordings were made firstly from the 4mm phantom channel; the transmitted power setting was selected to give the maximum intensity Doppler signal without saturation, and this value (equal to <1% maximum power output) was then used for all recordings from the three channels. Unlike the investigation by Hatab et al. (1997), no bone was placed in the beam path as saturation of signals could be more simply avoided by reducing the output power setting on the TCD system. A sample volume length setting of 0.85cm and filter setting "off" were used in all cases, and all signal recordings were of a one-minute duration. The sonogram for the signals was obtained using in-house spectral analysis software, with window lengths of 50ms for the 2mm channel, and 100ms for the 3mm and 4mm channels. An example of a sonogram derived for the 2mm channel of the flow phantom is shown in figure 3.3.

Power values were obtained from each Doppler signal recording by processing the sonogram information. The maximum frequency envelope was derived manually using a simple threshold method (Evans et al. 1989) and used in a foot-finding algorithm to divide the signal into beats (Evans 1988). A power value was obtained for each one-minute recording by selecting ten beats. Selection was initially based on elimination of any beats containing high intensity noise; an example of such noise is shown in figure 3.4. Ten beats were then chosen randomly from those remaining in order to prevent operator bias affecting the selection, and to help smooth any inherent time variations in the signal power. The total power for each beat was obtained by summing all the sonogram power values contained in the beat, and the mean signal power was then calculated as being equal to the mean of the total power values for the ten selected beats.

3.3.2 Recordings

To investigate the effect of transducer position on the signal power received from each of the phantom channels, Doppler signals were recorded for transducer positions on the phantom surface spaced at 0.5mm intervals across the width of each channel. The effect of sample depth setting on signal power was also investigated for each channel, in each case using the transducer position which was estimated to give the maximum power during the former set of recordings.

To establish whether it is feasible to compare power values derived from non-continuous signals recordings which have involved repositioning of the transducer, recordings for fifteen separate applications of the transducer to the phantom were made for each channel. For each application, the signal power was carefully maximised by eye, using the sonogram intensity and the power trace provided by the Doppler system.

The relationship between signal power and channel size was obtained by analysing the signals recorded at different sample depths and transducer positions from each channel (described above), and then selecting the maximum of the power values derived from these recordings. This method allowed

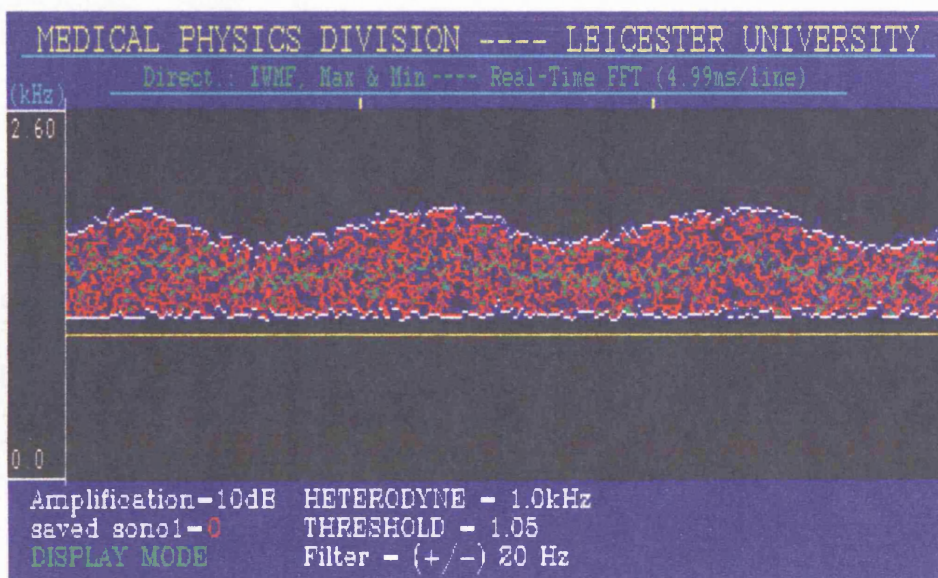


Figure 3.3 An example of the Doppler sonogram recorded from the 2mm channel of the flow phantom.

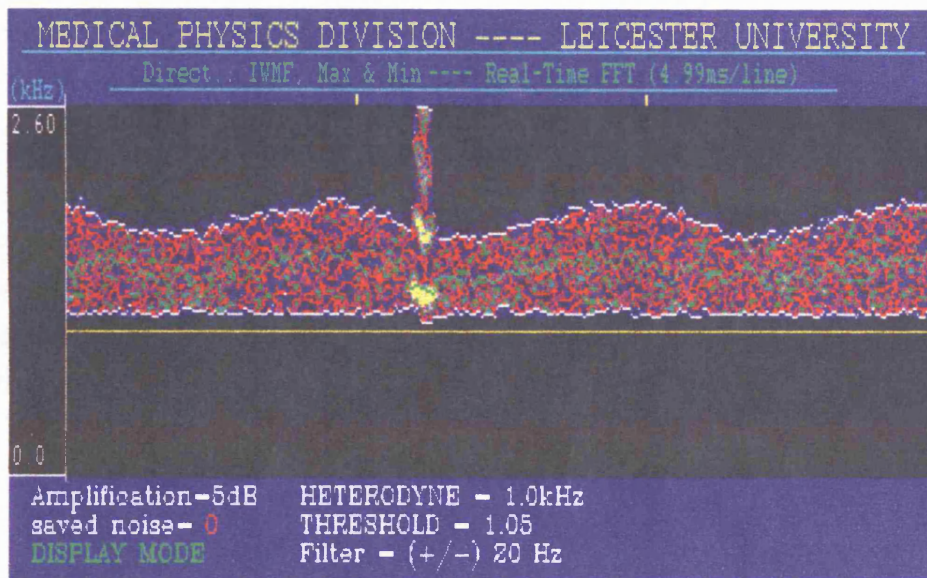


Figure 3.4 A Doppler signal recorded from the TMM flow phantom showing an example of high intensity noise caused by either air bubbles or a particle clump. Rejection of any beats containing noise prevents the calculation of an inaccurately large signal power value.

the assumption that each channel was being insonated with the same maximum intensity region of the ultrasound beam.

3.3.3 Signal Power Corrections

Correction for Path Length

Because the flow phantom used in this study was designed to have an identical distance between the surface and the centre of each channel, the precise path length to the upper wall of each channel was slightly different for each channel size. Relative to the path length for the 4mm diameter channel, the beam travelled through an additional 2.8mm of TMM for the 2mm channel and 1.4mm for the 3mm channel, producing total signal power values reduced by approximately 6% and 3% respectively. Power values for the 2mm and 3mm channels were therefore corrected accordingly.

Correction for Beam Shape

The total signal power received from each flow phantom channel was corrected for the effects of non-uniform insonation by dividing by a correction factor $C_{beam}(d)$. Correction factors were calculated from the ratio of the total raw signal power P_{raw} that would theoretically be received from a channel of diameter ' d ' when in the non-uniform beam, and the total power $P_{uniform}$ received for uniform insonation of the same channel:

$$C_{beam}(d) = \frac{P_{raw}}{P_{uniform}} \quad [3.1]$$

The value of P_{raw} for each of the phantom channel sizes was estimated from the received field beam shape of the 2MHz Scimed transducer; the received field is representative of both the transmission and the reception zone sensitivities of the transducer, and can be assumed to be proportional to the signal power received from different positions within a vessel. Pressure amplitude values were recorded from the beam of the transducer using a 0.25mm point hydrophone (model HP301, Precision Acoustics Ltd., Dorchester, UK), providing a three-dimensional array of values composed of a series of planes lying parallel to the face of the transducer. The array position was centred axially on the relevant sample depth and laterally on the centre of the transducer in order to coincide with the theoretical position of maximum intensity in the beam, and the array size covered the sample volume length (0.85cm). Pressure amplitude values were squared to provide an approximation of the transmitted field intensity, and the intensity values were in turn squared to provide an estimate of the overall sensitivity pattern of the transducer; the latter is shown in figure 3.5.

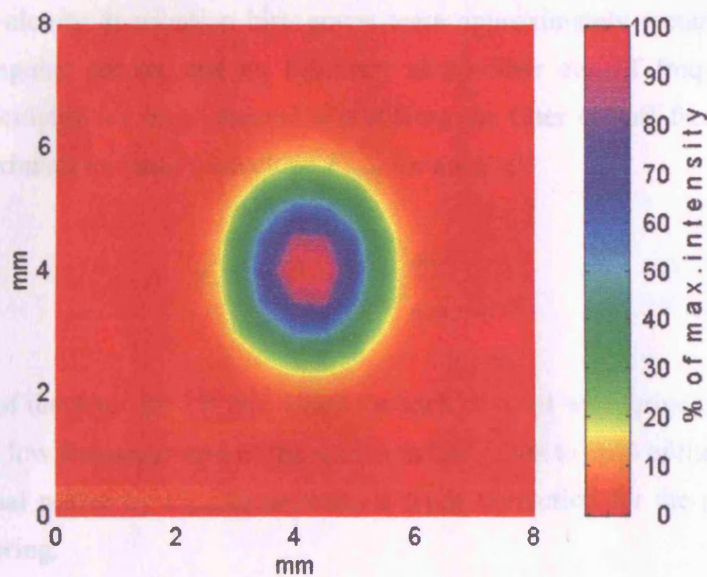
The contribution to the total signal power from each plane was calculated by summing the received field sensitivity values that intersected with the channel, and was dependent on the cross sectional area of the channel and its position within the plane. The position in each plane was determined by the orientation and location of the channel in the beam. For this investigation, the orientation was 45 degrees and the vessel was assumed to pass through the centre of the sample

volume (corresponding to the region of maximum beam sensitivity). An algorithm was used to locate and average those values incident at the vessel edges that contributed only partially to the received signal; this is described in detail in chapter 6.

The total power P_{total} theoretically received for uniform irradiation of each of the three phantom channels was calculated in the same way as P_{max} but using an array composed of values which were all equal to the maximum sensitivity in the recorded array of received field sensitivity values.

Correction for High Pass Filtering

An approximate filter correction was implemented for this in-vivo investigation. By deriving the theoretical velocity profiles and velocity distribution histograms for the signals recorded from each of the flow phantom channels, it was found that the profiles appeared parabolic, and that the corresponding velocity distribution histograms were approximately triangular (Figure 3.6). Hence, assuming rectangular filtering, the correction factor $C_{\text{rect}}(\omega)$ was calculated as a function of the filter cut-off frequency f_{cut} and the mean value of the signals \bar{v} (Equation 3.1).



The value of $C_{\text{rect}}(\omega)$ was then multiplied by the measured power P_{meas} to give the corrected power P_{corr} (Equation 3.2). The value of P_{corr} was then divided by the total power P_{total} to give the corrected field sensitivity S_{corr} (Equation 3.3).

3.4 Results

Figure 3.5 Received field sensitivity plot for a 2MHz Scimed TCD transducer, recorded at an axial distance of 5.0cm for a homogeneous beam path through water.

The results show that there is one transducer position for each channel size at which the received power is at a maximum. For positions away from this, the power decreases with distance. For all channel sizes, the received power falls by more than 25% within 1mm of the transducer position at which the maximum power is received.

Figure 3.7 depicts the normalised signal power received from each of the channels at various sample depth settings. The results again show that in each case the power is at a maximum for one particular sample depth setting and decreases for settings greater or smaller than this.

Figure 3.8 displays the variation in received power arising when the transducer is removed and then re-applied to the phantom surface. For each of the three channels, the received power is plotted for fifteen re-applications of the transducer, with the values normalised to the mean value for the 4mm channel. The mean and standard deviation of the normalised signal powers was calculated to be 0.51 ± 0.01 for the 2mm channel, 0.69 ± 0.04 for the 3mm channel and 1.00 ± 0.04 for the 4mm channel.

volume (corresponding to the region of maximum beam sensitivity). An algorithm was used to locate and amend those values incident at the vessel edges that contributed only partially to the received signal; this is described in detail in chapter 6.

The total power P_{uniform} theoretically received for uniform insonation of each of the three phantom channels was calculated in the same way as P_{raw} , but using an array composed of values which were all equal to the maximum sensitivity in the recorded array of received field sensitivity values.

Correction for High Pass Filtering

An approximate filter correction was implemented for this in-vitro investigation. By deriving the theoretical velocity profiles and velocity distribution histograms for the signals recorded from each of the flow phantom channels, it was found that the profiles appeared parabolic, and that the corresponding velocity distribution histograms were approximately rectangular (figure 3.6). Hence, assuming rectangular spectra and an infinitely sharp filter cut-off frequency, a correction factor $C_{\text{filter}}(d)$ was calculated for each channel size d from the filter cut-off frequency F_{filter} and the mean value of the maximum frequency envelope F_{mean} for a signal:

$$C_{\text{filter}}(d) = 1 - \frac{F_{\text{filter}}}{F_{\text{mean}}} \quad [3.2]$$

The value of the filter cut-off frequency for each channel was derived from the position at which the power at the low frequency end of the spectrum had fallen to 50% of the maximum value. Division of the total signal power by $C_{\text{filter}}(d)$ provides a crude correction for the proportion of the spectrum removed by filtering.

3.4 Results

Figure 3.7 shows the signal power received at different lateral transducer positions on the surface of the phantom, for the 2mm, 3mm and 4mm diameter channels. The values are normalised to the maximum power value received from the 4mm channel. The results show that there is one transducer position for each channel size at which the received power is at a maximum. For positions away from this, the power decreases with distance. For all channel sizes, the received power falls by more than 25% within 1mm of the transducer position at which the maximum power is received.

Figure 3.8 depicts the normalised signal power received from each of the channels at various sample depth settings. The results again show that in each case the power is at a maximum for one particular sample depth setting and decreases for settings greater or smaller than this.

Figure 3.9 displays the variation in received power arising when the transducer is removed and then reapplied to the phantom surface. For each of the three channels, the received power is plotted for fifteen re-applications of the transducer, with the values normalised to the mean value for the 4mm channel. The mean and standard deviation of the normalised signal powers was calculated to be 0.31 ± 0.01 for the 2mm channel, 0.69 ± 0.04 for the 3mm channel and 1.00 ± 0.04 for the 4mm channel.

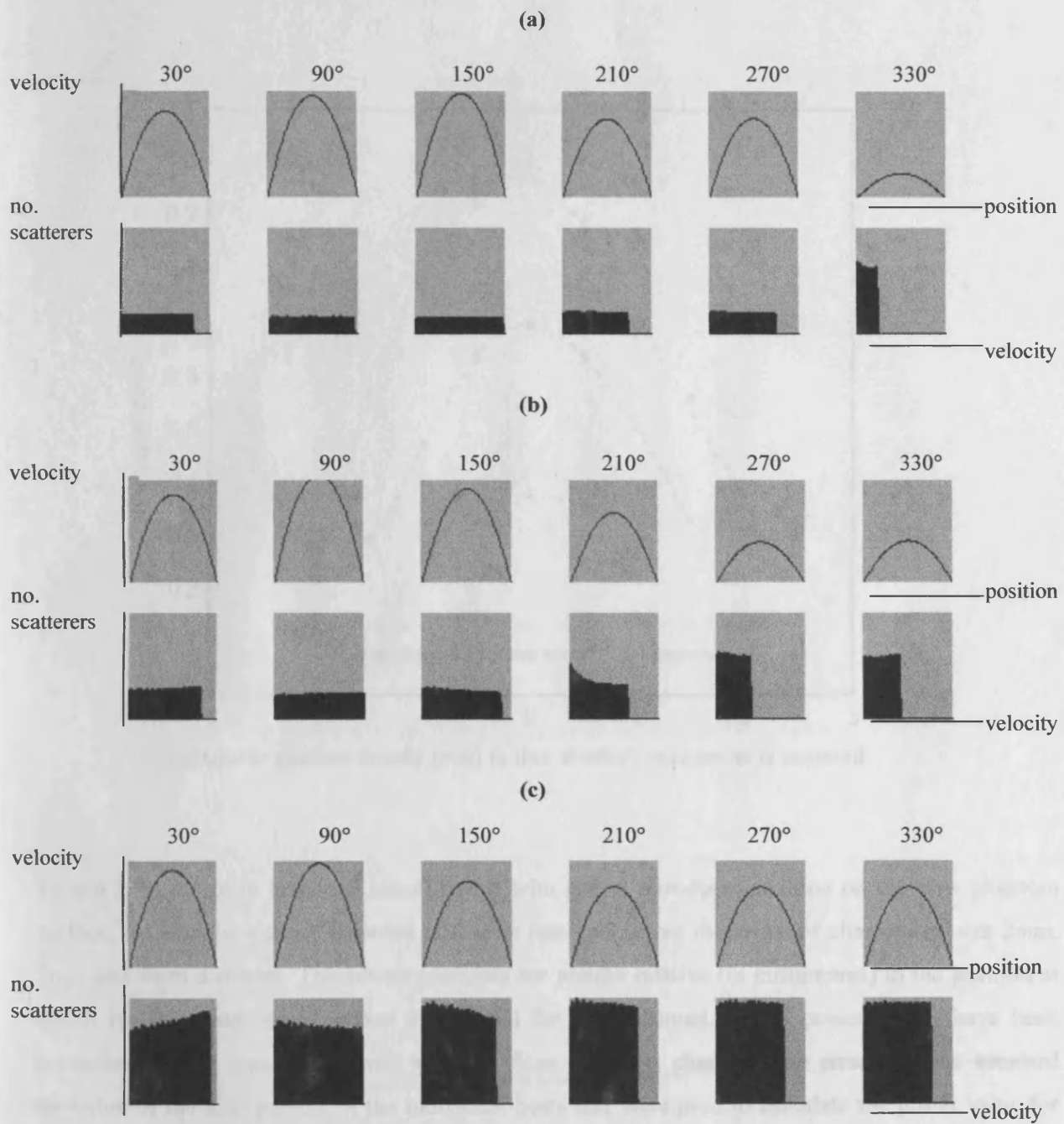


Figure 3.6 velocity profiles and velocity distribution histograms plotted at six cardiac phases, for flow phantom channels of diameter **(a)** 2mm, **(b)** 3mm and **(c)** 4mm.

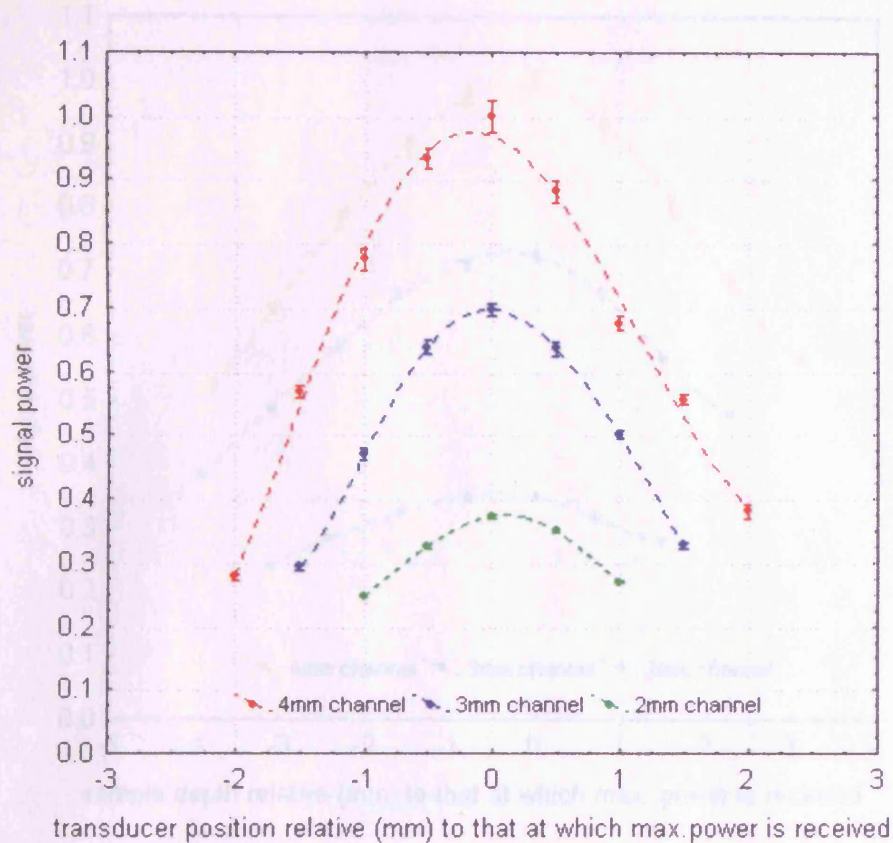


Figure 3.7 Change in total raw signal power with lateral transducer position on the flow phantom surface, for Doppler signals recorded at 0.5mm intervals across the width of channels of size 2mm, 3mm and 4mm diameter. Transducer positions are plotted relative (in millimetres) to the position at which the maximum signal power is received for each channel. Signal power values have been normalised to the maximum power received from the 4mm channel. The errors are the standard deviation of the total powers of the individual beats that were used to calculate the power value for each signal recording. The dashed lines represent a fifth order polynomial fit to the data points.

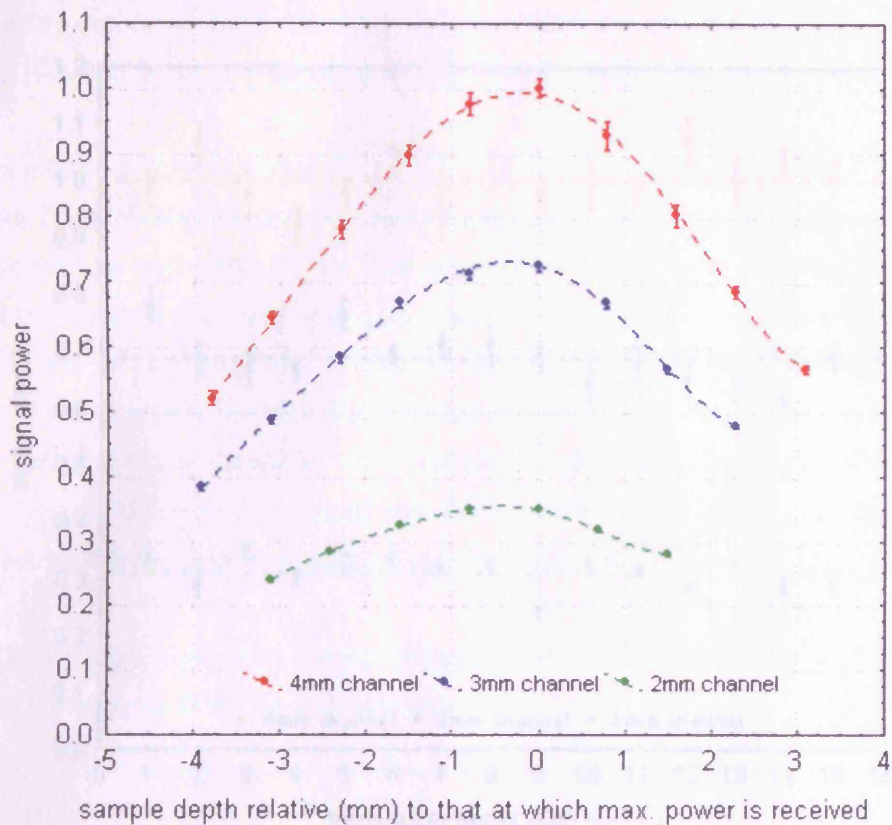


Figure 3.8 Change in total raw signal power with sample depth setting, for Doppler signals recorded from flow phantom channels of size 2mm, 3mm and 4mm diameter, in each case using the transducer position estimated from figure 3.7 to produce the maximum signal power. Sample depth settings are plotted relative (in millimetres) to the setting for which the maximum signal power is received for each channel. Signal power values have been normalised to the maximum power received from the 4mm channel. The errors are the standard deviation of the total powers of the individual beats that were used to calculate the power value for each signal recording. The dashed lines represent a fifth order polynomial fit to the data points.

These results show that for the 4mm channel, the variation in received power is approximately 2.7% from the mean. The variation is slightly greater for the 3mm and 4mm channels, ranging up to 13%.

Mean-averaged peak velocities of approximately 46cm/s, 27cm/s and 13cm/s were calculated for the signals recorded from the 4mm, 3mm and 2mm channels respectively. Maximum Doppler shift frequencies for the signals were approximately 375Hz, 475Hz and 325Hz respectively. The filter cut-off frequency was calculated to be approximately 150Hz for all three channels. Correction factors for high pass filtering are given in table 3.1.

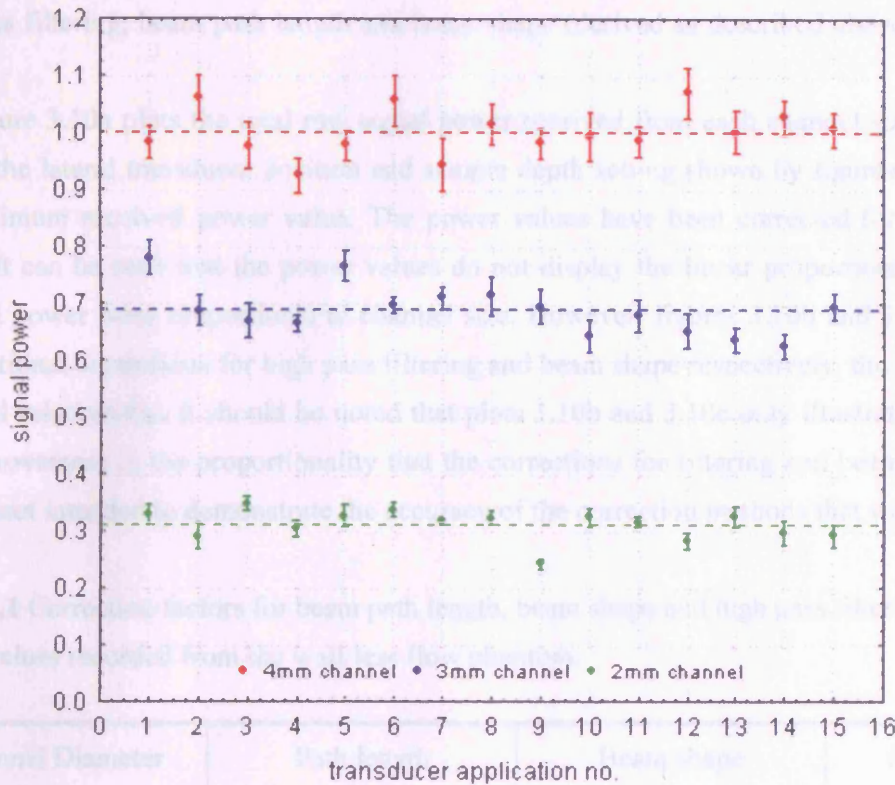


Figure 3.9 Variation of the total raw signal power received from flow phantom channels of diameter 2mm, 3mm and 4mm, for fifteen applications of the transducer to the phantom surface above each channel. For each application the received signal power was maximised using the Doppler sonogram intensity and the power trace provided by the Doppler system. The dotted lines represent the mean signal power received from each channel, and values have been normalised to the mean value for the 4mm channel. The errors are the standard deviation of the total powers of the individual beats that were used to calculate the power value for each signal recording.

The fragility of the flow phantom TMM material used in this investigation required low flow velocities to be used in order to prevent leakage. Although the backscatter properties of the TMM appear to be dependent on velocity at low velocities (Ramparino et al. 1999) the authors attributed this

These results show that for the 2mm channel, the variation in received power is approximately $\pm 3\%$ from the mean. The variation is slightly greater for the 3mm and 4mm channels, ranging up to $\pm 5\%$.

Time-averaged peak velocities of approximately 46cms^{-1} , 22cms^{-1} and 15cms^{-1} were calculated for the signals recorded from the 2mm, 3mm and 4mm channels respectively. Maximum Doppler shift frequencies for the signals were approximately 975Hz, 477Hz and 325Hz respectively. The filter cut-off frequency was calculated to be approximately 100Hz for all three channels. Correction factors for high pass filtering, beam path length and beam shape (derived as described above) are given in table 3.1.

Figure 3.10a plots the total raw signal power received from each channel size, recorded in each case at the lateral transducer position and sample depth setting shown by figures 3.7 and 3.8 to give the maximum received power value. The power values have been corrected for the effects of path length. It can be seen that the power values do not display the linear proportionality expected if the received power were proportional to channel size. However, figures 3.10b and 3.10c show that with the additional corrections for high pass filtering and beam shape respectively, the results approach the expected relationship. It should be noted that plots 3.10b and 3.10c only illustrate the likely scale of the improvement in the proportionality that the corrections for filtering and beam shape bring about, and are not intended to demonstrate the accuracy of the correction methods that were used.

Table 3.1 Correction factors for beam path length, beam shape and high pass filtering applied to signal power values recorded from the wall-less flow phantom.

Channel Diameter (mm)	Path length correction factor	Beam shape correction factor	High pass filter correction factor
2.0	1.067	0.22	0.78
3.0	1.033	0.19	0.60
4.0	1.00	0.16	0.49

3.5 Discussion

To date, the theoretical relationship between the Doppler signal power and vessel size has only been investigated using conventional tubing flow phantoms (Hatab et al. 1997), which may produce distortion in the signal power spectra due to the difference in the acoustic properties between the tube walls and the surrounding medium. In order to more closely model the in-vivo case, this study has used Doppler signals recorded from a wall-less flow phantom. Although the 45 degree beam-vessel angle used in the phantom is not the same as the zero degree angle usually assumed for insonation of the MCA, the fact that the latter can vary by up to ± 30 degrees (Martin et al. 1993, Martin et al. 1995) suggests that the flow phantom configuration is not unreasonable as a model of the in-vivo case.

The fragility of the flow phantom TMM material used in this investigation required low flow velocities to be used in order to prevent leakage. Although the backscatter properties of the BMF appear to be dependent on velocity at low velocities (Ramnarine et al. 1999), the authors attributed this

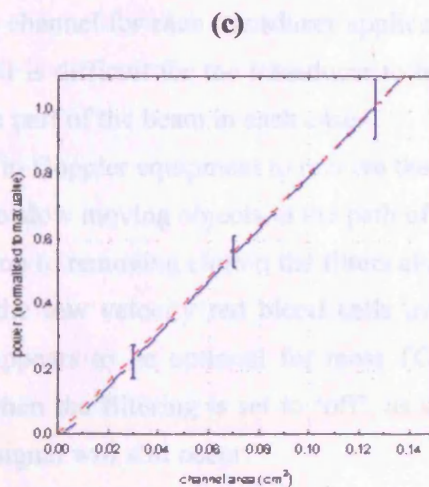
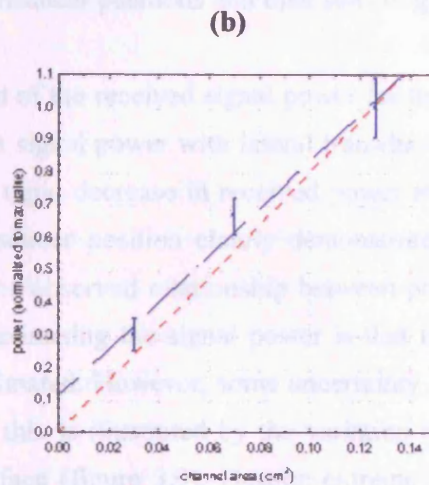
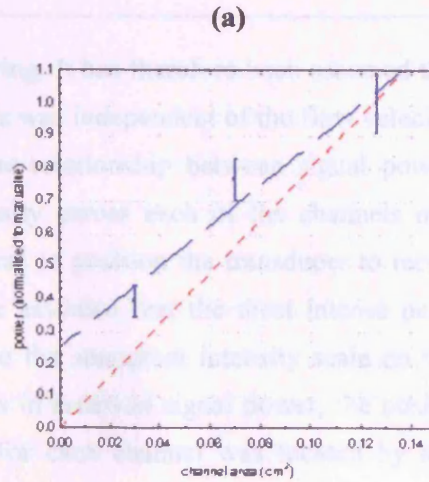


Figure 3.10(a-c) The relationship between the total signal power and channel area for intensity-maximised Doppler signals recorded from flow phantom channels of 2mm, 3mm and 4mm diameter (areas 0.031cm^2 , 0.071cm^2 and 0.126cm^2 respectively), for (a) raw signal power values, (b) signal power values corrected for high pass filtering, and (c) signal power values corrected for filtering and beam shape. The dotted red lines represent the proportional relationship expected from theory, and the dashed blue lines the best fit to the plotted signal power values. Power values have been normalised to that of the 4mm channel. The errors are the standard deviation of the total powers of the individual beats that were used to calculate the power value for each signal recording.

to the effects of high pass filtering. It has therefore been assumed that the backscatter power received from the flow phantom channels was independent of the flow velocity.

In order to obtain the true relationship between signal power and channel size for the flow phantom case, the beam intensity across each of the channels must be approximately equal. The simplest way to achieve this was to position the transducer to receive the maximum possible signal power; in this way it could be assumed that the most intense part of the beam was being used to insonate each channel. Because the sonogram intensity scale on the TCD system was not sensitive enough to detect small changes in received signal power, the position for which the received signal intensity was at a maximum for each channel was located by analysing the signals recorded for different sample depths and transducer positions and then selecting the maximum of the power values derived from these recordings.

The need for maximisation of the received signal power for the in-vitro case is illustrated by the results showing the variation in signal power with lateral transducer position (figure 3.7) and sample depth setting (figure 3.8). The rapid decrease in received power away from the maximum with both sample depth setting and transducer position clearly demonstrates that unless the signal power is maximised for each channel, the observed relationship between power and vessel size may be false. An additional advantage of maximising the signal power is that the position of each flow phantom channel in the beam can be estimated. However, some uncertainty remains as to the exact position of the channels in the beam, and this is illustrated by the variation in power for re-applications of the transducer to the phantom surface (figure 3.9). Despite extreme care being taken to maximise the signal power received from the channel for each transducer application, the values display a variation of up $\pm 5\%$. This suggests that it is difficult for the transducer to be positioned so that the channel is insonated with exactly the same part of the beam in each case.

High pass filtering is used in Doppler equipment to remove the low frequency clutter components in the signal which occur due to slow moving objects in the path of the beam, for example vessel wall movements. However, in addition to removing clutter, the filters also remove the low frequency signal components originating from the low velocity red blood cells travelling close to the vessel walls. Although high pass filtering appears to be optional for most TCD systems, all contain additional inherent filters. Hence, even when the filtering is set to 'off', as was the case for this investigation, some high pass filtering of the signal will still occur.

The fragility of the TMM used in this investigation meant that at high flow velocities there was a tendency for the phantom to leak at the join between the inlet tubes and the channels, and in the worst case for splits to develop in the material. Consequently, low flow rates were used for the recordings taken in this study; time-averaged peak velocities of approximately 46cm s^{-1} , 22cm s^{-1} and 15cm s^{-1} were calculated from the velocity envelopes of the signals recorded from the 2mm, 3mm and 4mm channels respectively. The effect of high pass filtering on the flow phantom signals was accentuated firstly by the fact that the low flow velocities caused a large proportion of the spectrum to be removed by the filter, and secondly by the fact that the different velocities in each channel resulted in a different proportion of the spectrum being removed in each case.

The difficulty in correcting for filtering lies in the uncertainty about the true spectral shape. The

precise effects of beam shape on the signal spectrum cannot be predicted unless the exact position of a channel in the beam is known. In addition, spectral estimate variance and noise may obscure the shape of the spectrum, and non-uniform attenuation of the signal by materials in the beam path may also cause unpredictable distortion. Because of the unknown influence of these factors, extrapolation of the spectrum to replace the filtered low frequency spectral components may not be accurate. To overcome these difficulties, a theoretical correction for the effects of high pass filtering on the signals recorded from each channel was derived using the assumptions that the signal power spectra are rectangular and that the high pass filter has an infinitely sharp cut-off frequency. The former assumption is unlikely to be precisely accurate owing to effects such as beam shape, spectral broadening and noise affecting the shape of the spectra, and the latter due to the limitations of electronic filters. However, because the main aim of the filter correction was merely to illustrate the scale of the filtering effects on the signal power recorded from the flow phantom, it was considered unnecessary at this stage to refine the corrections for the in-vitro case.

Using the method described in section 3.3.4, the filter cut-off frequency was calculated to be approximately 100Hz for all three channels. The calculation method was validated by the fact that this value was equal to that derived from a plot of the frequency response of the inherent high pass filters in the Scimed PC Dop842 system (see figure 7.4a in chapter 7). The maximum Doppler shift frequencies for the 2mm, 3mm and 4mm flow phantom channels were approximately 975Hz, 477Hz and 325Hz respectively. The application of corrections for high pass filtering to the signals recorded from the flow phantom (figure 3.10b) therefore had a significant influence on the relationship between power and channel size, bringing it closer to the theoretical one.

Non-uniform insonation of a vessel results in unequal weighting of the Doppler spectral power at different frequencies. The extent of the spectral distortion depends on the beam shape across the vessel. For the in-vitro case, if the received signal power is maximised for a channel then it can be assumed that the maximum beam intensity is approximately coincident with the central high-flow region of the vessel. Consequently, because the TMM is homogeneous and the size of each channel is known, the approximate beam shape across each channel can be estimated from a plot of the transducer sensitivity, allowing a correction for non-uniform insonation to be calculated. The accuracy of the correction factors used in this investigation was potentially limited by the fact that the channel positions were not known precisely, and also because the derivation of the correction factors from a beam plot required an approximation of the contribution of the intensity values falling at the edges of the channels. A further source of error arose because the beam plot was obtained for a homogeneous water path rather than a TMM path. A separate investigation of the effects of the TMM on beam shape was carried out by plotting the received field beam shape for a path through a TMM sample of thickness 5cm placed in the water tank between the transducer and the point hydrophone. It can be seen that the distortion effects relative to the beam shape for the homogeneous path appear to be minor (figures 3.11a and 3.11b). In addition, owing to the uncertainty of the precise effects on beam shape of the TMM path for each channel, errors would still be introduced if beam shape correction factors were derived from a TMM beam plot. The path in each case was therefore assumed to be homogeneous and the water path beam plot used for the derivation of beam shape corrections.

When using flow phantoms to investigate the relationship between signal power and vessel size, it is important that the beam path length is the same for each channel to ensure that the attenuation of the beam is equal in each case. This can be achieved by the correct positioning of the transducer on the phantom surface. However, because the flow phantom used in this study was designed to have an identical distance between the surface and the centre of each channel, the precise path length to the upper wall of each channel was slightly less for each channel size. Corrections for beam path length were therefore applied to the flow phantom graphs in order to account for the difference in TMM attenuation for

fitting and beam size was not used. Channel size was not used as the upper wall of the channel of inaccuracy was not negligible relative to

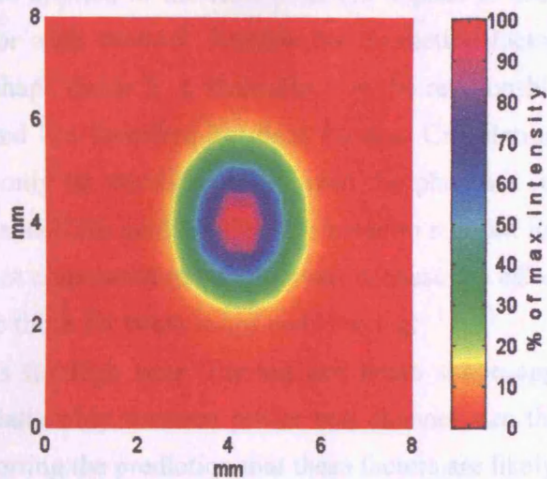
The corrections produced a final relationship (Figure 3.11(a)), supporting the prediction that these factors are likely to have a negligible influence on the shape for the in-vitro case.

3.4 Conclusions

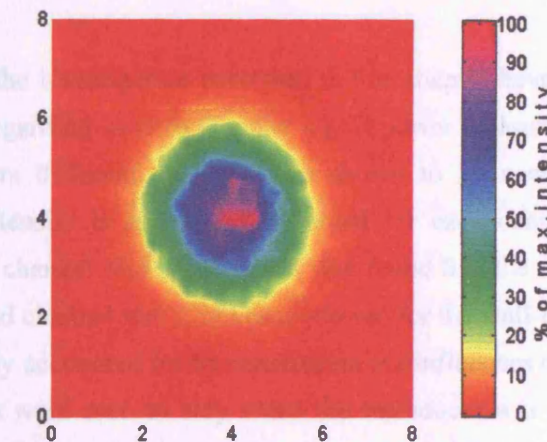
The results of the in-vitro investigation illustrated a number of previously unreported points regarding the relationship between power received from the in-vitro beam intensity and channel size. It can be concluded that the relationship between power and channel size is not linear, and that the two relationships between power and channel size are not the same. The relationship between power and channel size can be approximately described as a power law relationship. The relationship between power and channel size is not linear, and that the two relationships between power and channel size are not the same. The relationship between power and channel size can be approximately described as a power law relationship.

Although the in-vitro case is not identical to that of the flow phantom, many of the same points will apply. The relevance of the in-vitro findings to the in-vivo case will be discussed in the next chapter.

Figure 3.11 Received field sensitivity plots for a 2MHz Scimed TCD transducer, recorded at an axial distance of 5.0cm for (a) a homogeneous beam path through water, and (b) a beam path through a 5.0cm sample of TMM.



(a)



When using flow phantoms to investigate the relationship between signal power and vessel size, it is important that the beam path length is the same for each channel to ensure that the attenuation of the beam is equal in each case. This can be achieved by the correct positioning of the transducer on the phantom surface. However, because the flow phantom used in this study was designed to have an identical distance between the surface and the centre of each channel, the precise path length to the upper wall of each channel was slightly different for each channel size. Corrections for beam path length were therefore applied to the flow phantom signals in order to account for the difference in TMM attenuation for each channel. Because the correction factors were small relative to those for filtering and beam shape (table 3.1), their effect on the relationship between signal power and vessel size was minimal and has therefore not been plotted. Calculation of the correction factor for each channel was based only on the distance between the phantom surface and the closest point on the upper wall of the channel. No modification was made to account for the wall curvature, but this source of inaccuracy was not considered to be important because the effect of the beam path corrections was negligible relative to those for beam shape and filtering.

The corrections for high pass filtering and beam shape applied to the flow phantom signals produced a final relationship between power and channel size that was approximately proportional (figure 3.10c), supporting the prediction that these factors are likely to have most influence on spectral shape for the in-vitro case.

3.6 Conclusions

The results of the investigation described in this chapter have illustrated a number of previously unreported points regarding in-vitro Doppler signal power measurements. Maximisation of the signal power received from different channels was shown to be necessary in order to ensure that the insonating beam intensity is approximately equal for each channel and that the true relationship between power and channel size is plotted. It was found that the relationship between the maximised raw signal power and channel size is not proportional for the wall-less flow phantom case, but that this can be approximately accounted for by considering the influences of filtering and beam shape. Finally, signal power values were seen to vary when the transducer was removed and then reapplied to the phantom surface, despite careful maximisation of the signal intensity in each case.

Although the in-vivo case is not identical to that of the flow phantom, many of the same points will apply. The relevance of the in-vitro findings to the MCA will be discussed in the next chapter, along with additional factors that may affect Doppler signal power recordings from in-vivo vessels.

CHAPTER 4

The In-Vivo Doppler Power Spectrum

4.1 Introduction

The in-vitro investigation of the relationship between Doppler signal power and vessel size published by Hatab et al. (1997) included only superficial coverage of the relevance of the results to the in-vivo case, with a discussion of the possible effects of high pass filtering and haematocrit on the signal power recorded from in-vivo vessels. In order to more fully assess the accuracy of the Doppler power method for measuring changes in MCA size, this chapter gives a detailed analysis of all the factors which might affect the signal power, and discusses the relevance to the MCA case of the results obtained from the in-vitro investigation described in chapter 3.

4.2 Factors Affecting the In-Vivo Doppler Power Spectrum

One important difference between the in-vitro and in-vivo cases is that a single vessel is monitored in the latter. This eliminates the need to consider the influence of gross transducer movements or sample depth setting; provided that these factors remain constant during in-vivo recordings, they will not affect the signal power received from a vessel. Similarly, the effects of beam path are irrelevant for the single vessel case, as the path length and the physical properties of the tissues in the path will be constant if the transducer position remains stationary.

A further difference between the in-vitro and in-vivo cases is that the scale of the size changes occurring for in-vivo vessels are likely to be smaller than the difference between the flow phantom channel sizes used for the in-vitro investigation. This results in the need for even greater care when accounting for the factors which influence the signal power, as the errors introduced by these factors will be more significant with respect to the detection of smaller power changes.

Similarly to the in-vitro case, the relationship between transducer frequency and backscattered power can be disregarded if the insonating frequency does not change. In addition, the effects of spectral broadening can be considered to be constant for all vessel sizes if the beam-vessel angle does not change, and the effects of spectral noise can be reduced by optimising the SNR and averaging power values over time.

The remaining factors affecting the Doppler signal power which need to be considered more carefully for the in-vivo case are high pass filtering, non-uniform insonation, non-uniform attenuation, transducer position, flow conditions and scatterer concentration.

4.2.1 High Pass Filtering

As discussed in chapter 3, the high pass filtering of the Doppler signals recorded from different flow phantom channel sizes had a marked effect on the power spectra due to the low flow velocities necessitated by the fragility of the TMM. Relative to the in-vitro case, the in-vivo relationship between power and vessel size should be affected far less by filtering as the velocity of the blood in the cerebral

vessels is higher than that used in the flow phantom, and hence the proportion of red blood cells travelling at low velocities is reduced and a smaller percentage of the total power is removed by the filter. For example, the mean value of time-averaged peak velocity in the adult MCA is 51cm s^{-1} (Evans et al. 1989), which corresponds to a maximum Doppler shift frequency of approximately 1300Hz for an insonation angle of zero degrees and a transducer frequency of 2MHz. A filter cut-off frequency of 100Hz would therefore remove only 7.7% of the spectral power (assuming parabolic flow and a rectangular power spectrum).

As the filter cut-off frequency increases, so will the percentage of the power spectrum removed by the filter. The cut-off frequency should therefore be kept as low as possible if the effects of high pass filtering are to be minimised. However, the benefits of this are doubtful if the filter setting is too low to prevent the appearance of low frequency clutter signals in the spectrum. Even if it is possible to obtain clutter-free signals without using the optional high-pass filtering provided by the system, it should again be noted that use of a zero filter setting on most TCD systems does not mean that all high pass filtering is eliminated; the presence of inherent filters will unavoidably result in the loss of part of the low frequency spectrum. An example of this is given in figure 4.1, which shows a signal spectrum recorded from the 2mm channel of the wall-less flow phantom described in chapter 3. The signal was recorded with the Scimed PCDop842 high pass filter setting "off", but it can be seen that filtering up to approximately 100Hz is still present.

If the filter cut-off frequency and the flow velocity remain constant during recordings, then the proportionality to vessel size of any changes in power that are detected should not be adversely affected by high pass filtering. However, varying velocities may introduce a source of error to in-vivo power measurements, as any change in velocity alters the percentage of the power spectrum that is removed by the filter. This effect is inadvertently demonstrated by the results of Hatab et al. (1997), which show an increase in signal power with velocity that can be attributed to high pass filtering.

The consequences of high pass filtering for the Doppler signal power method depend on the circumstances of a recording. If a change in velocity occurs without an accompanying change in vessel size then the resultant increase or decrease in the total signal power caused by variation in the proportion of the power spectrum removed by the high pass filters could potentially be falsely interpreted as a change in vessel size. Alternatively, for a simultaneous change in velocity and vessel size, the relationship between power and vessel size could be affected and hence incorrect conclusions might be drawn about the scale of the vessel size change that has occurred.

For the in-vivo case, the change in power caused by filtering is likely to be small due to the relatively limited range of velocity changes that occur. For example, a high pass filter of 100Hz applied to a signal recorded for a peak flow velocity of 51cm s^{-1} will result in a loss of 7.7% of the spectrum under the conditions stated above. A change in velocity to 60cm s^{-1} will mean that only 6.5% of the spectrum is removed by the filter, resulting in a power increase of 1.2%. The scale of this power change is small, and the possible misinterpretation of it having been caused by a change in vessel size would therefore be unlikely to significantly influence any conclusions that are drawn. However, under different circumstances the error could be increased, for example for higher filter cut-off frequencies, lower flow velocities or greater changes in velocity. Hence, the presence of an error due to filtering

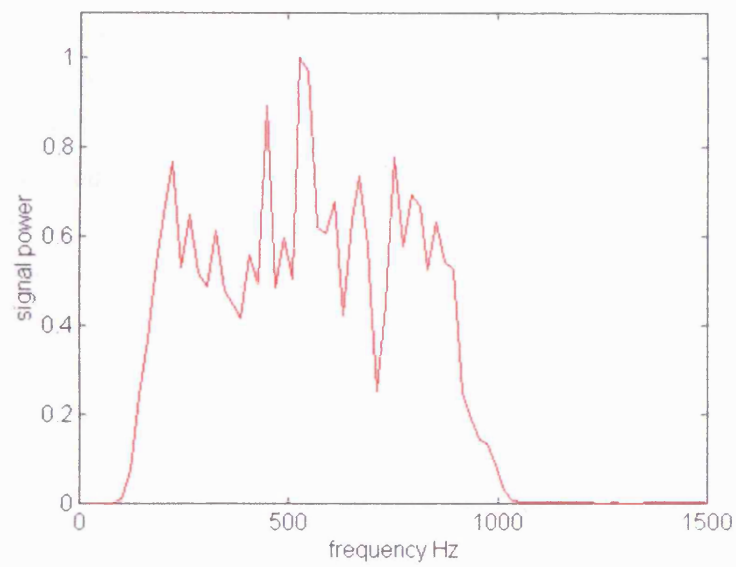


Figure 4.1 Signal spectrum showing presence of inherent high pass filtering in the Scimed PC Dop842 TCD system. The spectrum is the mean of ten peak systolic spectra extracted from the signal recorded from the 2mm channel flow phantom channel.

should always be considered when using the Doppler power method to detect size changes in in-vivo vessels.

4.2.2 Non-Uniform Insonation

The in-vitro investigation described in chapter 3 demonstrates that beam shape affects the signal power received from different sized flow phantom channels and hence alters the relationship between power and channel size. The effect of beam shape for Doppler power recordings from the MCA is likely to be even greater than that seen in-vitro due to the additional distortion of the beam by the temporal bone and inhomogeneous tissues in the beam path. Temporal bone is known to cause significant beam distortion (Fry and Barger 1978, White et al. 1978, Grolimund 1986) as the curvature of the skull bone in the temporal region, the varying thickness of the bone and the convoluted inner surface of the skull may all act to cause focusing and refraction of the beam and spatial variations in attenuation. Additional refraction may also occur due to the curved surface of the muscle and blood interface at the vessel wall (LaFollette and Ziskin 1986, Thompson and Aldis 1996). This effect may be accentuated if vascular disease is present, due to an increased impedance mismatch between calcified plaque and blood.

For the flow phantom investigation, correction factors for the effects of beam shape on signal power were derived for each channel using the available channel size, position and beam shape information. For in-vivo cerebral vessels, the derivation of specific correction factors is prevented by the fact that the size of the vessel is unknown, and also because the nature of beam shape distortion by temporal bone varies between individuals (Grolimund 1986).

4.2.3 Attenuation

For the in-vitro case, attenuation of the transmitted ultrasound beam and the backscattered Doppler signal was approximately uniform owing to the homogeneous TMM. For the in-vivo case, however, non-uniform attenuation of the beam will occur due to spatial variations in the physical properties of the various tissues lying between the transducer and vessel. The absorption component of attenuation is increased for rigid materials such as bone, and hence is significant for the case of the MCA due to the presence of the temporal bone. In addition, reflection is increased due to the large impedance mismatches at the bone interfaces.

Non-uniform attenuation will affect the total signal power by causing further distortion to the beam shape across the MCA, and by altering the shape of Doppler power spectrum during the passage of the Doppler signal from the vessel to the transducer. The effects on beam shape are likely to increase the probability of non-uniform insonation introducing inaccuracy to the relationship between power and vessel size. However, the effects on the shape of the Doppler spectrum when the signal is in transit should remain approximately constant for all size changes of the MCA provided that the beam path does not change.

4.2.4 Transducer Position

The in-vitro investigation of the effects of removing and then reapplying the transducer to the flow phantom surface illustrated the difficulty involved with positioning the transducer so that a channel was insonated with exactly the same part of the beam in each case. This difficulty is likely to be increased for recordings from in-vivo vessels due to the inhomogeneous nature of the tissues in the beam path causing more extreme differences in received power with small changes in transducer position or insonation angle. The flow phantom results emphasise the already well-understood need to maintain a stationary transducer position during the monitoring of changes in Doppler signal power from in-vivo vessels in order to prevent variations in power caused by movements of the transducer being misinterpreted as changes in vessel size. Furthermore, both the repositioning results and those showing changes in power with transducer position suggest that it is inadvisable to compare power values which are recorded before and after deliberate repositioning of the transducer, for example in the case of recordings taken on different days. It has been shown that even if the received signal power is carefully maximised to recreate the same insonation conditions in each case, the potential variation in power due to removal and re-application of the transducer is large enough to be misinterpreted as a significant change in vessel size. Although these findings prohibit the comparison of power values derived from non-continuous recordings, this has the hidden advantage that the effects of haematocrit on in-vivo signal power can be largely disregarded during a single recording; this is discussed in more detail in section 4.2.6.

The maintenance of transducer position for the in-vitro case was relatively simple, as operator input was the only factor likely to cause displacement. However, the feasibility of preventing transducer movements in-vivo may be limited, owing to patient motion and the less uniform surface to which the probe must be secured. This can only be overcome by taking great care to securely couple the transducer to the head, and by requesting that patients remain as still as possible. Beyond this, the transducer must be continuously observed to allow detection of any displacement, and the Doppler signal must also be monitored in order to identify any noise that arises in the signal from patient actions such as talking or swallowing.

4.2.5 Flow Conditions

For the in-vitro investigation presented in chapter 3, the backscatter properties of the BMF were assumed to be independent of the flow velocity for the range of velocities used in the investigation. For the in-vivo case, however, the power of the signal backscattered from blood can potentially be affected by changes in the flow conditions (Evans and McDicken 2000). As previously stated in chapter 2, both low and high shear rates can cause an increase in power due to cell aggregation and turbulent flow respectively (Angelsen 1980, Shung et al. 1984, Shung et al. 1992, Cloutier & Shung 1993, Bascom & Cobbold 1996).

A change in flow conditions in the MCA resulting in a change in backscattered power could only be identified if information about both the blood composition and vessel size was available. This is obviously not feasible during routine monitoring of the MCA. Consequently, the use of the Doppler

power method in-vivo should ideally be limited to cases for which shear rates are neither abnormally high nor low in order to reduce the possibility of fluctuations in red blood cell distribution causing changes in signal power that are unrelated to vessel size. Flow conditions can be reasonably assumed to be suitable if the flow is non-turbulent and the flow velocity is within normal limits.

4.2.6 Blood Composition

The relationship between blood haematocrit and backscattered power is not linear (Shung et al. 1976, 1992). Power initially increases with red blood cell concentration, reaching its maximum for a haematocrit value between approximately 15-20%. After this point, power decreases with increasing haematocrit. The effects of a change in haematocrit on the backscattered power will therefore depend on the initial value and the direction of change. For adults, normal haematocrit varies between 42%-47% (Dacie and Lewis 1968), therefore an increase will result in a fall in the backscattered power, and vice versa.

Variations in haematocrit that produce a significant change in the backscattered power could potentially be falsely interpreted as a change in vessel size. However, it is unlikely that haematocrit will change significantly over the duration of a recording; only moderate fluctuations of approximately $\pm 4\%$ occur over a 24 hour period (Eastham and Slade 1992) with variations most likely to be related to stimuli such as exercise, meals, fluid intake or strong emotions. Hence, changes in haematocrit large enough to significantly affect signal power are only likely to occur if recordings are taken over very long periods of time. In this case, it is probable that the effect of any haematocrit changes will be outweighed by changes in signal power arising from inadvertent movements of the transducer or changes in the coupling of the transducer to the head. Hatab et al. (1997) expressed concern about the effects of haematocrit changes on power recordings taken on different days, but this factor can be considered irrelevant as the comparison of non-continuous recordings of Doppler signal power is prohibited by the likelihood of spurious power changes being introduced by the change in transducer position (see section 4.2.4).

4.3 Conclusions

Provided that the transducer position remains stationary and that flow conditions and haematocrit are stable during recordings, it can be assumed that the theoretically proportional relationship between Doppler signal power and the size of the MCA will be altered primarily by beam shape and to a lesser extent by high pass filtering. The effect of filtering is likely to be less significant than for the in-vitro case due to the higher flow velocities in-vivo, whereas the effects of non-uniform insonation will probably be more pronounced owing to the distortion of beam shape by the temporal bone and the inhomogeneous tissues in the beam path.

In order to assess the importance of non-uniform insonation of the MCA with regard to the accuracy of the Doppler power method, further investigation is required of the nature of in-vivo beam shape distortion and the errors introduced by beam shape to signal power changes generated by changes in vessel size. These factors are explored in chapters 5 and 6 respectively.

CHAPTER 5

The Effects of Temporal Bone on TCD Beam Shape

5.1 Introduction

If the incident beam intensity is constant across a vessel and the red blood cells are uniformly distributed, then the power of the Doppler signal components backscattered from different positions in the vessel will theoretically be independent of their point of origin. However, if the beam intensity varies across a vessel, then the power of the signal components originating from different locations will be unequally weighted according to the intensity of the beam at the relevant positions. The consequence of significant non-uniform insonation of a vessel may be an alteration of the relationship between the Doppler signal power and vessel size, thereby potentially invalidating the assumption that power changes are proportional to vessel size changes. Such an effect has been demonstrated in chapter 3 for in-vitro signals recorded from a wall-less flow phantom. In addition, non-uniform insonation may cause inaccuracy in other parameters calculated from the Doppler signal power spectrum. Examples of situations where this could occur for recordings taken from the MCA include the detection and classification of microemboli in the cerebral circulation, and the calculation of mean blood velocity. A knowledge of the beam shape across the MCA is therefore desirable for many Doppler ultrasound applications.

For Doppler signals recorded from in-vivo vessels, it is unlikely that beam intensity will be uniform across many of the larger vessels as a lateral decrease in intensity away from the beam centre is an inherent characteristic of most ultrasound transducers. In addition, for cerebral arteries such as the MCA, the likelihood of significant intensity variations across the vessel is increased by spatial fluctuations in the acoustic and physical properties of the temporal bone in the beam path. White et al (1969) demonstrated that ultrasound beams are widely and irregularly scattered by passage through the living skull and brain, and that the pattern of scattering varies greatly with small movements of the transducer relative to the skull. A further study by White et al (1978) showed that refraction, absorption and scattering by temporal bone cause degradation of many of the properties of the ultrasound beam. Fry and Barger (1978) studied sound beam distortion after passage through skull bone samples and observed beam refraction, reductions in beam width and changes in the attenuation of the beam with lateral transducer displacement. Grolimund (1986) measured a wide range of energy losses in different skull samples and showed that focusing, refraction and multiple regions of high intensity arose from the presence of bone in the ultrasound beam. Finally, Hames et al. (1991) demonstrated a decrease in sample volume width when temporal bone samples were placed in the beam.

Although these studies have investigated the distortion of ultrasound beams by the skull bone, none have illustrated this for more than one of the samples that were investigated, and none have specifically extended their findings to estimate the resulting distortion of the Doppler signal spectrum. In order to assess the potential effects of beam shape on the signal spectra recorded from the MCA, the sensitivity pattern of the beam needs to be plotted. The sensitivity pattern is a combination of the

shapes of the transmitted field and the reception zones of a transducer, and the sensitivity value at any position in a vessel is therefore proportional to the Doppler signal power that will be backscattered from that point.

While it may not be possible to determine the precise beam shape for individual cases due to variations in the physical characteristics of the media in the beam path, information about the range of beam shapes that are likely to arise for in-vivo recordings of the Doppler signal power from the MCA may allow a prediction of the scale of the errors introduced by this factor, and potentially the derivation of some type of in-vivo correction. The aim of the work described in this chapter was therefore to investigate the range of beam shapes that may occur for TCD investigations of cerebral blood flow in the MCA, by illustrating the effects of transducer type and temporal bone on the sensitivity pattern across the vessel, and discussing the potential effects of these factors on the Doppler signal spectrum.

5.2 Methods and Materials

An assessment of the variability in beam shape between transducers was carried out by recording pressure amplitude arrays from four 2MHz commercial pulsed-wave transcranial Doppler transducers (manufacturers Scimed, EME, DWL and Rimed) for a homogeneous path through water. Crystal diameter was approximately 1cm for the Rimed transducer, and 2cm for the Scimed, EME and DWL transducers. The Scimed transducer was powered using a Scimed PC Dop842 system, and the other transducers were excited using a 15V peak-to-peak signal of frequency 2MHz, pulse length 10 μ s and pulse repetition frequency 15KHz. In each case the ultrasound beam was transmitted into a water tank using a transmission gel to couple the transducer face with an acoustic window in the side of the tank (figure 5.1a). Care was taken to ensure that no air bubbles were present in the gel.

To examine the potential inter-subject variation in beam shape across the MCA, four additional pressure amplitude arrays were recorded for beam paths through temporal bone using the Scimed transducer. Bone samples of size approximately 2x2cm were obtained at post mortem from the temporal window region of the skull of male cadavers aged 25, 78, 83 and 84 years. Following extraction, the bone was stored in formalin. Samples were placed in the beam path between the transducer face and the tank acoustic window (figure 5.1b) with a transmission gel on both surfaces to ensure good coupling.

The possible variations in beam shape arising for an individual were investigated by recording two further pressure amplitude arrays after removal and re-application of the transducer to one of the bone samples (cadaver age 84). The transducer positioning was random for each recording; however, due to the similarity in the cross-sectional area of the bone sample surface and that of the transducer face, any changes in transducer position and angle were small. Once again, extreme care was taken to ensure air-free contact between surfaces in order to prevent variations in coupling affecting the beam shape.

For each beam field, a two-dimensional array of pressure amplitude values centred laterally on the beam axis was recorded at an axial distance of 5.0cm from the transducer face, using a 0.25mm point hydrophone (Precision Acoustics Ltd., Dorchester, UK) to record values at 0.25mm intervals.

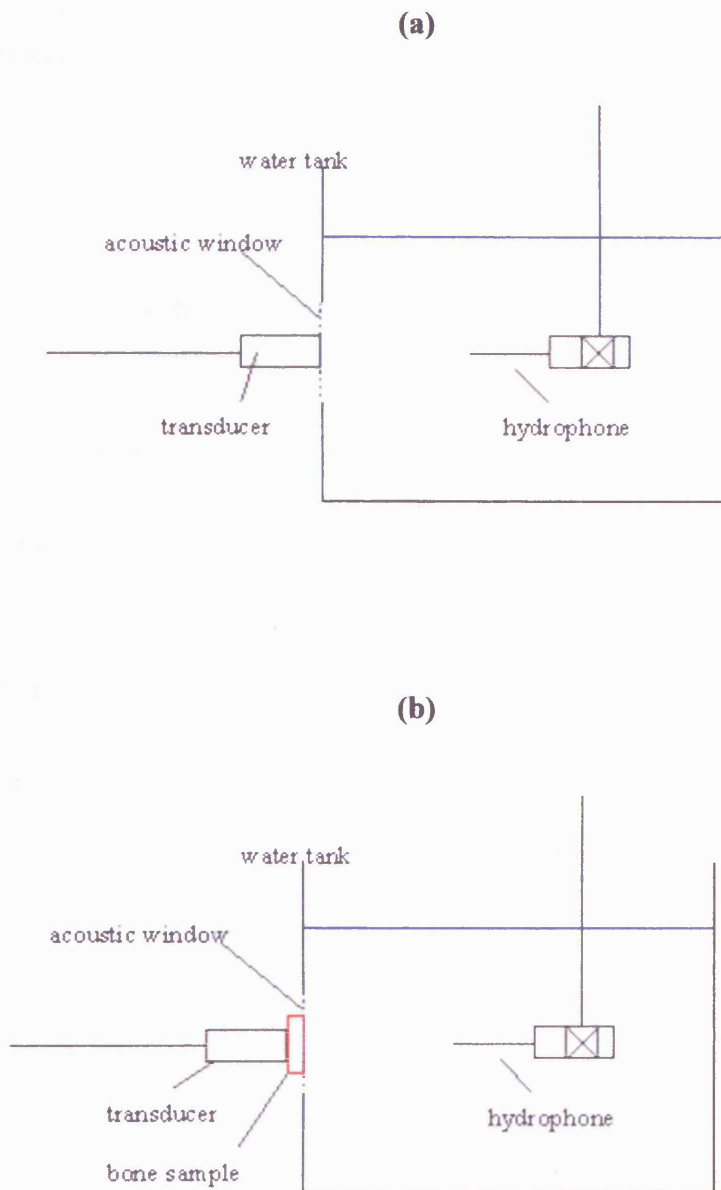


Figure 5.1 Schematic diagrams showing the equipment configuration used for obtaining beam plots through **(a)** a homogeneous water path, and **(b)** a temporal bone sample.

The 5.0cm axial distance was chosen on the basis that most TCD recordings for the MCA are acquired at this approximate depth. Pressure amplitude values were squared to provide an approximation of the intensity pattern of the transmitted beam; these values were in turn squared to provide an estimate of the received field sensitivity pattern of the transducer. Because the sensitivity pattern is representative of both the transmission field and the reception zone of the transducer, its value at any position in a vessel is proportional to the signal power that will be received from that point.

5.3 Results

Results were plotted using the MATLAB software package, with received field sensitivity values expressed as a percentage of the maximum value in each plot. The intensity percentage scale was chosen over the conventional decibel representation as even relatively small changes in sensitivity will have a dramatic effect on some Doppler measurements.

Figures 5.2a-d show the received field sensitivity plots for a Scimed transducer and the EME, DWL and Rimed transducers respectively. In all cases it can be seen that beam sensitivity decreases approximately uniformly away from a central maximum. Figure 5.3 shows the lateral decrease in beam sensitivity for each transducer along a line taken in an arbitrary direction through the maximum value in each beam, and demonstrates that the rate of decrease is approximately equal for the Scimed, EME and Rimed transducers, and slightly more rapid for the DWL transducer. For all the transducers, the beam sensitivity falls to between 50-60% of the maximum within approximately 1mm of the central maximum value, and to between 20-30% within approximately 1.5mm.

Figures 5.4a-d show the beam sensitivity plots recorded with the Scimed transducer for beam paths through the four temporal bone samples taken from cadavers aged 25, 78, 83 and 84 years respectively. The beam shape is seen to be distorted for all bone samples, exhibiting multiple regions of maximum sensitivity and a loss of uniformity in the decrease in sensitivity away from these regions. A large degree of variability can be seen in the distortion arising for different samples. Figures 5.5a-c portray repeated beam plots for removal and reapplication of the transducer to one bone sample, and also demonstrate a large degree of variability in the distortion.

5.4 Discussion

Prediction of the TCD beam shape across the MCA may allow estimation of the potential influence of non-uniform insonation on the relationship between the Doppler signal power and vessel size. The investigation described in this chapter has looked at the effects of transducer type and temporal bone on beam shape, as these are likely to be the main sources of variation in the beam sensitivity across a vessel.

The sensitivity plots for the four commercial transducers show that the beam shapes appear to be similar for all cases (figures 5.2a-d). This is verified by figure 5.3, which demonstrates that the rate of decrease in beam sensitivity away from the central maximum value is approximately equal for all the transducers. The slight difference in the rate of decrease seen for the DWL transducer is probably due only to the arbitrary direction of the line through the beam plot maximum for which the values were

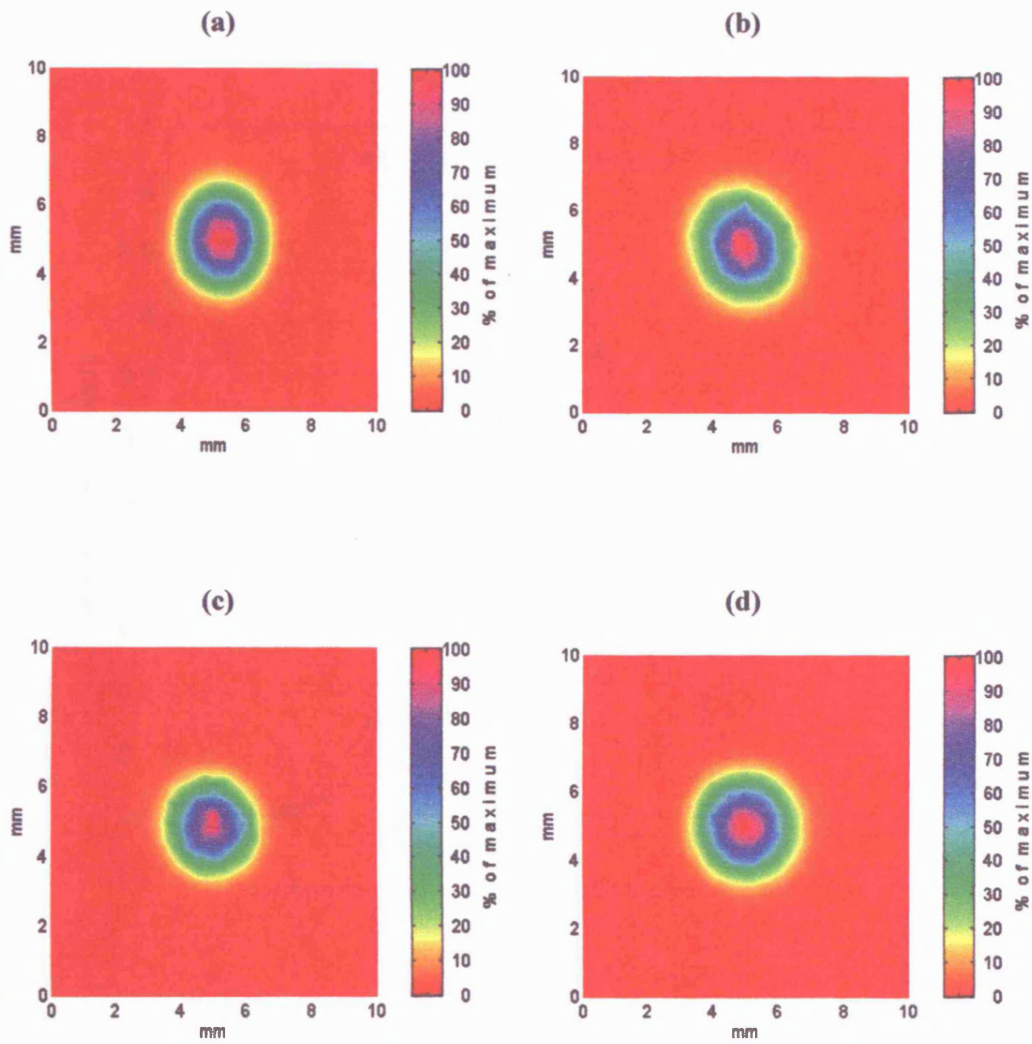


Figure 5.2(a-d) Received field beam sensitivity for four commercial TCD transducers (a) Scimed, (b) EME, (c) DWL, (d) Rimed, plotted at an axial distance of 5.0cm from the transducer face for a beam path through water

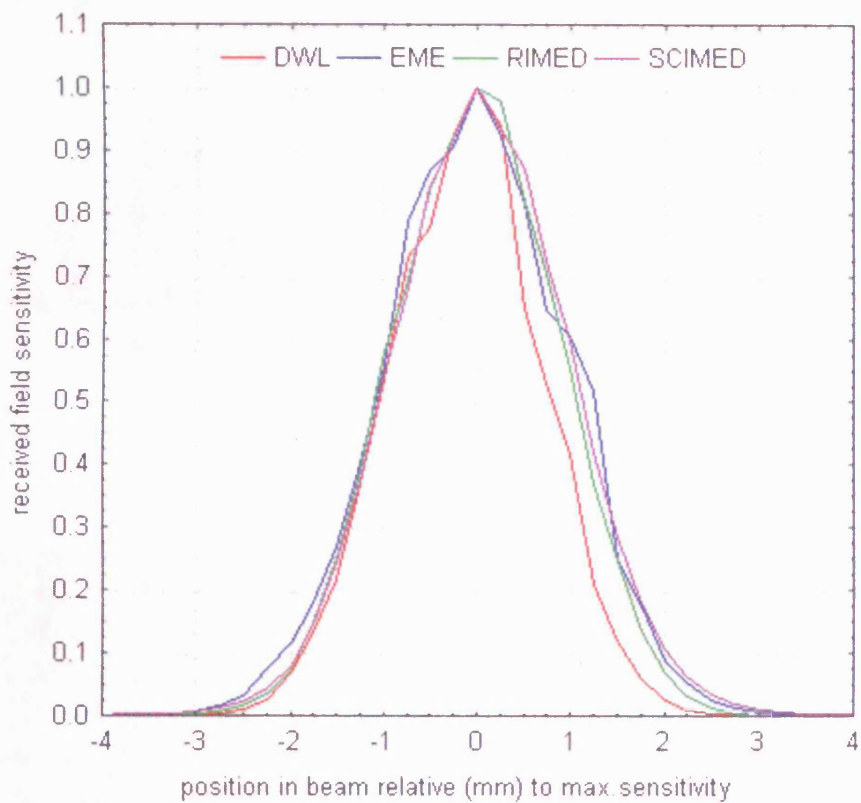


Figure 5.3 Lateral decrease in beam sensitivity for four commercial transducers, taken from the received field sensitivity plots shown in figure 5.2a-d. Position in each beam is plotted relative to the position at which maximum sensitivity occurs

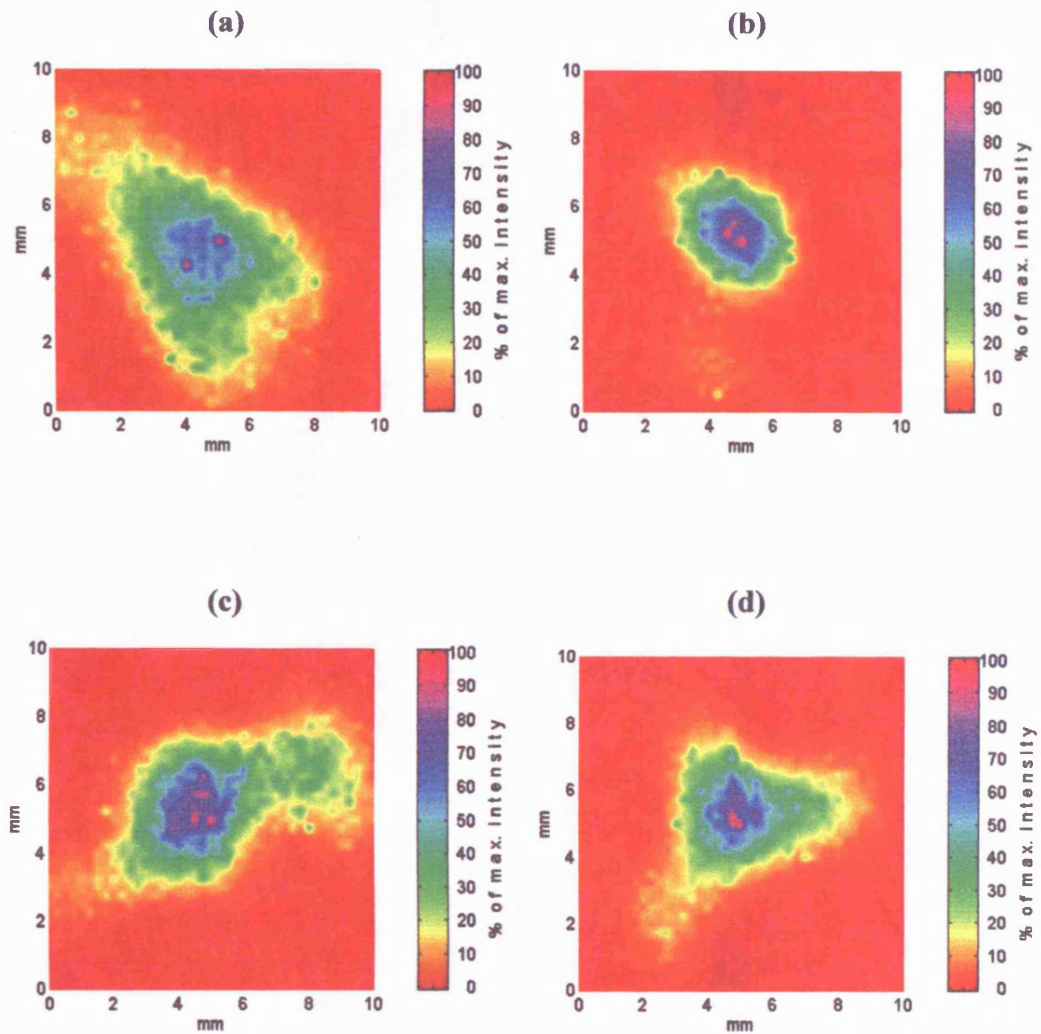


Figure 5.4(a-d) Received field beam sensitivity of a Scimed transducer, plotted at an axial distance of 5.0cm from the face of the transducer for beam paths through four temporal bone samples.

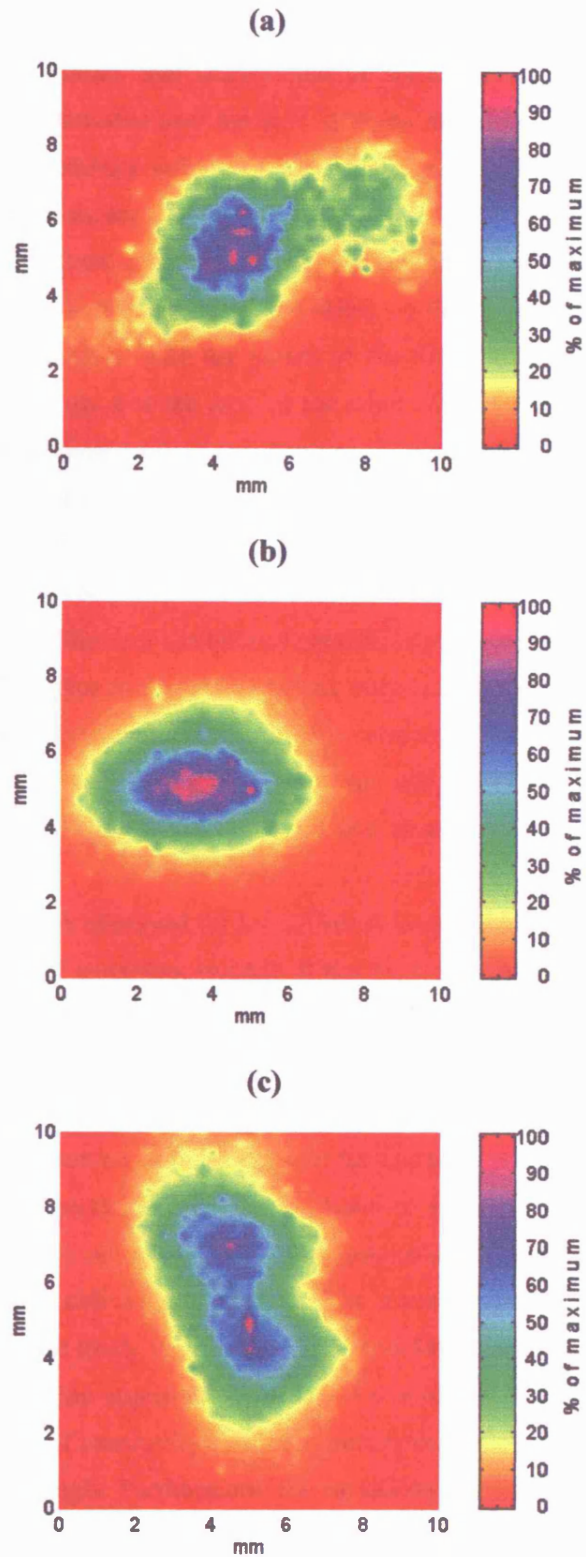


Figure 5.5(a-c) Received field beam sensitivity of a Scimed transducer, plotted at an axial distance of 5.0cm from the face of the transducer for three different applications of the transducer to one temporal bone sample.

extracted. The fact that there appears to be relatively little variation in beam shape between the four commercial transducers is encouraging as it indicates that the initial shape is likely to be independent of the transducer used. It is possible that there might be some variability in beam shape between transducers made by the same manufacturer but it is unlikely that this will be significant enough to cause the rate of decrease in sensitivity away from the beam centre to deviate greatly from that of the four transducers investigated in this study.

The recorded beam plots show that the rate of decrease in sensitivity away from the central maximum value is rapid enough to have a significant effect on the shape of the Doppler signal power spectra received from in-vivo vessels, with the extent of the distortion depending on the size of the vessel and its position in the beam. For the case of the adult MCA, sizes have been shown to range between 2.3mm and 3.5mm in diameter (van der Zwan et al. 1993). If it is assumed that the region of maximum sensitivity is incident on the central axis of a vessel and that the red blood cells are uniformly distributed, then the effect of the beam shapes recorded in this study on the power spectrum of a signal received from a vessel of diameter 3mm would be a gradual increase in spectral power with Doppler shift frequency, with the low frequency spectral components originating from the low velocity red blood cells at the edges of the vessel having only approximately 20% of the magnitude of those components originating from the highest velocity cells in the centre of the vessel. This could produce a significant error in the calculation of the intensity weighted mean frequency of a signal, the estimation of changes in vessel size, or the detection and classification of emboli travelling at the vessel edges.

The distortion to beam shape observed for the different temporal bone samples (figures 5.4a-d) is assumed to be equivalent to that occurring in-vivo; it has been shown that the acoustic properties of cadaver skull bone do not differ greatly from those of living skull (White et al. 1969) and that the properties do not change significantly due to preservation in formalin (White et al. 1978). Although seven bone samples were initially obtained for this investigation, three of these had to be rejected due to the fact that they had been removed from the edge of the temporal window region and therefore did not provide an adequate cross-sectional area for the beam to pass through. The limited number of samples means that the study does not provide an ideal representation of the true variation in distortion that might be expected between individuals. However, the results do provide a preliminary picture of the range of beam shapes that are likely to arise for TCD recordings from the MCA.

Because beam shape distortion appears to be greatly variable between samples, it may be difficult to accurately predict the nature of sensitivity variations across the MCA due to differences in temporal bone properties between individuals. Furthermore, the variability in beam shape distortion seen for the three different applications of the transducer to one of the bone samples (figures 5.5a-c) verifies that the in-vivo beam shape across the MCA will be significantly affected by the path that the beam takes through the temporal bone. This emphasizes the care that must be taken to maintain a stationary transducer position when using the Doppler power method in-vivo, and the inadvisability of comparing power values derived from non-continuous recordings where the transducer has been removed and then reapplied.

Owing to the non-uniformity of the beam shape after passage of the beam through temporal bone,

it is unsuitable to illustrate the lateral changes in beam sensitivity by taking values from a single line across the beam plot, as was the case for figure 5.3. Instead, sensitivity variations for the bone-distorted beams are portrayed two-dimensionally (figure 5.6a-d) by superimposing a vessel of diameter 3mm onto the beam plots shown in figure 5.4. In each case the vessel is positioned to give the maximum total signal power value (equal to the sum of the sensitivity values encompassed by the vessel). These plots more clearly illustrate the potential inter-subject differences in beam shape distortion, and also demonstrate that the effects of beam shape on signal power are likely to be more pronounced after passage of the beam through temporal bone; in all cases sensitivity falls to less than 20% of the maximum at the vessel edges, compared to the 20-30% seen for a 3mm vessel in the transducer beams (figures 5.2a-d).

Even if it was possible to predict the beam shape across individual vessels, the nature of the distortion caused by temporal bone may cause difficulties in correcting the signal power for the effects of beam shape. Specific corrections would require information about the vessel position in the beam; currently this can only be predicted by maximising the received signal power during recordings in order to allow the assumption that the maximum beam intensity is incident somewhere in the central region of the vessel. Maximisation of the signal means that it is unlikely that the maximum beam intensity will coincide with the edge regions of the vessel, as for this case the spectral components with the greatest magnitude will have low Doppler shift frequencies owing to the slower blood velocities at the vessel edges and are likely to be attenuated by the inherent high pass filters, thereby noticeably reducing the received signal power. The fact that the distorted beams appear to commonly exhibit more than one region of maximum intensity adds further complications to the derivation of correction factors.

5.5 Conclusions

The study of TCD beam shapes carried out in this chapter has shown that there appears to be relatively little variation in the sensitivity patterns for the commercial transducers that were investigated and hence implies that the beam shape across the MCA will not be influenced by this factor. However, a high degree of variability was seen in the distortion caused by different samples of temporal bone and also in the distortion arising from different beam paths through the bone. This suggests that the influence of beam shape on the relationship between the Doppler signal power and the MCA size may vary both between individuals and for individual recordings if transducer displacements occur. The potential scale of the errors introduced by beam shape to Doppler power measurements is investigated in chapter 6.

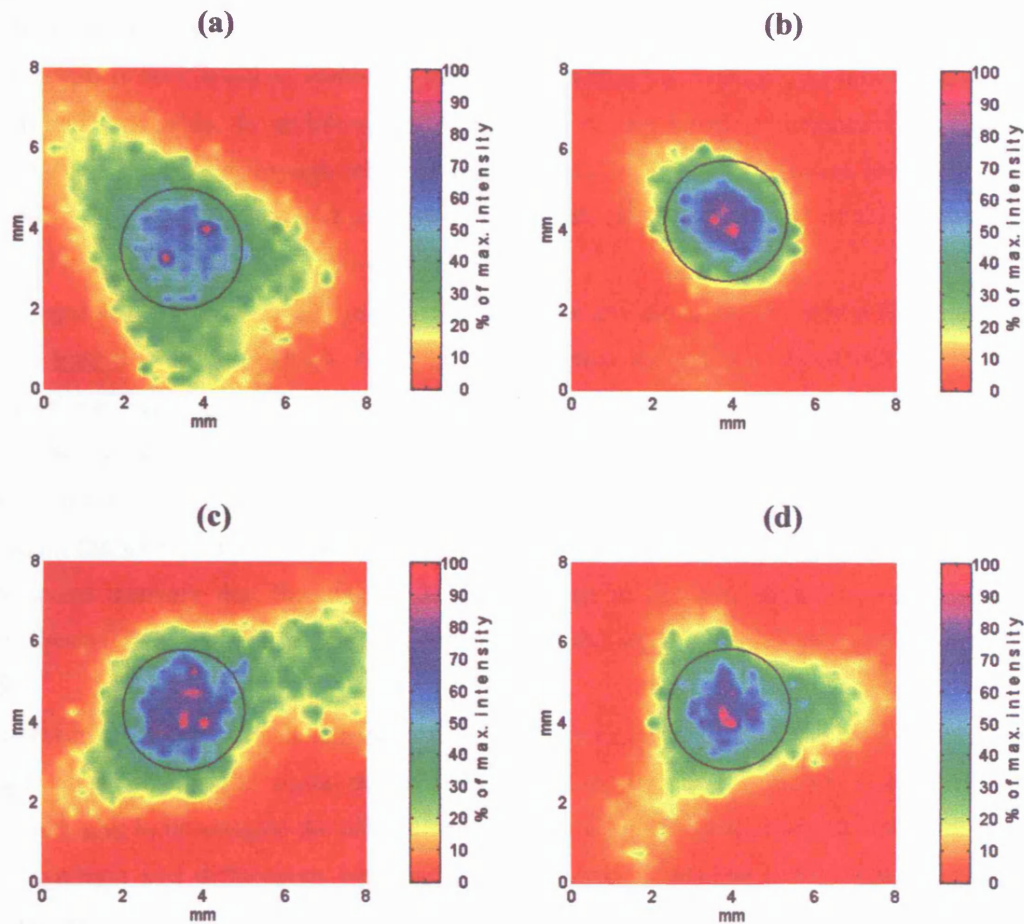


Figure 5.6(a-d) Two dimensional plots of the beam sensitivity across a 3mm diameter vessel, for each of the bone-distorted beams shown in figure 5.4a-d. The vessel has been positioned at the point in the beam giving the maximum total power value. Sensitivity values are plotted as a percentage of the maximum value.

CHAPTER 6

The Effects of Beam Shape on the Ability to Predict Changes in Vessel Size Using the Doppler Power Method

6.1 Introduction

Proportionality between signal power and vessel size can only be assumed if the intensity of the incident beam is uniform across a vessel for all changes in its size. This is unlikely to be the case unless the vessel is very small as variations in intensity within the beam are an inherent characteristic of most ultrasound fields. In addition, the final shape of the beam is dependent on the physical characteristics of the media through which it passes. This is especially relevant for TCD recordings from the MCA due to the temporal bone in the beam path causing distortion of the beam shape (Fry and Barger 1978, White et al. 1978, Grolimund 1986).

The magnitude of the Doppler signal originating from any particular point in a vessel is a function of the beam intensity at that position. Any variations in intensity across a vessel will result in unequal weighting of the signal spectral components at different frequencies, producing a distortion of the spectrum. The nature of the distortion and its effect on the total signal power will depend on the shape of the beam in the region that is incident on the vessel. Beam shape will vary for different vessel sizes depending on the extent and position of the region of the beam covering the vessel in each case. It therefore seems unlikely that the magnitude of a change in the total signal power arising from a change in vessel size will be exactly proportional to the magnitude of the area change that has occurred.

The objective of the work described in this chapter was to create a model that would predict the percentage change in Doppler signal power arising from dilation or contraction of a vessel in a non-uniform beam, and to investigate the effects on the power change of initial vessel size, area changes of varying magnitude and differences between increasing and decreasing vessel size. The percentage power changes for a zero degree insonation angle were modelled for beam paths through a homogeneous medium and through each of five temporal bone samples. The aim of investigating different bone samples was to provide an estimate of in-vivo variability in the errors introduced by beam shape to the Doppler power method, as previous research has shown that the beam distortion caused by temporal bone is highly sample-dependent (see chapter 5). Because the insonation angle for in-vivo recordings from the MCA may reach 30 degrees in extreme cases (Martin et al. 1993, Martin et al. 1995), the effects of variations in beam angle were investigated by simulating angles of 15 and 30 degrees and modeling the percentage power changes for these cases.

6.2 Method

The shape of a Doppler ultrasound beam is determined by the combination of the shapes of the transmission field and the reception zone; these are identical for single crystal PW transducers. It is generally assumed that the transmitted intensity at any point is equal to the square of the pressure amplitude of the beam at that point. Hence, following the reciprocity principle, beam shape can be

calculated from the fourth power of the pressure amplitude. The power of the signal received from a vessel was therefore modelled using the assumption that the backscattered power from any small element of a blood vessel is equal to the fourth power of the pressure amplitude at that point. By recording an array of pressure amplitude values from the transducer beam using a point hydrophone and using this to calculate a corresponding array of backscattered power values, the total power received from a vessel can be calculated from the sum of the array values that coincide with the vessel position.

6.2.1 Beam Intensity Recordings

Pressure amplitude fields were recorded from the beam of a 2MHz pulsed wave TCD transducer (Scimed PCDop842, Bristol, UK) for a homogeneous beam path through water and for paths through water and each of four temporal bone samples (details of the four samples are given in the previous chapter). In each case a 0.25mm point hydrophone (Precision Acoustics Ltd., Dorchester, UK) was used to acquire a three-dimensional array of pressure amplitude values centred axially on the sample depth (5.0cm) and laterally on the axis of the beam, to coincide with the theoretical position of maximum intensity in the beam. Values were acquired at intervals of 0.25mm over a distance of 20mm laterally and 8.5mm axially. The pressure amplitude array for the fifth temporal bone beam path was recorded prior to the start of this project by another researcher (Dr. Julia Smith) using a similar method.

Once recorded, the pressure amplitude array for each beam path was used to calculate two corresponding arrays of transmitted intensity and backscattered power values. Figures 6.1a-f show the backscattered power values at an axial distance of 5.0cm from the transducer face for the homogeneous water path, the pre-recorded temporal bone path and the four additional temporal bone paths respectively.

6.2.2 Calculation of the Theoretical Signal Power Received From a Vessel

Calculation of the power backscattered from a theoretical vessel was carried out for each beam path by separating the relevant array into a series of planes lying parallel to the face of the transducer. For the zero degree insonation angle, the power calculation was simplified by adding the values from corresponding positions in the parallel planes; this produced a two-dimensional array composed of values equal to the total power of the signal received from the sample volume at each point across the beam. The two-dimensional arrays for simulated insonation angles of 15 and 30 degrees were derived by shifting the parallel planes with respect to each other before summing values at corresponding positions; the size of the shift for each plane was determined by the required angle and the position of the plane relative to the centre of the sample volume.

Because the original pressure amplitude values were recorded at fairly coarse intervals owing to the finite size of the hydrophone and to time and array size constraints, a two-dimensional linear interpolation was implemented in order to generate an array with values spaced at 0.05mm intervals. This allowed calculation of the total power received from a circular vessel using the relatively simple

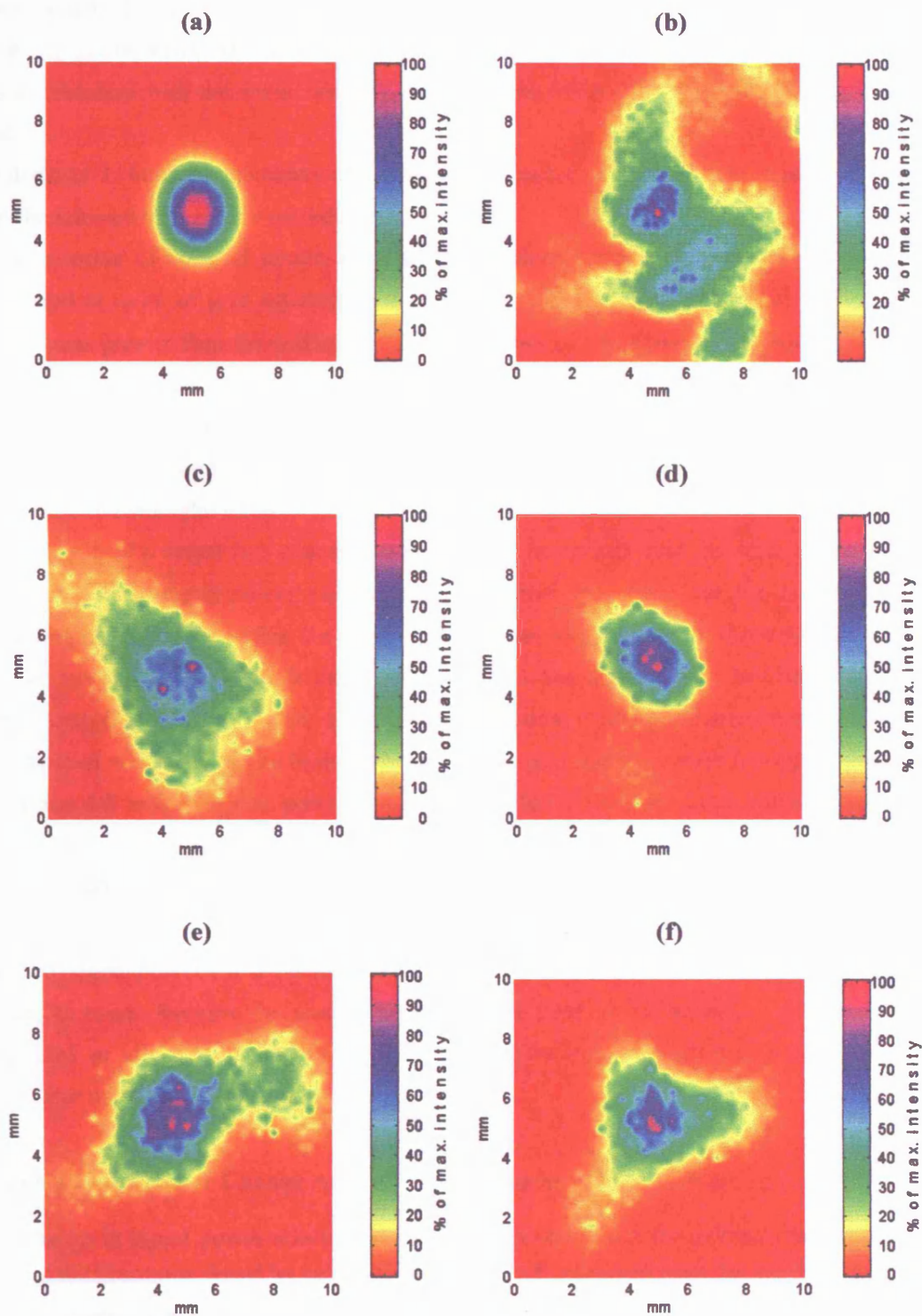


Figure 6.1 Plots of received field sensitivity recorded at an axial distance of 5.0cm from the face of a 2MHz Scimed transducer for (a) a homogeneous water path, (b) a temporal bone path recorded prior to the start of this project by another researcher, (c-f) a further four temporal bone paths.

method described below:

It was assumed that the values in the interpolated arrays formed a grid, with each grid square corresponding to one value. By labelling the position of each grid square by its corner co-ordinates, the values coincident with the vessel were located using the following method for each grid square in the plane:

- The distance 'L' between the centre of the vessel and each corner of the grid square was calculated from the relevant grid square co-ordinates.
- For each corner of the grid square, the distance to the centre was compared to the vessel radius (calculated in units of grid squares); a corner was assumed to fall outside of the vessel if this distance was greater than the radius, and inside the vessel if the distance was equal to or less than the radius.
- If between one and four corners of the grid square fell inside the vessel, then the backscattered power value corresponding to the grid square position was assumed to contribute to the total power received from the vessel.

The cross-section of a vessel was assumed to be circular, hence reducing the contribution to the total power of any backscattered power values originating from the edges due the corresponding grid squares falling only partially within the vessel. Edge values were defined as those whose grid squares had between one and three corners falling inside the vessel. Because the array had been interpolated to give values spaced at very small intervals, a crude approximation of the contribution of an edge value to the total power was made on the basis of the number of grid square corners falling inside the vessel; if three corners fell inside then the power value was included in the sum, if two corners fell inside then half of the power value was added and if only one corner fell inside then the value was rejected. The method was tested for vessels in a theoretical uniform intensity beam and found to produce an estimate of power which was within $\pm 1\%$ of the relevant vessel area in all cases.

The total signal power value calculated using this method depends on the size of the vessel and its location in the beam. Because the precise location in the beam is unknown in-vivo, the total power was calculated at all lateral positions of the vessel in the array to demonstrate variations in the received power with vessel position in the beam.

6.2.3 Calculation of Power Change Arising From a Change in Vessel Size

The change in signal power arising from a change in vessel size for different lateral positions of the vessel in the beam was found by calculating the power P_0 received from the original vessel and the power P_1 received from the vessel after a contraction or dilation in area of $\pm \Delta a\%$. The change in power $\Delta P\%$ was derived as the difference between these two power values expressed as a percentage of the power received from the original vessel:

$$\Delta P\% = \frac{100(P_1 - P_0)}{P_0} \quad [6.1]$$

For the theoretical situation where the beam is of uniform intensity, a percentage change $\pm\Delta a\%$ in the size of a vessel should produce an equal percentage change $\pm\Delta P\%$ in the power of the received signal.

All calculations were carried out for each of the recorded beam intensity fields (homogeneous path and five temporal bone sample paths). The total power was calculated for three base-line vessel sizes (2.0mm, 3.0mm and 4.0mm diameter), for lateral positions spaced at 0.05mm intervals across the beam, and for changes in the vessel area of $\pm 10\%$ and $\pm 20\%$ at each position. The percentage change in power generated by the change in vessel area was found for each case. The vessel sizes were selected to encompass the potential range of MCA sizes as determined by van der Zwan et al. (1993), who measured MCA diameters of between 2.31mm and 3.46mm from adult human cadavers. The percentage values for the vessel area changes were chosen to simulate feasible in-vivo area changes.

6.3 Results

The variation in received field sensitivity across the beam at an axial distance of 5.0cm from the transducer face is shown for the homogeneous beam path and the five temporal bone beam paths in figures 6.1a-f respectively. For the homogeneous beam path, the beam sensitivity can be seen to decrease approximately uniformly from a central region of maximum intensity. In comparison, the variation seen for the beam path through temporal bone is highly distorted, with a much more rapid decrease away from more than one point of high beam sensitivity. This is characteristic of the beam shapes for all of the temporal bone samples that were investigated.

For most clinical recordings the transducer is generally positioned to maximise the intensity of the received signal. The following results are therefore shown only for those lateral positions of a vessel where the received power P is greater than 25% of the maximum possible power received from the vessel for ideal placement of the transducer; this cut-off limit has been estimated to represent the most extreme case of poor transducer positioning. The plots are centred on the vessel position $(x,y)_{max}$ at which the maximum power is received.

The total signal power received for zero degree insonation of vessels at different lateral positions in the beam is shown for the homogeneous beam path in figures 6.2a-c for vessels of diameter 2.0mm, 3.0mm and 4.0mm respectively. Figures 6.3a-c display the corresponding data for one of the temporal bone beam paths (that shown in figure 6.1c). As would be expected from the relevant beam intensity plots shown in figure 6.1, the results for the homogeneous beam path show that P decreases approximately uniformly away from $(x,y)_{max}$, whereas the results for the temporal bone beam path illustrate a distortion in the pattern of decrease around $(x,y)_{max}$.

Figures 6.4a-c depict the percentage change in power $\Delta P\%$ arising from a 10% increase in area of vessels of 2.0mm, 3.0mm and 4.0mm diameter respectively, for zero degree insonation at different lateral vessel positions in the beam for the homogeneous beam path. Similarly, figures 6.5a-c show the percentage changes for a 20% increase in vessel area, figures 6.6a-c for a 10% decrease and figures 6.7a-c for a 20% decrease. Figures 6.8-6.11 show the corresponding results for a beam path through temporal bone.

The results for the homogeneous beam path show that $\Delta P\%$ close to $(x,y)_{max}$ is smaller than the

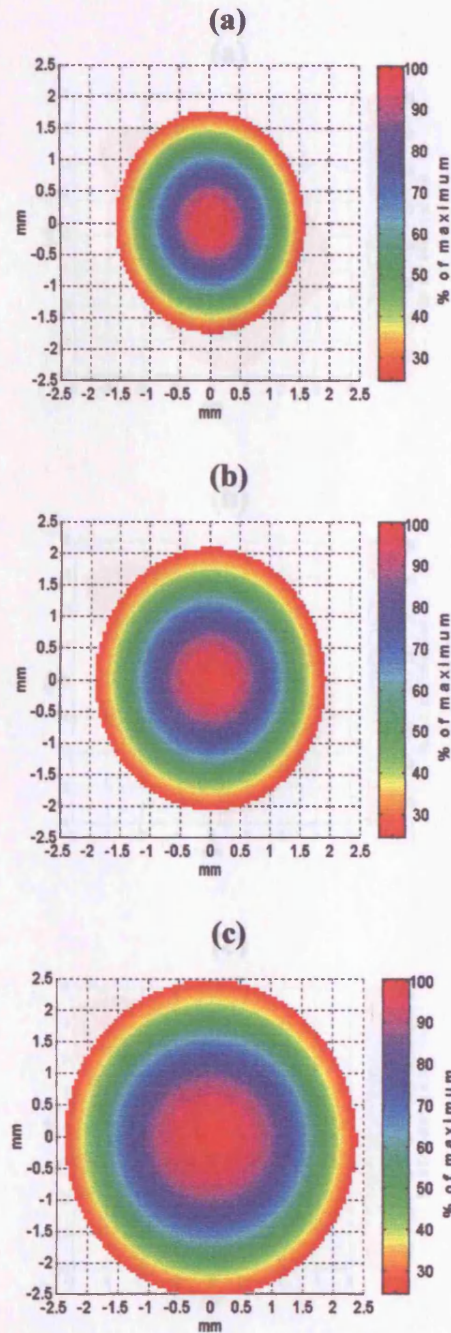


Figure 6.2 Surface plots for a homogeneous beam path showing the modelled values of the total signal power received at different vessel positions in the beam for (a) 2.0mm, (b) 3.0mm and (c) 4.0mm diameter vessels. Lateral positions of the vessels in the beam are plotted relative to the position at which the maximum total power is received for each vessel size. Values are plotted only for those vessel positions at which the total power is greater than 25% of the maximum value, and are expressed as a percentage of this maximum.

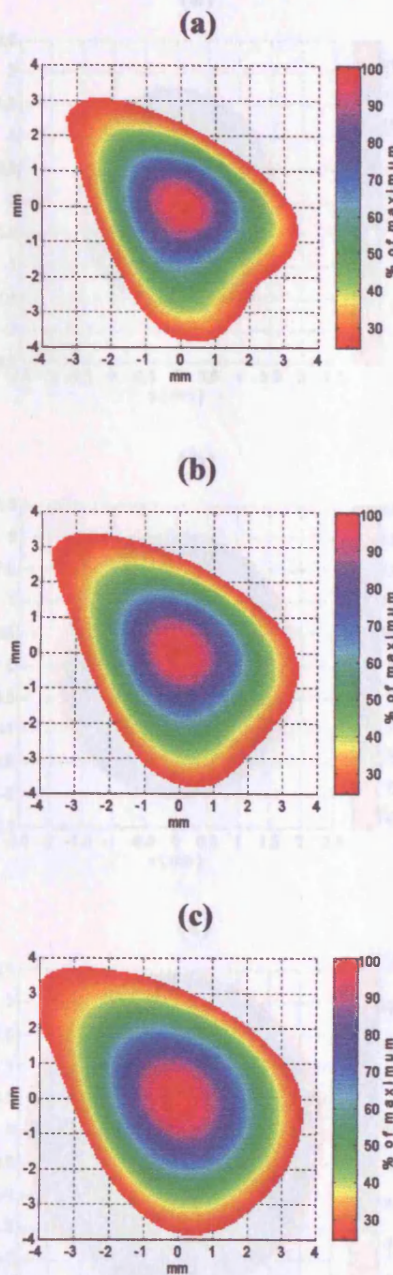


Figure 6.3 Surface plots for a beam path through temporal bone showing the modelled values of the total signal power received at different vessel positions in the beam for (a) 2mm, (b) 3mm and (c) 4mm diameter vessels. Lateral positions of the vessels in the beam are plotted relative to the position at which the maximum total power is received for each vessel size. Values are plotted only for those vessel positions at which the total power is greater than 25% of the maximum value, and are expressed as a percentage of this maximum.

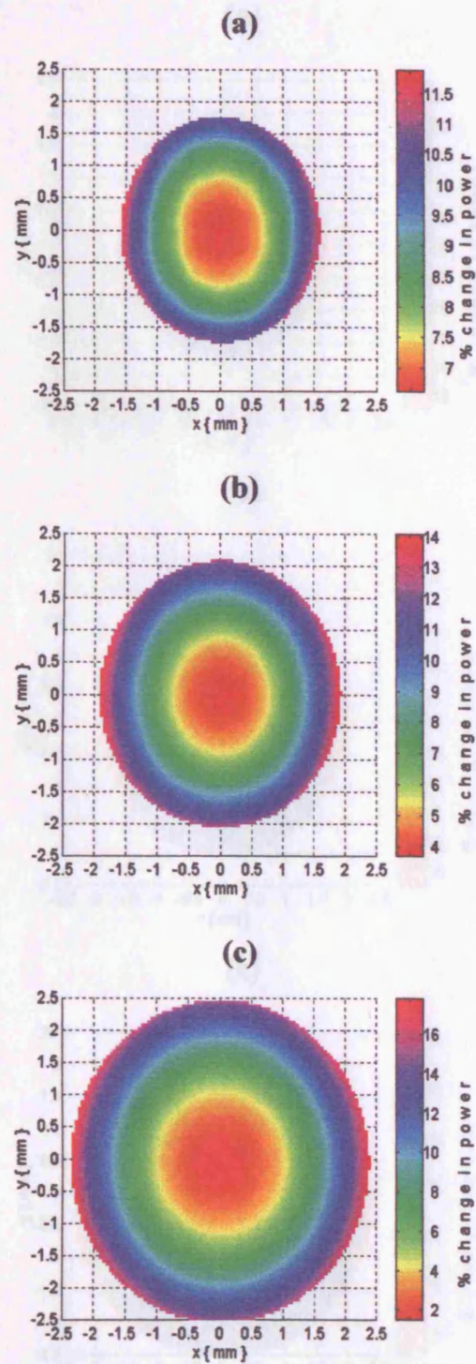


Figure 6.4 Surface plots for a homogeneous beam path showing the percentage change in the modelled values of the total signal power received from vessels of diameter (a) 2mm, (b) 3mm and (c) 4mm power undergoing a 10% dilation in size at different positions in the beam. Vessel positions (x,y) are plotted relative to the position for which the total power is at a maximum when the vessels are in their base-line state. Values are plotted only for vessel positions in the beam at which the total power exceeds 25% of this maximum value.

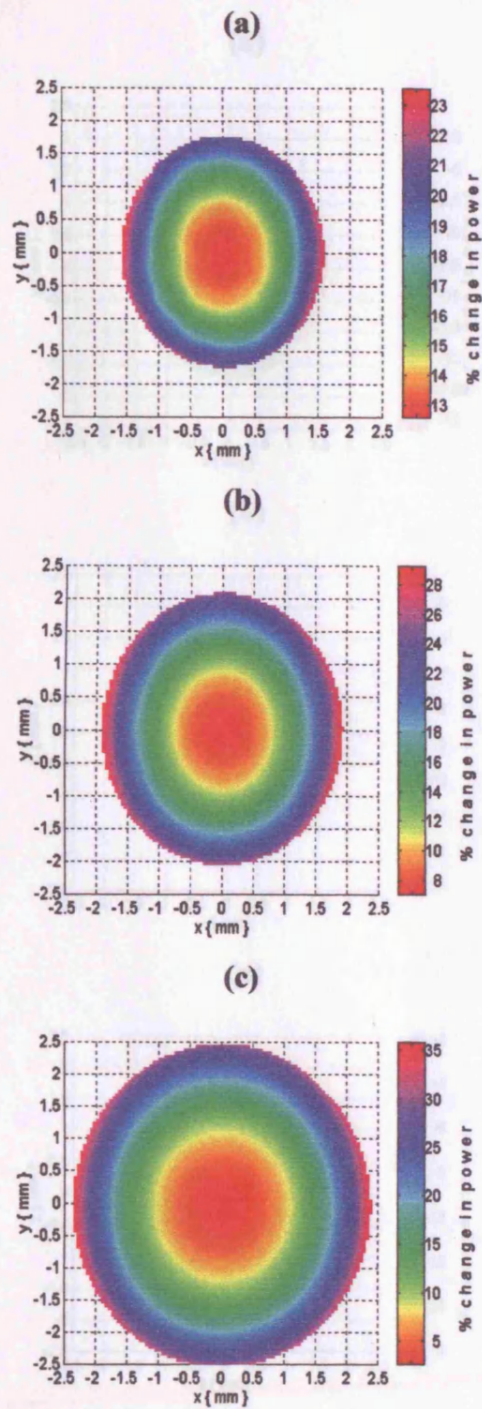


Figure 6.5 Surface plots for a homogeneous beam path showing the percentage change in the modelled values of the total signal power received from vessels of diameter (a) 2mm, (b) 3mm and (c) 4mm power undergoing a 20% dilation in size at different positions in the beam. Vessel positions (x,y) are plotted relative to the position for which the total power is at a maximum when the vessels are in their base-line state. Values are plotted only for vessel positions in the beam at which the total power exceeds 25% of this maximum value.

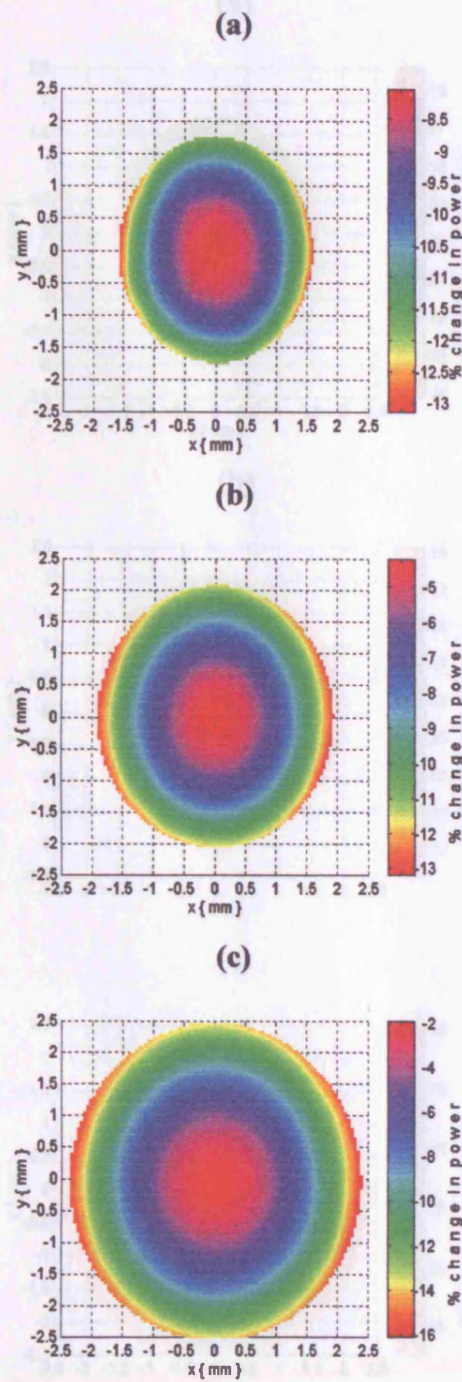


Figure 6.6 Surface plots for a homogeneous beam path showing the percentage change in the modelled values of the total signal power received from vessels of diameter (a) 2mm, (b) 3mm and (c) 4mm power undergoing a 10% contraction in size at different positions in the beam. Vessel positions (x,y) are plotted relative to the position for which the total power is at a maximum when the vessels are in their base-line state. Values are plotted only for vessel positions in the beam at which the total power exceeds 25% of this maximum value.

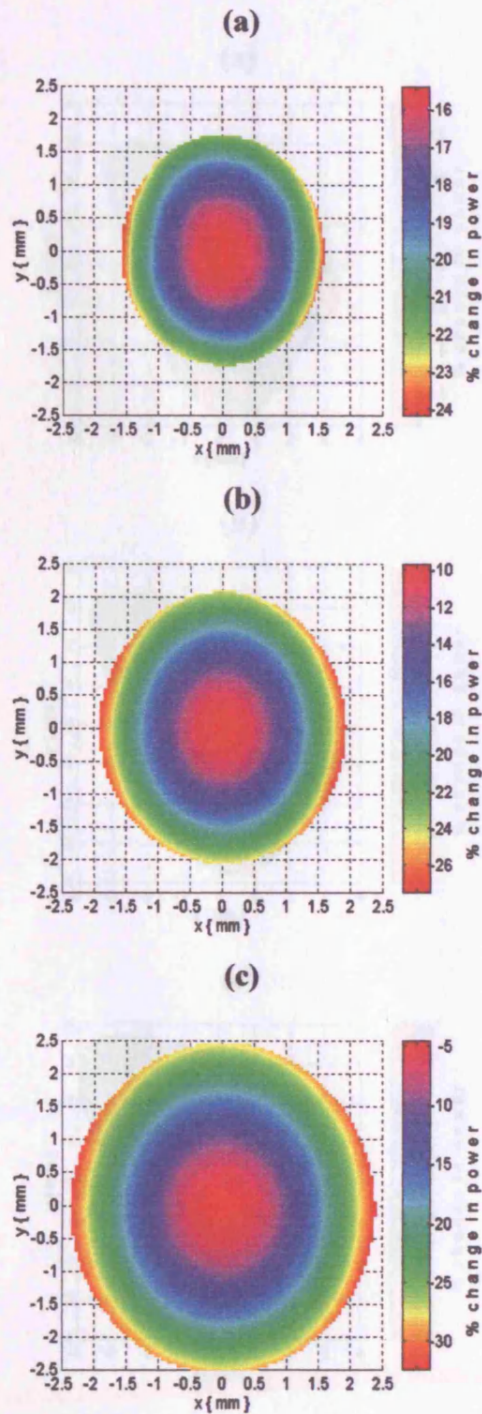


Figure 6.7 Modelled surface plots for a beam path through normal bone, showing the percentage

Figure 6.7 Surface plots for a homogeneous beam path showing the percentage change in the modelled values of the total signal power received from vessels of diameter (a) 2mm, (b) 3mm and (c) 4mm power undergoing a 20% contraction in size at different positions in the beam. Vessel positions (x,y) are plotted relative to the position for which the total power is at a maximum when the vessels are in their base-line state. Values are plotted only for vessel positions in the beam at which the total power exceeds 25% of this maximum value.

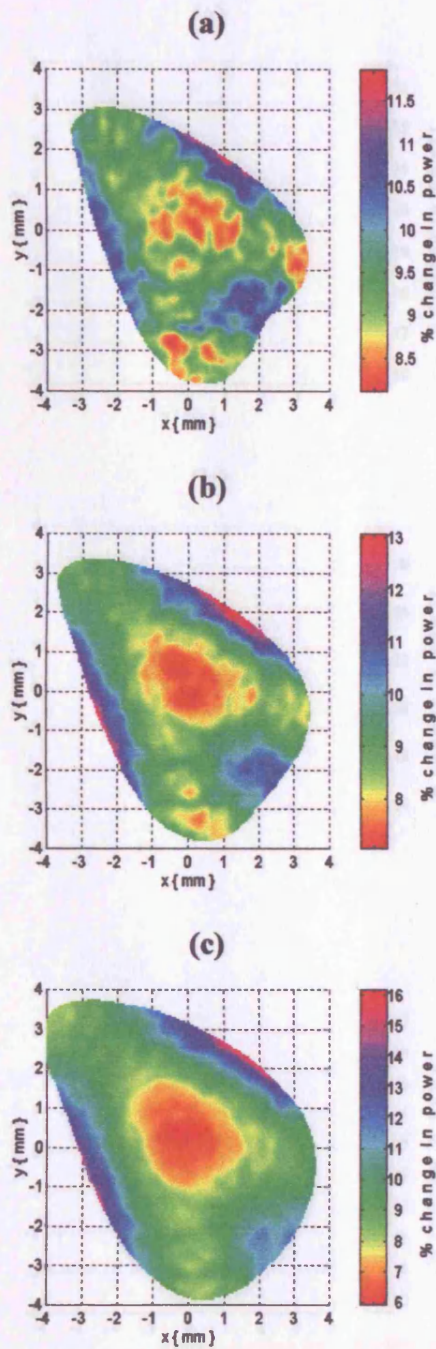


Figure 6.8 Modelled surface plots for a beam path through temporal bone, showing the percentage change in the total signal power received for 0° insonation of vessels of diameter (a) 2mm, (b) 3mm and (c) 4mm power undergoing a 10% dilation in size at different positions in the beam. Vessel positions (x,y) are plotted relative to the position for which the total power is at a maximum when the vessels are in their base-line state. Values are plotted only for vessel positions in the beam at which the total power exceeds 25% of this maximum value.

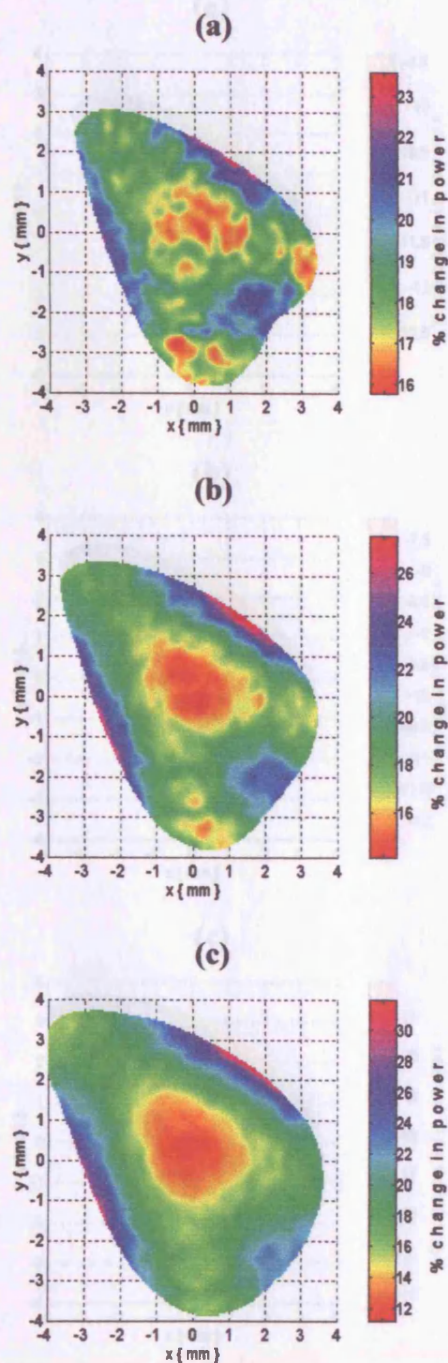


Figure 6.9 Modelled surface plots for a beam path through temporal bone, showing the percentage change in the total signal power received for 0° insonation of vessels of diameter (a) 2mm, (b) 3mm and (c) 4mm power undergoing a 20% dilation in size at different positions in the beam. Vessel positions (x,y) are plotted relative to the position for which the total power is at a maximum when the vessels are in their base-line state. Values are plotted only for vessel positions in the beam at which the total power exceeds 25% of this maximum value.

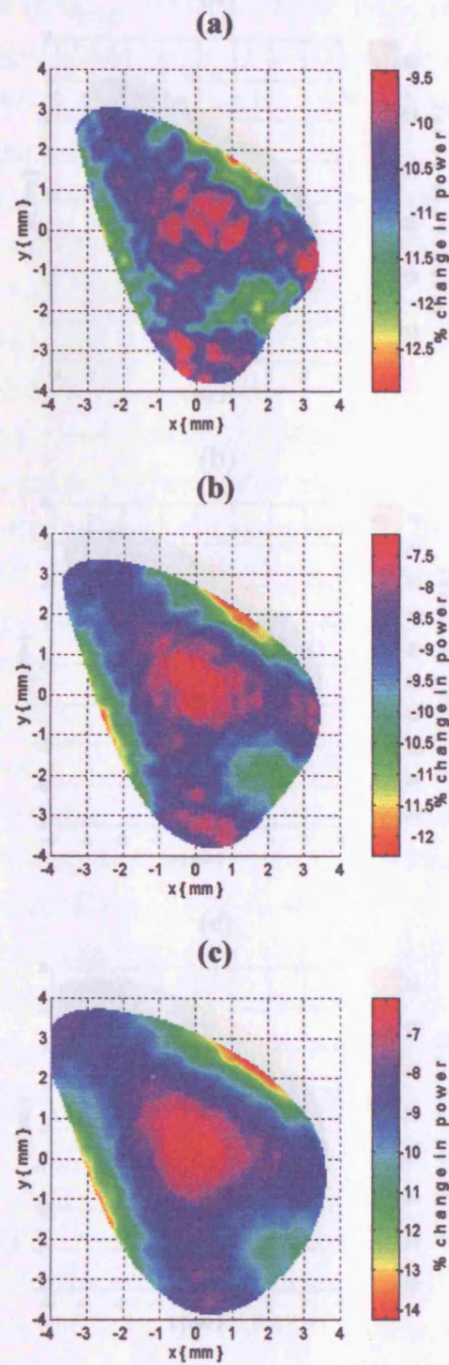


Figure 6.10 Modelled surface plots for a beam path through temporal bone, showing the percentage change in the total signal power received for 0° insonation of vessels of diameter (a) 2mm, (b) 3mm and (c) 4mm power undergoing a 10% contraction in size at different positions in the beam. Vessel positions (x,y) are plotted relative to the position for which the total power is at a maximum when the vessels are in their base-line state. Values are plotted only for vessel positions in the beam at which the total power exceeds 25% of this maximum value.

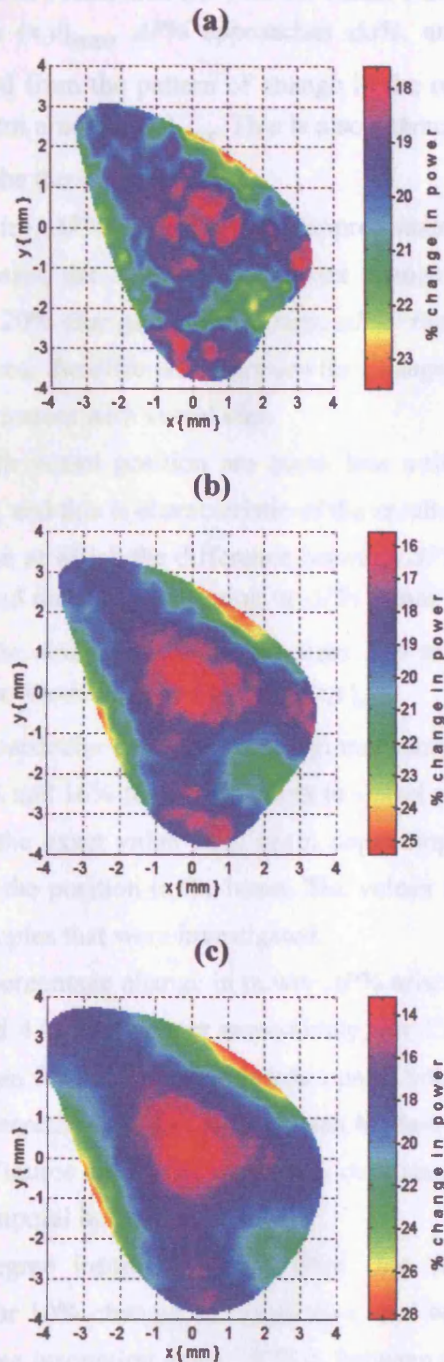


Figure 6.11 Modelled surface plots for a beam path through temporal bone, showing the percentage change in the total signal power received for 0° insonation of vessels of diameter (a) 2mm, (b) 3mm and (c) 4mm power undergoing a 20% contraction in size at different positions in the beam. Vessel positions (x,y) are plotted relative to the position for which the total power is at a maximum when the vessels are in their base-line state. Values are plotted only for vessel positions in the beam at which the total power exceeds 25% of this maximum value.

corresponding percentage change in vessel area $\Delta\alpha\%$ for all vessel sizes. As the vessel position in the beam moves further away from $(x,y)_{max}$, $\Delta P\%$ approaches $\Delta\alpha\%$, and eventually equals and then exceeds it. As would be expected from the pattern of change in the received signal power P (figure 6.2), the change in $\Delta P\%$ is uniform around $(x,y)_{max}$. This is also characteristic of the results seen for a 20% dilation and contraction of the three vessel sizes.

For 10% changes in vessel size, $\Delta P\%$ ranges between approximately 2% and 17%, with the value depending on the size of the vessel, the direction of the size change that it has undergone and the vessel position in the beam. For 20% changes in vessel size, $\Delta P\%$ ranges between 3% and 35%. For both 10% and 20% changes in area, the difference between the change in received signal power $\Delta P\%$ and the expected change $\Delta\alpha\%$ increases with vessel size.

The variations in $\Delta P\%$ with vessel position are much less uniform for a beam path through temporal bone (figures 6.8-6.11), and this is characteristic of the results seen for all of the investigated bone samples. The vessel position at which the difference between $\Delta P\%$ and $\Delta\alpha\%$ is greatest does not always coincide with $(x,y)_{max}$ and the spatial variation in $\Delta P\%$ is not uniform. However, similarly to the homogeneous beam path, the results for all vessel sizes and area changes show that $\Delta P\%$ is consistently smaller than $\Delta\alpha\%$ for vessel positions close to $(x,y)_{max}$.

The results plotted for this particular beam path through temporal bone show that values of $\Delta P\%$ range between approximately 5% and 16% for 10% changes in vessel area, and between 12% and 31% for 20% changes in area, with the exact value once again depending on the initial vessel size, the direction of the size change and the position in the beam. The values are representative of the ranges obtained from the other bone samples that were investigated.

Figures 6.12a-c depict the percentage change in power $\Delta P\%$ arising from a 10% increase in area of vessels of 2.0mm, 3.0mm and 4.0mm diameter respectively, for 15 degree insonation at different lateral vessel positions in the beam for a temporal bone beam path. Similarly, figures 6.13a-c show the percentage changes for a 10% decrease in vessel area, figures 6.14a-c for a 20% increase and figures 6.15a-c for a 20% decrease. Figures 6.16-6.19 show the corresponding results for a 30 degree insonation angle for the same temporal bone beam path.

The results for the 15 degree insonation angle show that values of $\Delta P\%$ range between approximately 6.5% and 15% for 10% changes in vessel area, and between 13% and 30% for 20% changes in area. For the 30 degree insonation angle, $\Delta P\%$ is between approximately 7% and 14% for 10% changes in vessel area, and between 14% and 29% for 20% changes in area. These values are again representative of the ranges obtained for the other bone samples. A reduction in the range of values with increasing insonation angle was observed for all samples.

6.4 Discussion

It is known that non-uniform insonation of a vessel may affect the backscattered power and hence alter the relationship between total signal power and the size of the vessel from which the signal originates. It is also known that variations in intensity are an inherent feature of ultrasound transducers, and that beam shape in-vivo is likely to be distorted by tissue inhomogeneities in the beam path. Plots of beam intensity for a homogeneous beam path (figure 6.1a) and a temporal bone

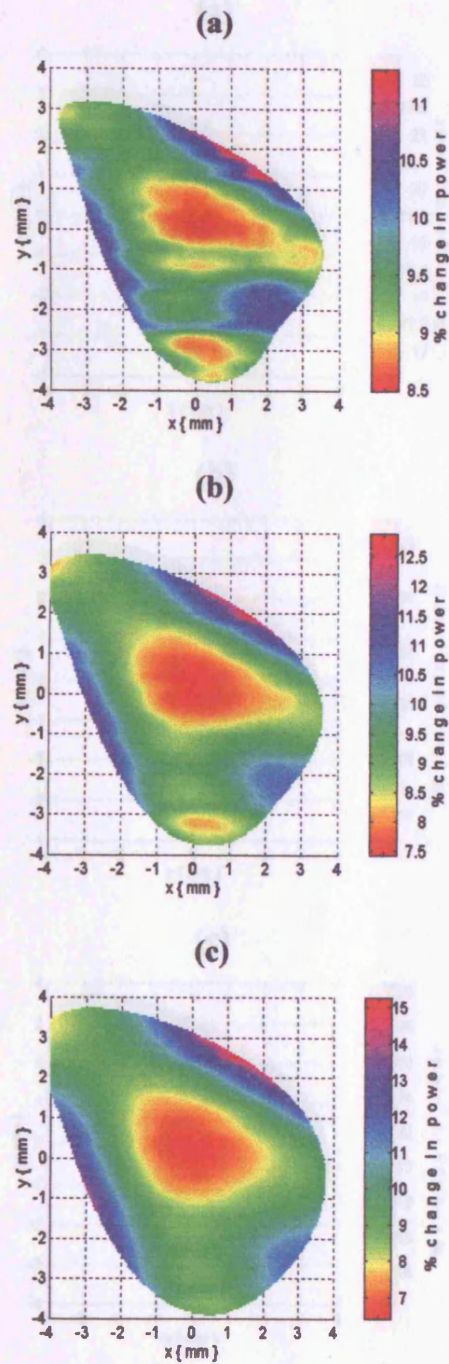


Figure 6.12 Modelled surface plots for a beam path through temporal bone, showing the percentage change in the total signal power received for 15° insonation of vessels of diameter (a) 2mm, (b) 3mm and (c) 4mm power undergoing a 10% dilation in size at different positions in the beam. Vessel positions (x,y) are plotted relative to the position for which the total power is at a maximum when the vessels are in their base-line state. Values are plotted only for vessel positions in the beam at which the total power exceeds 25% of this maximum value.

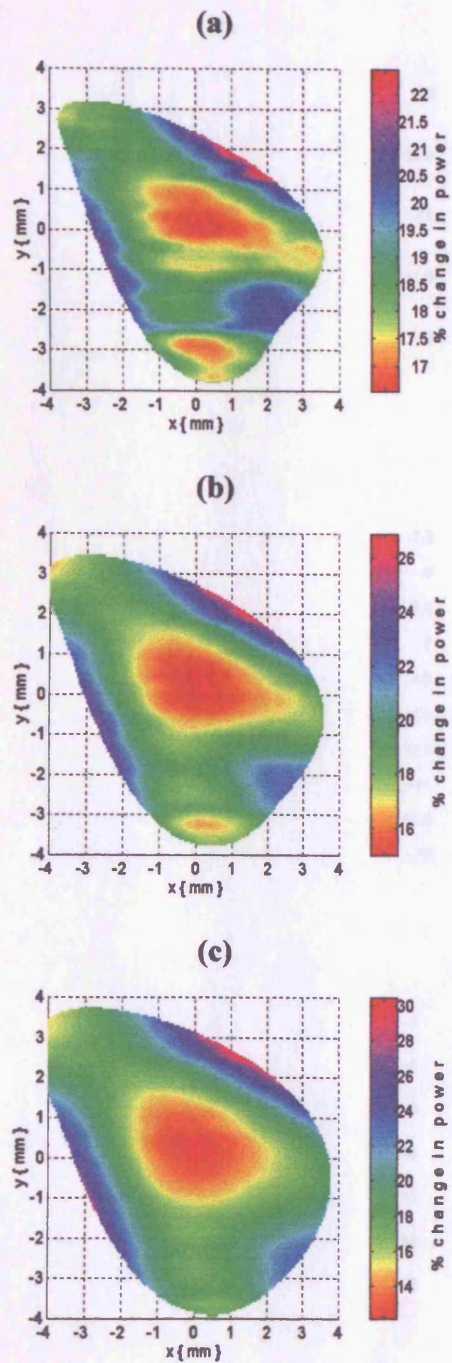


Figure 6.13 Modelled surface plots for a beam path through temporal bone, showing the percentage change in the total signal power received for 15° insonation of vessels of diameter (a) 2mm, (b) 3mm and (c) 4mm power undergoing a 20% dilation in size at different positions in the beam. Vessel positions (x,y) are plotted relative to the position for which the total power is at a maximum when the vessels are in their base-line state. Values are plotted only for vessel positions in the beam at which the total power exceeds 25% of this maximum value.

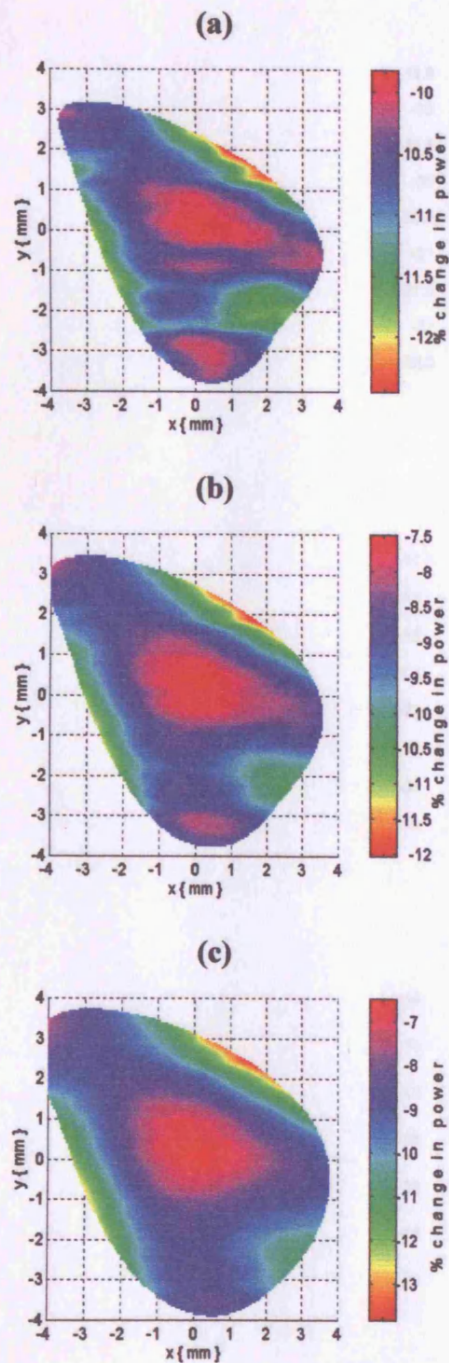


Figure 6.14 Modelled surface plots for a beam path through temporal bone, showing the percentage change in the total signal power received for 15° insonation of vessels of diameter (a) 2mm, (b) 3mm and (c) 4mm power undergoing a 10% contraction in size at different positions in the beam. Vessel positions (x,y) are plotted relative to the position for which the total power is at a maximum when the vessels are in their base-line state. Values are plotted only for vessel positions in the beam at which the total power exceeds 25% of this maximum value.

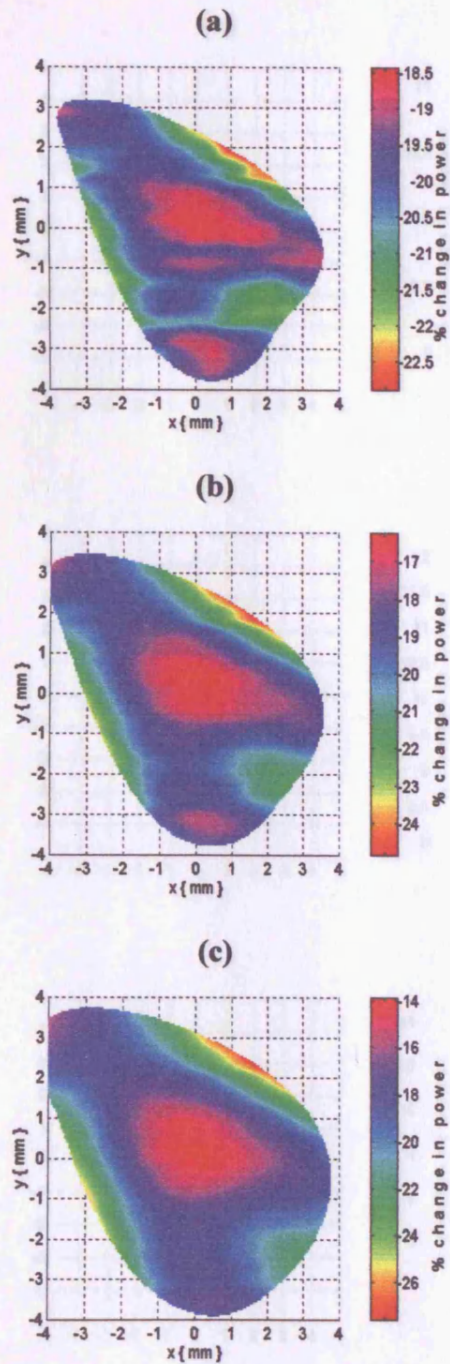


Figure 6.15 Modelled surface plots for a beam path through temporal bone, showing the percentage change in the total signal power received for 15° insonation of vessels of diameter (a) 2mm, (b) 3mm and (c) 4mm power undergoing a 20% contraction in size at different positions in the beam. Vessel positions (x,y) are plotted relative to the position for which the total power is at a maximum when the vessels are in their base-line state. Values are plotted only for vessel positions in the beam at which the total power exceeds 25% of this maximum value.

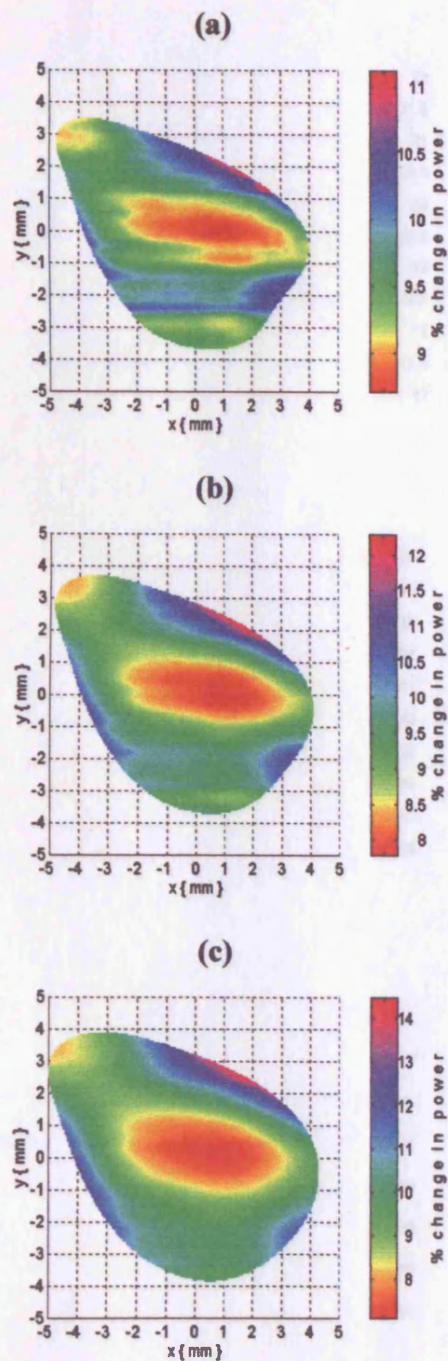


Figure 6.16 Modelled surface plots for a beam path through temporal bone, showing the percentage change in the total signal power received for 30° insonation of vessels of diameter (a) 2mm, (b) 3mm and (c) 4mm power undergoing a 10% dilation in size at different positions in the beam. Vessel positions (x,y) are plotted relative to the position for which the total power is at a maximum when the vessels are in their base-line state. Values are plotted only for vessel positions in the beam at which the total power exceeds 25% of this maximum value.

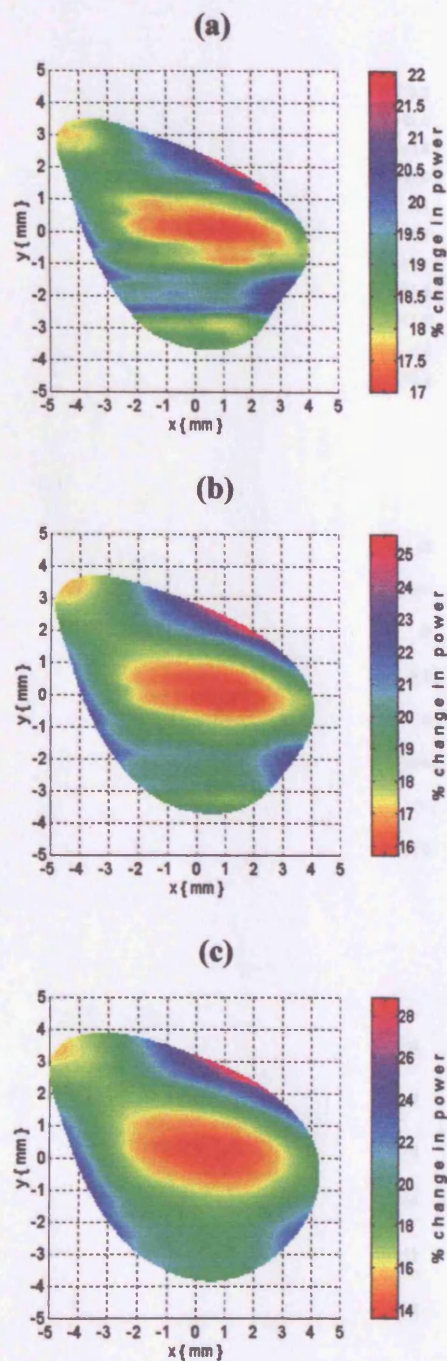


Figure 6.17 Modelled surface plots for a beam path through temporal bone, showing the percentage change in the total signal power received for 30° insonation of vessels of diameter (a) 2mm, (b) 3mm and (c) 4mm power undergoing a 20% dilation in size at different positions in the beam. Vessel positions (x,y) are plotted relative to the position for which the total power is at a maximum when the vessels are in their base-line state. Values are plotted only for vessel positions in the beam at which the total power exceeds 25% of this maximum value.

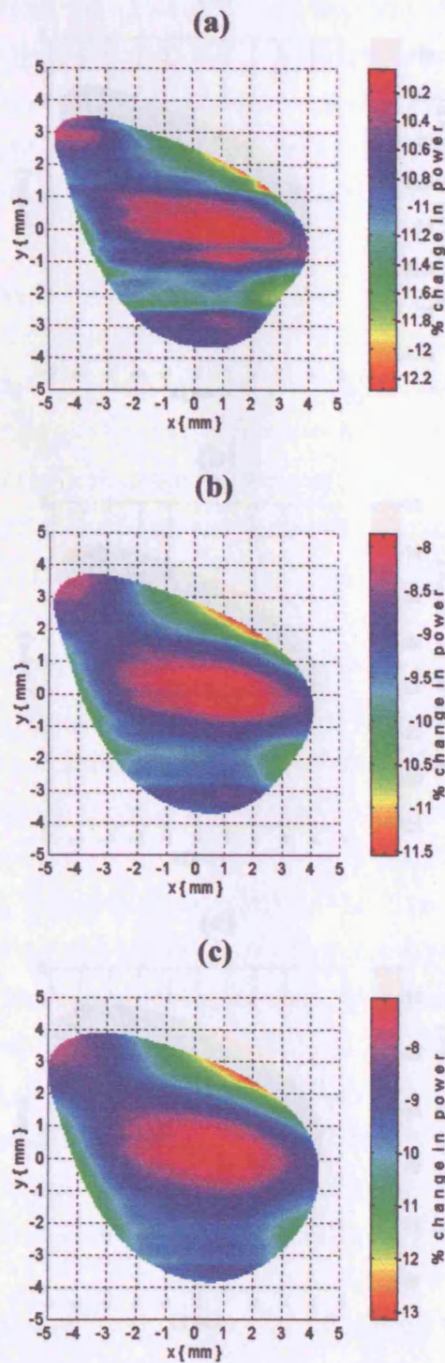


Figure 6.18 Modelled surface plots for a beam path through temporal bone, showing the percentage change in the total signal power received for 30° insonation of vessels of diameter (a) 2mm, (b) 3mm and (c) 4mm power undergoing a 10% contraction in size at different positions in the beam. Vessel positions (x,y) are plotted relative to the position for which the total power is at a maximum when the vessels are in their base-line state. Values are plotted only for vessel positions in the beam at which the total power exceeds 25% of this maximum value.

beam path (figure 6.1b) show that intensity variations of up to 10% occur within a range of less than 0.5mm. This illustrates that changes in signal intensity arising from changes in the size of cerebral vasculature as the MCA was highly

in this chapter, a model of the vessel was used in order to demonstrate the effects of percentage change in power due to vessel size and size changes through each of five vessel diameters on both in-vivo and in-vivo power slope between commercial transducers.

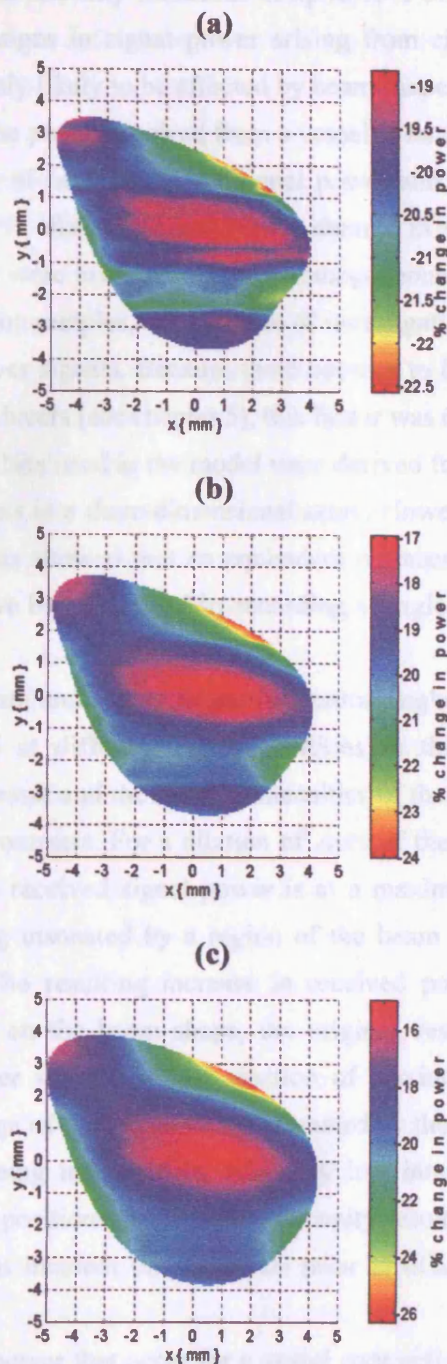
The background power level used in the model was derived from the projection of values of relevant axial and lateral positions of the vessel diameter. However, for a zero degree angle of rotation, additional calculations were required across the beam width to provide a value at the required axial distance.

For a cylindrical beam path (figures 6.4-6.7) showing a 20% contraction in vessel diameter, the vessel position in the beam is very close to that for which the received power is at a maximum, there are increases in area works in the vessel being increased by 20% of the beam with lower intensity than that incident at the vessel centre. The percentage change in received power is therefore smaller than expected, with 20% depending on the vessel size and the axial of the vessel. If the vessel lies further from the centre of the beam and other edges of the beam approach 20% of the vessel diameter, the percentage change in received power is smaller, hence approximating the original beam width.

The percentage change in power due to vessel contraction is at a particular way. For a vessel positioned close to the point at which a maximum power is received, a decrease in size of a vessel is equivalent to this over the cross section

Figure 6.19 Modelled surface plots for a beam path through temporal bone, showing the percentage change in the total signal power received for 30° insonation of vessels of diameter (a) 2mm, (b) 3mm and (c) 4mm power undergoing a 20% contraction in size at different positions in the beam. Vessel positions (x,y) are plotted relative to the position for which the total power is at a maximum when the vessels are in their base-line state. Values are plotted only for vessel positions in the beam at which the total power exceeds 25% of this maximum value.

and the resulting change in the received signal power due to the contraction will be approximately proportional to the magnitude of the size change.



beam path (figure 6.1b) show that intensity variations of up to 10% occur within a range of less than 0.5mm. This illustrates that changes in signal power arising from changes in the size of cerebral vessels such as the MCA are highly likely to be affected by beam shape.

In this chapter, a model of the power received from a vessel in an ultrasound beam was created in order to demonstrate the effects of beam shape on signal power and to provide a prediction of the percentage change in power $\Delta P\%$ likely to arise from a change in vessel size. A range of vessel positions, sizes and size changes were investigated for a homogeneous beam path and for beam paths through each of five temporal bone samples, with the aim of investigating the influence of beam shape on both in-vitro and in-vivo power signals. Because there appears to be very little variation in beam shape between commercial transducers (see chapter 5), this factor was disregarded.

The backscattered power values used in the model were derived from the summation of values at relevant axial and lateral positions in a three-dimensional array. However, for a zero degree angle of insonation, additional calculations showed that an equivalent representation of backscattered power values across the beam could have been obtained by recording a single plane of values at the required axial distance.

For a homogeneous beam path and a zero degree insonation angle, the shape of the surface plots (figures 6.4-6.7) showing $\Delta P\%$ at different vessel positions in the beam can be explained by considering the position of the vessel and the relative intensities of the regions of the beam that cover the vessel if it either dilates or contracts. For a dilation of $\Delta a\%$, if the vessel position in the beam is very close to that for which the received signal power is at a maximum, then any increase in area results in the vessel edges being insonated by a region of the beam with lower intensity than that incident at the vessel centre. The resulting increase in received power is therefore smaller than expected, with $\Delta P\%$ depending on the beam shape, the original vessel size and the extent of the dilation. If the vessel lies further away from the position of maximum received signal power, an increase in size results in one edge of the vessel being insonated by the higher intensity central region of the beam and other edges being insonated by relatively low intensity parts of the beam. $\Delta P\%$ approaches $\Delta a\%$ at these vessel positions, as the mean intensity resulting from the higher and lower intensity regions approaches that incident on the vessel prior to dilation, hence approximating the uniform beam case.

The percentage changes in power that occur for a vessel contraction arise in a similar way. For a vessel positioned close to the point at which maximum power is received, a decrease in area means that the less intense regions of the beam initially incident at the vessel edges are no longer contributing to the received signal. $\Delta P\%$ is therefore smaller than expected due to the relatively high beam intensity across the contracted vessel compared to that across the original. As for the vessel dilation case, $\Delta P\%$ approaches $\Delta a\%$ for positions of the vessel further away from the point at which maximum power is received; because some edge areas of the vessel coincide with higher intensity regions of the beam than others, the average beam intensity at the vessel edges is similar to that in the central region of the vessel. Hence the mean beam intensity over the whole vessel is equivalent to that over the contracted vessel and the resulting change in the received signal power due to the contraction will be approximately proportional to the magnitude of the area change.

The varying percentage changes in power modeled for a zero degree insonation angle and a beam path through temporal bone (figures 6.8-6.11) originate in the same way as those for the homogeneous beam path. However, for the latter the beam shape is fairly uniform (figure 6.1a) and hence the variation in $\Delta P\%$ with the position of the vessel in the beam is similar for all directions away from the point at which maximum signal power is received. In comparison, the beam shape for a path through bone is greatly distorted (figures 6.1b-f), and consequently the variation in $\Delta P\%$ with vessel position is non-symmetric.

The results derived from the bone-distorted beam shapes for a zero degree insonation angle show that for positions of a vessel in the beam at which the received power is greater than 25% of the maximum, $\Delta P\%$ can vary substantially from that expected from the relevant size change $\Delta a\%$. For in-vivo recordings of signal power the location of the vessel in the beam can be assumed to be close to the position at which maximum signal power is received provided that the transducer is placed carefully to receive the strongest possible signal from a vessel. Using this assumption, the results for zero degree insonation of the five bone-distorted beams show that $\Delta P\%$ for a 10% change in vessel area is between 3% and 9% for vessels with diameters 2mm, 3mm and 4mm. For a 20% change in area, $\Delta P\%$ is between 5% and 17.5%. The individual results for each beam and vessel size are shown in figures 6.20a-d. Although it is possible that $\Delta P\%$ could reflect the vessel area change more closely if the transducer was moved less than 1mm relative to the vessel, it is equally as likely for a small transducer movement to increase the difference between $\Delta P\%$ and $\Delta a\%$.

The actual error in $\Delta P\%$ that these values represent is substantial; for example, a 7% change in power detected when a 10% change is expected can be expressed as a 30% error in $\Delta P\%$. In these terms, the error associated with a power change arising from a change in vessel size has been shown to be between 10% and 75% for a zero degree beam-vessel angle and the particular beam shapes, vessel sizes and size changes that were investigated. If the beam distortion caused by the five temporal bone samples used in this investigation is representative of that arising in-vivo, then the magnitude of the modelled error values suggests that non-uniform insonation of the MCA can potentially lead to Doppler power measurements of the scale of vessel size changes being grossly inaccurate.

In order to simulate the effects of the varying insonation angles used for in-vivo recordings from the MCA, the percentage change in power $\Delta P\%$ was also modelled for beam-vessel angles of 15 and 30 degrees. The results obtained for the five bone-distorted beams show that the range of values of $\Delta P\%$ is reduced with increasing insonation angle in all cases. Once again using the assumption that the transducer is positioned to receive the strongest possible signal from a vessel, the results for the five bone-distorted beams show that for a 15 degree insonation angle, $\Delta P\%$ is between 4% and 9.75% for vessels with diameters 2mm, 3mm and 4mm undergoing a 10% change in vessel area, and between 7% and 18.5% for 20% changes in area. For a 30 degree insonation angle, $\Delta P\%$ is between 5.5% and 10% for 10% area changes, and between 11% and 19% for a 20% area changes. The individual results for each beam and vessel size are shown in figures 6.21a-d and 6.22a-d for 15 and 30 degree insonation angles respectively. By comparing these values to those given above for a zero degree insonation angle, it can be seen that the discrepancy between $\Delta P\%$ and the percentage change in area becomes smaller as the insonation angle increases. However, the error in $\Delta P\%$ for a 30 degree beam-

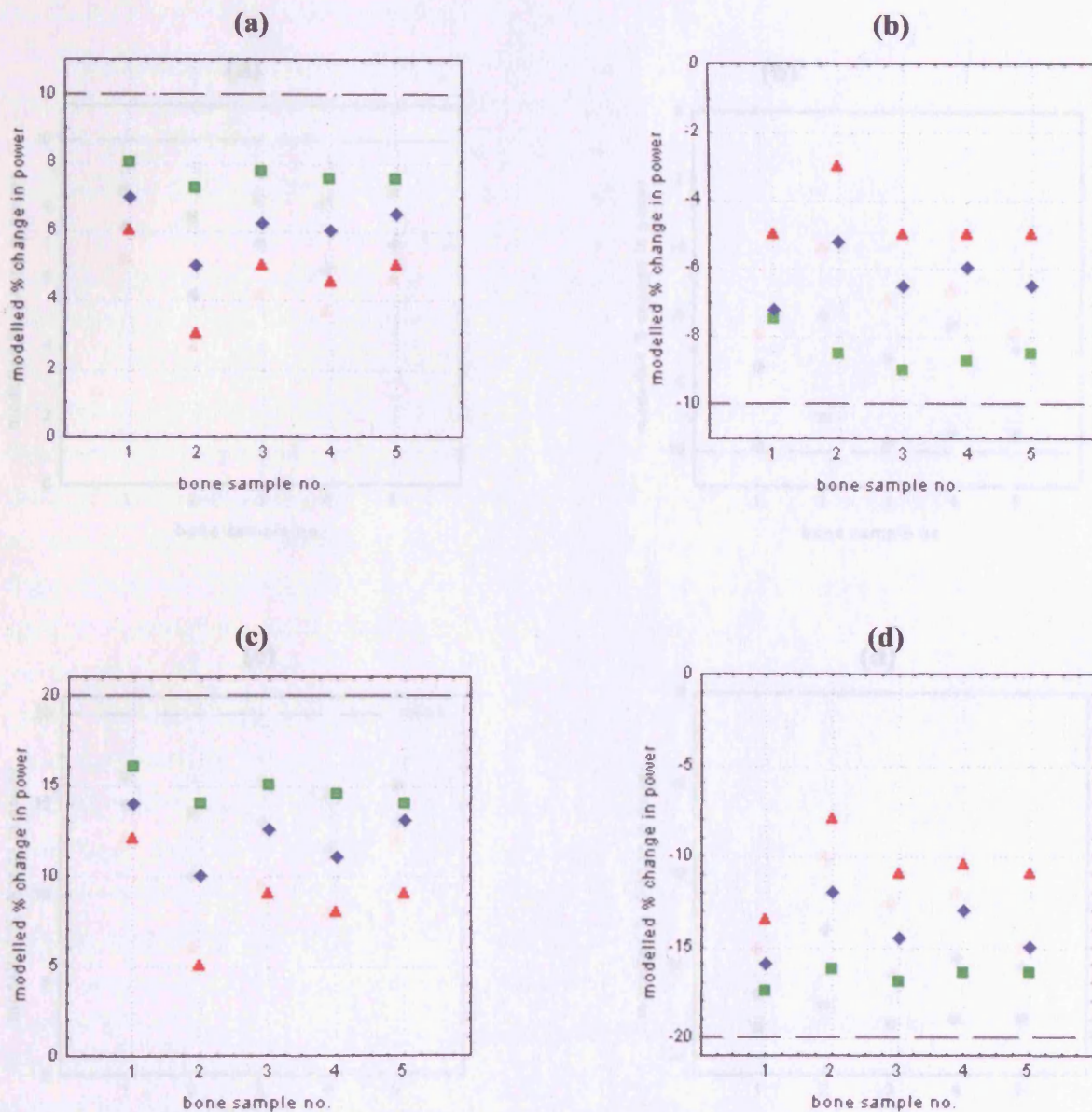


Figure 6.20 The percentage changes in total signal power arising from changes in the cross-sectional area of vessels of diameter 2mm (■), 3mm (◆) and 4mm (▲), modelled for beam shapes produced by zero degree insonation of five different temporal bone samples with 2MHz Scimed transducer beam. Percentage power change values are plotted for (a) 10% increases in vessel areas, (b) 10% decreases in vessel areas, (c) 20% increases in vessel areas, (d) 20% decreases in vessel areas, for the vessel position giving the maximum total signal power in each beam. The dashed lines represent the expected percentage change in signal power.

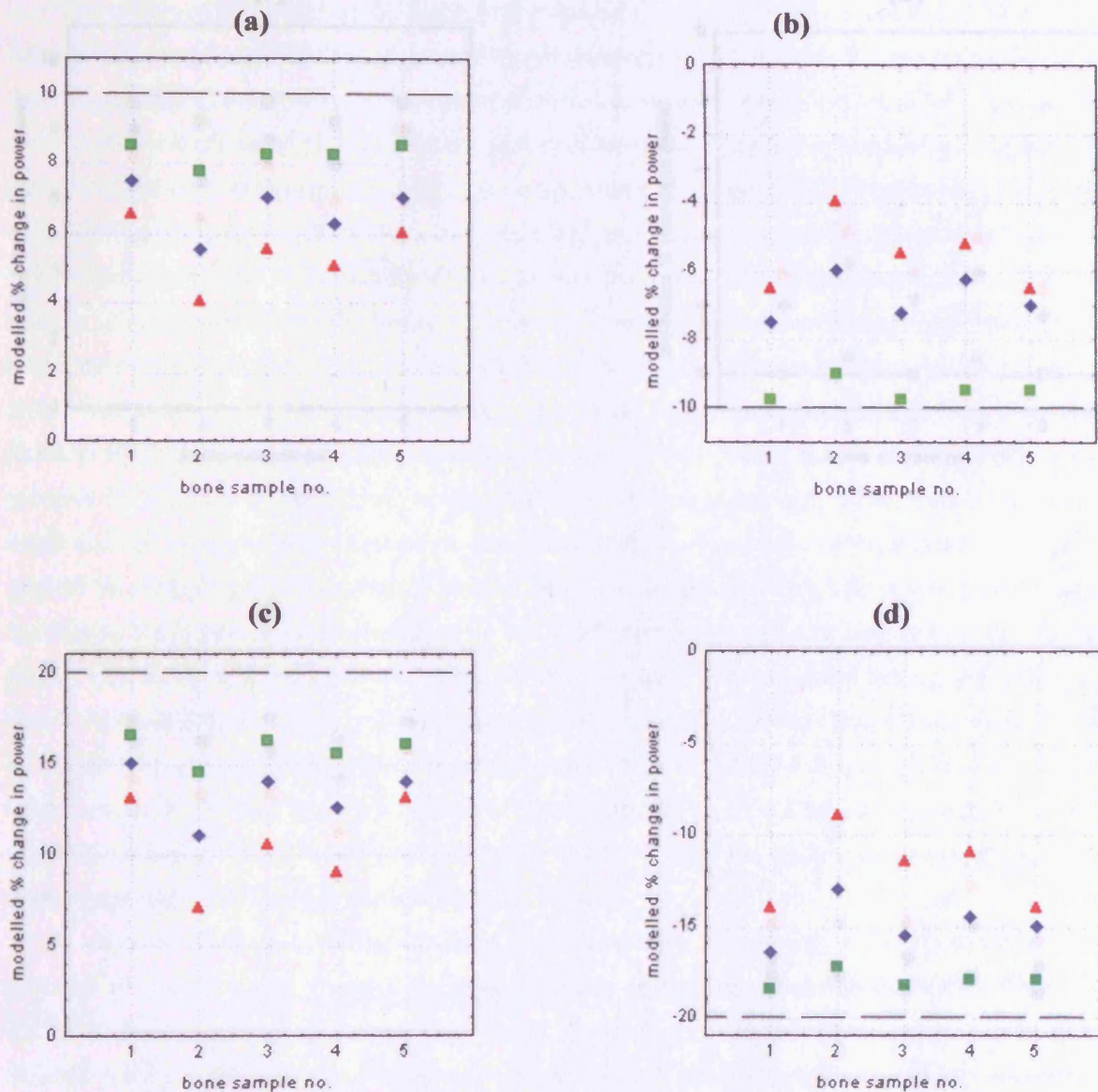


Figure 6.21 The percentage changes in total signal power arising from changes in the cross-sectional area of vessels of diameter 2mm (■), 3mm (◆) and 4mm (▲), modelled for beam shapes produced by 15 degree insonation of five different temporal bone samples with 2MHz Scimed transducer beam. Percentage power change values are plotted for (a) 10% increases in vessel areas, (b) 10% decreases in vessel areas, (c) 20% increases in vessel areas, (d) 20% decreases in vessel areas, for the vessel position giving the maximum total signal power in each beam. The dashed lines represent the expected percentage change in signal power.

vessel angle (representing the maximum angle of insonation that is likely to occur for the MCA) has been shown to reach 50%, and therefore may still result in a further misinterpretation of the scale of the change in vessel area that has occurred.

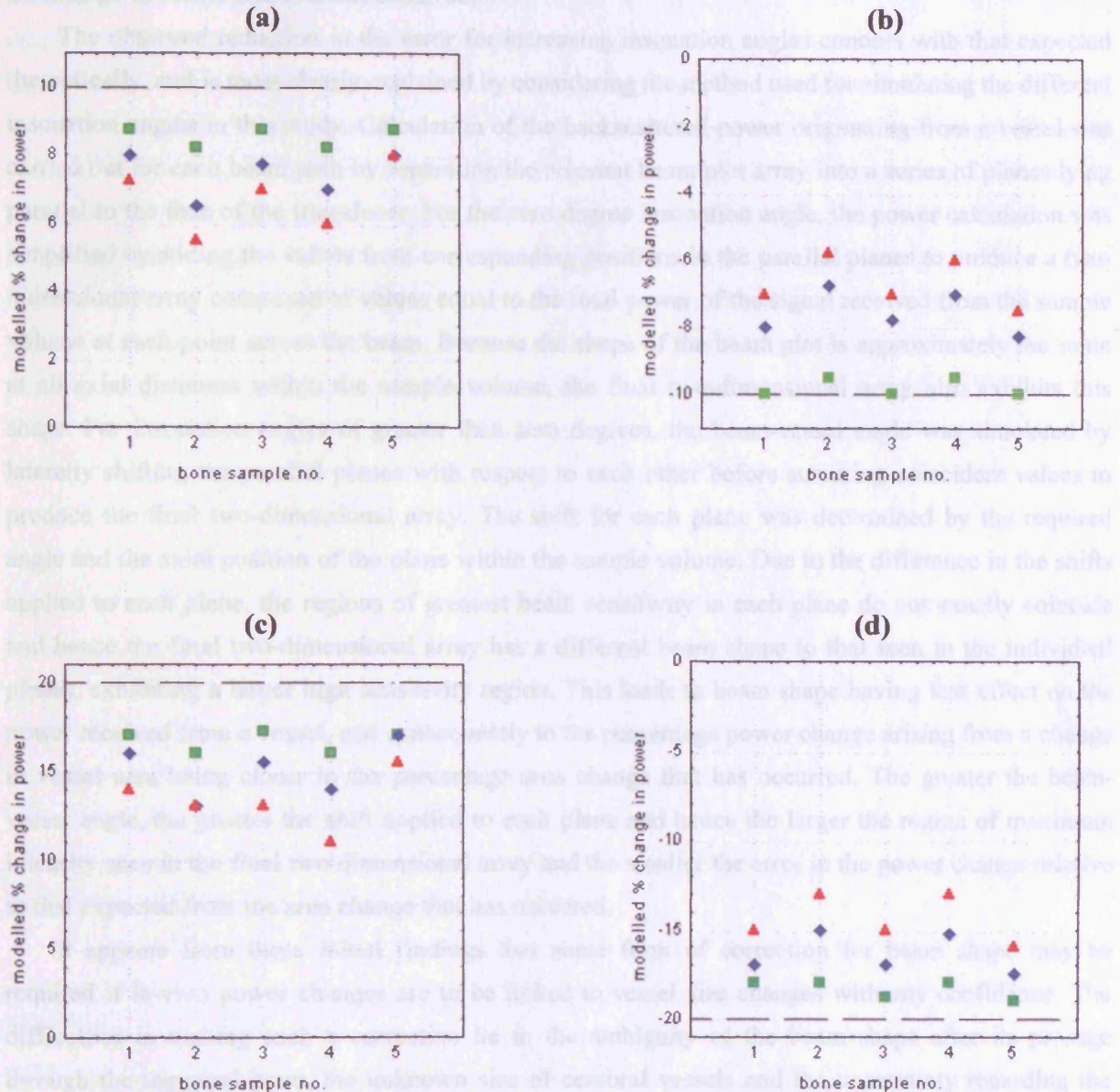


Figure 6.22 The percentage changes in total signal power arising from changes in the cross-sectional area of vessels of diameter 2mm (■), 3mm (◆) and 4mm (▲), modelled for beam shapes produced by 30 degree insonation of five different temporal bone samples with 2MHz Scimed transducer beam. Percentage power change values are plotted for (a) 10% increases in vessel areas, (b) 10% decreases in vessel areas, (c) 20% increases in vessel areas, (d) 20% decreases in vessel areas, for the vessel position giving the maximum total signal power in each beam. The dashed lines represent the expected percentage change in signal power.

For a 10% change in vessel area, the expected percentage change in signal power is 5% and 17.5% for a 20% change in area. These values have been predicted for zero degree insonation of 2mm, 3mm and 4mm diameter vessels by beams which have undergone distortion by temporal bone, representing errors of between 10% and 15% in

vessel angle (representing the maximum angle of insonation that is likely to occur for the MCA) has been shown to reach 50%, and therefore may still result in a serious misinterpretation of the scale of the change in vessel area that has occurred.

The observed reduction in the error for increasing insonation angles concurs with that expected theoretically, and is most clearly explained by considering the method used for simulating the different insonation angles in this study. Calculation of the backscattered power originating from a vessel was carried out for each beam path by separating the relevant beam plot array into a series of planes lying parallel to the face of the transducer. For the zero degree insonation angle, the power calculation was simplified by adding the values from corresponding positions in the parallel planes to produce a two-dimensional array composed of values equal to the total power of the signal received from the sample volume at each point across the beam. Because the shape of the beam plot is approximately the same at all axial distances within the sample volume, the final two-dimensional array also exhibits this shape. For insonation angles of greater than zero degrees, the beam-vessel angle was simulated by laterally shifting the parallel planes with respect to each other before summing coincident values to produce the final two-dimensional array. The shift for each plane was determined by the required angle and the axial position of the plane within the sample volume. Due to the difference in the shifts applied to each plane, the regions of greatest beam sensitivity in each plane do not exactly coincide and hence the final two-dimensional array has a different beam shape to that seen in the individual planes, exhibiting a larger high sensitivity region. This leads to beam shape having less effect on the power received from a vessel, and consequently to the percentage power change arising from a change in vessel area being closer to the percentage area change that has occurred. The greater the beam-vessel angle, the greater the shift applied to each plane and hence the larger the region of maximum intensity seen in the final two-dimensional array and the smaller the error in the power change relative to that expected from the area change that has occurred.

It appears from these initial findings that some form of correction for beam shape may be required if in-vivo power changes are to be linked to vessel size changes with any confidence. The difficulties in making such a correction lie in the ambiguity of the beam shape after its passage through the temporal bone, the unknown size of cerebral vessels and the uncertainty regarding the position of a vessel in the beam. A potential alternative to correcting for beam shape might seem to be the use of a larger beam for signal power recordings, with the aim of improving uniformity in the beam shape across the insonated vessel. However, owing once again to the unknown nature of the distortion of the beam by the skull, the benefits are dubious for the in-vivo case.

6.5 Conclusions

The results of the study described in this chapter suggest that the proportionality between power changes and MCA area changes is likely to be substantially influenced by the beam shape across the vessel. Assuming that the transducer is positioned to receive the maximum signal, changes in power of between 3% and 9% for a 10% change in vessel area and 5% and 17.5% for a 20% change in area have been predicted for zero degree insonation of 2mm, 3mm and 4mm diameter vessels by beams which have undergone distortion by temporal bone, representing errors of between 10% and 75% in

the power change. The values for the zero degree insonation angle are likely to represent the maximum error range as it has been shown that the discrepancy between a vessel area change and the resulting power change is reduced for increasing angle of insonation. However, because the predicted errors for a 30 degree beam-vessel angle reached 45%, it appears likely that the Doppler signal power method can potentially have poor accuracy even for the largest angles of insonation.

The modelled changes in power have been shown to be dependent on the beam shape itself, the position of the vessel in the beam, the original size of the vessel and the change in area that occurs. The fact that these variables are unknown in-vivo means that it is difficult to determine the exact effects that beam shape will have on a change in signal power detected from the MCA. If the errors derived in this study are representative of those arising for in-vivo recordings from the MCA then it appears that some form of correction for beam shape is required before a proportional relationship between changes in signal power and vessel size can be assumed with any confidence.

CHAPTER 7

Correcting the Doppler Signal Power For the Effects of Beam Shape and Filtering

7.1 Introduction

The results presented in the previous chapter demonstrate that non-uniform insonation of a vessel arising from distortion of the Doppler ultrasound beam shape by temporal bone causes a loss of proportionality between changes in vessel size and the resultant changes in total power for most vessel positions in the beam. Assuming that the vessel position in the beam is such that the received signal intensity is at a maximum, the change in total power arising from a change in vessel area has been shown to be consistently smaller than expected, with the difference between the expected and actual values varying with beam shape. These findings suggest that some form of correction for beam shape is required before changes in signal power recorded from the MCA can be confidently related to the scale of the size change that the vessel has undergone.

The results of the investigation of beam shape distortion by temporal bone described in chapter 5 suggest that the distortion occurring for in-vivo Doppler recordings from the MCA will vary unpredictably between individuals. Because the exact nature of the distortion cannot be predicted, and because neither the size nor the precise position of an in-vivo vessel in the beam is known, the effects of non-uniform insonation of a vessel on the shape and magnitude of the signal power spectrum cannot be specifically determined for individual cases. The only solution is therefore some form of universal correction which will at least approximately compensate for the loss of proportionality between vessel size changes and changes in the total signal power that is caused by non-uniform insonation. Ideally, the correction should also compensate for high-pass filtering in order to eliminate this potential source of error, albeit small for the in-vivo case.

This chapter firstly describes a modelling technique used to provide a simulation of the Doppler power spectra arising for specific vessel size, insonation and flow conditions. This is followed by the description of a spectral averaging method, and a spectral correction method. In both cases, the simulated Doppler spectra are used to investigate the relationship between total power and vessel size, in order to assess the suitability of the methods for use with in-vivo signals.

7.2 Modelling the Doppler Power Spectrum

The advantage of using a theoretical model to simulate the Doppler signal power spectrum is that spectra can be generated for very precise insonation and flow conditions; these factors are unknown for in-vivo signals, and can only be estimated for flow phantom signals. In addition, vessel sizes and vessel area changes can be specified.

The simulation of a Doppler power spectrum was based on the division of a theoretical vessel of radius R into 1551 laminae of equal thickness, and simultaneously into sectors of angle 10 degrees, resulting in each lamina being divided into 36 sections of equal area. Figure 7.1 shows a schematic representation of this area division for fewer laminae and sectors. It was assumed that the distribution of red blood cells was uniform throughout the vessel, and hence that the backscattered signal from

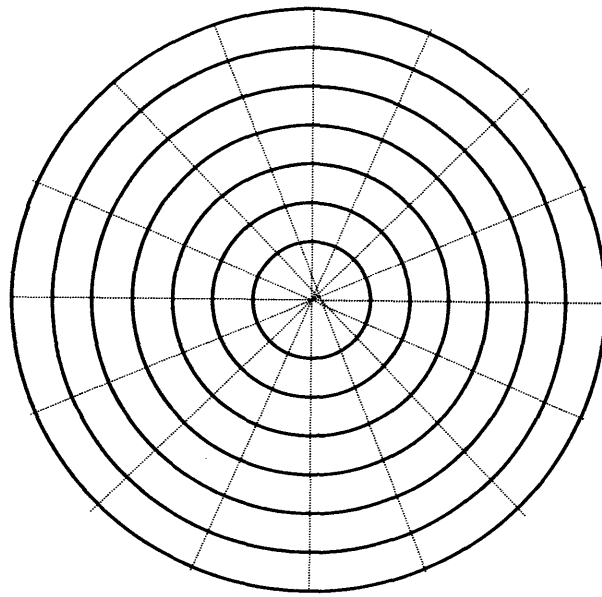


Figure 7.1 Schematic illustration of the division of a theoretical vessel into sections, using laminae of equal thickness and sectors of equal angle.

each section of lamina was proportional to the cross-sectional area (this forms the basis of the theory behind the Doppler power method).

The velocity of the blood for each lamina was calculated using the assumption that the velocity profile was parabolic. For parabolic flow, the velocity V at any radial position r in a vessel can be calculated from the equation:

$$V(r) = V_{\max} \left(1 - \frac{r^2}{R^2} \right) \quad [7.1]$$

where R is the vessel radius and V_{\max} is the maximum central stream velocity (Evans and McDicken 2000). The assumption of parabolic flow was based on the likelihood that flow in the MCA will have a parabolic profile owing to its small diameter and unidirectional flow.

In order to generate the spectrum, the velocity range (equal to V_{\max}) was divided into 32 bins of equal width. The Doppler shift frequency corresponding to the upper and lower limits of each bin was calculated using the Doppler equation (chapter 2), assuming a transducer frequency of 2MHz and an insonation angle of zero degrees (standard values for Doppler investigations of the MCA). The contribution of each section of vessel lamina to the spectrum depended firstly on its center velocity, which determined the spectral bin to which the lamina contributed, and secondly on the area of the lamina section, which determined the magnitude of the contribution to the relevant bin. Division of the vessel into a large number of laminae allowed a more accurate spectral shape to be generated; fewer lamina provided only a crude estimate.

The area of each section of lamina was calculated using the following equations:

$$\text{width of each lamina : } \Delta r = \frac{R}{N} \quad [7.2]$$

$$\text{area of each section of lamina: } A(r) = \frac{\pi(r)^2 - \pi(r - \Delta r)^2}{36} \quad [7.3]$$

where R is the radius of the vessel, N the number of laminae that the vessel is divided into, and r the radial distance from the centre of the vessel to the outer edge of each lamina.

Figure 7.2b shows the spectrum created for the parabolic velocity profile shown in figure 7.2a; as would be expected, the spectral shape is approximately rectangular. This is due to the fact that for parabolic flow the rate of decrease of velocity away from the vessel centre is proportional to the distance from the centre of the vessel, but the area of the equal width laminae increases in proportion to their distance from the vessel centre. Exact cancellation of these two effects means that the volume of blood travelling at any velocity is independent of the velocity.

7.2.1 Non-Uniform Insonation

The magnitude of the change in power arising from an in-vivo change in vessel size is dependent on the relative intensities of the area of beam covering the vessel before and after its size change. An

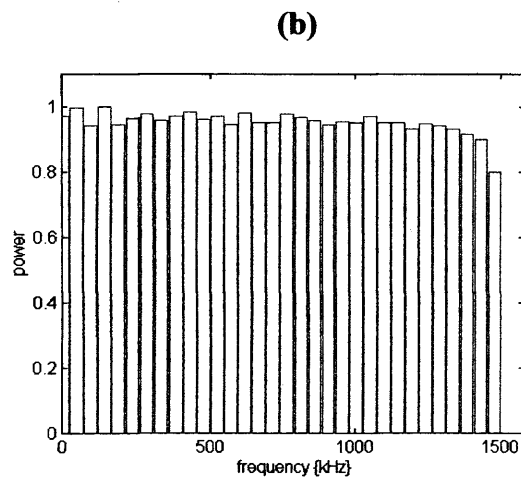
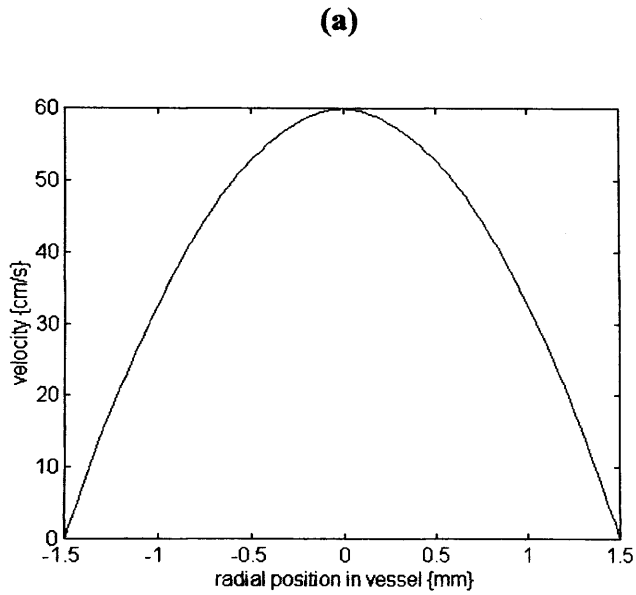


Figure 7.2 (a) parabolic velocity profile for a vessel of diameter 3mm. **(b)** the power spectrum generated by the spectrum model for this velocity profile, for uniform insonation of the vessel. Power values have been normalised to the maximum.

estimate of these relative intensities is only possible if the beam shape and the vessel position in the beam are known. The derivation of an accurate correction factor for non-uniform insonation of in-vivo cerebral vessels is limited by the fact that the size of the vessel is unknown, and also because the beam shape is likely to be distorted by the presence of the temporal bone in the beam path (Fry and Barger 1978, White et al. 1978, Grolimund 1986).

It has been demonstrated that an ultrasound beam exhibits significant distortion after passage through temporal bone (chapter 5), with the pattern of distortion varying for different bone samples. The consequence of such distortion on the Doppler signals recorded from the MCA will be non-uniform insonation of the vessel, with the effects on spectral shape depending on the beam sensitivity pattern across the vessel.

The variability of the beam distortion caused by temporal bone suggests that the effects of non-uniform insonation on the total signal power cannot be accurately predicted for individual cases. This is also supported by the work described in chapter 6, which showed that the change in power observed for various changes in vessel size varied with the insonation pattern across a vessel. A universal correction is therefore required which will at least approximately compensate for the effects of non-uniform insonation in every case.

The effects of non-uniform insonation were introduced to the spectral model using the bone-distorted beam sensitivity plots recorded in chapter 5. The theoretical vessel was positioned in each plot at the point corresponding to that for which the total received power was at a maximum (this is shown in figure 7.3a for a 3mm diameter vessel in one of the bone-distorted beam plots). As described previously, the vessel was then divided into 1551 equal width laminae, and simultaneously into sectors of angle 10° , resulting in each lamina being divided into 36 sections of equal area. The magnitude of the contribution of each lamina section to the spectral model was dictated by the area of the section and the beam sensitivity value at the relevant position, hence simulating the effects of non-uniform insonation. Figure 7.3b shows a spectrum modelled for the vessel-beam configuration shown in figure 7.3a and a peak flow velocity of 60cms^{-1} , and illustrates the loss of the rectangular spectral shape due to the lower beam intensities incident at the vessel edges.

7.2.2 High Pass Filtering

High pass filtering of Doppler signals is inherent to all TCD systems in order to remove the low frequency clutter signals arising from transducer movement and slow tissue movements in the beam path. The disadvantage of such filtering is that it also removes the low frequency Doppler signal originating from the red blood cells which are travelling at low velocities close to the vessel walls. Although the proportion of the spectrum that is filtered from in-vivo signals is likely to be small due to the relatively high Doppler shift frequencies compared to the filter cut-off frequency, the effects of filtering on spectral shape should still be considered when attempting to model the Doppler signal spectrum and apply corrections for the factors that may be affecting the relationship between signal power and vessel size, in order to accurately represent the in-vivo case.

In order to simulate the effects of high pass filtering on the shape of the modelled Doppler spectrum, the frequency response characteristics of the inherent high-pass filtering of the Scimed

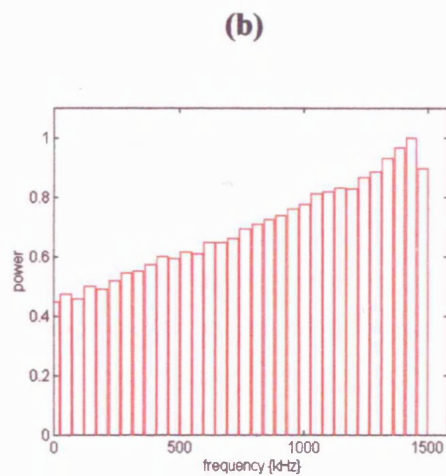
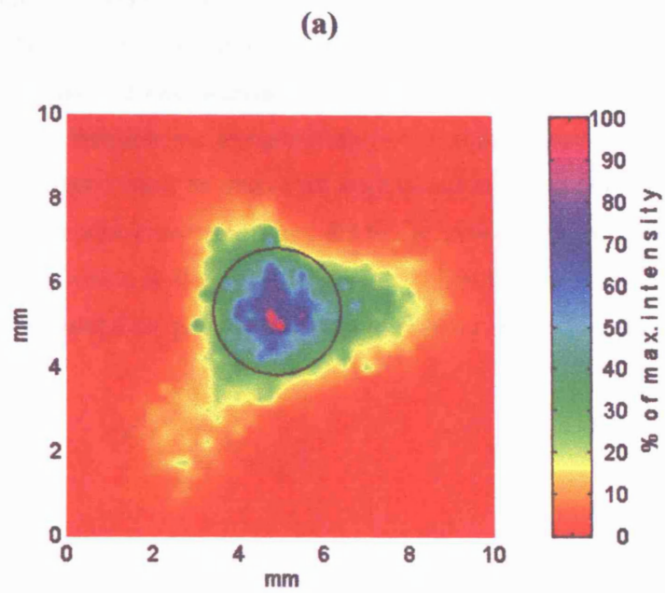


Figure 7.3 (a) Received field beam sensitivity of a Scimed transducer, plotted at an axial distance of 5.0cm from the face of the transducer, for a beam path through a temporal bone sample. A vessel of size 3mm diameter has been superimposed on the plot at the position giving the maximum total power value. **(b)** The modelled power spectrum produced for this insonation pattern. Power values have been normalised to the maximum.

PCDop 842 recording system were required. These were derived from the system circuit diagrams using the EDWIN (Electronic Design for Windows) computer package (Norlinvest Ltd., BVI). The magnitude and phase of the frequency response are shown in figure 7.4a.

The filter frequency response characteristics were applied to the modelled power spectrum by calculating the Doppler shift frequency corresponding to the centre velocity of each spectral bin. The frequency for each bin was then used to derive an amplification value from the frequency response plot. The amplification value was converted from dB to an intensity ratio using the standard decibel equation [7.4] and the power value in the relevant bin multiplied by this ratio. The effects of the high-pass filter simulation on the modelled power spectrum are shown in figure 7.4b.

$$dB = 10 \log \left(\frac{I}{I_0} \right) \quad [7.4]$$

7.3 Testing the Doppler Power Spectrum Model

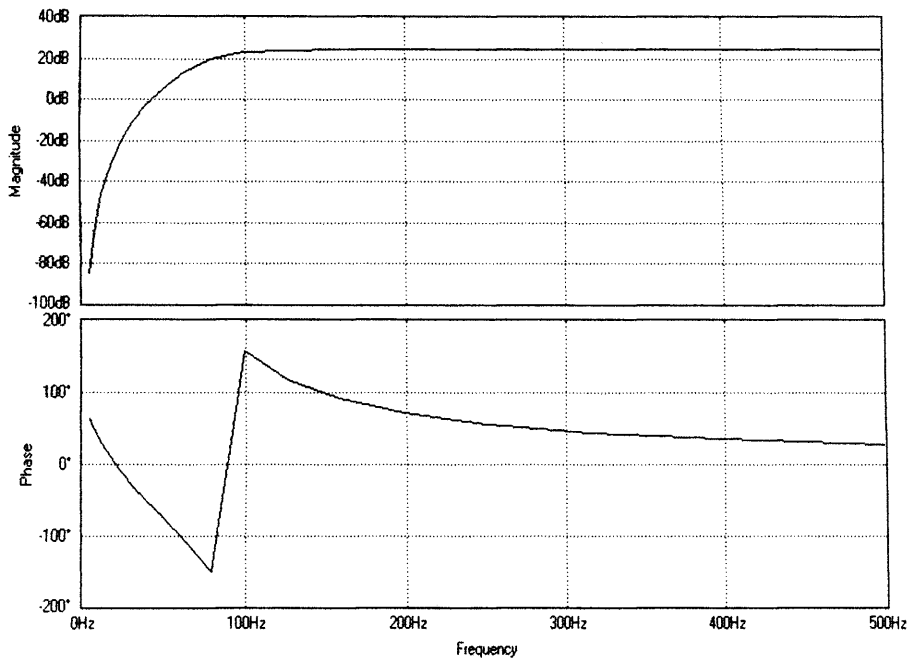
The basis of the Doppler power method is that changes in vessel size produce proportional changes in signal power which are independent of any simultaneous changes in velocity that occur. This theory was used to test the accuracy of the spectrum model, by creating spectra for both steady and pulsatile flow in the following circumstances:

- changes in the flow velocity for a constant vessel size
- changes in vessel size for a constant flow velocity
- changes in both velocity and vessel size, but a constant flow rate.

Because the Doppler power method is based on the theory that the total power is affected only by the volume of blood in a vessel, the modelled spectra were initially created for conditions of uniform insonation, and without high pass filtering. Vessel sizes were chosen to reflect those of the MCA (van der Zwan et al. 1993), and flow velocities were selected from the normal range of time-averaged peak values for this artery (Evans et al. 1989).

Maximum frequency envelope waveforms were generated for steady flow and for one cardiac cycle of pulsatile flow (figures 7.5a and 7.12a respectively). For pulsatile flow, the maximum frequency envelope waveform was derived from one cardiac cycle of a Doppler signal recorded from the MCA of a healthy adult at rest (see chapter 8 for details of envelope derivation and beat marking methods), and was smoothed using a five-point moving average technique. For steady flow, the maximum frequency envelope was created to have a constant value equal to the mean value of the pulsatile flow waveform. To simulate variations in the flow velocity, the pulsatile waveform was normalised to its mean value and then multiplied by the frequency corresponding to the required time-averaged peak velocity. The steady flow frequency envelope values in each case were again set to equal to the time-averaged velocity of the pulsatile flow envelope. For both steady and pulsatile flow, the total power value for the waveform was calculated by summing the power values in all frequency bins of the modelled spectra.

(a)



(b)

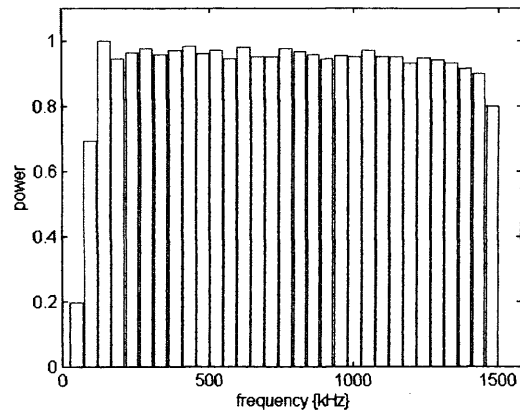


Figure 7.4 (a) frequency and phase response of the inherent high pass filters in the Scimed PcDop842 transcranial Doppler system. **(b)** the effect of the inherent filters on the shape of the modelled power spectrum. Power values have been normalised to the maximum.

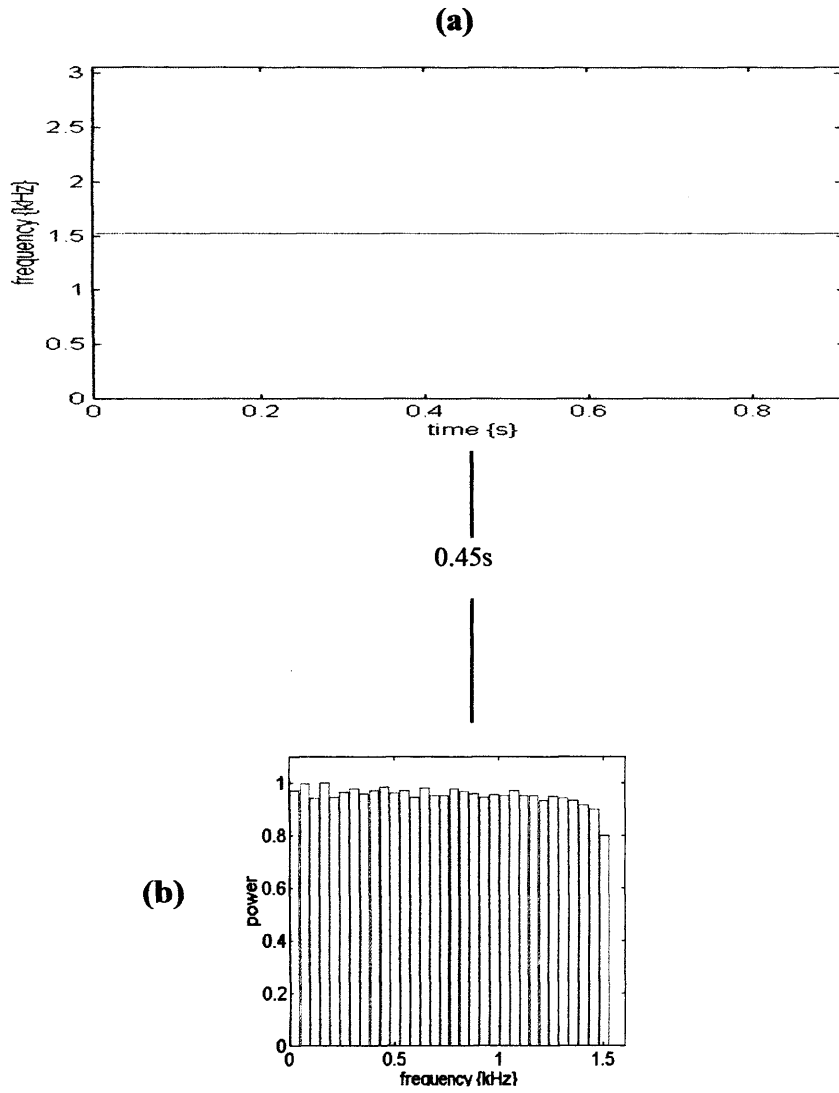


Figure 7.5 (a) steady flow maximum frequency waveform envelope corresponding to a time-averaged peak velocity of 60cm s^{-1} . (b) modelled power spectrum for an arbitrary time in the steady flow waveform.

7.3.1 Steady Flow

Figure 7.5b shows the power spectrum generated by the spectrum model for a vessel of diameter 3mm, at an arbitrary time in a steady flow envelope with peak velocity 60cm s^{-1} . As would be expected from theory, the spectrum is approximately rectangular in shape owing to the assumption of parabolic flow, and the maximum frequency (F_{max}) of 1530Hz corresponds to the steady flow peak velocity value of 60cm s^{-1} . Figures 7.6a-e show the power spectra produced by the spectrum model at a single arbitrary time in steady flow envelopes with peak velocity values of 50cm s^{-1} , 55cm s^{-1} , 60cm s^{-1} , 65cm s^{-1} and 70cm s^{-1} respectively. These plots verify that the spectral shape remains rectangular at all velocities, that the maximum spectral frequency corresponds to the peak velocity value in each case, and that the magnitude of the spectral power values varies in order to maintain a constant total power value. The relationship between velocity and the total power values derived from the modelled spectra is plotted in figure 7.7. It can be seen that the total power is independent of velocity, as would be expected from theory.

Figures 7.8a-e show the modelled power spectra created for vessels with diameters of 1.5mm, 2mm, 2.5mm, 3mm and 3.5mm respectively, in each case at a single arbitrary time in a flow envelope with a steady flow peak velocity of 60cm s^{-1} . It can be seen that the maximum frequency is equal for each spectra, due to the same peak velocity value being used in the model in each case, but that the magnitude of the spectral power varies with the size of the vessel. The relationship between vessel area and the total power values derived from the modelled spectra is plotted in figure 7.9. The graph shows that the two parameters are proportional, as predicted by the theory behind the Doppler power method.

Figures 7.10a-e show the spectra generated for five combinations of velocity and vessel diameter values, with the product of vessel cross-sectional area and velocity giving an identical flow rate value in each case. Values for each spectrum are given in table 7.1. Both the maximum spectral frequency and the magnitude of the spectral power values can be seen to vary, but the relationship between total power and vessel area is still proportional (figure 7.11), demonstrating that power changes arising under conditions of simultaneous changes in velocity and vessel size remain unaffected by velocity.

7.3.2 Pulsatile Flow

Figure 7.12b shows the power spectra generated by the spectrum model for a vessel of diameter 3mm at five arbitrary times in a pulsatile flow envelope with a time-averaged peak velocity of 60cm s^{-1} . The spectra are once again approximately rectangular in shape owing to the assumption of parabolic flow, but the maximum frequency varies in each case depending on the value of the flow envelope at the relevant time in the cardiac cycle.

In addition to this plot, inspection of the modelled spectra created for pulsatile flow conditions was carried out for various values of time-averaged peak velocity and for changes in vessel size, as described previously for the steady flow case. In all cases, the spectra fulfilled the relevant theoretical criteria in terms of shape, and plots of total power against velocity and vessel area were identical to those shown for steady flow (figures 7.7, 7.9 and 7.11).

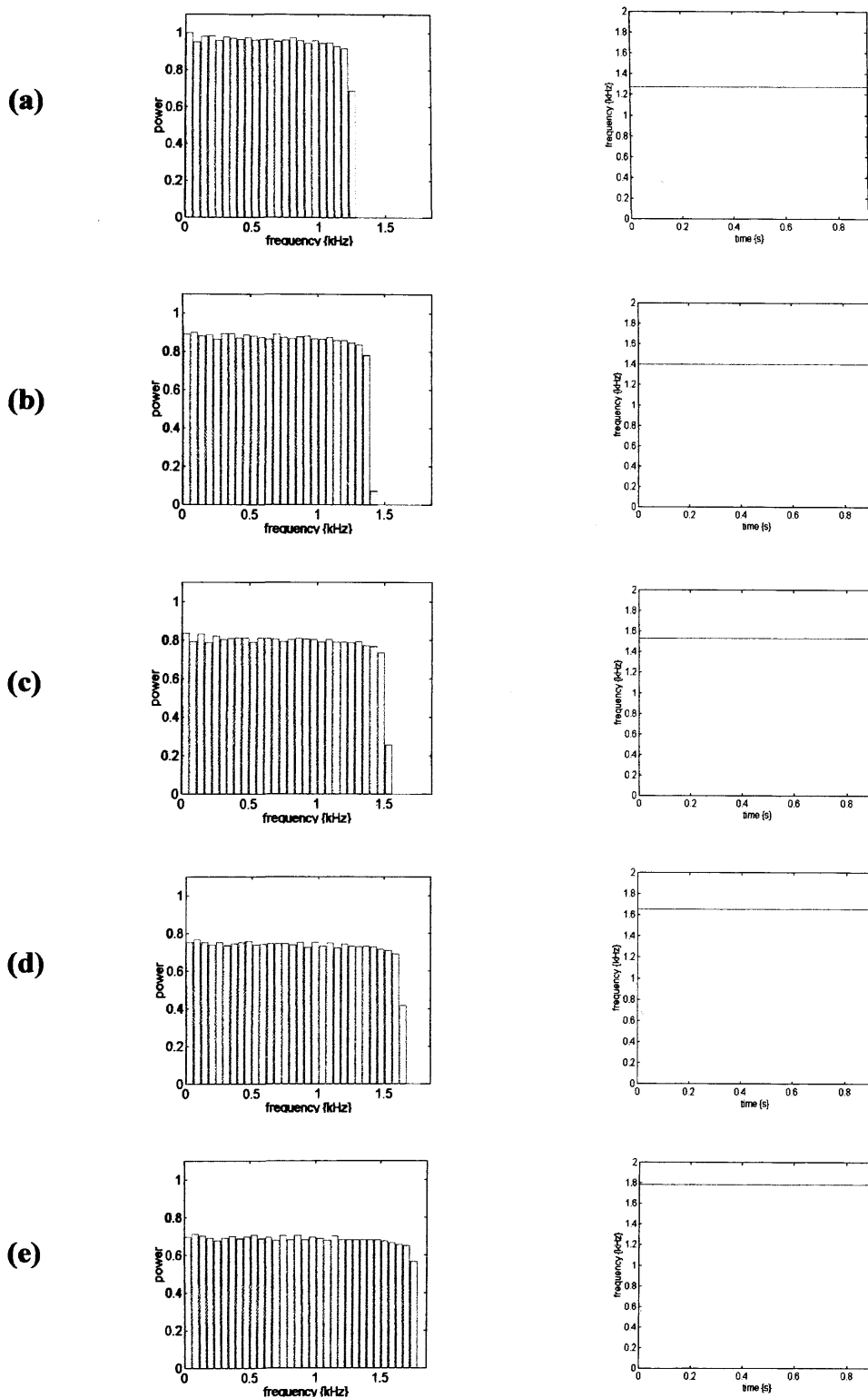


Figure 7.6(a-e) Modelled power spectra generated for a vessel of diameter 3mm and steady flow time-averaged peak velocity values of 50 cm s^{-1} , 55 cm s^{-1} , 60 cm s^{-1} , 65 cm s^{-1} and 70 cm s^{-1} respectively. In each case, the power spectrum is plotted for an arbitrary time in the steady flow waveform shown alongside.

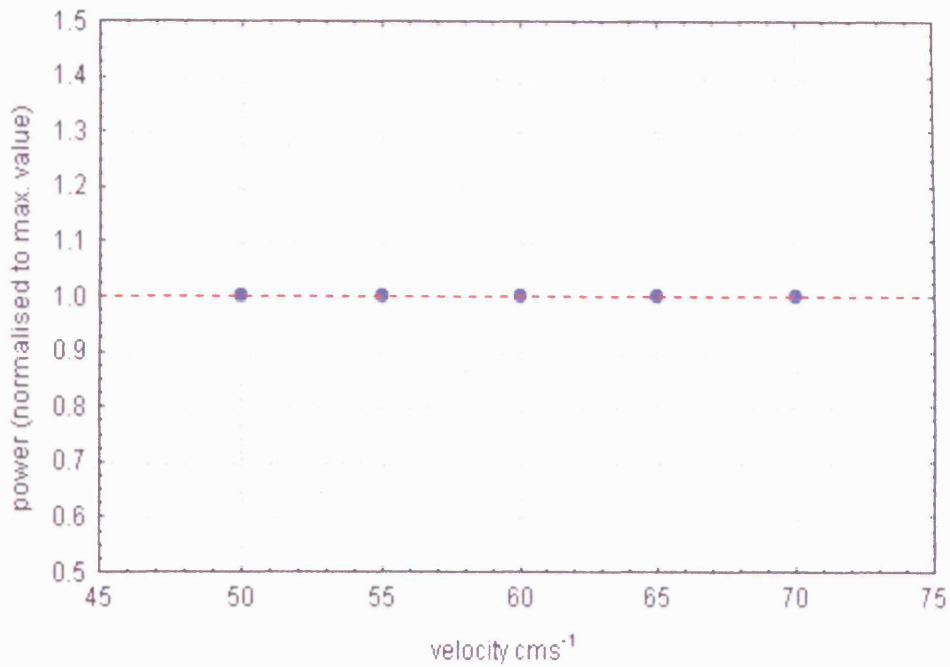


Figure 7.7 The relationship between velocity and the total power contained in the modelled spectra. Modelled spectra were generated for a vessel of diameter 3mm containing steady flow waveforms with time-averaged peak velocities of 50cms^{-1} , 55cms^{-1} , 60cms^{-1} , 65cms^{-1} and 70cms^{-1} respectively. Power values have been normalised.

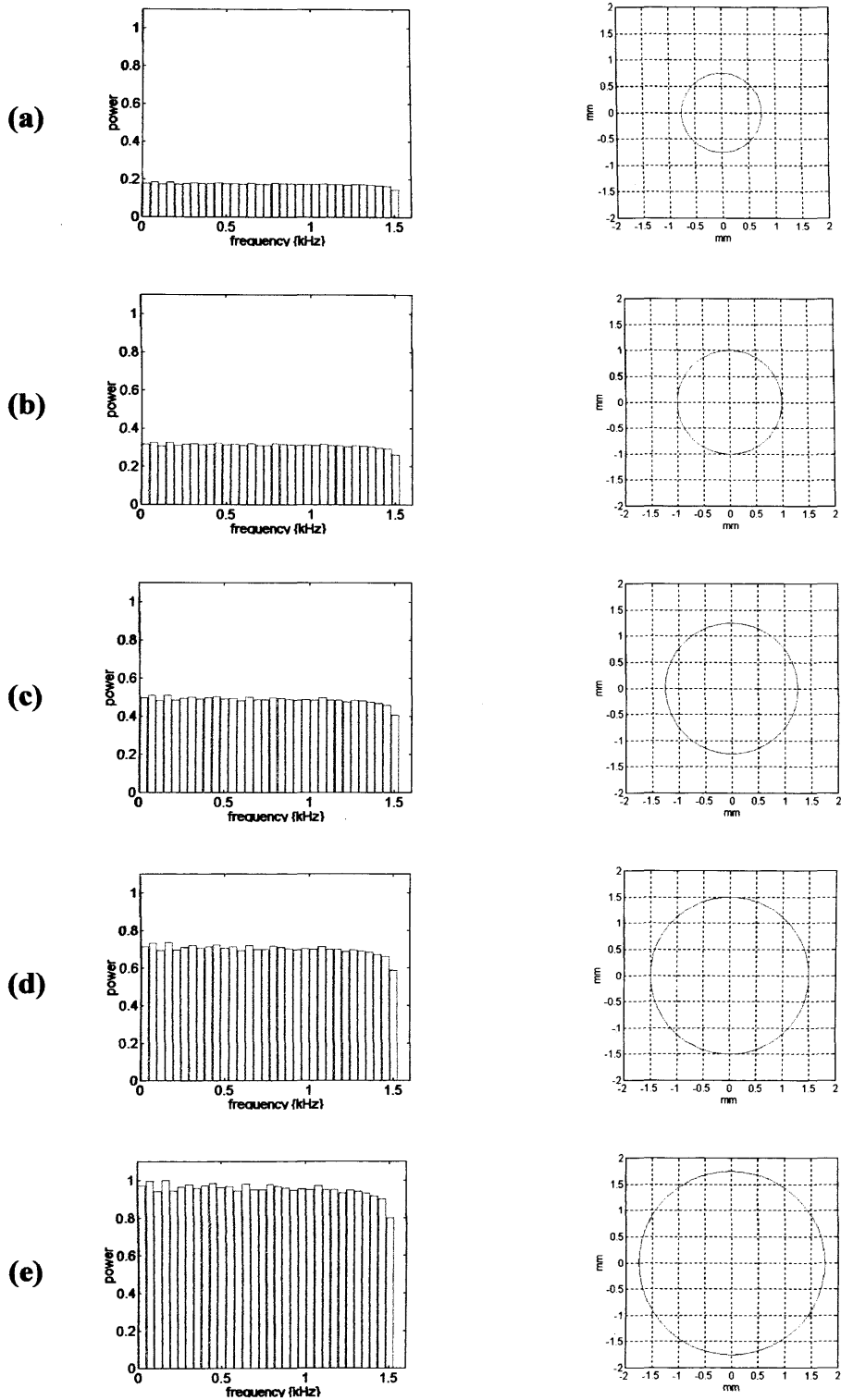


Figure 7.8(a-e) Modelled power spectra generated for a steady flow time-averaged peak velocity value of 60cms^{-1} , for vessel diameters of 1.5mm, 2mm, 2.5mm, 3mm and 3.5mm respectively. In each case the power spectrum is plotted for an arbitrary time in the steady flow waveform, and the relevant vessel size is shown alongside.

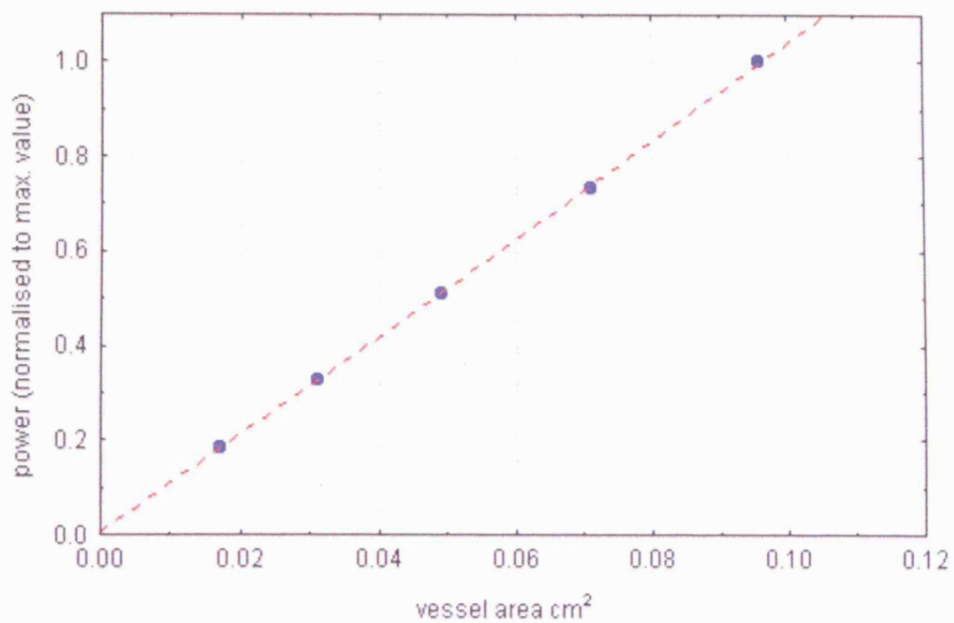


Figure 7.9 The relationship between vessel area and the total power contained in the modelled spectra. Modelled spectra were generated for vessels of diameter 1.5mm, 2mm, 2.5mm, 3mm, 3.5mm (corresponding to areas 0.017cm², 0.031cm², 0.049cm², 0.071cm² and 0.096cm² respectively) containing a steady flow waveform with a time-averaged peak velocity of 60cms⁻¹. Power values have been normalised to the maximum.

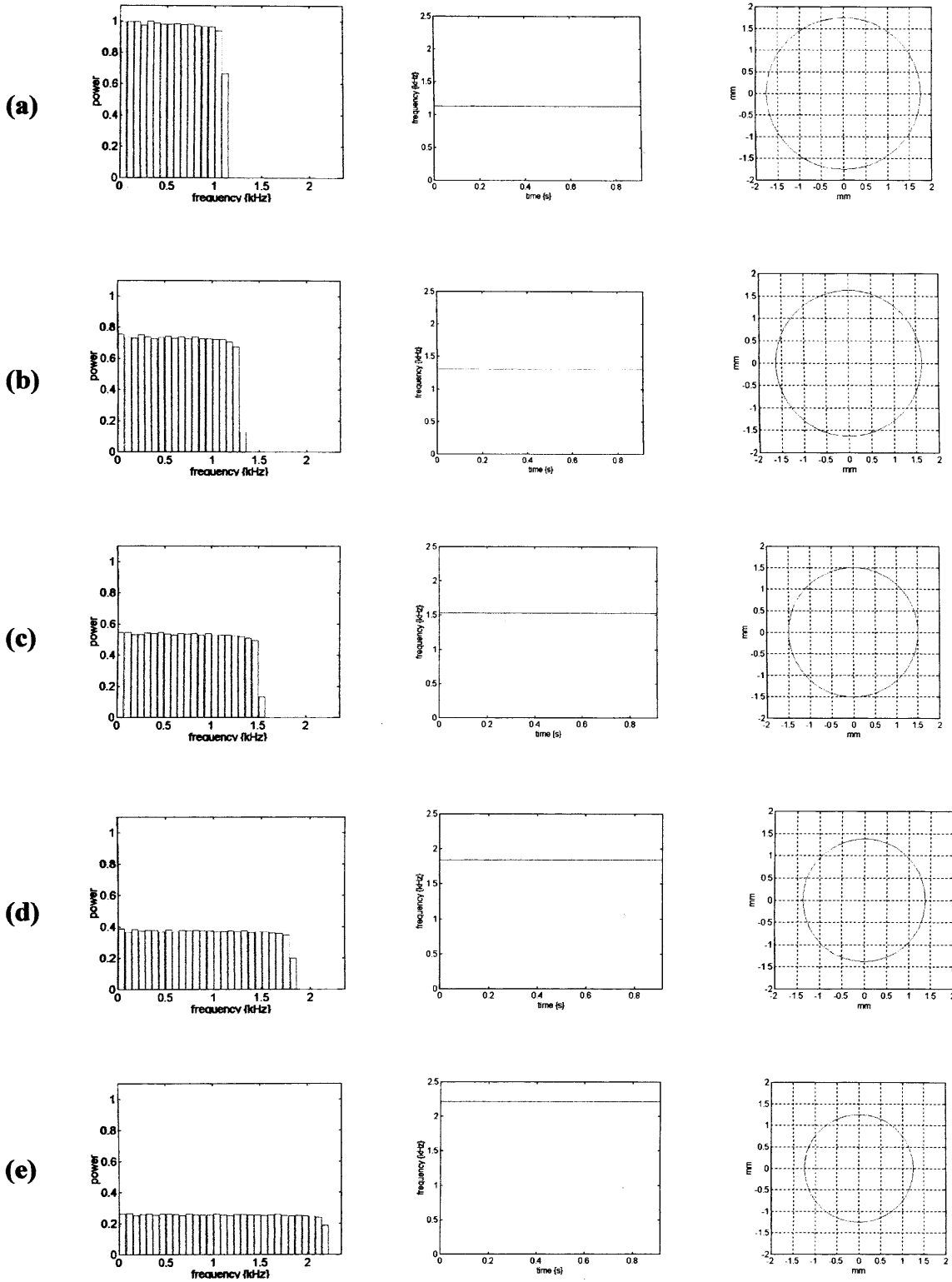


Figure 7.10(a-e) Modelled power spectra generated for five combinations of flow velocity and vessel diameter values giving equal volume flow rates (values given in table 7.1). In each case the power spectrum is shown alongside the relevant steady flow waveform and vessel size, and is plotted for an arbitrary time in the waveform.

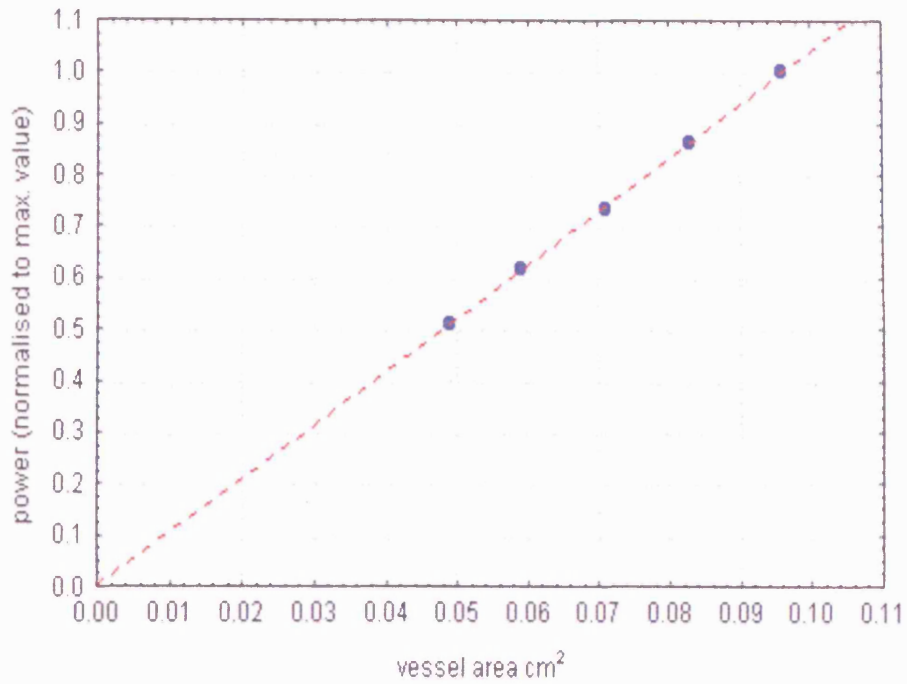


Figure 7.11 The relationship between vessel area and the total power contained in the modelled spectra. Modelled spectra were generated for steady flow, using five sets of vessel area and time-averaged peak velocity values to provide identical values for volume flow (see table 7.1 for values). Power values have been normalised to the maximum.

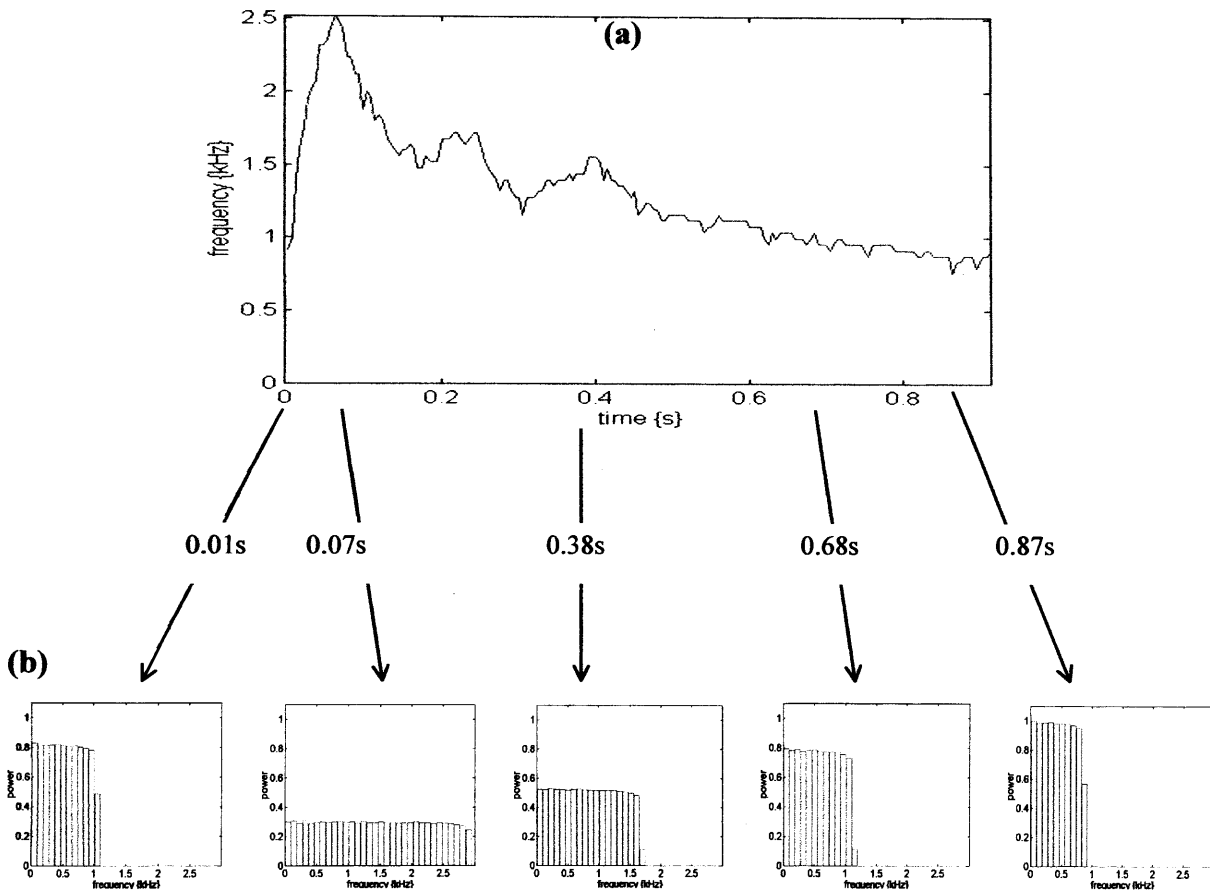


Figure 7.12 (a) pulsatile flow maximum frequency waveform envelope corresponding to a time-averaged peak velocity of 60cm s^{-1} . **(b)** modelled power spectra for five arbitrary times in the pulsatile flow waveform.

7.4 The Ensemble Mean Spectrum Correction Method

Owing to the uncertainty of both the beam shape across an in-vivo vessel and the position of the vessel in the beam, a precise correction for the effects of non-uniform insonation on the total Doppler signal power cannot be derived for individual cases. An alternative approach is therefore required, with one possibility being the reconstruction of the raw Doppler spectrum to give a spectral shape similar to that occurring for conditions of uniform insonation. Because in-vivo Doppler signals are inherently noisy, a correction applied to the spectrum occurring at any single sample time would be subject to inaccuracy. However, this source of error can be reduced by averaging the individual spectra over time and hence increasing the signal-to-noise ratio.

This section describes a simple spectral averaging method which can be applied to Doppler signals. In order to verify that the total spectral power obtained after averaging will still accurately reflect the signal power changes expected for specific changes in vessel area, average spectra were calculated for different flow conditions using the modelled spectra described in the previous section.

7.4.1 Derivation of the Ensemble Mean Spectrum

Spectral analysis of a Doppler signal produces a time series of power spectra (figure 7.13) which are used to generate the Doppler sonogram. The ensemble mean spectrum is formed for a beat (or any section of the signal in the case of steady flow) by taking the relevant individual spectra and averaging the power values in corresponding frequency bins over the number of spectra. The power $P_{ems}(f)$ in each frequency bin f of the ensemble mean spectrum is therefore given by:

$$P_{ems}(f) = \frac{\sum_{t=1}^{t=T} P(f,t)}{T} \quad [7.5]$$

where the parameter T represents the number of individual spectra in the beat.

If it is assumed that the flow profiles in a vessel are parabolic, and hence that the signal power spectrum at any instant in time is approximately rectangular, then the shape of the ensemble mean spectrum can be predicted. This shape will depend on whether the flow in the vessel is steady or pulsatile. For steady flow, all of the individual spectra will have the same maximum frequency value, and hence the ensemble mean spectrum will remain approximately rectangular (figure 7.14). For pulsatile flow, the maximum frequency values of the individual spectra will vary due to the changing blood velocity over the cardiac cycle. The ensemble mean spectrum will therefore only be rectangular in shape below the frequency corresponding to the minimum value of the maximum frequency envelope. All of the individual spectra have components below this frequency, and every spectrum therefore contributes to the ensemble mean spectrum power. With increasing frequency above this point, progressively fewer individual spectra have components and hence the ensemble mean spectrum power gradually decreases (figure 7.15).

The predicted ensemble mean spectrum shapes for steady and pulsatile flow can be verified using a simple model. For pulsatile flow, a maximum frequency envelope waveform (figure 7.17a) was

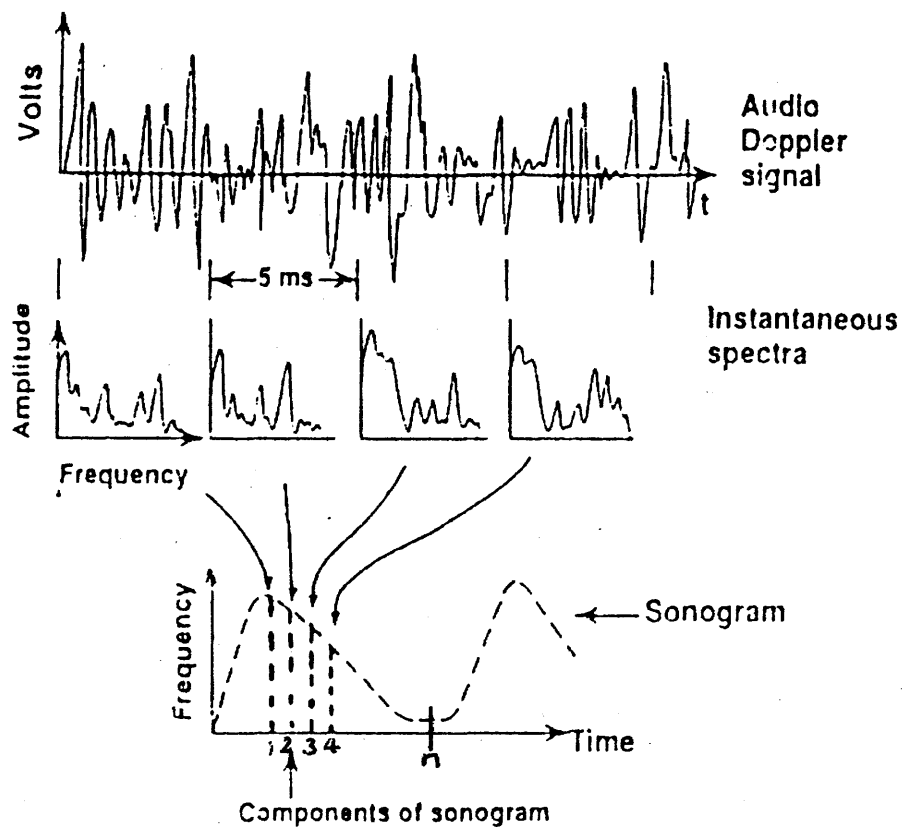


Figure 7.13 Formation of the Doppler sonogram (McDicken 1990)

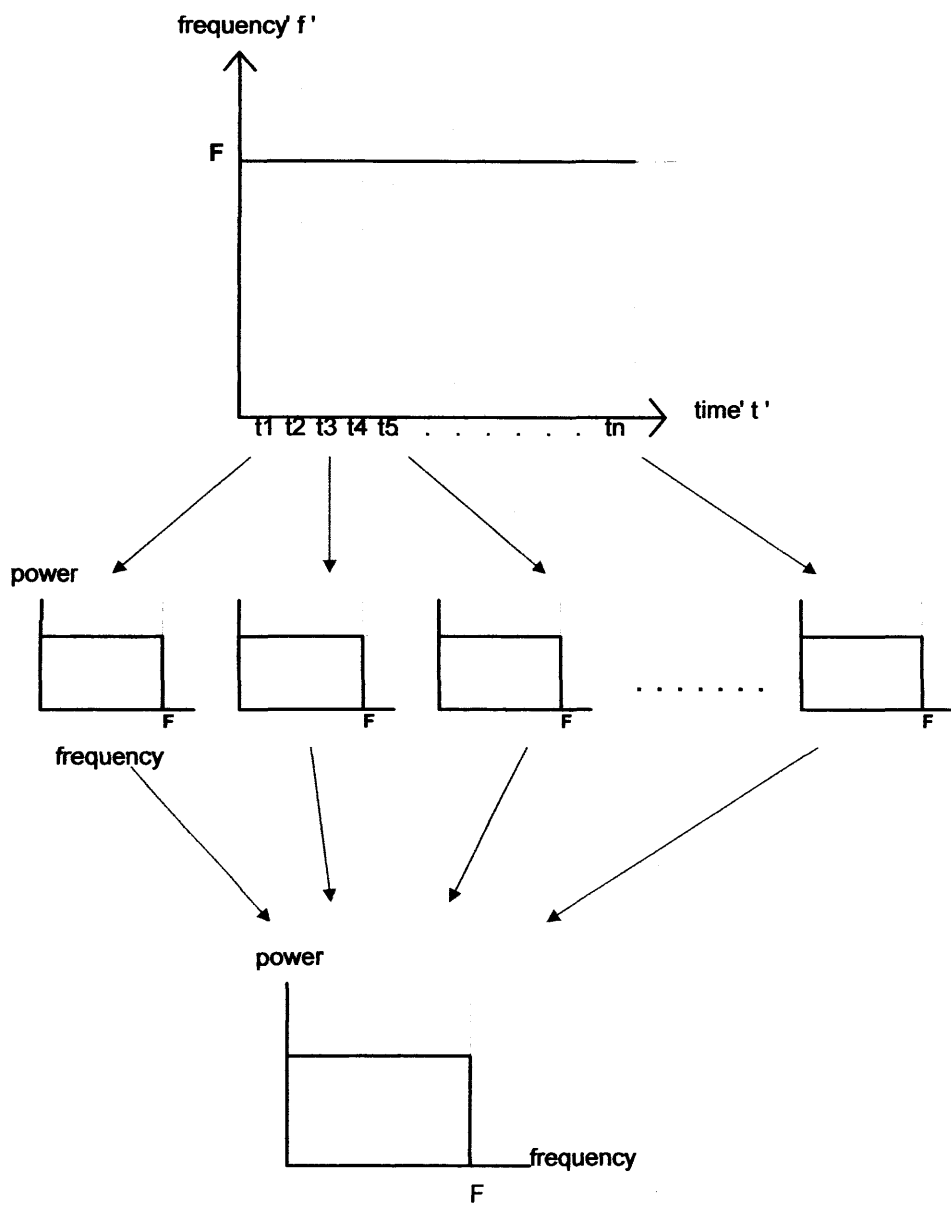


Figure 7.14 The generation of the ensemble mean spectrum from the spectral components of steady flow.

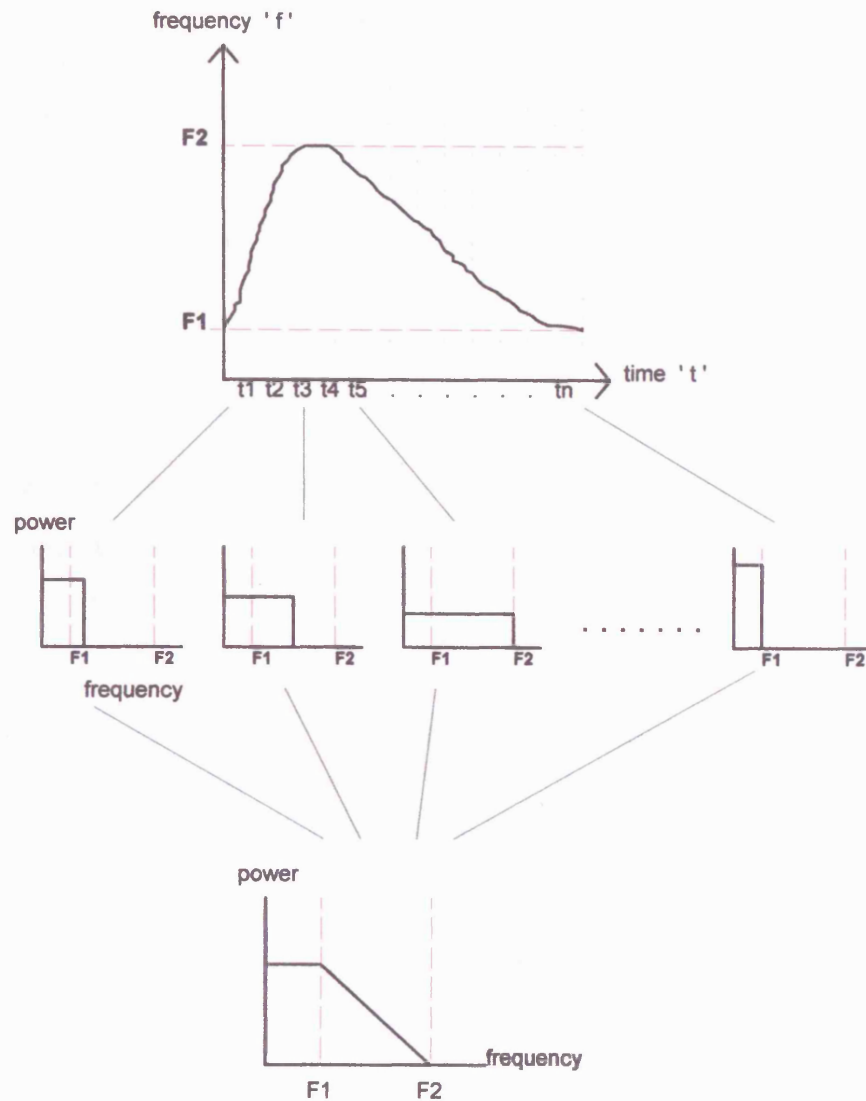


Figure 7.15 The generation of the ensemble mean spectrum from the spectral components of pulsatile flow. It should be noted that the decay in power between $F1$ and $F2$ is not necessarily a straight line.

derived from one cardiac cycle of a Doppler signal recorded from the MCA of a healthy adult at rest (see chapter 8 for envelope derivation and beat marking methods), and was smoothed using a five-point rectangular moving average technique. For steady flow, the maximum frequency envelope was created to have a constant value equal to the mean value of the pulsatile flow waveform (figure 7.16a), hence giving identical time-averaged peak velocity values for the pulsatile and steady flow cases. Assuming that the total power remained constant with time for both flow types (figures 7.16a and 7.17a), spectra were created at time intervals of 0.005 seconds throughout each waveform using this power value and the maximum frequency envelope value for the relevant time. Examples of these individual spectra are shown in figures 7.16b and 7.17b for steady and pulsatile flow respectively.

The ensemble mean spectrum was calculated for each type of flow by averaging the power values in corresponding frequency bins of the individual spectra over the number of spectra in the signal. The shape in each case can be seen to be close to that predicted; for steady flow the ensemble mean spectrum is approximately rectangular (figure 7.16c), and for pulsatile flow it is rectangular up to the frequency corresponding to the frequency envelope minimum value, but beyond this 'knee' frequency the power gradually decreases (figure 7.17c).

7.4.2 Testing the Ensemble Mean Spectrum

In order to verify that the use of this averaging method will provide an accurate representation of signal power changes arising from changes in vessel area, ensemble mean spectra were calculated for a range of flow conditions using the modelled spectra generated for pulsatile flow in the previous section.

Figures 7.18a-e show the ensemble mean spectra that were calculated for a vessel diameter of 3mm and time-averaged peak flow velocities of 50cms⁻¹, 55cms⁻¹, 60cms⁻¹, 65cms⁻¹ and 70cms⁻¹ respectively. A plot of velocity against the total power P_{ems} in each ensemble mean spectrum is given in figure 7.19, and verifies that power remains independent of velocity when values are calculated from the ensemble mean spectrum. Figures 7.20a-e show the ensemble mean spectra that were calculated for a time-averaged peak velocity of 60cms⁻¹ and vessel diameters of 1.5mm, 2mm, 2.5mm, 3mm and 3.5mm respectively, and the corresponding plot of P_{ems} against vessel area exhibits the correct proportional relationship (figure 7.21). Finally, the ensemble mean spectra were calculated for simultaneous changes in both velocity and vessel size (figures 7.22a-e), values for velocity and vessel area given in table 7.1), and the proportional relationship between P_{ems} and vessel area verified for this case (figure 7.23).

7.4.3 Theoretical Background to the Ensemble Mean Spectrum Correction

For in-vivo recordings from the MCA, the theoretical shape of the ensemble mean spectrum (figure 7.17c) will be distorted due to the effects of beam shape and high-pass filtering on the individual spectra from which it is calculated. High-pass filtering of the Doppler signal affects only the low frequency portion of the signal spectrum, but non-uniform insonation arising from spatial variations in beam intensity is likely to influence the power at all frequencies, with the extent of the

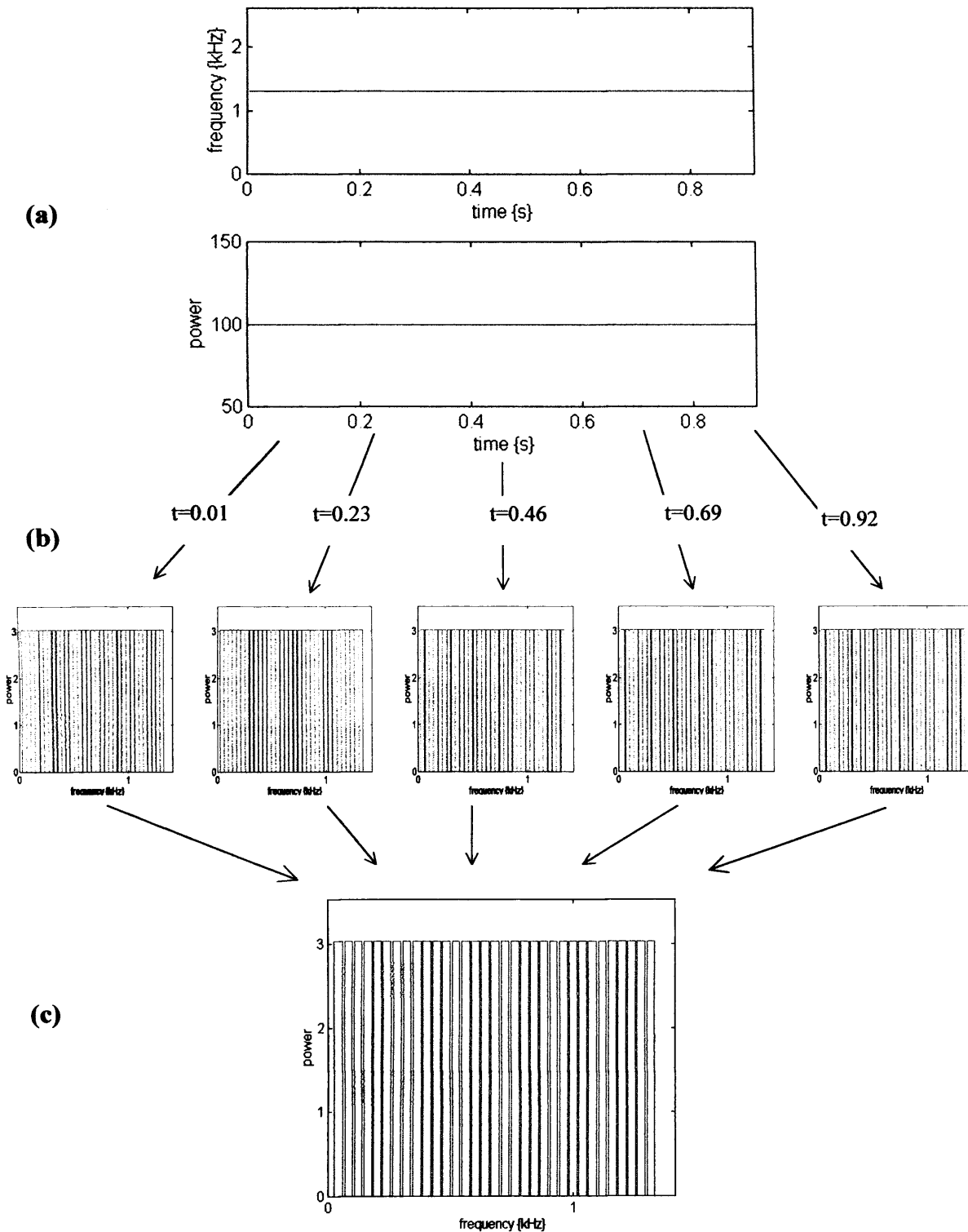


Figure 7.16 The Ensemble Mean Spectrum shape for steady flow. The assumption that total spectral power remains constant with time has been used to generate the power spectra at time intervals of 0.005 seconds in the steady flow waveform. Averaging the power values at each frequency over the number of spectra in the waveform produces the Ensemble Mean Spectrum. (a) shows the maximum frequency envelope and total power of the steady flow waveform, (b) examples of the spectra created at various times in the waveform, and (c) the resulting Ensemble Mean Spectrum shape. The units of power are arbitrary.

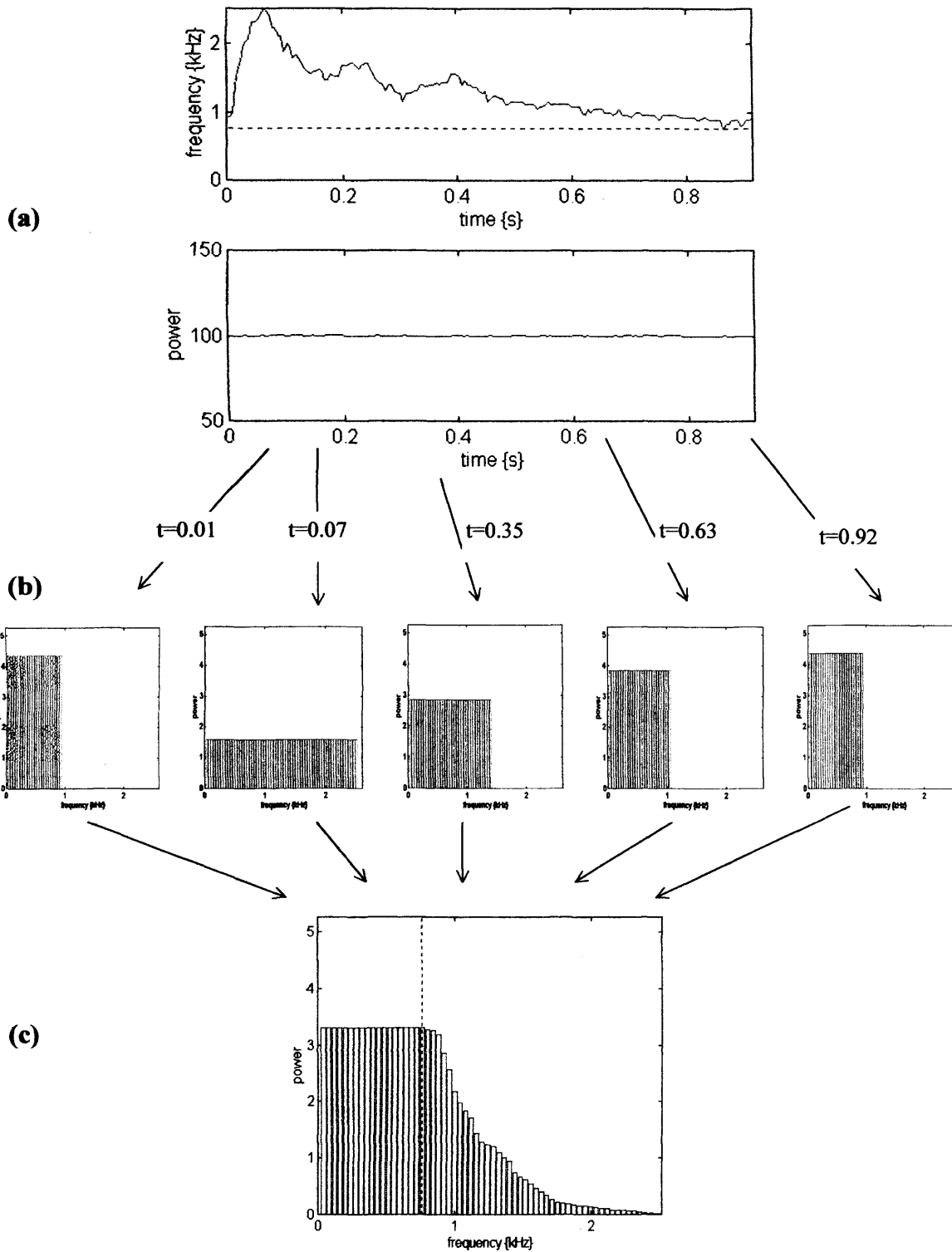


Figure 7.17 The Ensemble Mean Spectrum shape for pulsatile flow. The assumption that total spectral power remains constant with time has been used to generate the power spectra at time intervals of 0.005 seconds in the pulsatile waveform. Averaging the power values at each frequency over the number of spectra in the waveform produces the Ensemble Mean Spectrum. (a) shows the maximum frequency envelope and total power of the pulsatile waveform, (b) examples of the spectra created at various times in the waveform, and (c) the resulting Ensemble Mean Spectrum shape. The units of power are arbitrary.

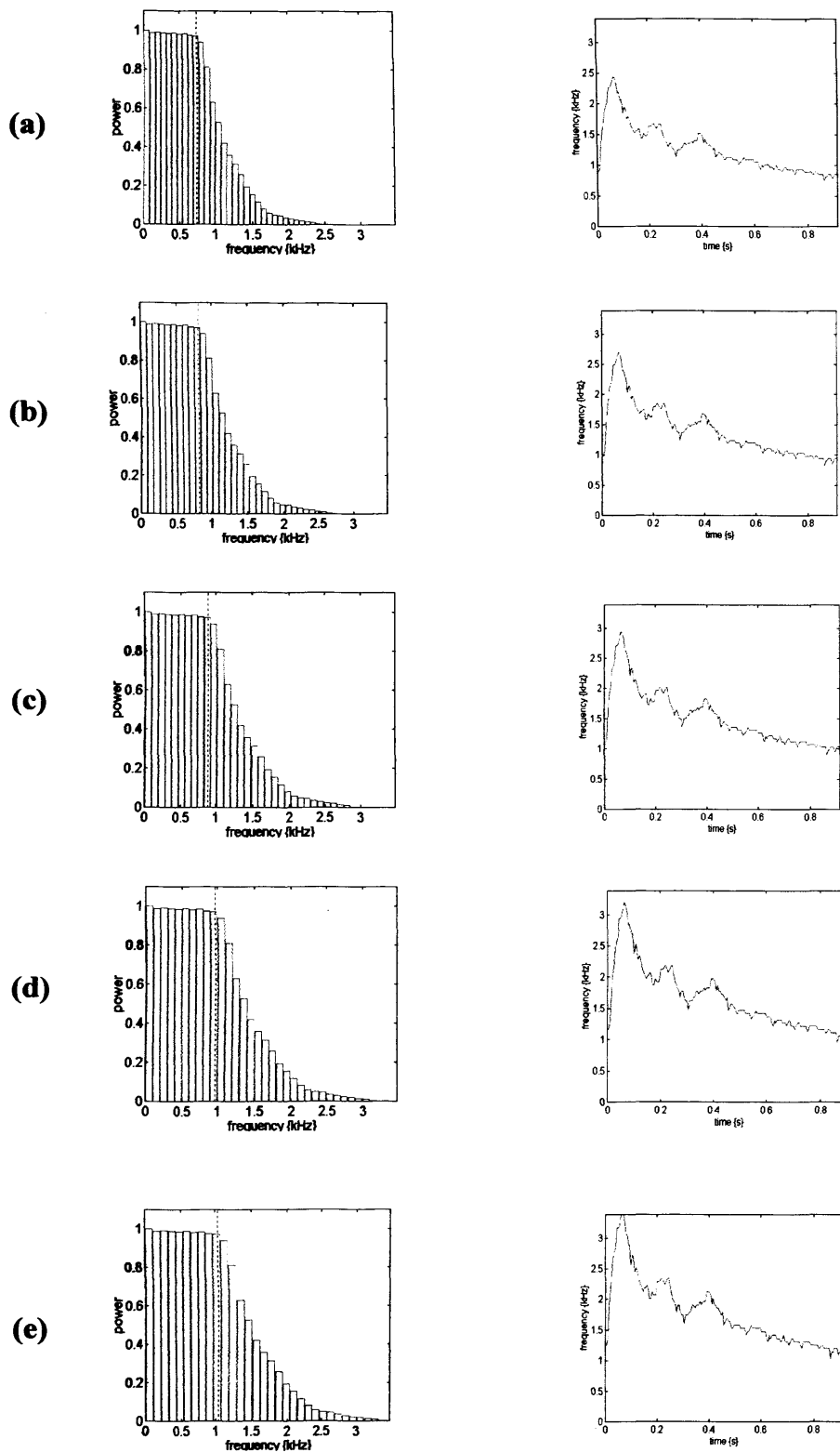


Figure 7.18(a-e) Ensemble mean spectra calculated from the modelled power spectra generated for a uniformly insonated vessel of diameter 3mm containing pulsatile flow with a time-averaged peak velocity of 50cm s^{-1} , 55cm s^{-1} , 60cm s^{-1} , 65cm s^{-1} and 70cm s^{-1} respectively. The maximum frequency waveform envelope is shown alongside the ensemble mean spectrum in each case.

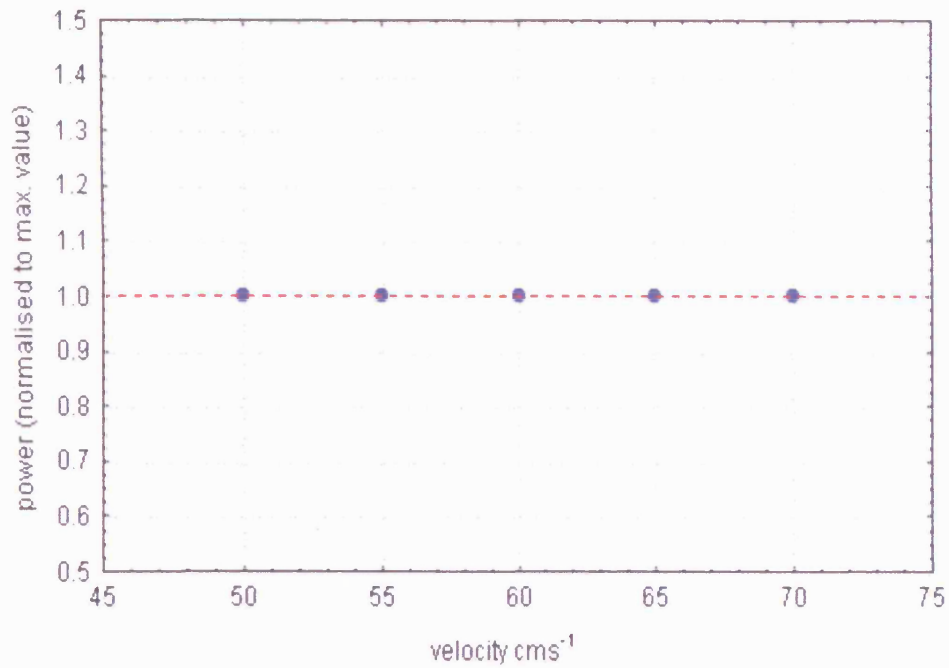


Figure 7.19 The relationship between velocity and the total power contained in the ensemble mean spectra derived from the modelled power spectra which were generated for a vessel of diameter 3mm containing pulsatile flow with a time-averaged peak velocity of 50cms⁻¹, 55cms⁻¹, 60cms⁻¹, 65cms⁻¹ and 70cms⁻¹ respectively. Power values have been normalised.

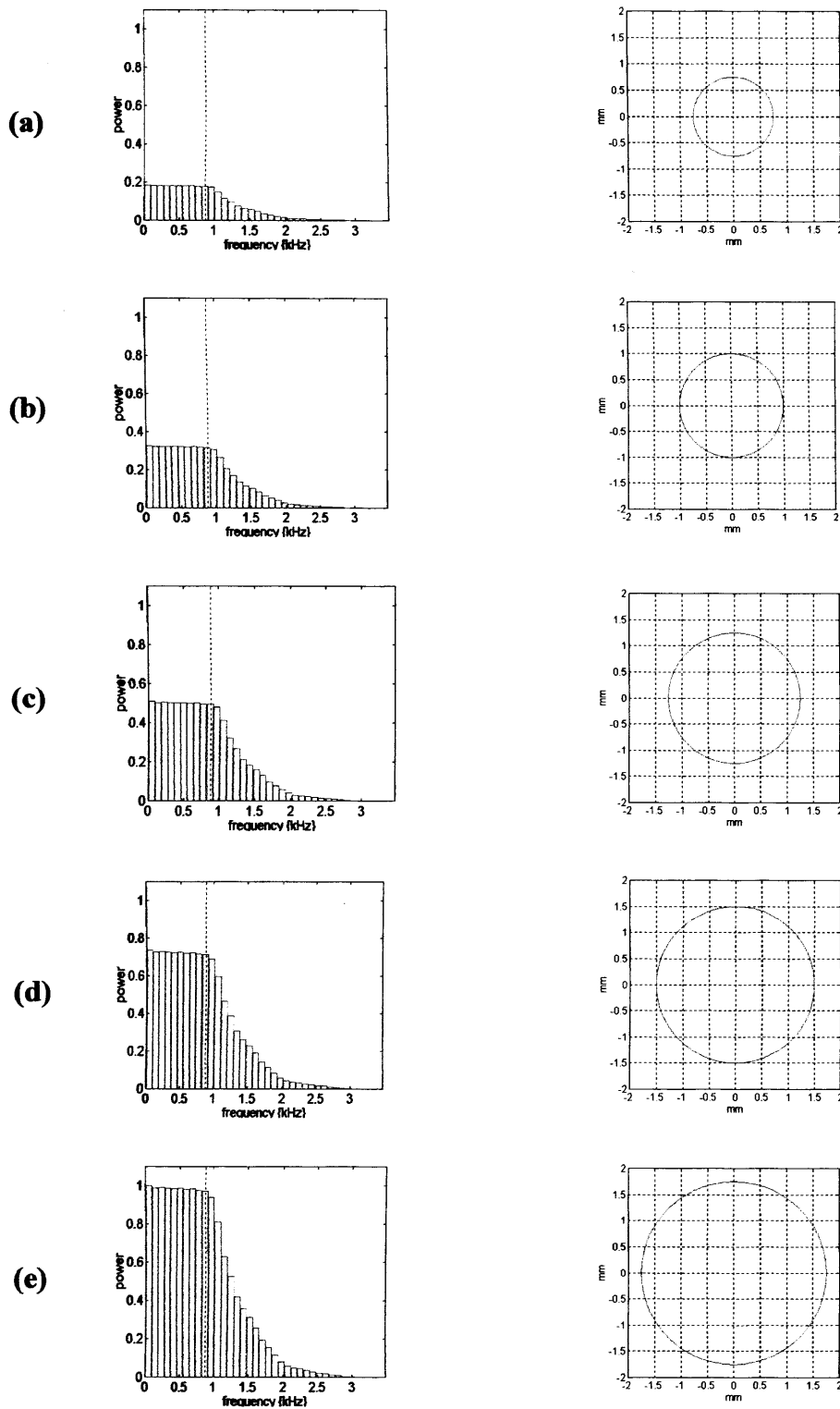


Figure 7.20(a-e) Ensemble mean spectra calculated from the modelled power spectra generated for uniformly insonated vessels of diameter 1.5mm, 2mm, 2.5mm, 3mm and 3.5mm respectively, containing pulsatile flow with a time-averaged peak velocity values 60cms^{-1} . The relevant vessel size is shown alongside the ensemble mean spectrum in each case.

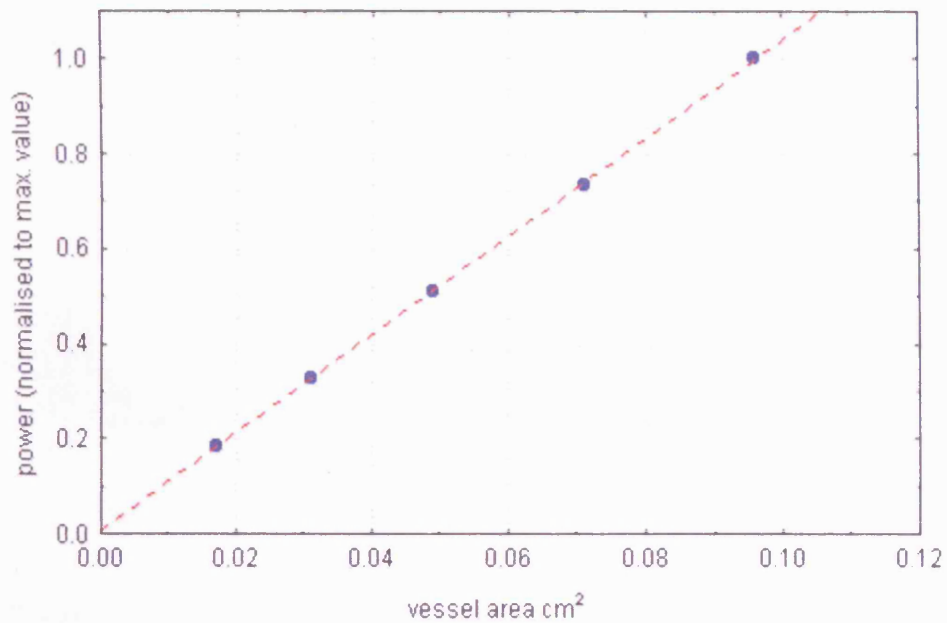


Figure 7.21 The relationship between velocity and the total power contained in the ensemble mean spectra derived from the modelled power spectra which were generated for vessels of diameter 1.5mm, 2mm, 2.5mm, 3mm, 3.5mm (corresponding to areas 0.017cm², 0.031cm², 0.049cm², 0.071cm² and 0.096cm² respectively) containing pulsatile flow with a time-averaged peak velocity of 60cms⁻¹. Power values have been normalised to the maximum.

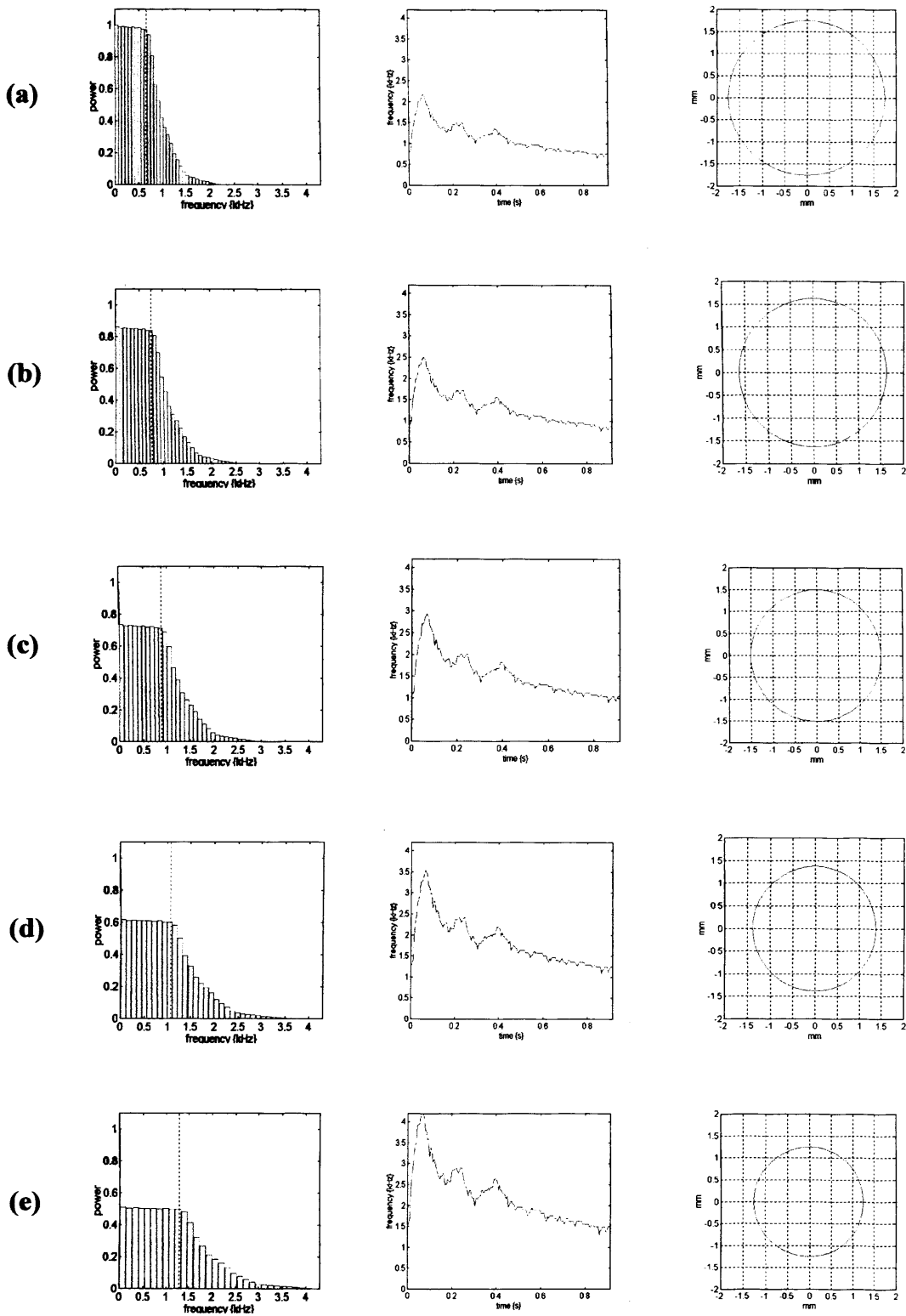


Figure 7.22(a-e) Ensemble mean spectra calculated from the modelled power spectra generated for uniform insonation and five combinations of flow velocity and vessel diameter values giving equal volume flow rates (values given in table 7.1). In each case the relevant pulsatile waveform and vessel size are plotted alongside the ensemble mean spectrum.

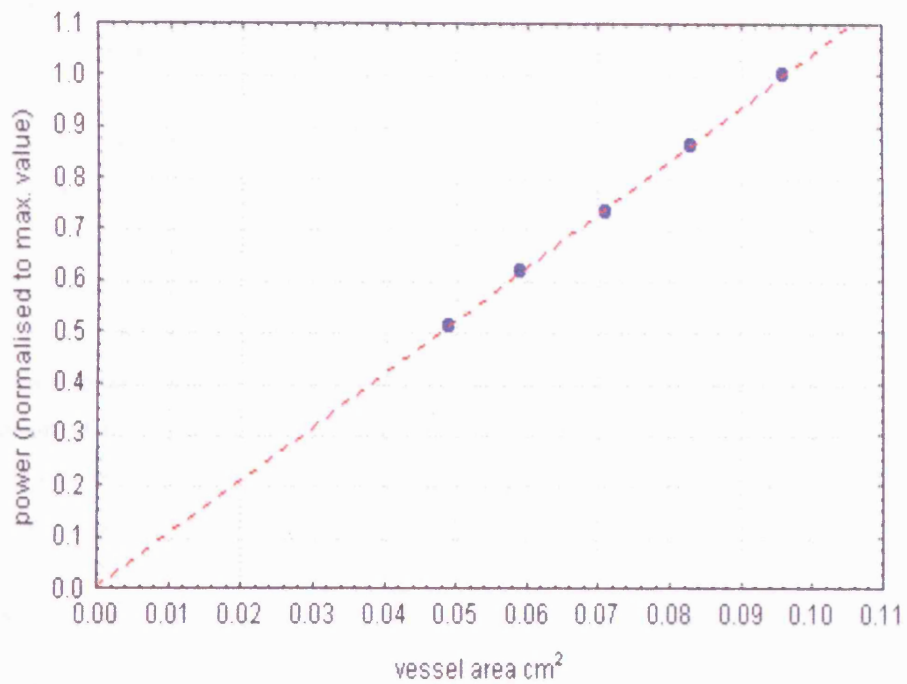


Figure 7.23 The relationship between velocity and the total power contained in the ensemble mean spectra derived from the modelled power spectra which were generated for pulsatile flow using five sets of vessel area and time-averaged peak velocity values to provide identical values for volume flow (see table 7.1 for values). Power values have been normalised to the maximum.

effect at each frequency depending on the beam shape across the vessel.

The effect of non-uniform insonation on the shape of the ensemble mean spectrum above the 'knee' frequency is unlikely to be obvious relative to the overriding effect of the averaging technique causing a gradual reduction in the power of the spectral components with frequencies above this. For the low frequency components below the knee, however, the rectangular shape that is present under conditions of uniform insonation is likely to be distorted, with the nature of the distortion depending on the insonation pattern across the vessel.

The proposed ensemble mean correction is based on approximate compensation for the effects of beam shape on the power values in each of the frequency bins above the knee frequency, plus the reconstruction of the theoretical rectangular shape of the ensemble mean spectrum below the knee frequency. The correction has the additional advantage of simultaneously compensating for the loss of spectral power caused by high-pass filtering.

Figure 7.24a shows a sketch of a Doppler sonogram and maximum velocity envelope $V_{max}(t)$ for a single cardiac cycle. The position of one frequency bin is given, and the velocity values corresponding to the upper and lower frequency limits of the bin are marked as V_1 and V_2 respectively. At any time in the beat, the maximum flow velocity V_{max} in the vessel is determined by the value of the maximum envelope at the relevant time. The velocity profile for parabolic flow at time t is shown in figure 7.24b, and the position of the frequency bin is marked. The volume of blood travelling with the velocities defined by this frequency bin will be contained within a single annulus in the vessel (figure 7.24c). The position and size of the annulus will depend on the upper and lower bin velocities, the maximum flow velocity and the radius of the vessel.

Equation 7.1 gave an expression for the blood velocity at a radius r in a vessel of radius R containing a parabolic flow profile with a maximum velocity V_{max} . For a particular bin f , rearranging this equation and substituting the upper and lower velocities (V_1 and V_2 respectively) gives expressions for the radial positions r_1 and r_2 corresponding to the blood flowing at these velocities at a time t :

$$r_1(f, t) = R \sqrt{1 - \frac{V_1(r_1)}{V_{max}(t)}} \quad [7.7a]$$

$$r_2(f, t) = R \sqrt{1 - \frac{V_2(r_2)}{V_{max}(t)}} \quad [7.7b]$$

For parabolic flow, the radial distance r_2 corresponding to the blood travelling with the minimum velocity for the bin will be greater than the radial distance r_1 corresponding to the maximum blood velocity. The cross-sectional area A of the annulus containing the blood travelling with velocities within the range covered by the bin f at a time t is therefore equal to:

$$A(f, t) = \pi \cdot r_2(f, t)^2 - \pi \cdot r_1(f, t)^2 \quad [7.8]$$

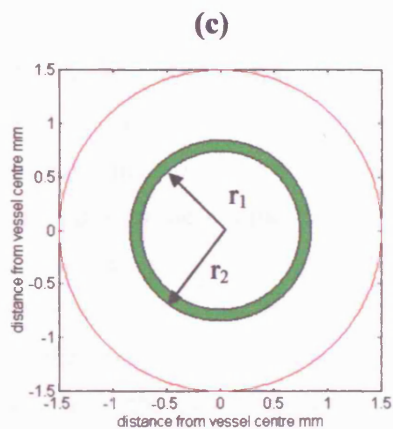
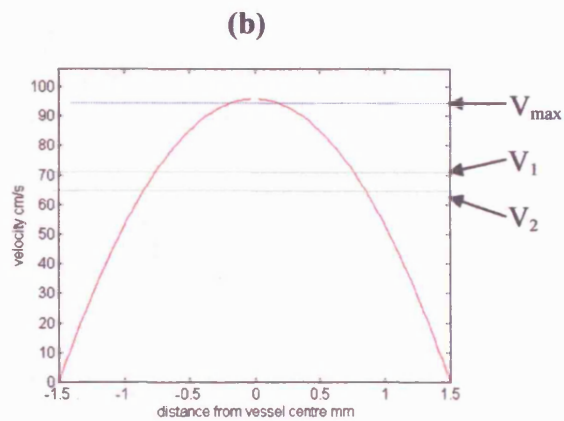
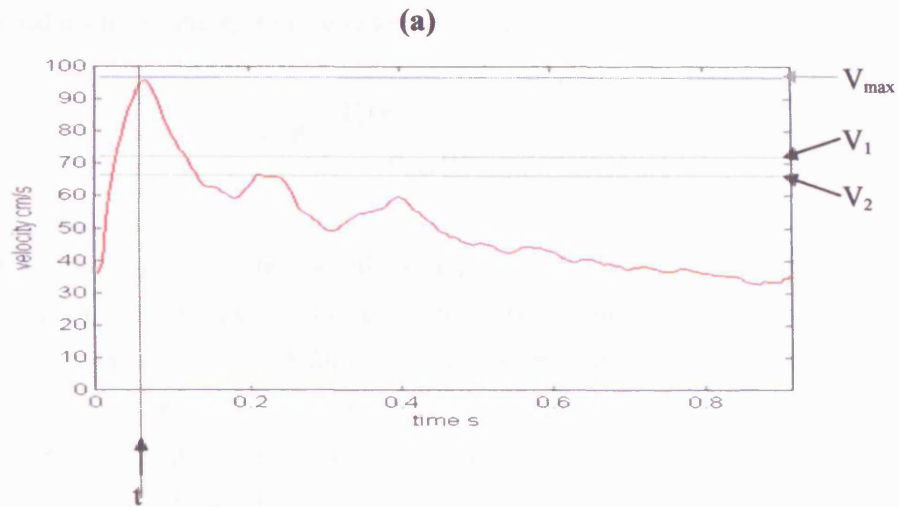


Figure 7.24 (a) a sketch of a Doppler sonogram and maximum velocity envelope for a single cardiac cycle, showing the upper and lower velocity limits V_1 and V_2 corresponding to a single frequency bin, and the maximum flow velocity V_{max} at time t in the cycle (b) the velocity profile for parabolic flow at time t , showing the the same velocities (c) a cross-sectional plot of a 3mm diameter vessel showing the position of the annulus at the specified time t in the cycle which contains the volume of blood travelling with the velocities relevant to the frequency bin shown in (a).

Substituting the values for r_1 and r_2 from equations 7.7a and 7.7b gives:

$$A(f, t) = \pi \cdot R^2 \left(\frac{V_1(r_1) - V_2(r_2)}{V_{\max}(t)} \right) \quad [7.9]$$

Figure 7.25a shows the position on the Doppler sonogram of the maximum frequency bin f_{\max} , which corresponds to the times in the cardiac cycle at which the maximum flow velocity is greatest. The velocity profile is shown in figure 7.25b for the time t corresponding to the greatest value of maximum flow velocity in the cycle. For this particular time in the beat it can be seen that the highest blood velocity contributing to the bin f_{\max} is equal to the maximum flow velocity. The value of r_1 is therefore zero (equation 7.7a) and the position of the vessel annulus containing the blood travelling with velocities falling within bin f_{\max} is at the vessel centre (figure 7.25c).

Because the annulus covers the centre of the vessel, its cross-sectional area can be defined by the radial distance $r_{\max 2}$ corresponding to the lower velocity $V_{\max 2}$ of the maximum frequency bin f_{\max} :

$$r_{\max 2}(f_{\max}, t) = R \sqrt{1 - \frac{V_{\max 2}(r_{\max 2})}{V_{\max}(t)}} \quad [7.10]$$

$$A(f_{\max}, t) = \pi \cdot r_{\max 2}(f_{\max}, t)^2 = \pi \cdot R^2 \left(\frac{V_{\max}(t) - V_{\max 2}(r_{\max 2})}{V_{\max}(t)} \right) \quad [7.11]$$

For an unfiltered Doppler signal, the magnitude of the power of the signal backscattered from a small unit area at any position in a vessel is theoretically equal to the product of the area and the sensitivity S of the received field of the transducer at that position (as discussed in chapters 5 and 6, received field sensitivity is equal to the square of the transmitted beam intensity I). The total power received from several such small areas is therefore equal to the product of the total area and the mean value of the beam sensitivities incident on the individual areas.

Following from this theory, the total signal power $P(f, t)$ contributing to a specific frequency bin f at any instant in time is equal to the product of the volume of blood flowing with the relevant velocities and the mean sensitivity $S(f, t)$ of the area of the beam covering the annulus of the vessel in which the blood is contained. For a constant sample volume length, the volume of blood is proportional to the cross-sectional area $A(f, t)$ of the relevant annulus. The signal power can therefore be expressed as:

$$P(f, t) = S(f, t) \cdot A(f, t) \quad [7.12]$$

An expression for the mean sensitivity of the area of the beam affecting the signal power contained in a frequency bin f at time t can be obtained from equation 7.12 by rearranging and substituting for $A(f, t)$ using equation 7.9:

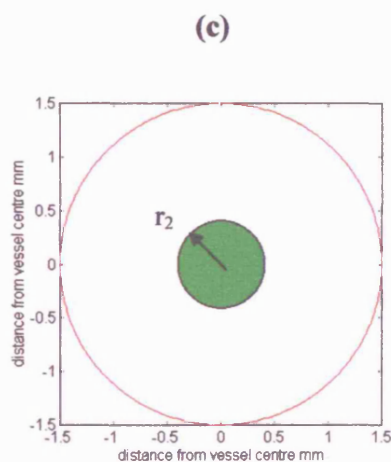
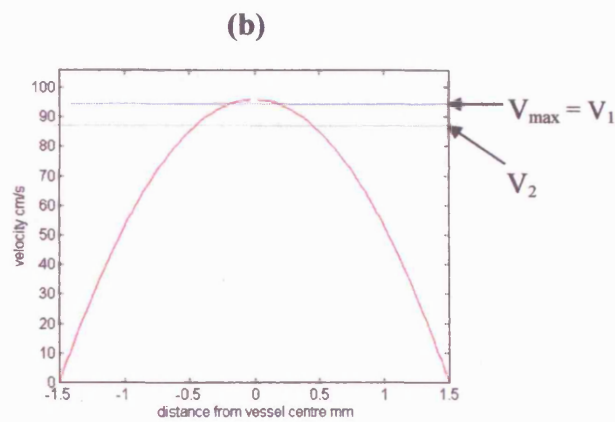
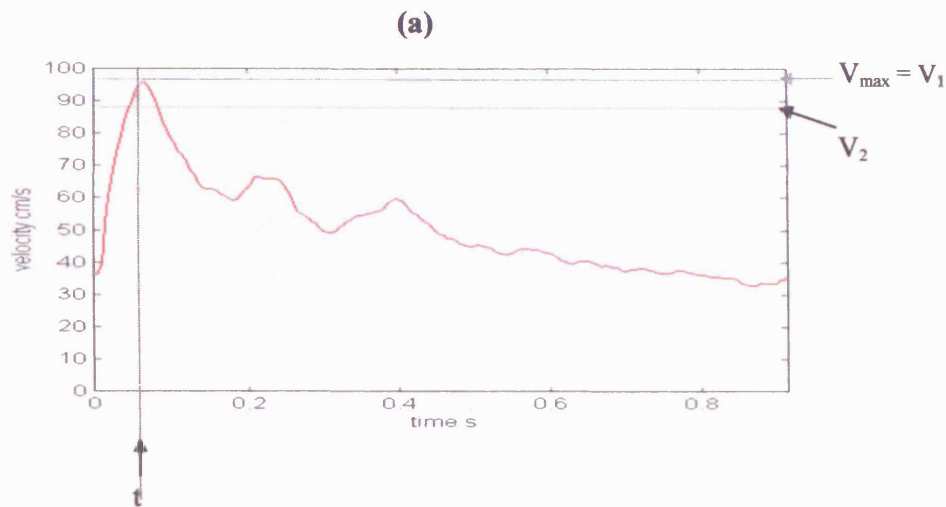


Figure 7.25 (a) a sketch of a Doppler sonogram and maximum velocity envelope for a single cardiac cycle, showing the upper and lower velocity limits V_1 and V_2 corresponding to the maximum frequency bin, and the maximum flow velocity V_{max} at time t in the cycle (b) the velocity profile for parabolic flow at time t , showing the the same velocities (c) a cross-sectional plot of a 3mm diameter vessel showing the position of the annulus at the specified time t in the cycle which contains the volume of blood travelling with the velocities relevant to the frequency bin shown in (a).

$$S(f, t) = \frac{P(f, t)}{A(f, t)} = \frac{P(f, t) \cdot V_{\max}(t)}{\pi \cdot R^2 (V_1(r_1) - V_2(r_2))} \quad [7.13]$$

Similarly, an expression for the mean sensitivity of the area of the beam affecting the signal power contained in the maximum frequency bin f_{\max} at time t can be obtained by substituting for $A(f_{\max}, t)$ using equation 7.11:

$$S_{\max}(f, t) = \frac{P(f_{\max}, t)}{A(f_{\max}, t)} = \frac{P(f_{\max}, t) \cdot V_{\max}(t)}{\pi \cdot R^2 (V_{\max}(t) - V_{\max 2}(r_{\max 2}))} \quad [7.14]$$

Because the maximum flow velocity V_{\max} in a vessel changes with time, so also will the position of the blood volume that is travelling with velocities relevant to a particular bin, owing to the dependence of the radial position on this parameter (equations 7.7a and b). Consequently, the mean beam sensitivity value that corresponds to the signal contributing to a particular frequency bin will also vary with time. Figure 7.26a shows a sketch of the Doppler sonogram and maximum frequency envelope for a single cardiac cycle, with the position of one frequency bin marked. The shaded block represents the area of the sonogram contributing to the total signal power for this bin, and illustrates the fact that the vessel contains blood travelling at velocities relevant to this bin during the time interval $T(f)$. At times T_1 and T_2 , the value of the maximum frequency envelope is approximately equal to the upper frequency limit of the bin, and hence the value of r_1 (equation 7.7a) is equal to zero. The annulus containing the blood travelling at the relevant velocities therefore falls at the centre of the vessel, as seen in figure 7.26b. For times between T_1 and T_2 , the value of the maximum frequency envelope is greater than the upper frequency limit of the bin, giving a value of r_1 that is greater than zero, and the annulus in each case is therefore positioned away from the vessel centre. The largest displacement of the annulus from the vessel centre occurs at the time for which the value of the maximum frequency envelope is greatest.

It can be deduced from figure 7.26b that the mean beam sensitivity $S(f)$ for a frequency bin f is equal to the average of the sensitivity values that occur at each time t within the relevant time interval $T(f)$ in the beat:

$$S(f) = \frac{\sum_{T_1(f)}^{T_2(f)} S(f, t)}{T(f)} \quad [7.15]$$

Substituting for $S(f, t)$ using equation 7.13 gives:

$$S(f) = \frac{1}{T(f) \pi \cdot R^2 (V_1(r_1) - V_2(r_2))} \cdot \left[\sum_{T_1(f)}^{T_2(f)} P(f, t) \cdot V_{\max}(t) \right] \quad [7.16]$$

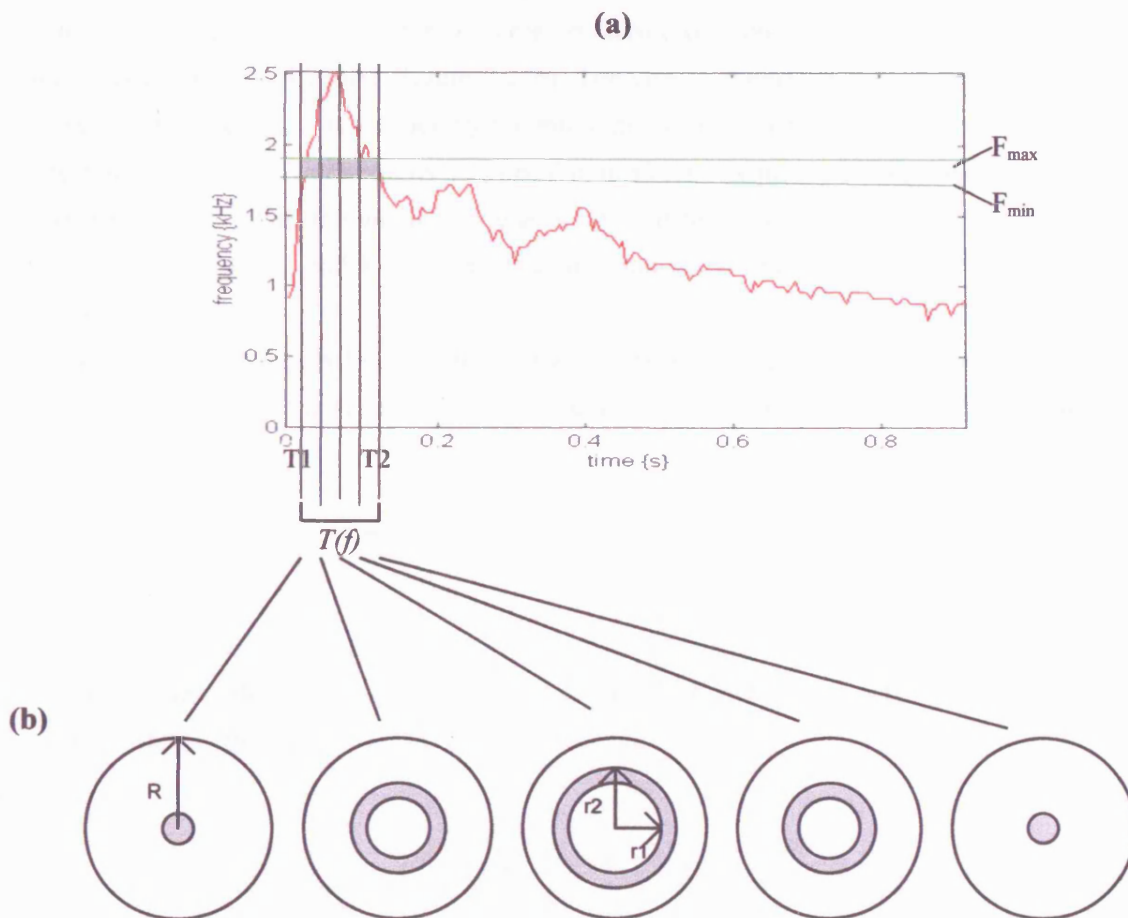


Figure 7.26 (a) The Doppler sonogram and maximum frequency envelope for a single cardiac cycle. The shaded block represents the region of the sonogram contributing to the total signal power for the marked frequency bin, and illustrates that the vessel contains blood travelling at velocities relevant to this bin during the time interval $T(f)$. **(b)** schematic representation of the variation in position with time of the vessel annulus containing the blood travelling with these velocities, shown for five different times within the interval $T(f)$. The true inner and outer radii (r_1 and r_2 respectively) of the annulus at each time are determined by the vessel radius R , the upper and lower limits (F_{\max} and F_{\min} respectively) of the relevant frequency bin, and the value of the maximum velocity envelope (see equations 7.7a & b).

The same theory can be applied to the maximum frequency bin f_{max} ; figure 7.27a shows the position of this bin on the Doppler sonogram, with the shaded block representing the area of the sonogram contributing to the total signal power at the relevant frequencies. For this case, however, the highest blood velocity contributing to the bin is equal to the maximum flow velocity V_{max} at all times within the interval $T(f_{max})$. The value of r_1 is therefore zero (equation 7.7a) and the position of the vessel annulus is at the vessel centre (figure 7.27b). The cross-sectional area of the annulus at any time t within the interval $T(f_{max})$ is defined by the maximum flow velocity V_{max} and the radial distance r_{max2} corresponding to the lower velocity V_{max2} of the maximum frequency bin f_{max} (equation 7.10). Hence, as seen in figure 7.27b, the annulus size is greatest at the time within the interval $T(f_{max})$ when the difference between V_{max} and V_{max2} is greatest, and smallest at times T_1 and T_2 when V_{max} and V_{max2} are closest in value.

As for other frequency bins, the mean beam sensitivity $S(f_{max})$ for the maximum frequency bin f_{max} is equal to the mean of the sensitivity values occurring within the time interval $T(f_{max})$ in the beat:

$$S(f_{max}) = \frac{\sum_{T_1(f_{max})}^{T_2(f_{max})} S(f_{max}, t)}{T(f_{max})} \quad [7.17]$$

Substituting the value for $S(f_{max}, t)$ given in equation 7.14 provides an expression for the mean beam sensitivity $S(f_{max})$ for the maximum frequency bin f_{max} :

$$S(f_{max}) = \frac{1}{T(f_{max})\pi \cdot R^2} \cdot \left[\sum_{T_1(f_{max})}^{T_2(f_{max})} P(f_{max}, t) \cdot \frac{V_{max}(t)}{(V_{max}(t) - V_{max2}(r_{max2}))} \right] \quad [7.18]$$

For equation 7.18, the time interval $T_1(f_{max})$ to $T_2(f_{max})$ is relatively short, and hence the variation of $V_{max}(t)$ over this interval is small. It can therefore be assumed that the value of V_{max} is constant with time. In order to give a better estimate of the maximum velocity envelope over the relevant interval, the value of the constant is set to be equal to the mean value of the maximum velocity envelope, $V_{mean}(f_{max})$, calculated for the relevant time interval $T(f_{max})$. Because the value of the lower bin velocity $V_{max2}(r_{max2})$ is also constant with time, the whole velocity term can be removed from the summation. The remaining summation of the power $P(f_{max}, t)$ is proportional to the power value $P_{ems}(f_{max})$ in the corresponding frequency bin of the ensemble mean spectrum (see equation 7.5), and can therefore be replaced by this value. Equation 7.18 therefore becomes:

$$S(f_{max}) \approx \frac{1}{T(f_{max})\pi \cdot R^2} \cdot \frac{V_{mean}(f_{max})}{(V_{mean}(f_{max}) - V_{max2}(r_{max2}))} \cdot P_{ems}(f_{max}) \quad [7.19]$$

Making the same assumption of constant maximum velocity over the time interval $T_1(f)$ to $T_2(f)$ for equation 7.16 again allows removal of the velocity term from the summation, and hence the replacement of the power summation with the relevant ensemble mean power $P_{ems}(f)$, although it

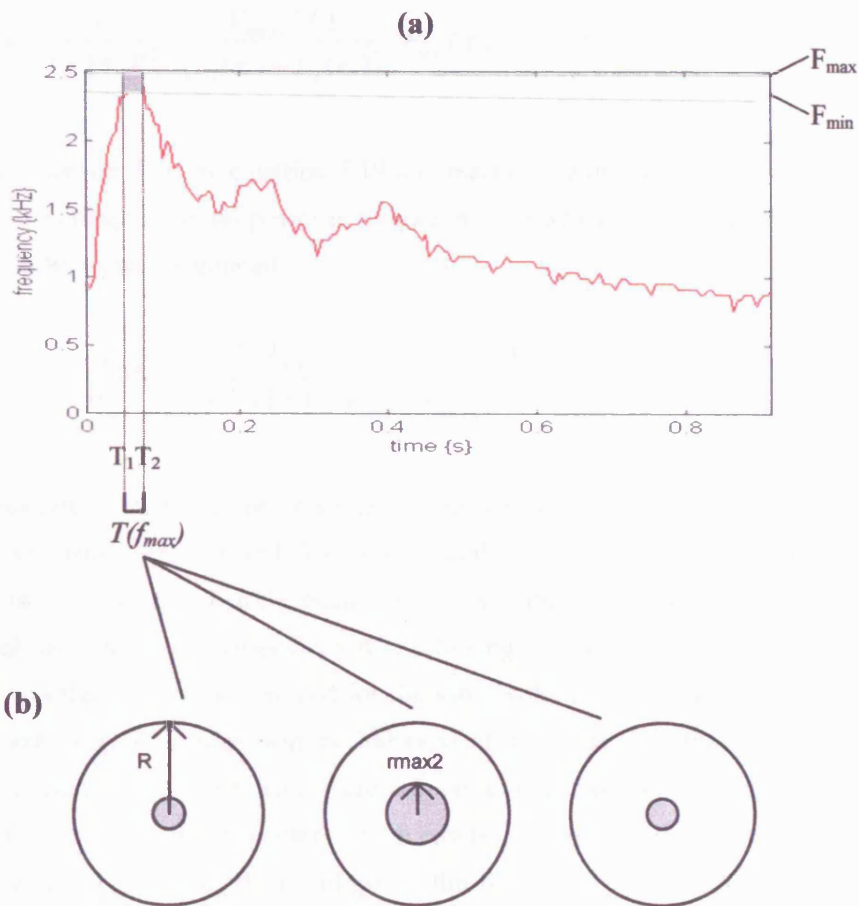


Figure 7.27 (a) The Doppler sonogram and maximum frequency envelope for a single cardiac cycle. The shaded block represents the region of the sonogram contributing to the total signal power for the marked maximum frequency bin, and illustrates that the vessel contains blood travelling at velocities relevant to this bin during the time interval $T(f_{max})$. **(b)** schematic representation of the variation in position with time of the vessel annulus containing the blood travelling with these velocities, shown for three different times within the interval $T(f_{max})$. At each time, the maximum flow velocity for this bin is equal to the value of the maximum velocity envelope, and the annuli therefore cover the central region of the vessel. The true radius r_{max2} of the annulus at each time is defined by equation 7.10.

should be noted that the accuracy of the assumption of constant maximum velocity will be increasingly reduced for the lower frequency bins owing to the longer time intervals $T(f)$ over which the signal originates in the cardiac cycle. Equation 7.16 therefore becomes:

$$S(f) \approx \frac{1}{T(f)\pi \cdot R^2} \cdot \frac{V_{mean}(f)}{(V_1(r_1) - V_2(r_2))} \cdot P_{ems}(f) \quad [7.20]$$

Finally, dividing equation 7.20 by equation 7.19 and rearranging provides an expression for the mean beam sensitivity affecting the signal power in frequency bin f which is independent of the radius of the vessel from which the signal originated:

$$S(f) \approx S(f_{max}) \cdot \frac{P_{ems}(f)}{P_{ems}(f_{max})} \cdot \frac{T(f_{max})}{T(f)} \cdot \frac{V_{mean}(f)}{V_{mean}(f_{max})} \cdot \frac{(V_{mean}(f_{max}) - V_{max2}(r_{max2}))}{(V_1(r_1) - V_2(r_2))} \quad [7.21]$$

Figure 7.27b illustrates that the Doppler signals contributing to the maximum frequency bins of an ensemble mean spectrum are received from the central region of the vessel. If the position of the vessel in the beam is stationary, then the beam sensitivity pattern at the centre of a vessel will not vary even if the vessel increases or decreases in size. Following from this, if the value of $P_{ems}(f_{max})$ for any ensemble mean spectrum is always derived for the same volume of blood, then the intensity pattern across the relevant central annulus will be identical at all times, and the value of $S(f_{max})$ will be approximately constant. This term can therefore be eliminated from equation 7.20, leaving an expression for $S(f)$ composed of parameters which can be calculated directly from the ensemble mean spectrum and the maximum velocity envelope of the relevant beat. The derivation of $P_{ems}(f_{max})$ is discussed below.

Calculation of $P_{ems}(f)$

The values of $P_{ems}(f)$ can be extracted directly from the ensemble mean spectrum. However, in order to reduce the effects of speckle on the spectrum, a more robust evaluation of the true power in each of the frequency bins is obtained by averaging the values from the relevant bin and those on either side.

Calculation of $P_{ems}(f_{max})$

As stated previously, to allow elimination of the term $S(f_{max})$ from equation 7.20, the value of $P_{ems}(f_{max})$ for any ensemble mean spectrum calculated from a particular Doppler signal must always be derived for a central annulus of the same radius so that it can be assumed that the beam sensitivities affecting this power value remain constant.

In order to define the maximum frequency section of an ensemble mean spectrum that corresponds to the signal received from a central annulus of a known fixed radius, it is necessary to know the flow velocity of the blood travelling at the edge of the annulus. This can be calculated from

equation 7.1. However, it can be seen that the velocity value is dependent on the radius R of the vessel, a parameter which is unknown and potentially variable for clinical Doppler recordings. Consequently, the assumption of a constant central annulus radius can only be an approximation for any signal, owing to the possibility that the vessel may change in size during the recording.

To optimise the approximation, a method of extracting a value for $P_{ems}(f_{max})$ which minimises any variation in the size of the central annulus is required. Equation 7.1 can be rearranged to give an expression for the radius of a centre annulus before (r_{c1}) and after (r_{c2}) a change in vessel radius from R_1 to R_2 respectively:

$$r_{c1} = R_1 \sqrt{1 - \frac{V(r_{c1})}{V_{max}}} \quad [7.22a]$$

$$r_{c2} = R_2 \sqrt{1 - \frac{V(r_{c2})}{V_{max}}} \quad [7.22b]$$

By setting the ratio of the flow velocity $V(r_c)$ at the edge of the central annulus and the centre stream maximum flow velocity V_{max} to equal a constant value, the square root term in equations 7.22a and b can be denoted as a constant k , and the radius of the centre annulus will therefore depend only on the vessel radius. An expression for the magnitude of the change in the radius $|\Delta r_c|$ of the central annulus in terms of the magnitude of the change in vessel radius $|\Delta R|$ can be derived from the difference between equations 7.22a and b:

$$|\Delta r_c| = |\Delta R| \cdot k \quad [7.23]$$

If the vessel changes in size, then the radius of the centre annulus will also change by an amount determined by the chosen value of the velocity ratio. If the velocity at the edge of the annulus is selected to be close to the centre maximum velocity then the ratio will approach unity, and hence the constant k will be small and any variation in the size of the centre annulus will be minimised. However, the closer the values of $V(r_c)$ and V_{max} , the smaller the size of the centre annulus and therefore the smaller the volume of blood that is contributing to the relevant section of the ensemble mean spectrum. If the signal contributing to the value of $P_{ems}(f_{max})$ originates from a small volume of blood, then the estimate of the blood volume that the power value provides is likely to be less accurate, and hence the ensemble mean spectrum correction becomes less robust.

In order to overcome these conflicting requirements, a compromise must be reached by assigning a value to the velocity ratio of $V(r_c)$ and V_{max} which maximises the volume of blood contributing to the value of $P_{ems}(f_{max})$ but minimises any changes in the size of the central annulus. This velocity ratio value can be derived by progressively decreasing the ratio value and observing the effects on the relationship between total power and vessel size that is obtained after the ensemble mean spectrum correction has been implemented; the smallest ratio value for which a proportional relationship is still observed can be assumed to be the optimum value for use in the correction. The derivation of a

suitable ratio value for ensemble mean spectra calculated from modelled Doppler spectra is described in section 7.4.4 below.

Calculation of the Velocity Parameters

The value of V_{max} in equation 7.16 is equal to the maximum value of the maximum velocity envelope of the beat from which the ensemble mean Doppler spectrum has been calculated. The remaining velocity parameters in the equation relate to the upper and lower frequency limits of each bin f , and can be derived from the frequency bin size and the relevant bin frequency.

7.4.4 Correcting the Ensemble Mean Spectrum

Dividing the ensemble mean spectrum power in each frequency bin by the calculated sensitivity value $S(f)$ theoretically provides a value which is directly proportional to the cross-sectional area of the vessel that contains blood travelling with velocities corresponding to those covered by the relevant bin (equation 7.21). By implementing this procedure for each frequency bin from the knee frequency upwards, the ensemble spectrum power in this frequency range is therefore corrected for the effects of non-uniform insonation. The effects of beam shape on the spectral power below the knee frequency can be eliminated by reconstructing the theoretical rectangular shape of the spectrum, by extrapolating the corrected power value for the knee frequency bin to replace the power values below this frequency.

In order to apply the correction described above to any ensemble mean spectrum, a suitable value must first be derived for the velocity ratio defining the size of the central vessel annulus and hence the value of $P_{ems}(f_{max})$. This was estimated for simulated Doppler signals by generating spectra for five combinations of velocity and vessel diameter values, for vessel positions giving the maximum total signal power received from a beam recorded for a homogeneous path through water. In each case, the vessel cross-sectional area and the flow velocity were selected to give an identical flow rate (values are given in table 7.1). The simulated power spectra were used to calculate the ensemble mean spectrum for each vessel, and the total power in each ensemble mean spectrum was calculated before and after correction for beam shape and filtering using the method described in section 7.4.3. These total power values are shown in figure 7.28a-f, for correction factors derived using $P_{ems}(f_{max})$ values defined by velocity ratio values of 0.95, 0.925, 0.9, 0.85, 0.8 and 0.7 respectively. It can be seen that the ensemble mean spectrum correction re-establishes an approximately proportional relationship between total power and vessel size for $P_{ems}(f_{max})$ values calculated for velocity ratio values of 0.95 and 0.925, but for values below this the proportionality increasingly degenerates. The plots demonstrate that for the lower velocity ratio values, the detrimental effect on the correction of the greater change in the area of the central annulus caused by the changing vessel size outweighs the benefit of the larger central annulus size.

As stated previously, the smallest velocity ratio value producing $P_{ems}(f_{max})$ values for which a proportional relationship between corrected total power and vessel size is still observed can be assumed to be the optimum value for use in the correction. Based on the results seen in figure 7.28, a

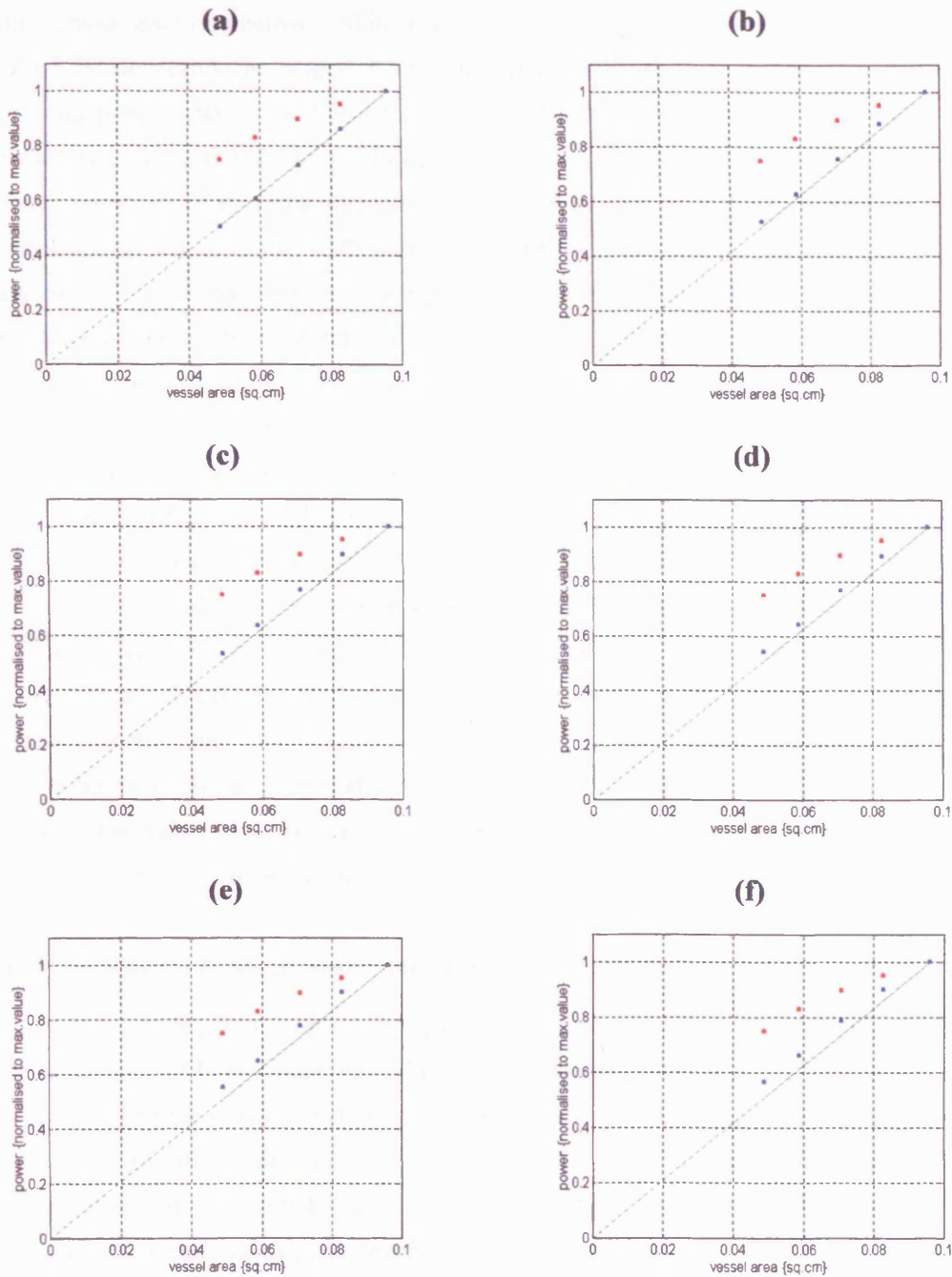


Figure 7.28 The relationship between Doppler power and vessel cross-sectional area for simultaneous changes in velocity and vessel size (see table 7.1 for values). The dotted line (---) illustrates the proportional relationship predicted by theory. Power values are calculated as the total power in the ensemble mean spectra derived from Doppler signals modelled for conditions of non-uniform insonation using a beam shape recorded for a homogeneous water path, and are plotted before (●) and after (●) correction for beam shape and filtering, with the value of $P_{ems}(f_{max})$ in the correction factor being defined by a velocity ratio of (a) 0.95 (b) 0.925 (c) 0.9 (d) 0.85 (e) 0.8 (f) 0.7.

velocity ratio value of 0.925 was therefore used for all investigations of the ensemble mean spectrum correction method described below, and in all following sections of this chapter.

Figure 7.29 illustrates the stages of the correction procedure for an ensemble mean spectrum generated from power spectra modelled for a 3.5mm diameter vessel containing pulsatile parabolic flow with a time-averaged velocity of 44.4cm s^{-1} . Figure 7.29a shows the ensemble mean spectrum obtained for conditions of uniform insonation, which can be seen to display the shape expected from theory (see section 7.4.1). Figure 7.29b shows the ensemble mean spectrum obtained for non-uniform insonation of the vessel by a beam shape plotted for a homogeneous water path, plus high-pass filtering of the modelled power spectra, and illustrates the distortion in shape occurring below the knee frequency and a reduction in spectral magnitude at all frequencies. Figure 7.29c displays the ensemble mean spectrum after correction for the effects of non-uniform insonation on the spectral components between the knee and the maximum frequency using the method described in section 7.4.3, and demonstrates that partial compensation is achieved for the reduction in magnitude caused by non-uniform insonation at these frequencies. The fact that the correction does not wholly compensate for the loss of power at the knee frequency may not be important if the amount of the shortfall is dependent on vessel size. Finally, figure 7.29d shows the ensemble mean spectrum after extrapolation of the corrected power value at the knee to replace the spectrum values below this frequency, and demonstrates that the final shape much more closely resembles that seen for conditions of uniform insonation in figure 7.29a. In order that this final stage of the spectrum correction is not dependent on a single value, the value used for the extrapolation is calculated from the mean power in the knee frequency bin and the bin on either side.

7.5 Testing the Ensemble Mean Spectrum Correction Method

The accuracy of the proposed ensemble mean spectrum correction method in counteracting the distorting influences of beam shape and filtering on the relationship between total power and vessel size was investigated for a range of flow velocities and vessel sizes, using modelled spectra generated for pulsatile flow waveforms derived from an in-vivo MCA signal and from the signals recorded from the wall-less flow phantom described in chapter 3. The effects of high-pass filtering and beam shape on the spectra were simulated using the methods described in sections 7.2.1 and 7.2.2 respectively. For the latter, a range of non-uniform insonation conditions were investigated using the beam shapes recorded for a beam path through water and for beam paths through five bone samples (chapters 5 and 6). By applying the proposed correction to the ensemble mean spectrum derived from the modelled spectra, the ability of the correction method to re-establish the proportional relationship between total power and vessel size could be observed.

7.5.1 MCA Pulsatile Flow

Changes in Blood Flow

For each beam shape, the vessel position giving the maximum total signal power value for the

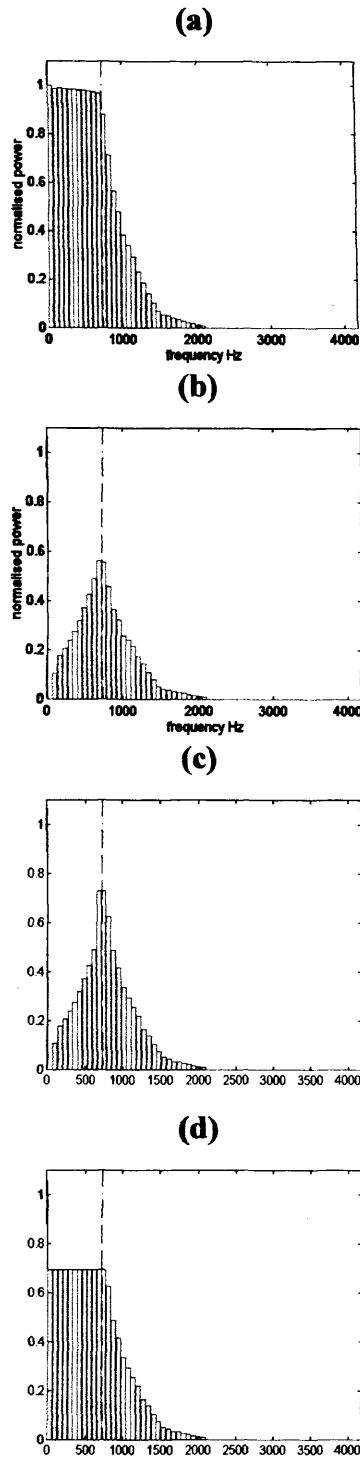


Figure 7.29 (a) The ensemble mean spectrum generated from the power spectra modelled for uniform insonation of a 3.5mm diameter vessel containing pulsatile parabolic flow with a time-averaged velocity of 44.4cms-1 (b) the ensemble mean spectrum generated from high-pass filtered power spectra modelled for non-uniform insonation of the same vessel by a beam shape plotted for a homogeneous water path (c) the ensemble mean spectrum after correction for the effects of non-uniform insonation on the spectral components between the knee and the maximum frequency (d) the ensemble mean spectrum after correction for the effects of non-uniform insonation and filtering on the spectral components below the knee frequency, by extrapolation of the corrected power value at the knee to replace the spectrum values below this frequency.

3mm vessel was found. This position was then used to generate the ensemble mean spectrum for five combinations of velocity and vessel diameter values, with the product of vessel cross-sectional area and velocity giving an identical flow rate value in each case. Values for each spectrum are given in table 7.1. The total power in each ensemble mean spectrum was calculated before and after correction for beam shape and filtering using the method described in sections 7.4.3 and 7.4.4, and is shown in figures 7.30a-f for the beam shapes recorded for a water path and five temporal bone paths respectively. It can be seen that in all cases the ensemble mean spectrum correction method re-establishes an approximately proportional relationship between total power and vessel size.

A point of interest at this stage is that the relationship between the vessel size and the uncorrected modelled power values resembles that seen for the raw power values recorded from the wall-less flow phantom described in chapter 3 (figure 3.10a). This similarity provides verification that the in-vitro results were recorded correctly.

Changes in Vessel Size

For each beam shape, ensemble mean spectra were generated for vessels with diameters of 1.5mm, 2mm, 2.5mm, 3mm and 3.5mm, in each case for a time-averaged peak velocity of 60cms^{-1} and at the position in each beam giving the maximum total signal power for the 3mm vessel. Figures 7.31a-e show the total power values calculated before and after correction of each ensemble mean spectrum, for the beam shapes recorded for a water path and five temporal bone paths respectively. It can be seen once again that the ensemble mean spectrum correction method re-establishes an approximately proportional relationship between total power and vessel size for all beam shapes.

Changes in Flow Velocity

Ensemble mean spectra were generated for time-averaged peak velocities of 50cms^{-1} , 55cms^{-1} , 60cms^{-1} , 65cms^{-1} and 70cms^{-1} , in each case for a vessel diameter of 3mm at the position in each beam giving the maximum total signal power. Figures 7.32a-f show the total power values calculated before and after correction of each ensemble mean spectrum, for the beam shapes recorded for a water path and five temporal bone paths respectively. In each case the best fit lines to the raw and corrected values are plotted, and it can be seen that the raw power increases with velocity for all beam shapes. Although the increase is very small over the investigated range of flow velocities, it is further reduced for the corrected values, producing a relationship between velocity and the total power that is approximately independent of velocity and therefore closer to that expected from theory. The slight variation in power with velocity prior to correction is likely to be due to the high pass filter removing a decreasing percentage of the ensemble mean spectrum with increasing velocity, and the improvement in the relationship after correction illustrates the ability of the correction method to compensate for the effects of filtering as well as those of beam shape.

Vessel Position in Beam

The ensemble mean spectra created for the varying flow conditions described above were generated by positioning each vessel at the point in each beam which gave the maximum total signal

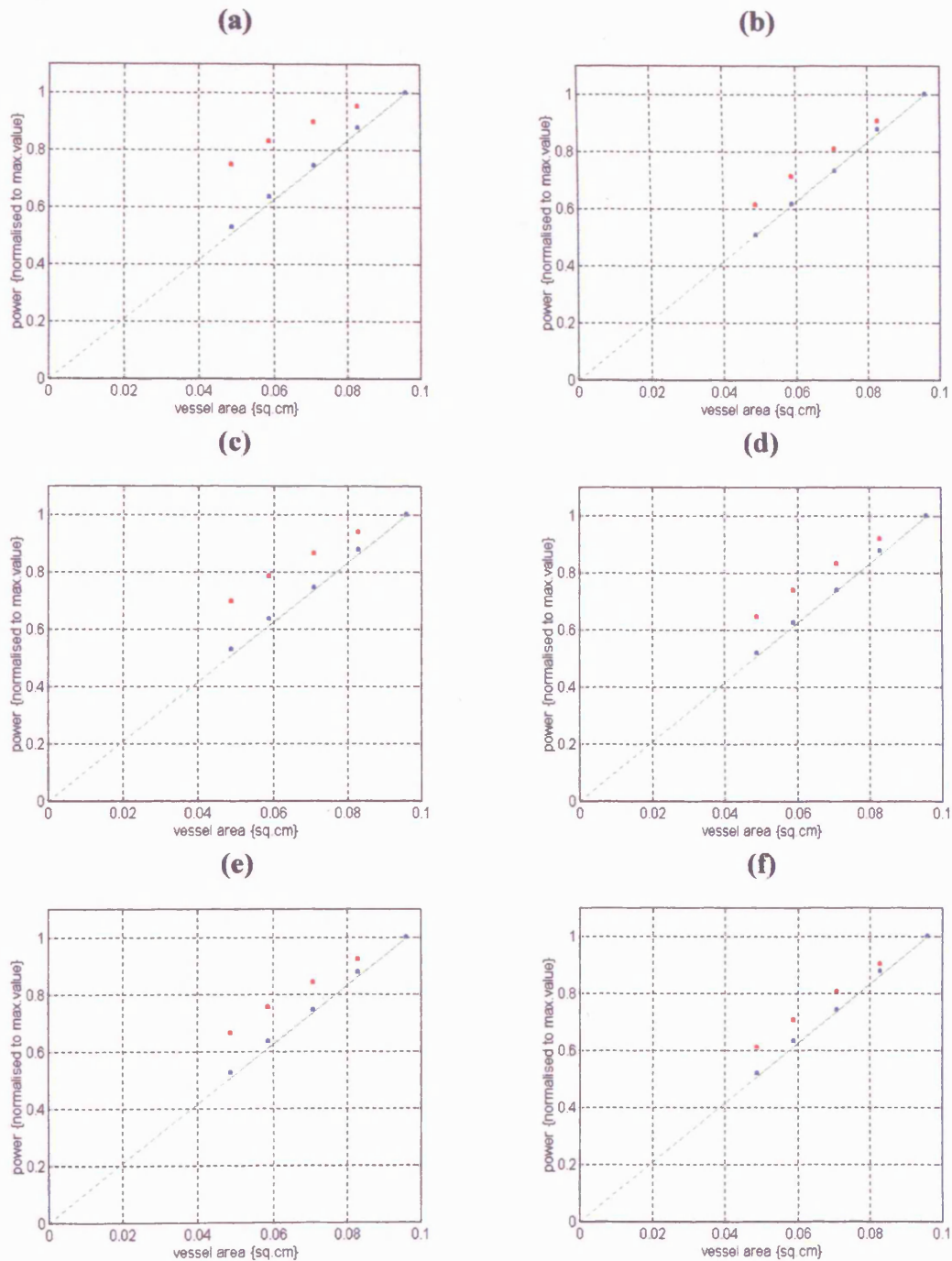


Figure 7.30 The relationship between Doppler power and vessel cross-sectional area for simultaneous changes in velocity and vessel size (see table 7.1 for values). Power values are calculated as the total power in the ensemble mean spectra modelled for conditions of non-uniform insonation using beam shapes plotted for (a) a homogeneous water path and (b-f) paths through five samples of temporal bone. Power values are plotted before (●) and after (●) correction for beam shape and filtering. The dotted line (---) illustrates the proportional relationship between power and vessel size that is predicted by theory.

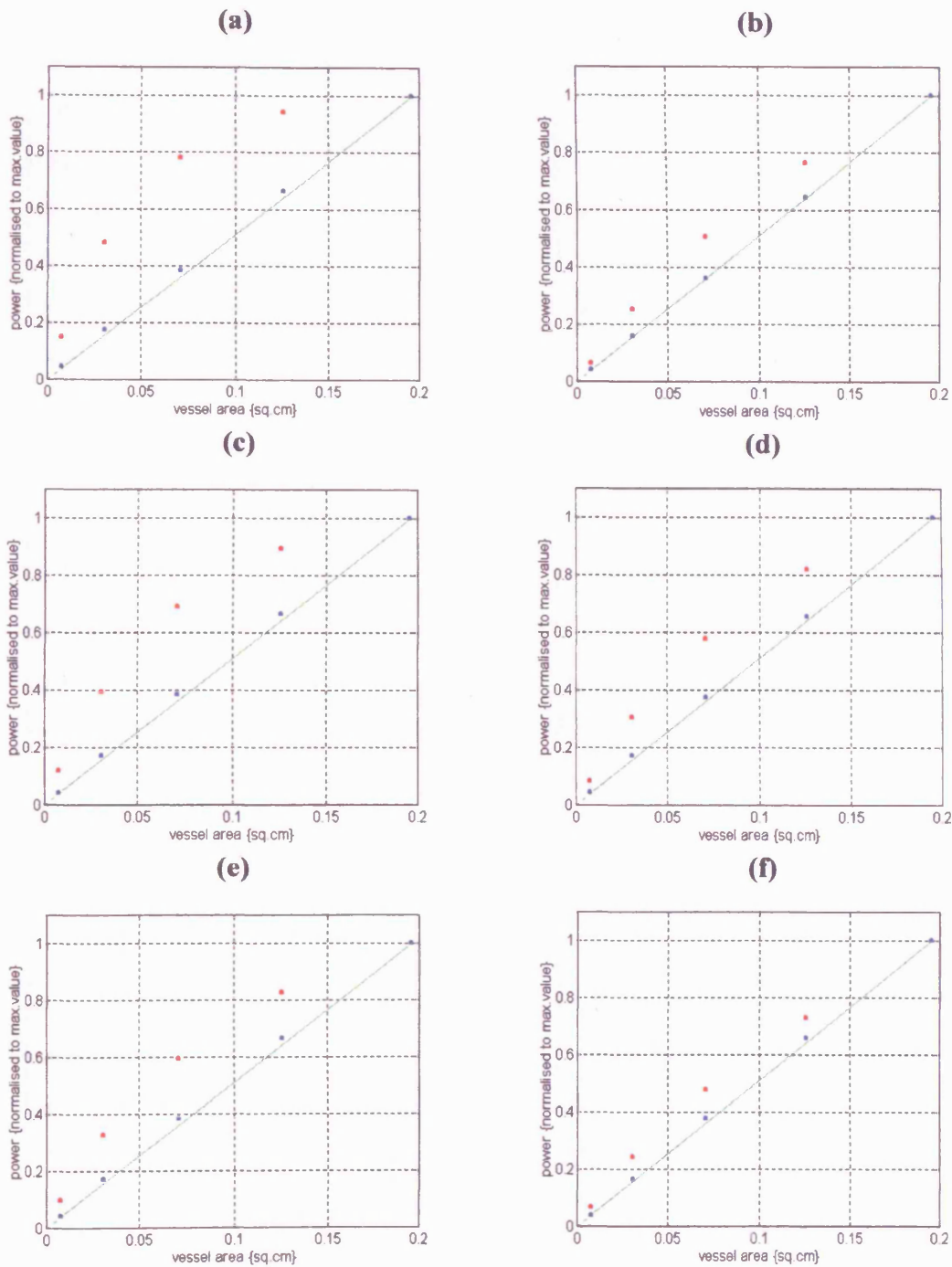


Figure 7.31 The relationship between Doppler power and vessel cross-sectional area for changing vessel size and a fixed flow velocity of 60cm s^{-1} . Power values are calculated as the total power in the ensemble mean spectra modelled for conditions of non-uniform insonation using beam shapes plotted for (a) a homogeneous water path and (b-f) paths through five samples of temporal bone. Power values are plotted before (●) and after (●) correction for beam shape and filtering. The dotted line (--) illustrates the proportional relationship between power and vessel size that is predicted by theory.

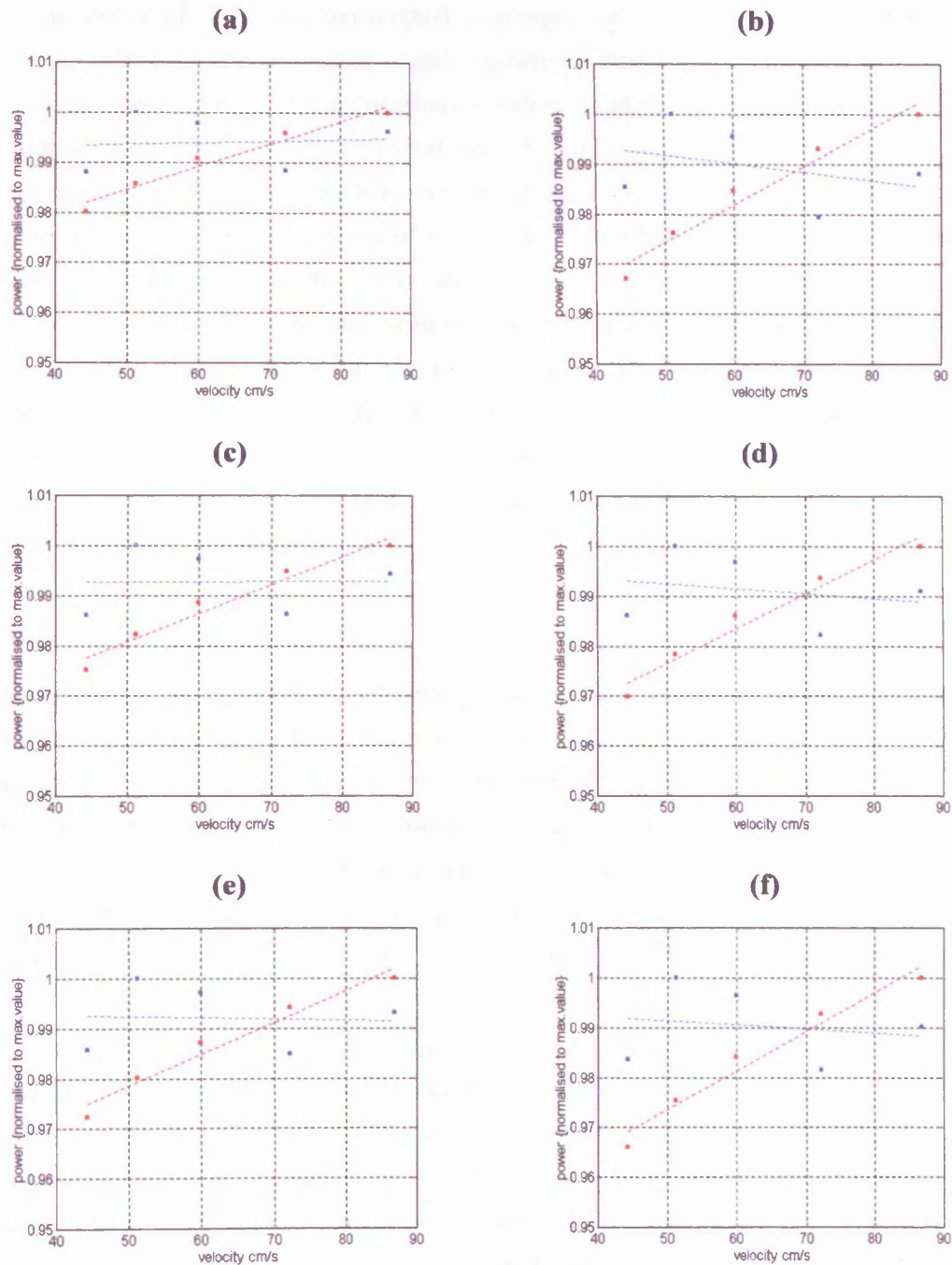


Figure 7.32 The relationship between Doppler power and flow velocity for changing velocities in a vessel of diameter 3mm. Power values are calculated as the total power in the ensemble mean spectra modelled for conditions of non-uniform insonation using beam shapes plotted for (a) a homogeneous water path and (b-f) paths through five samples of temporal bone. Power values are plotted before (●) and after (●) correction for beam shape and filtering. The dotted lines show the best fit relationship between power and velocity in each case.

power value for a 3mm diameter vessel. In order to investigate the effects of vessel position in the beam on the ability of the correction method to compensate for beam shape, the ensemble mean spectra were created for nine different vessel positions separated by 1mm intervals in each beam (figures 7.33a-7.38a), for the five combinations of velocity and vessel diameter values given in table 7.1 at each position. The separation interval was chosen as being sufficient to alter the incident position of the highest beam intensity from the central region of a 3mm vessel to the edge region; this can be assumed to cover the likely range of insonation conditions for the in-vivo case, assuming that the received signal power is carefully maximised.

Figures 7.33b-7.38b show the relationship between total power and vessel size before and after correction at each of the nine positions, for the water path beam and five bone path beams respectively. It can be seen that the ensemble mean spectrum correction re-establishes an approximately proportional relationship at all positions in each beam. The ability of the correction to compensate for the effects of non-uniform insonation can therefore be assumed to be independent of the position of a vessel in a beam.

Vessel Movement During Flow Changes

In the above investigations of the ensemble mean spectrum correction, spectra were generated for changing flow conditions using a stationary vessel position in each beam. For the in-vivo case, it is possible that small movements of the vessel in the beam may occur simultaneously to flow changes, due to movements of the patient and/or transducer during recordings. In order to investigate the effects of such movements on the ability of the correction to compensate for beam shape, ensemble mean spectra were generated for the five combinations of velocity and vessel diameter values given in table 7.1, but in each case the vessel position was displaced by a fixed distance in a random direction from the position giving the maximum total power for the 3mm vessel. Displacements of 0.25mm, 0.5mm and 1mm were carried out for each beam shape.

Figures 7.39a-7.44a show the relationship between total power and vessel size before and after correction for random displacements of the vessel by 0.25mm for the water-path beam and five bone-path beams respectively. Figures 7.39b-7.44b show the corresponding results for random displacements of 0.5mm, and figures 7.39c-7.44c for random displacements of 1mm. It can be seen that for vessel displacements of 0.25mm, the ensemble mean spectrum correction still produces an approximately proportional relationship between power and vessel size for five out of the six beam shapes, although the corrected power values show slightly more variation from proportionality than seen for the case where the vessel position remains stationary during changes in velocity and vessel size (figures 7.30a-f). However, for one of the beam shapes, the correction method fails to produce a proportional relationship (figure 7.44a).

The results for vessel displacements of 0.5mm and 1mm show that for all beam shapes, the ability of the ensemble mean correction to re-establish a proportional relationship between power and vessel size is reduced as the size of the vessel displacement increases, although the degree of inaccuracy varies for different beam shapes; comparing figures 7.41 and 7.43 illustrates this for the bone-distorted beams that were investigated.

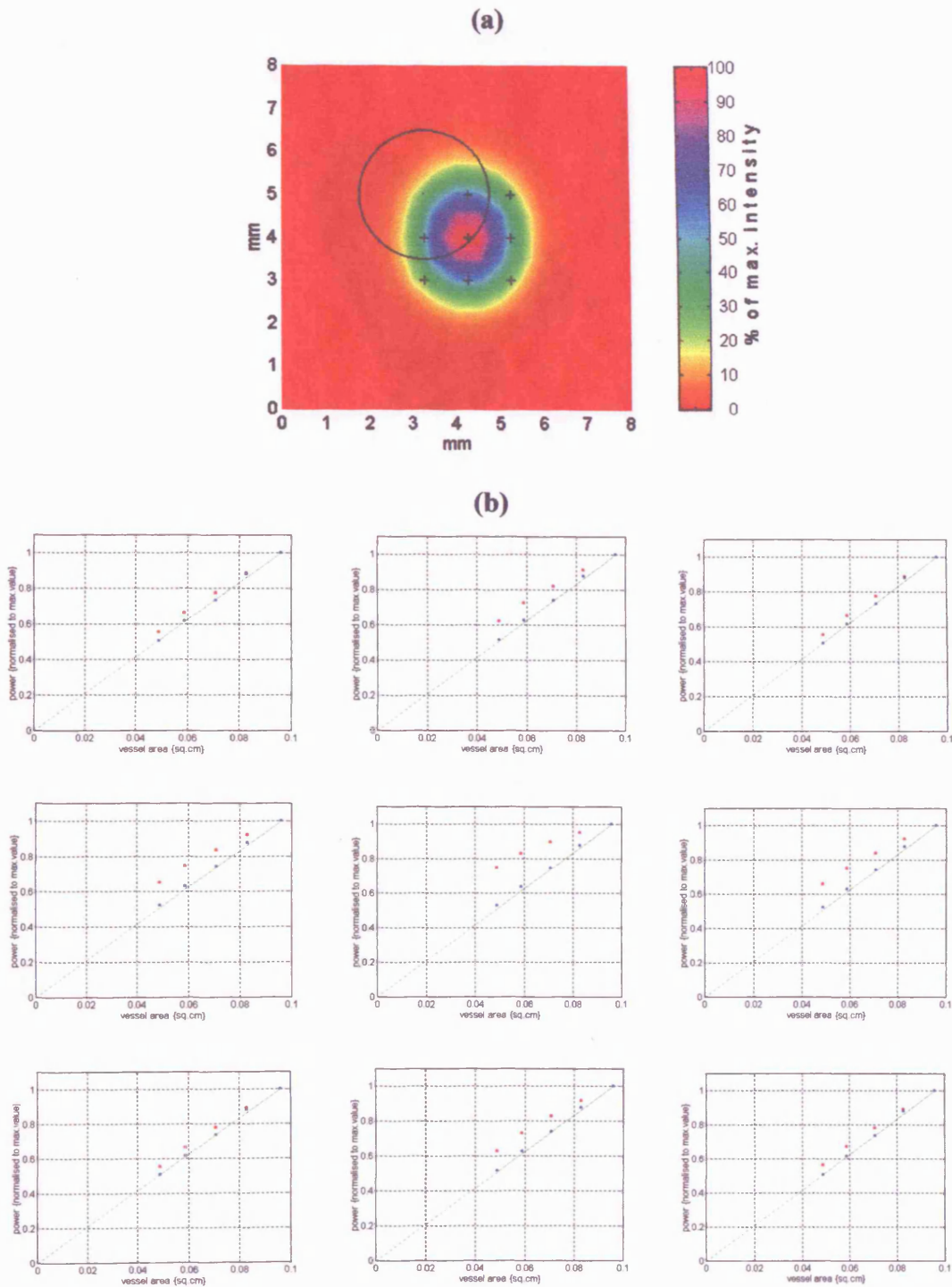


Figure 7.33 The relationship between total ensemble mean spectrum power and vessel cross-sectional area for simultaneous changes in velocity and vessel size (see table 7.1 for values) at nine different locations in the homogeneous water path beam shown in (a). The vessel centre position for each location in the beam is marked on the beam plot. Power values are plotted before (●) and after (●) correction for beam shape and filtering. The dotted line (---) illustrates the proportional relationship between power and vessel size predicted by theory.

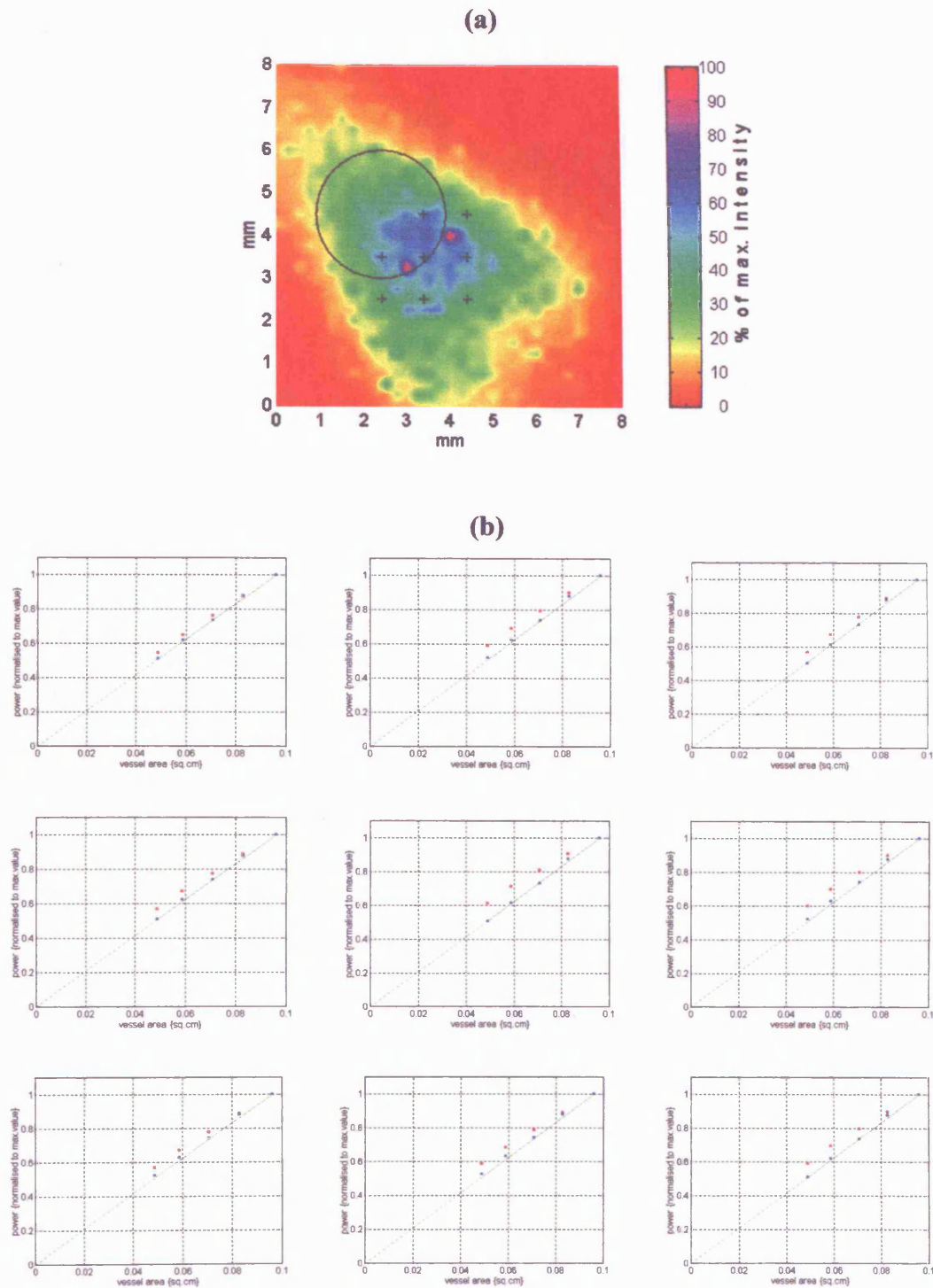


Figure 7.34 The relationship between total ensemble mean spectrum power and vessel cross-sectional area for simultaneous changes in velocity and vessel size (see table 7.1 for values) at nine different locations in the temporal bone path beam shown in (a). The vessel centre position for each location in the beam is marked on the beam plot. Power values are plotted before (●) and after (●) correction for beam shape and filtering. The dotted line (---) illustrates the proportional relationship between power and vessel size predicted by theory.

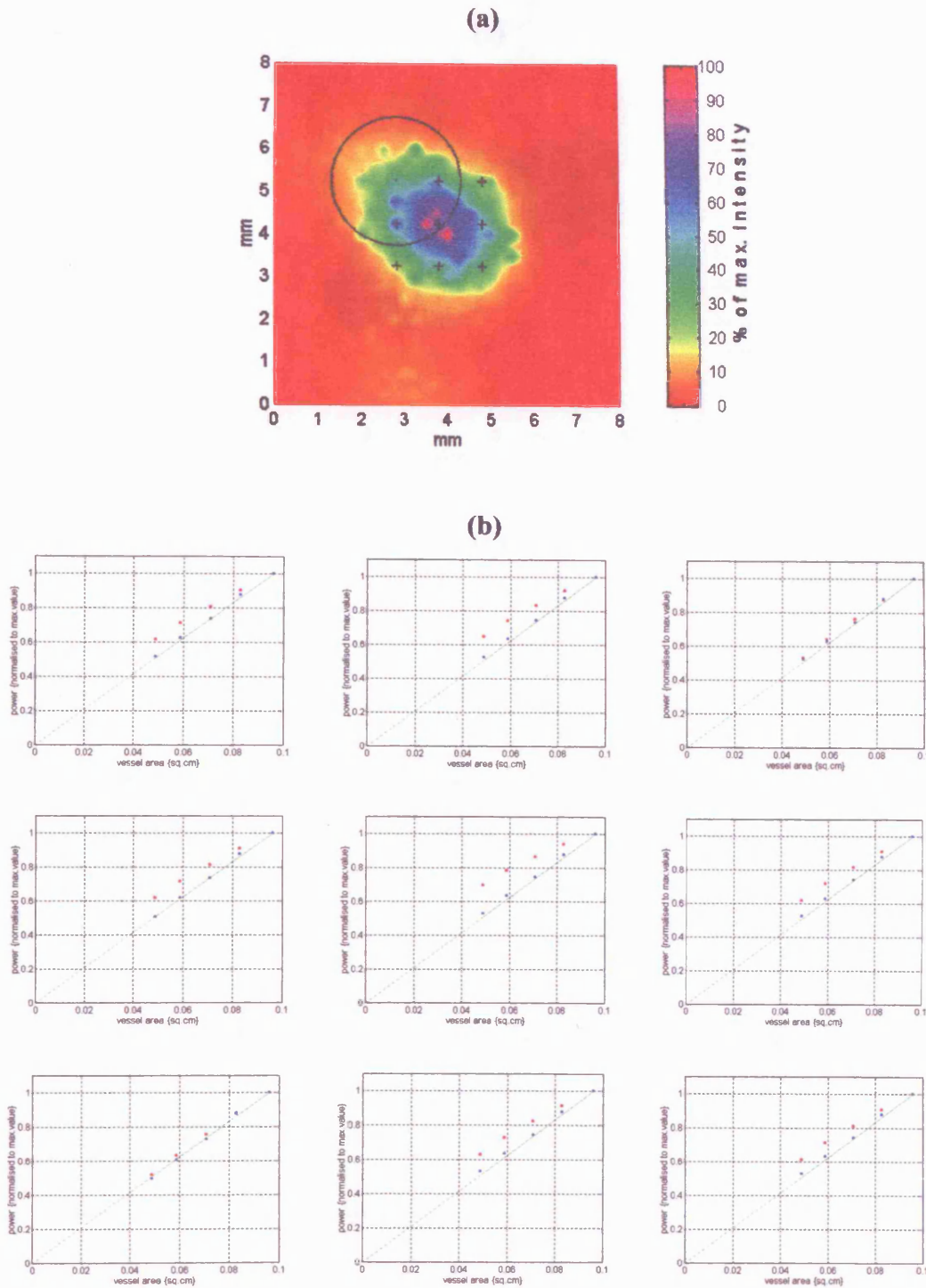


Figure 7.35 The relationship between total ensemble mean spectrum power and vessel cross-sectional area for simultaneous changes in velocity and vessel size (see table 7.1 for values) at nine different locations in the temporal bone path beam shown in (a). The vessel centre position for each location in the beam is marked on the beam plot. Power values are plotted before (●) and after (●) correction for beam shape and filtering. The dotted line (---) illustrates the proportional relationship between power and vessel size predicted by theory.

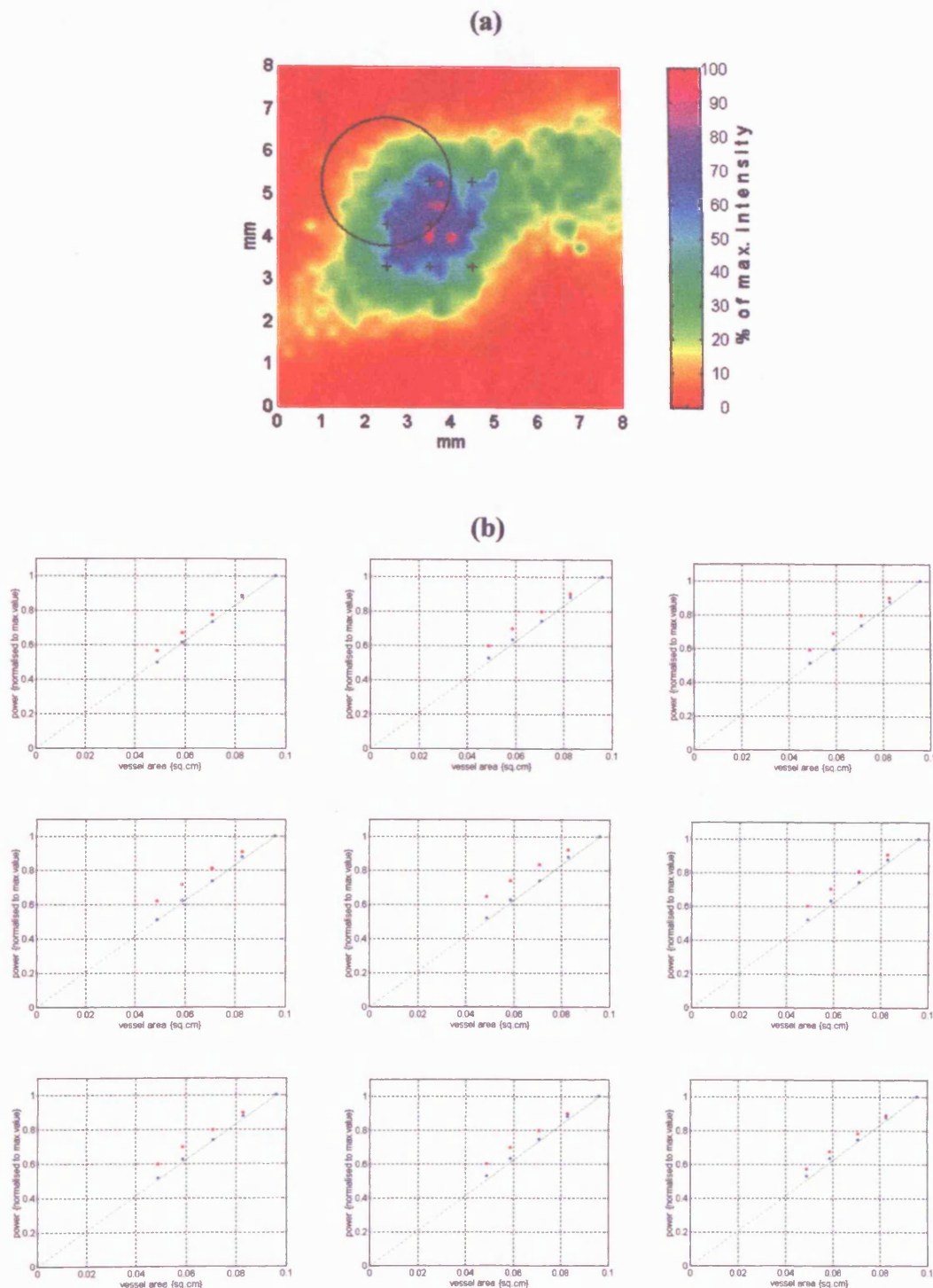


Figure 7.36 The relationship between total ensemble mean spectrum power and vessel cross-sectional area for simultaneous changes in velocity and vessel size (see table 7.1 for values) at nine different locations in the temporal bone path beam shown in (a). The vessel centre position for each location in the beam is marked on the beam plot. Power values are plotted before (●) and after (●) correction for beam shape and filtering. The dotted line (---) illustrates the proportional relationship between power and vessel size predicted by theory.

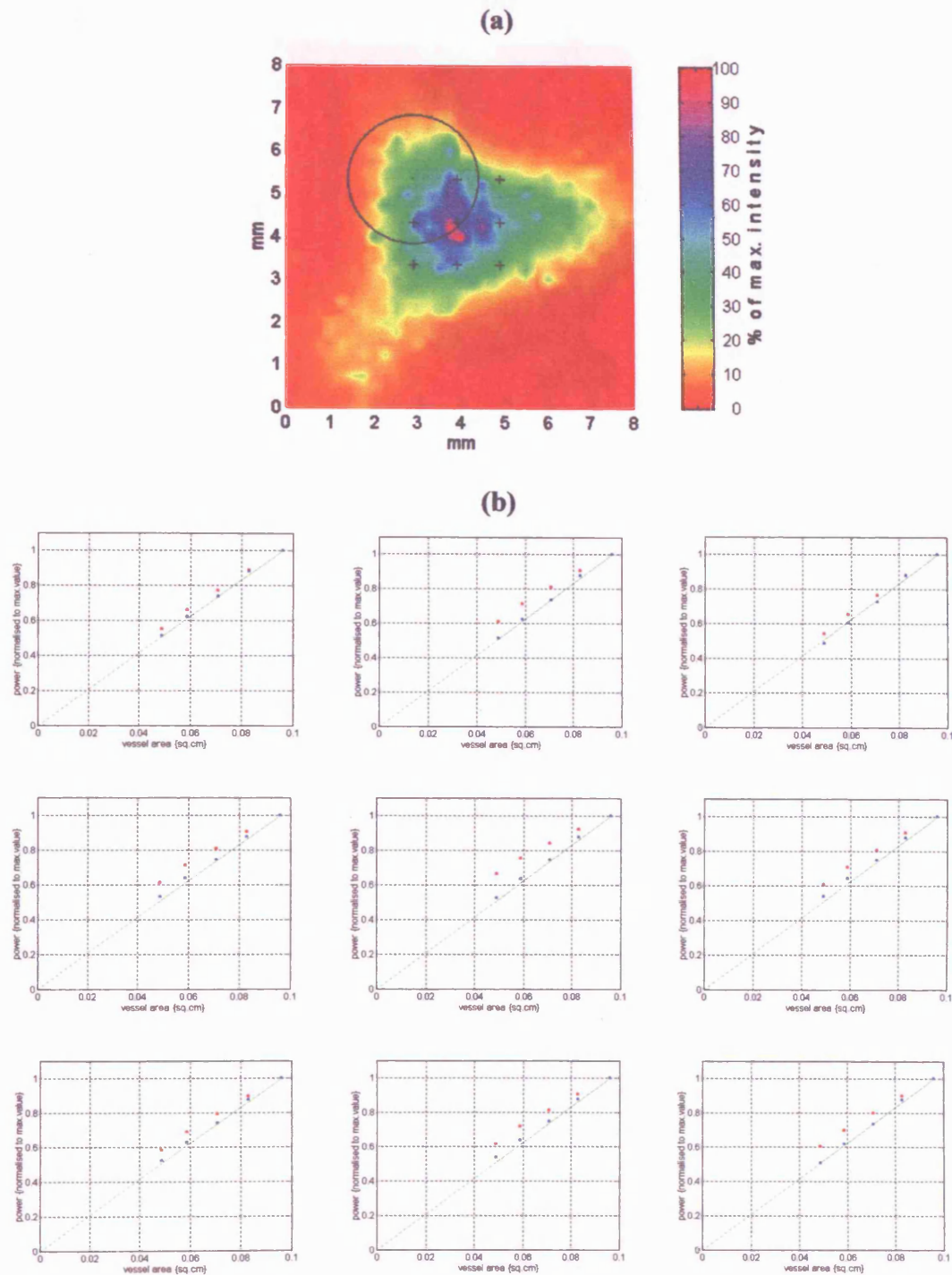


Figure 7.37 The relationship between total ensemble mean spectrum power and vessel cross-sectional area for simultaneous changes in velocity and vessel size (see table 7.1 for values) at nine different locations in the temporal bone path beam shown in (a). The vessel centre position for each location in the beam is marked on the beam plot. Power values are plotted before (●) and after (●) correction for beam shape and filtering. The dotted line (---) illustrates the proportional relationship between power and vessel size predicted by theory.

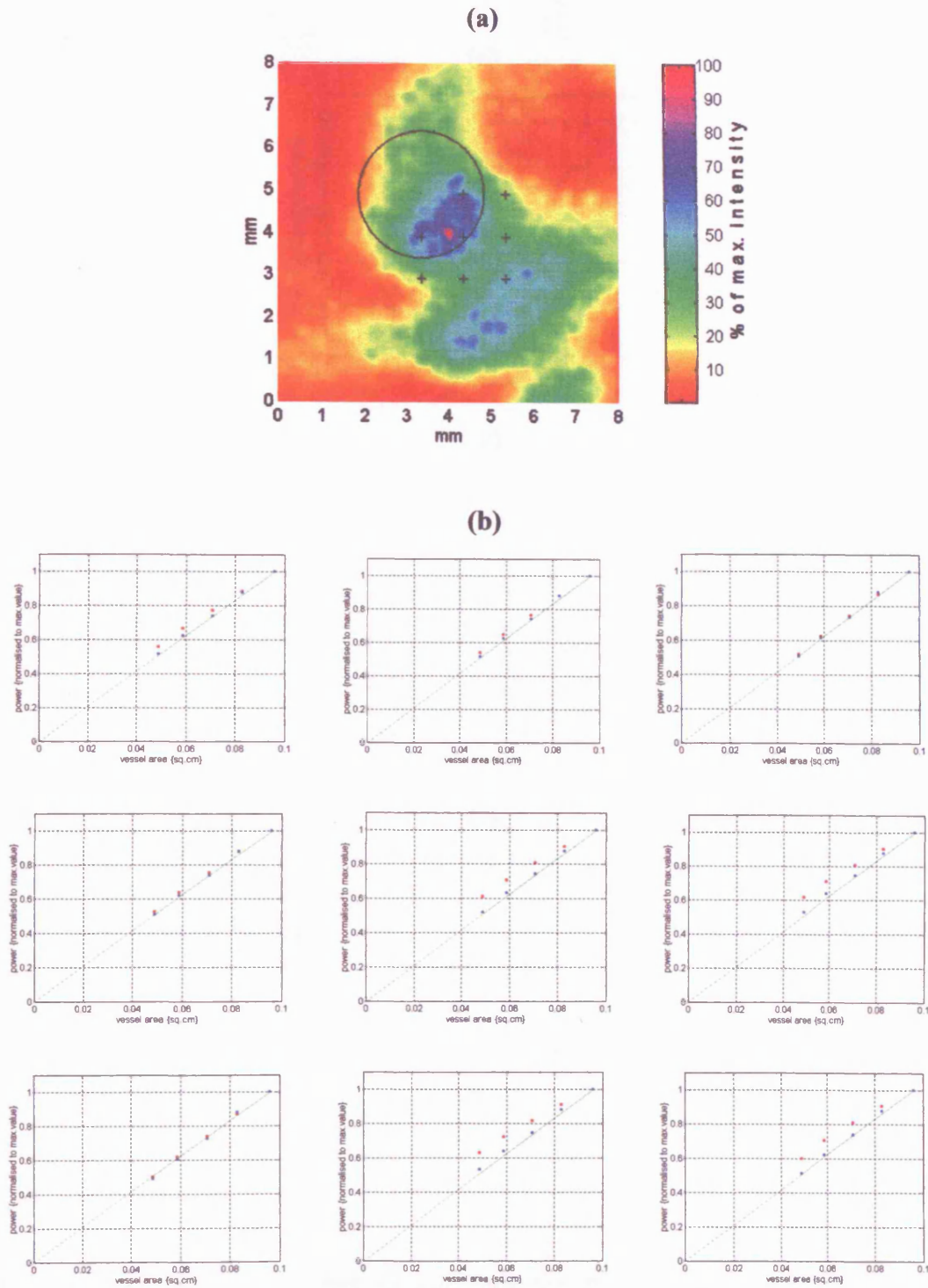


Figure 7.38 The relationship between total ensemble mean spectrum power and vessel cross-sectional area for simultaneous changes in velocity and vessel size (see table 7.1 for values) at nine different locations in the temporal bone path beam shown in (a). The vessel centre position for each location in the beam is marked on the beam plot. Power values are plotted before (●) and after (●) correction for beam shape and filtering. The dotted line (---) illustrates the proportional relationship between power and vessel size predicted by theory.

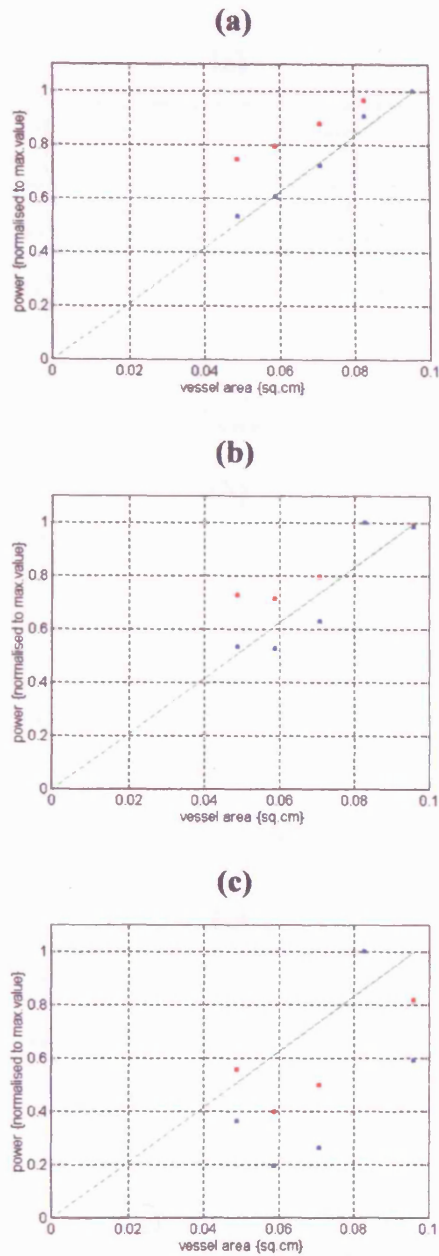


Figure 7.39 The relationship between the total ensemble mean spectrum power and vessel cross-sectional area for simultaneous changes in velocity and vessel size (see table 7.1 for values), with each ensemble mean spectrum modelled for a vessel position displaced in a random direction by (a) 0.25mm, (b) 0.5mm and (c) 1mm from the position giving the maximum total power value in the homogeneous water path beam (see figure 7.33a for beam shape). Power values are plotted before (●) and after (●) correction for beam shape and filtering. The dotted line (---) illustrates the proportional relationship between power and vessel size that is predicted by theory.

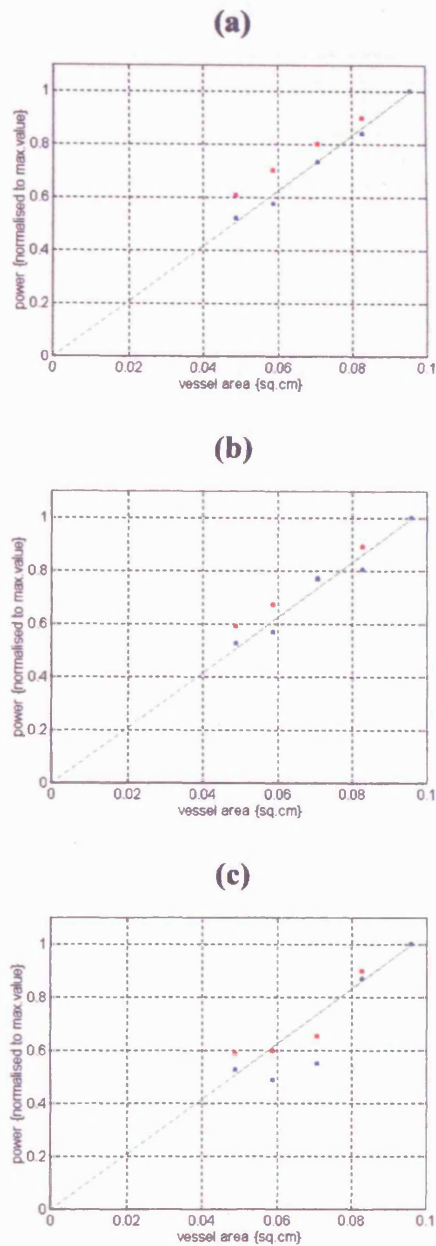


Figure 7.40 The relationship between the total ensemble mean spectrum power and vessel cross-sectional area for simultaneous changes in velocity and vessel size (see table 7.1 for values), with each ensemble mean spectrum modelled for a vessel position displaced in a random direction by (a) 0.25mm, (b) 0.5mm and (c) 1mm from the position giving the maximum total power value in a temporal bone-distorted beam (see figure 7.34a for beam shape). Power values are plotted before (●) and after (●) correction for beam shape and filtering. The dotted line (---) illustrates the proportional relationship between power and vessel size that is predicted by theory.

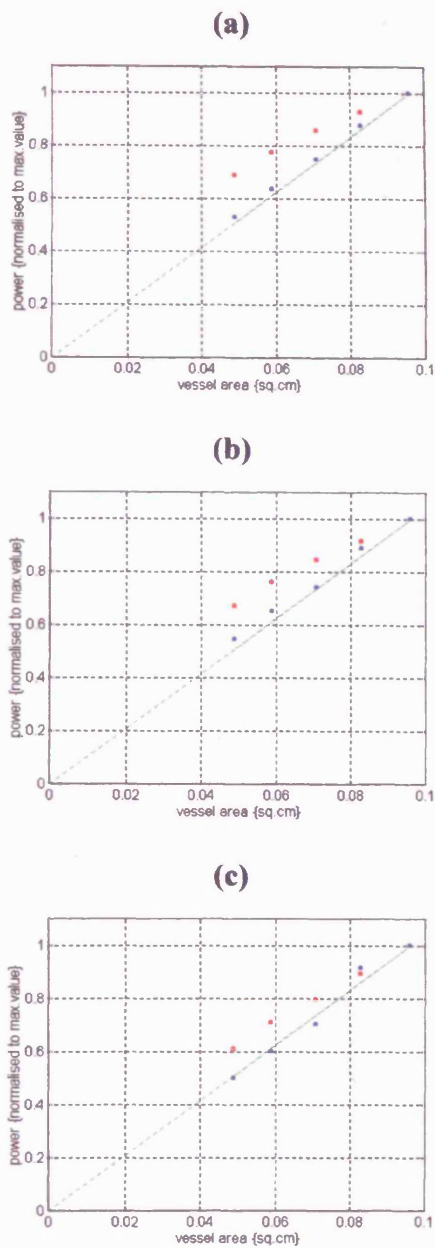


Figure 7.41 The relationship between the total ensemble mean spectrum power and vessel cross-sectional area for simultaneous changes in velocity and vessel size (see table 7.1 for values), with each ensemble mean spectrum modelled for a vessel position displaced in a random direction by (a) 0.25mm, (b) 0.5mm and (c) 1mm from the position giving the maximum total power value in a temporal bone-distorted beam (see figure 7.35a for beam shape). Power values are plotted before (●) and after (●) correction for beam shape and filtering. The dotted line (---) illustrates the proportional relationship between power and vessel size that is predicted by theory.

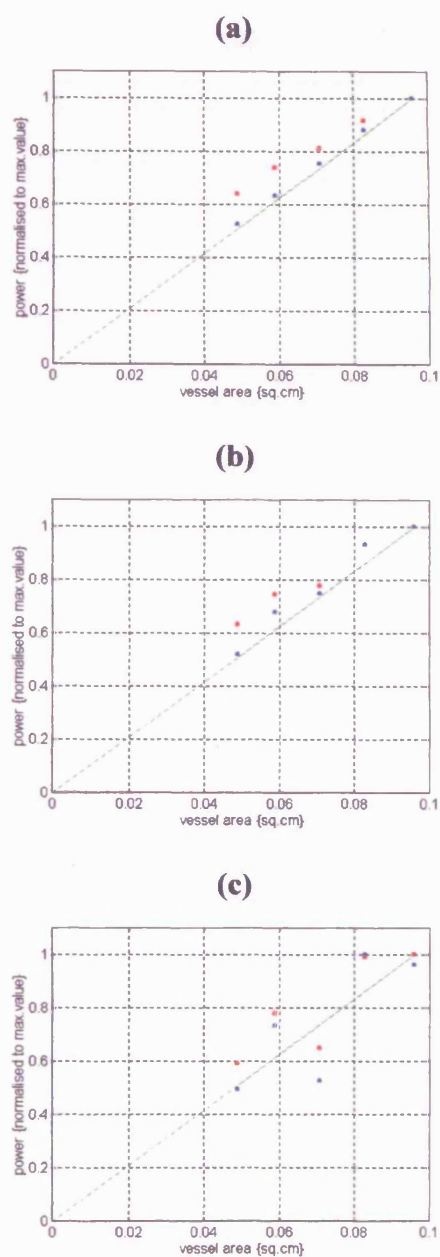


Figure 7.42 The relationship between the total ensemble mean spectrum power and vessel cross-sectional area for simultaneous changes in velocity and vessel size (see table 7.1 for values), with each ensemble mean spectrum modelled for a vessel position displaced in a random direction by (a) 0.25mm, (b) 0.5mm and (c) 1mm from the position giving the maximum total power value in a temporal bone-distorted beam (see figure 7.36a for beam shape). Power values are plotted before (●) and after (●) correction for beam shape and filtering. The dotted line (---) illustrates the proportional relationship between power and vessel size that is predicted by theory.

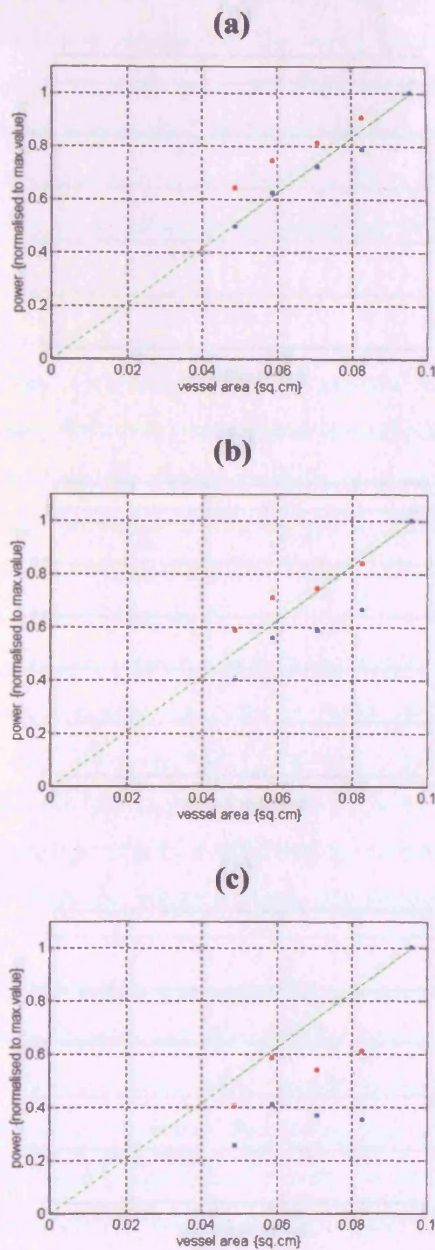


Figure 7.43 The relationship between the total ensemble mean spectrum power and vessel cross-sectional area for simultaneous changes in velocity and vessel size (see table 7.1 for values), with each ensemble mean spectrum modelled for a vessel position displaced in a random direction by (a) 0.25mm, (b) 0.5mm and (c) 1mm from the position giving the maximum total power value in a temporal bone-distorted beam (see figure 7.37a for beam shape). Power values are plotted before (●) and after (●) correction for beam shape and filtering. The dotted line (---) illustrates the proportional relationship between power and vessel size that is predicted by theory.

The results observed for the simulation of vessel movements during flow changes agree with what would be expected for the ensemble mean spectrum correction under these circumstances. The theory behind the correction method assumes that the beam intensity at the centre of each vessel remains constant for all changes in vessel size and position. In practice, any movement of the vessel therefore potentially violates this assumption. However, the larger the displacement of the vessel, the larger the variation in the beam intensity at the centre of each vessel, and hence the less likely the correction method is to produce accurate results.

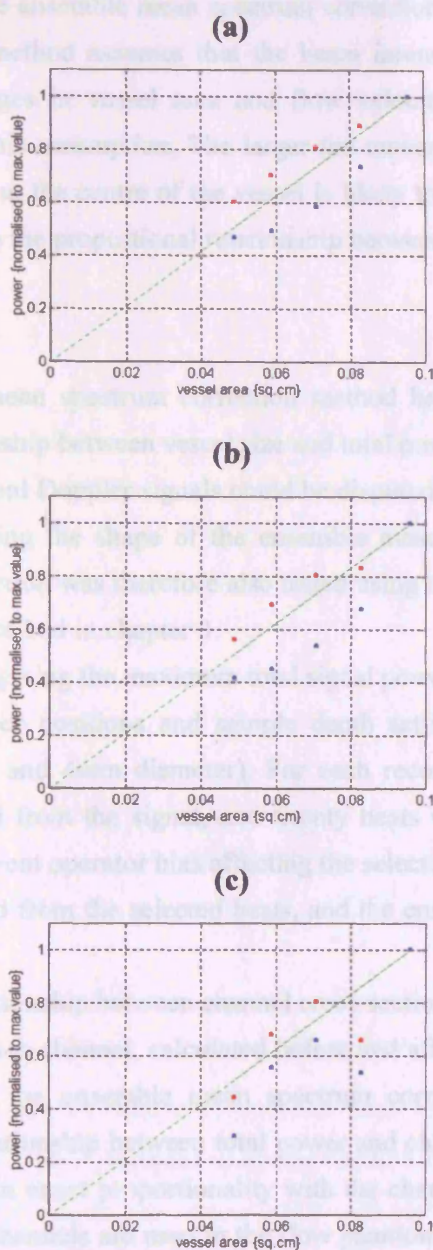
7.5.1 Flow Phantom Signal

Although the ensemble mean spectrum correction method has been shown to effectively re-establish a proportional relationship between vessel cross-sectional area and total power for well-defined Doppler spectra, the validity of the method for real flow phantoms is less certain due to the presence of additional factors such as vessel deformation and the shape of the vessel cross-section.

The ensemble mean spectrum correction method was applied to the data from the flow phantom recordings. The vessel cross-sectional area was determined for each channel using the method described in section 3.2.1.5. The vessel area was selected for each flow phantom channel (Dumb, Flow and Flow Phantom) using the method described in section 3.2.1.5. The ensemble mean spectrum for each channel was calculated from the selected data, and the ensemble mean spectrum correction applied.

Figure 7.44 shows the relationship between the total ensemble mean spectrum power and vessel cross-sectional area for simultaneous changes in velocity and vessel size (see table 7.1 for values), with each ensemble mean spectrum modelled for a vessel position displaced in a random direction by (a) 0.25mm, (b) 0.5mm and (c) 1mm from the position giving the maximum total power value in a temporal bone-distorted beam (see figure 7.38a for beam shape). Power values are plotted before (●) and after (●) correction for beam shape and filtering. The dotted line (---) illustrates the proportional relationship between power and vessel size that is predicted by theory.

Figure 7.44 The relationship between the total ensemble mean spectrum power and vessel cross-sectional area for simultaneous changes in velocity and vessel size (see table 7.1 for values), with each ensemble mean spectrum modelled for a vessel position displaced in a random direction by (a) 0.25mm, (b) 0.5mm and (c) 1mm from the position giving the maximum total power value in a temporal bone-distorted beam (see figure 7.38a for beam shape). Power values are plotted before (●) and after (●) correction for beam shape and filtering. The dotted line (---) illustrates the proportional relationship between power and vessel size that is predicted by theory.



The results observed for the simulation of vessel movements during flow changes agree with what would be expected for the ensemble mean spectrum correction under these circumstances. The theory behind the correction method assumes that the beam intensity at the centre of each vessel remains constant for all changes in vessel area and flow velocity; any movement of the vessel therefore potentially violates this assumption. The larger the movement of the vessel, the larger the variation in the beam intensity at the centre of the vessel is likely to be, and hence the less likely the correction method is to produce the proportional relationship between power and vessel size.

7.5.2 Flow Phantom Signals

Although the ensemble mean spectrum correction method has been shown to effectively re-establish a proportional relationship between vessel size and total power for modelled Doppler spectra, the validity of the method for real Doppler signals could be disputed due to the presence of additional factors such as noise influencing the shape of the ensemble mean spectrum. The accuracy of the ensemble mean spectrum correction was therefore also tested using the Doppler signals recorded from the wall-less flow phantom described in chapter 3.

The one-minute recording giving the maximum total signal power value (see section 3.3.1) for the investigated range of transducer positions and sample depth settings was selected for each flow phantom channel (2mm, 3mm and 4mm diameter). For each recording, any beats containing high intensity noise were eliminated from the signal, and twenty beats were then chosen randomly from those remaining in order to prevent operator bias affecting the selection. The ensemble mean spectrum for each channel was calculated from the selected beats, and the ensemble mean spectrum correction applied.

Figure 7.45 shows the relationship between channel cross-sectional area and the total power in the ensemble mean spectrum for each channel, calculated before and after correction for beam shape and filtering. It can be seen that the ensemble mean spectrum correction method re-establishes an approximately proportional relationship between total power and channel size. The small variation of the corrected power values from exact proportionality with the channel area may possibly be caused by the fact that three separate channels are used in the flow phantom case, requiring movement of the transducer. The beam intensity at the centre of each vessel may therefore vary slightly, causing some inaccuracy in the correction method.

7.6 Conclusions

Due to the unpredictable distortion of the shape of an ultrasound beam after passage through temporal bone, the effects on the signal power spectrum of non-uniform insonation of the MCA cannot be precisely determined for individual cases. Some form of universal correction is therefore required which will at least approximately compensate for the loss of proportionality between vessel size changes and changes in the total signal power caused by non-uniform insonation.

This chapter describes the modeling technique used to create simulations of the Doppler power spectra arising for various vessel size, insonation and flow conditions, and the use of the ensemble

mean spectrum as a signal averaging method. It has been demonstrated, for conditions of uniform illumination and without the presence of high pass filters, that the Doppler spectra created by the model provide an accurate description of the expected changes in spectral shape for varying vessel sizes and flow velocities. In addition, it has been shown that the calculation of total signal power from the ensemble mean spectrum is a valid method for accurately measuring changes in signal power.

A method for correcting the ensemble mean spectrum for the effects of beam shape and filtering was investigated using the ensemble mean spectra calculated from the modelled Doppler spectra. The results show that the correction method is consistent with an approximately proportional relationship between vessel area and signal power for arbitrary vessel and flow velocity changes under the non-uniform illumination conditions produced by six different beam shapes. The correction method has been used to correct the ensemble mean spectra recorded from the vessel phantoms up to approximately 0.35mm, but for larger vessel displacements the correction breaks down; this behaviour is to be expected as the beam diameter becomes a significant fraction of the vessel diameter at the centre of a vessel cross-section. For all Doppler spectra obtained from the vessel phantoms, the effectiveness of the correction method for the vessel phantoms is independent of the vessel position in the beam.

The ensemble mean spectra recorded from the vessel phantoms with the correction method using real Doppler signals recorded from the wall-less phantom described in chapter 3, show again, an approximately proportional relationship between vessel area and signal power.

The work presented in this chapter has shown that the ensemble mean spectrum correction method potentially provides a way of correcting in-vivo signals for the effects of beam shape and high-pass filtering, and should allow changes in signal power to be more confidently related to the scale of any vessel size changes that occur. The application of the correction method to in-vivo signals will be reported in the next chapter.

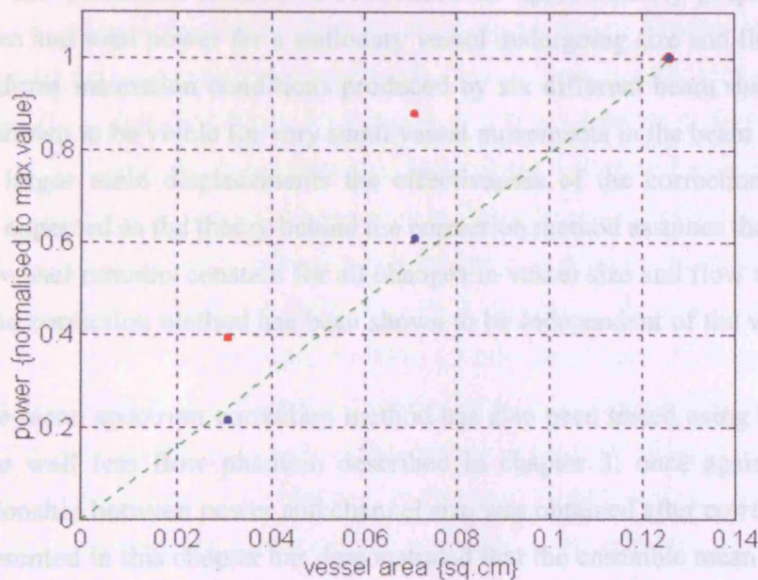


Figure 7.45 The relationship between Doppler power and channel cross-sectional area for the signals recorded from 2mm, 3mm and 4mm diameter channels (areas 0.031cm², 0.071cm² and 0.126cm² respectively) in the wall-less flow phantom. Power values are calculated as the total power in the ensemble mean spectra and are plotted before (●) and after (●) correction for beam shape and filtering. The dotted line (---) illustrates the proportional relationship between power and vessel size that is predicted by theory.

mean spectrum as a signal averaging method. It has been demonstrated, for conditions of uniform insonation and without the presence of high pass filters, that the Doppler spectra created by the model provide an accurate simulation of the expected changes in spectral shape for varying vessel sizes and flow velocities. In addition, it has been shown that the calculation of total signal power from the ensemble mean spectrum is a valid method for accurately monitoring changes in signal power.

A method for correcting the ensemble mean spectrum for the effects of beam shape and filtering was investigated using the ensemble mean spectra calculated from the modeled Doppler spectra. The results show that the correction method re-establishes an approximately proportional relationship between vessel area and total power for a stationary vessel undergoing size and flow velocity changes under the non-uniform insonation conditions produced by six different beam shapes. The correction method has been shown to be viable for very small vessel movements in the beam up to approximately 0.25mm, but for larger scale displacements the effectiveness of the correction breaks down; this behaviour is to be expected as the theory behind the correction method assumes that the beam intensity at the centre of a vessel remains constant for all changes in vessel size and flow velocity. Finally, the effectiveness of the correction method has been shown to be independent of the vessel position in the beam.

The ensemble mean spectrum correction method has also been tested using real Doppler signals recorded from the wall less flow phantom described in chapter 3; once again, an approximately proportional relationship between power and channel size was obtained after correction.

The work presented in this chapter has demonstrated that the ensemble mean spectrum correction method potentially provides a way of correcting in-vivo signals for the effects of beam shape and high-pass filtering, and should allow changes in signal power to be more confidently related to the scale of any vessel size changes that occur. The application of the correction method to in-vivo signals will be reported in the next chapter.

CHAPTER 8

Application of the Ensemble Mean Spectrum Correction to In-Vivo Doppler Signals

8.1 Introduction

The results of the modelling described in chapter 6 show that the non-uniform insonation of the MCA arising from distortion of the Doppler ultrasound beam shape by temporal bone is likely to cause a loss of proportionality between a change in vessel size and the resultant change in total power. It therefore appears that some form of correction for beam shape may be required before the magnitude of any changes in signal power recorded from the MCA can be confidently related to the scale of the size change that the vessel has undergone. Unfortunately it is not feasible to derive correction factors that are specific to individuals; the investigation of beam shape distortion by temporal bone described in chapter 5 showed that there is substantial variation in the pattern of distortion occurring for different bone samples and for different beam paths through the bone, leading to the conclusion that the beam shape for in-vivo Doppler recordings from the MCA is likely to vary unpredictably between individuals, and also for different transducer positions in individual cases. At the present time, the only solution is therefore some form of universal correction that will approximately compensate for the loss of proportionality between vessel size changes and changes in the total signal power in all cases.

Chapter 7 described a method for obtaining an averaged Doppler signal spectrum (the ensemble mean spectrum), and a method for correcting the ensemble mean spectrum for the effects of beam shape and high pass filtering. The theory behind the correction is based on a prediction of the shape of the ensemble mean spectrum for uniform insonation conditions and requires the assumption that the flow in a vessel is parabolic and the signal spectra are therefore rectangular in shape. This can be reasonably assumed for the MCA case if the flow is stable and unidirectional. The correction also requires that the beam intensity at the centre of a vessel remains approximately constant for all changes in size and flow velocity that occur. This can be assumed for an in-vivo vessel if the vessel position in the beam does not change during a recording, a criteria which is vital anyway for recordings of Doppler signal power in order to prevent spurious changes in power arising from changes in the insonation pattern across the vessel. The results obtained in chapter 7 suggest that the correction method is reliable for any position of a vessel in a beam provided that the position remains approximately constant during a recording. This finding is important with regard to the in-vivo case due to the fact that it is not currently possible to ascertain the precise position of an in-vivo vessel in a beam.

In chapter 7, tests of the proposed correction method using both simulated and in-vitro Doppler power spectra provided results suggesting that the application of the correction to in-vivo Doppler signals recorded with the transducer in a stationary position should potentially allow the magnitude of any changes in signal power to be more confidently related to the scale of any vessel size changes that occur. The following chapter investigates the effects of the correction on Doppler signal power using data recorded from healthy volunteers undergoing carbon dioxide reactivity testing, and assesses the feasibility of using the correction with clinical data.

8.2 Adapting the Ensemble Mean Spectrum Correction for Use With In-Vivo Signals

As explained in chapter 7, the value $P_{ems}(f_{max})$ of the power in the maximum frequency bin of each ensemble mean spectrum calculated from a particular Doppler signal must always be derived for a central vessel annulus of the same radius so that it can be assumed that the beam sensitivities affecting this power value remain constant. In order to define the maximum frequency section of an ensemble mean spectrum corresponding to the signal received from a central annulus of a known fixed radius, the flow velocity of the blood travelling at the edge of the annulus must be known. However, this velocity value is dependent on the radius of the vessel (see equation 7.1) and consequently the assumption of a constant central annulus radius can only be an approximation for any signal owing to the possibility of vessel size changes during the recording.

To optimise this approximation, a method of extracting a value for $P_{ems}(f_{max})$ that minimises any variation in the size of the central annulus is required. If the ratio of the flow velocity at the edge of the central annulus $V(r_c)$ and the centre stream maximum flow velocity V_{max} is set to equal a constant value, the radius of the centre annulus will consequently depend only on the vessel radius. Hence, if the vessel changes in size, then the radius of the centre annulus will also change by an amount determined by the chosen value of the velocity ratio (see equation 7.23).

In order to apply the correction to any ensemble mean spectrum a suitable value must first be derived for the velocity ratio. As stated previously, the smallest velocity ratio value producing $P_{ems}(f_{max})$ values for which a proportional relationship between corrected total power and vessel size is still observed can be assumed to be the optimum value for use in the correction, as it will provide a compromise between maximising the area of the central annulus and minimising any changes in its size. In chapter 7, the optimum velocity ratio was estimated to be equal to 0.925 using simulated Doppler signals; this value was seen to produce correction factors which successfully compensated for the effects of non-uniform insonation and filtering, for both flow phantom signals and for simulated signals created for a range of flow and vessel size changes at different positions in various beam shapes. For the simulated signals, vessel sizes of between 2.5mm and 3.5mm diameter were used; this effectively represents a change of the order of 15% in the diameter of a 3mm vessel. For a velocity ratio value of 0.925 these vessel sizes produced a change of the central annulus radius of 0.07mm (derived using equation 7.23), suggesting that this is the maximum magnitude of variation in the size of the central annulus that can occur before the effectiveness of the correction is compromised by this source of inaccuracy.

For the in-vivo case, the range of MCA size changes is likely to be smaller than that chosen for the simulated Doppler signals used in chapter 7. The largest measured change in MCA diameter found in the literature review given in chapter 1 is 8% (Huber and Handa 1967). This must be considered when deriving a suitable velocity ratio value for use when correcting in-vivo signals, as smaller changes in vessel size will produce smaller changes in the size of the central annulus and hence allow a larger volume of blood to be used in the derivation of the value of $P_{ems}(f_{max})$ before the correction breaks down.

Because the actual size of the MCA is unknown for clinical recordings, it is not possible to optimise the value of $P_{ems}(f_{max})$ for any one recording, and hence only a general case can be

considered. In order to estimate the potential scale of any changes in the size of the central annulus for the in-vivo case, the largest possible MCA size and size change need to be considered, as these will give rise to the greatest changes in vessel size for any given percentage change in diameter. The largest MCA diameter recorded by van der Zwan et al. (1993) was 3.46mm; rounding this value to 4mm ensures that most potential MCA sizes should be covered. Similarly, increasing the largest observed change in MCA diameter (given above as 8%) to 10% should theoretically cover the majority of MCA size changes. Using these predicted values in equation 7.23 along with a range of velocity ratio values, it was found that a ratio of 0.875 produces a change of approximately 0.07mm in the radius of the central annulus. Because this was the value of the maximum change in the central annulus size for which the correction still successfully compensated for the effects of beam shape and filtering on simulated Doppler signals, it was assumed that the same limit would apply to in-vivo signals. Hence, a velocity ratio value of 0.875 was selected when deriving the value of $P_{ems}(f_{max})$ to be used in the correction applied to all in-vivo signals.

8.3 The Carbon Dioxide (CO₂) Reactivity Test

Elevated blood CO₂ levels are known to cause significant increases in the velocities detected in the cerebral arteries (Markwalder 1984), plus potential vasodilation of these arteries (Huber & Handa 1967). The latter investigation used angiography exposures to measure changes in the size of various cerebral vessels when subjected to different stimuli, including hypercapnia. For vessels in the size range of the MCA, the largest observed total increase in vessel diameter was 8%. Although this value appears to be small, changes of this scale may still adversely affect the accuracy of any estimate of the change in blood flow made from velocity alone. This can be illustrated by considering the example of a vessel of diameter 3mm containing blood flowing with a time-averaged peak velocity of 60cm s⁻¹ (standard values for the MCA). If the vessel diameter increases by 8% and the velocity increases to 80cm s⁻¹, then the flow rate (equal to the product of velocity and vessel area) can be calculated to have increased by approximately 56%. However, if only the velocities are used to estimate the flow change, then the percentage increase in flow rate is found to be approximately 33%. This value is a substantial underestimation of the true value.

To date, three investigations (Aaslid 1989, Poulin 1996a, 1996b) have attempted to assess the extent of MCA size variations in healthy subjects breathing increased levels of CO₂ in air. All of these studies used Doppler signal power values to measure vessel size changes, and concluded that no changes of a magnitude large enough to significantly affect blood flow were detected. However, as stated previously, the ability of Doppler signal power values to quantify vessel size changes in-vivo is dubious.

The primary aim of this study was to establish the effects of the correction method on the recorded data, in order to ascertain the feasibility of using the correction with in-vivo signals, and to illustrate the possible advantages and disadvantages of both the Doppler power method and the correction technique. A secondary aim was to compare the observed changes in signal power (both before and after correction) with those reported in the above publications.

8.3.1 Method and Subjects

The technique used for the CO₂ reactivity test was based on that described by Bishop (1986) and utilised in other studies (Aaslid 1989, 1991, Widder 1989). Baseline values of cerebral blood flow velocity, arterial blood pressure and end-tidal carbon dioxide were recorded for an initial period of five minutes while subjects breathed normal air. This was followed by a two-minute recording with each subject breathing a mixture of 5% CO₂ in air, administered using a Douglas bag and elephant tubing leading to a one-way valve in a closely fitting face mask. Finally, a five-minute recording of recovery data was taken with the subject once again breathing normal air.

Fifteen healthy adult volunteers (10 males and 5 females) between the ages of 23 and 51 took part in the investigation. Subjects were only included if they had no history of vascular disease, heart problems, hypertension, migraine, epilepsy, cerebral aneurysm, intra-cerebral bleeding or other pre-existing neurological conditions. The study was approved by the Leicestershire Research Ethics Committee, and informed consent was obtained in all cases.

All recordings were made with subjects in the supine position with the head elevated. Cerebral blood flow velocity was monitored from the right MCA using a Scimed QVL-120 transcranial Doppler system (Bristol, UK) in conjunction with a 2MHz transducer held in position by a Scimed elastic headband device. Arterial blood pressure was monitored non-invasively using a finger cuff device (Ohmeda 2300 Finapres BP monitor). End-tidal CO₂ levels were monitored using an infra-red capnograph (Datex Normocap 200) connected to a face mask worn by the volunteer. All signals were recorded to DAT tape using an eight channel recorder (Sony PC-108M).

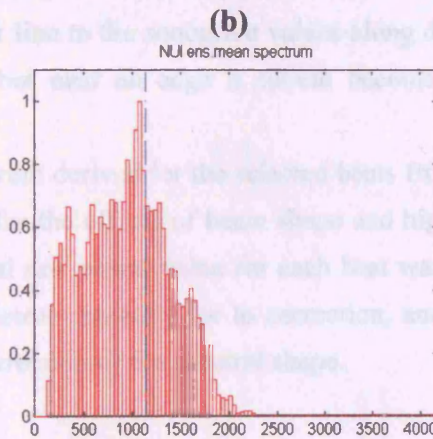
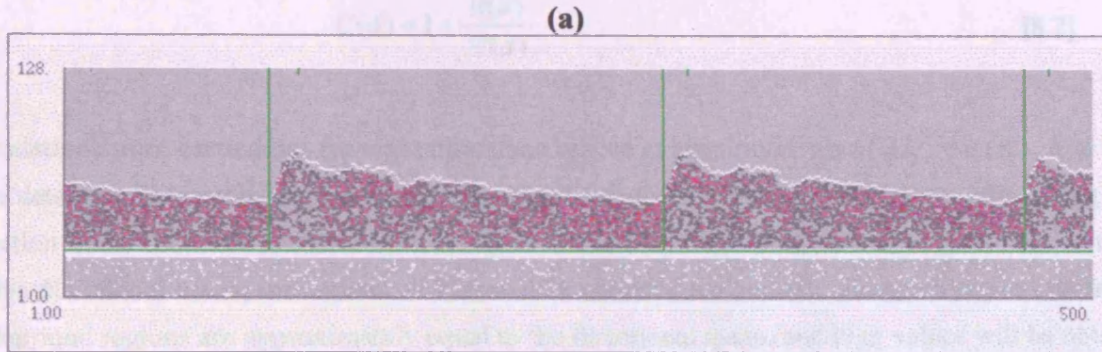
8.3.2 Analysis of Doppler Signal Power

For each subject, a five-minute section of signal encompassing the two-minute period of CO₂ inhalation was extracted from the DAT tape recording using an in-house software package. The maximum frequency envelope was derived from the signal sonogram using a simple threshold method (Evans et al. 1989), and was then used in a foot-finding algorithm (Evans 1988) to divide the signal into beats (figure 8.1a). Those beats having accurate foot markers and a good quality envelope were selected, and the ensemble mean spectrum was calculated for each selected beat using the method described in section 7.4.1. The ensemble mean spectrum for one beat is shown in figure 8.1b.

In order to attempt to reduce the distorting effects of noise on the Doppler power spectrum, the signal recorded for each subject was processed using a noise smoothing algorithm as described by Hoskins et al. (1990). The directional filter was chosen from the three algorithms described by the authors owing to it having the best overall performance in terms of noise reduction and the bias and distortion introduced to the maximum frequency envelope. Smoothing was implemented by considering that the sonogram display was an image, with each power value in the sonogram representing an image pixel. Each pixel was placed at the centre of a 9x9 pixel window, and the corresponding smoothed value calculated using the following filter output equation:

$$O(x, y) = \frac{\sum_{d=1}^{d=8} m(d).C(d)}{\sum_{d=1}^{d=8} C(d)} \quad [8.1]$$

where avg is the mean value of elements in a $M \times N$ window A span along the direction d , and $C(d)$ is a local average measure along the same direction that dictates the amount of correction depending on whether the power value is in a uniform area, or close to the edge of the sonogram. The value of $C(d)$ was derived using the following equation:



8.2.1 Results

Figure 8.1a shows a section of unfiltered Doppler sonogram (i.e. no speckling algorithm applied) taken from the signal recorded from one of the volunteers taking part in the CO₂ metabolic

Figure 8.1 (a) A section of the Doppler signal sonogram recorded from the MCA of a healthy adult volunteer, showing the maximum frequency envelope and beat foot markers. **(b)** the ensemble mean spectrum derived from the first beat seen in the signal.

The mean spectrum derived from this filtered sonogram for the beat corresponding to this trial is shown in the unfiltered ensemble mean spectrum seen in figure 8.1b.

Figures 8.2-8.12 show the MCA maximum flow velocity, arterial blood pressure and expired carbon dioxide values for each of the fifteen subjects, in each case for the five minute section of signal selected to encompass the two-minute period of 10% CO₂ rebreath. The period of CO₂ rebreath can be identified from the elevated velocity and reduced CO₂ levels during this time. Also shown for each subject is the variation in the total power with time, plotted before and after the ensemble mean spectrum correction has been applied. The power values seen in plot *d* of each figure are calculated from the ensemble mean spectra derived from the beats selected from the unfiltered sonogram, and are normalised to the mean of the uncorrected values in each case. Similarly, plot *e* in each figure shows

where $m(d)$ is the mean value of elements in a 3x9 window aligned along the direction d , and $C(d)$ is a local image measure along the same direction that dictates the amount of smoothing depending on whether the power value is in a uniform area or close to the edge of the sonogram. The value of $C(d)$ was derived using the following equation:

$$C(d) = 1 + \frac{R(d)}{Sl(d)} \quad [8.2]$$

Calculations were carried out for eight directions spaced at equal intervals of 22.5 degrees. $R(d)$ is an edge detection parameter calculated from the mean value of the sonogram elements lying along each direction d and the mean values of the sonogram elements in the 'background' regions on either side of this directional mean; low values of $R(d)$ will be obtained for uniform sonogram regions where the background regions are approximately equal to the directional mean, and high values will be obtained for sonogram edge regions where the directional mean is aligned parallel to the edge and the background values are consequently not equal. $Sl(d)$ is a measure of local image uniformity equal to the slope of the least-squares-fit line to the sonogram values along direction d ; for a uniform area the slope will have a low value, but near an edge it should become higher as the sonogram values decrease.

Each ensemble mean spectrum derived for the selected beats from both the filtered and unfiltered Doppler signals was corrected for the effects of beam shape and high pass filtering using the method described in chapter 7. The total raw power value for each beat was calculated as being equal to the sum of the ensemble mean spectrum power prior to correction, and the total corrected power value equal to the power sum after correction of the spectral shape.

8.3.3 Results

Figure 8.1a shows a section of unfiltered Doppler sonogram (i.e. no smoothing algorithm applied) taken from the signal recorded from one of the volunteers taking part in the CO₂ reactivity investigation. Figure 8.1b shows the ensemble mean spectrum derived from the first beat seen in figure 8.1a. The effect of the directional filter on the sonogram is shown in figure 8.2a for the same section of signal, and figure 8.2b shows the ensemble mean spectrum derived from this filtered sonogram for the beat corresponding to that used to obtain the unfiltered ensemble mean spectrum seen in figure 8.1b.

Figures 8.3-8.17 show the MCA maximum flow velocity, arterial blood pressure and end-tidal carbon dioxide values for each of the fifteen subjects, in each case for the five minute section of signal selected to encompass the two-minute period of 5% CO₂ inhalation. The period of CO₂ inhalation can be identified from the elevated velocity and end-tidal CO₂ levels during this time. Also shown for each subject is the variation in the total power with time, plotted before and after the ensemble mean spectrum correction has been applied. The power values seen in plot d of each figure are calculated from the ensemble mean spectra derived from the beats selected from the unfiltered sonogram, and are normalised to the mean of the uncorrected values in each case. Similarly, plot e in each figure shows

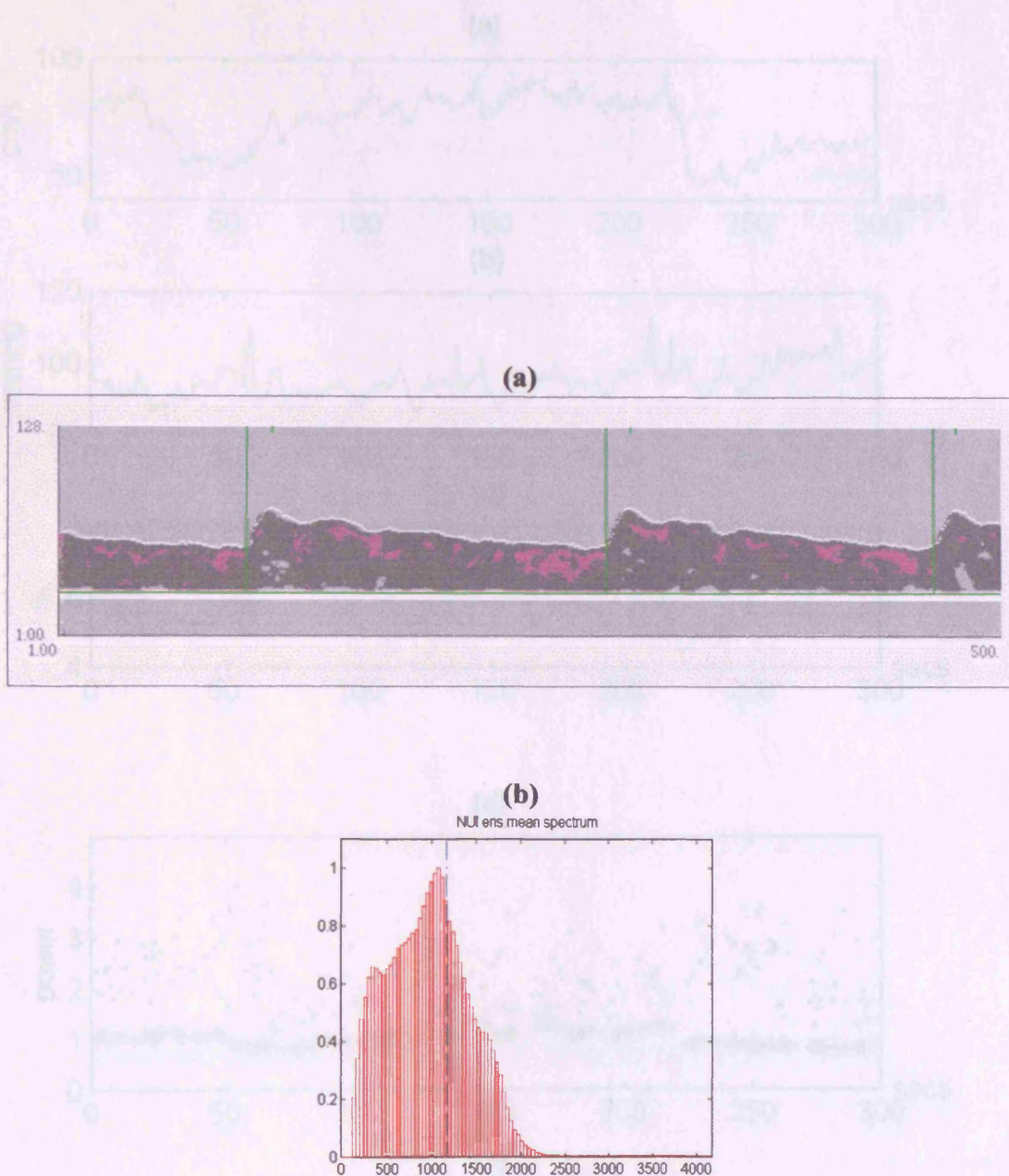


Figure 8.2 (a) A section of the Doppler signal sonogram recorded from the MCA of a healthy adult volunteer. A directional filter noise-smoothing algorithm has been applied to the sonogram. **(b)** the ensemble mean spectrum derived from the first beat seen in the signal.

Figure 8.1 CFS raw data for subject 1, showing (a) measured blood flow velocity (b) arterial blood pressure (c) and heart rate (d) raw (++) and corrected (x) power values derived from the unfiltered Doppler sonogram (e) raw (++) and corrected (x) power values derived from the filtered Doppler sonogram.

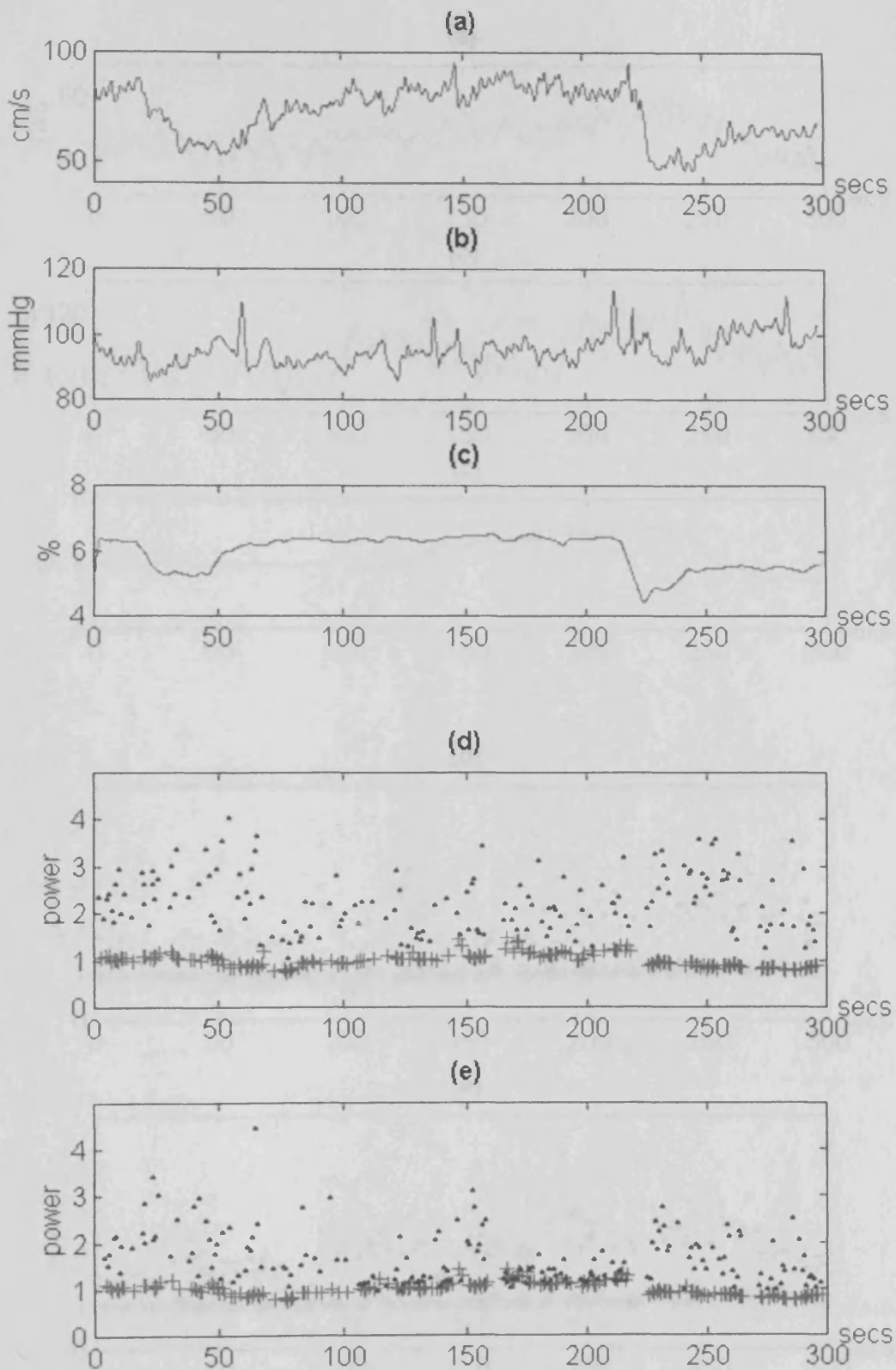


Figure 8.3 CO₂ reactivity data for subject 1, showing (a) maximum blood flow velocity (b) arterial blood pressure (c) end tidal CO₂ (d) raw (+) and corrected (•) power values derived from the unfiltered Doppler sonogram (e) raw (+) and corrected (•) power values derived from the filtered Doppler sonogram

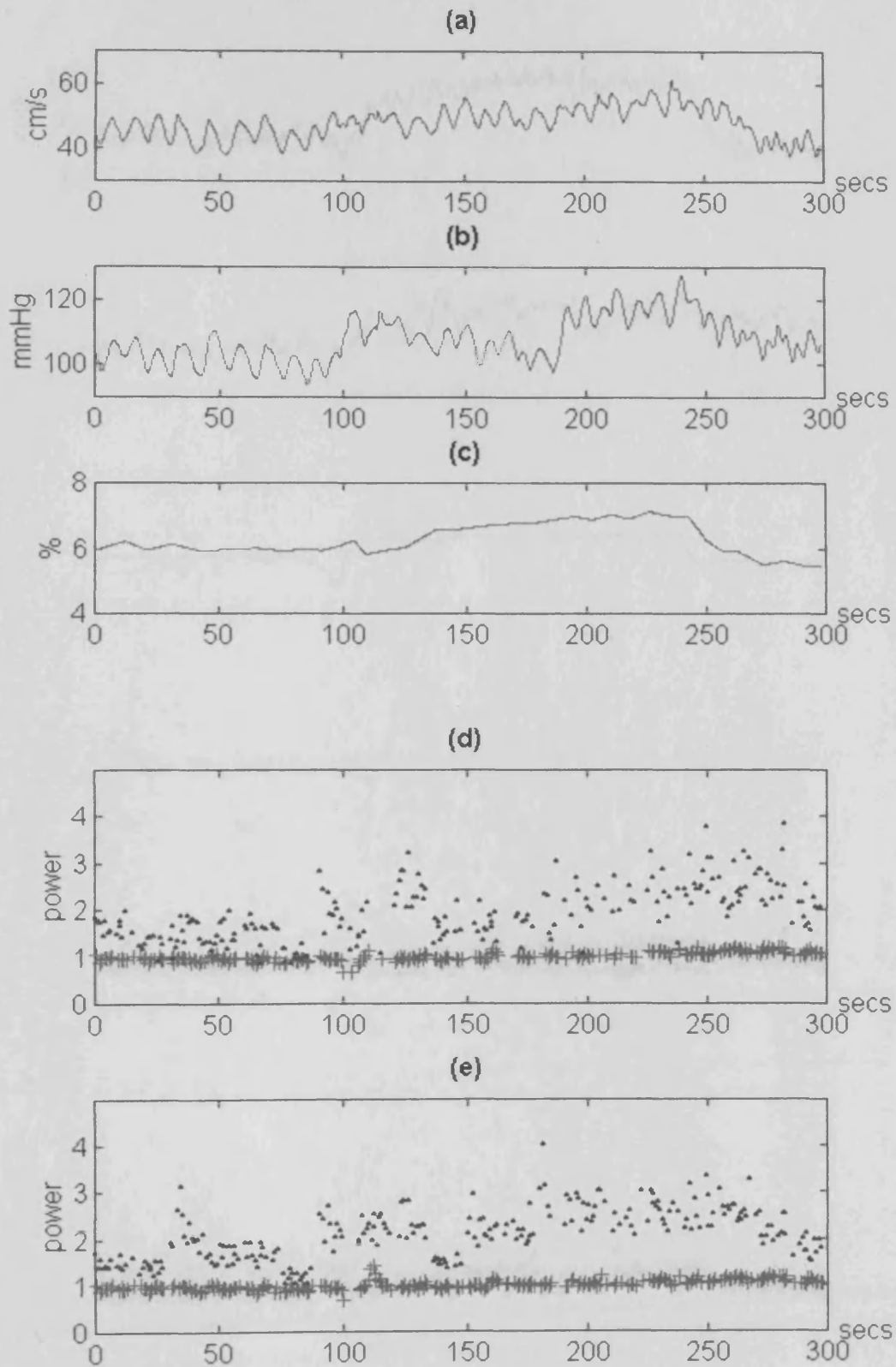


Figure 8.4 CO₂ reactivity data for subject 2, showing (a) maximum blood flow velocity (b) arterial blood pressure (c) end tidal CO₂ (d) raw (+) and corrected (•) power values derived from the unfiltered Doppler sonogram (e) raw (+) and corrected (•) power values derived from the filtered Doppler sonogram

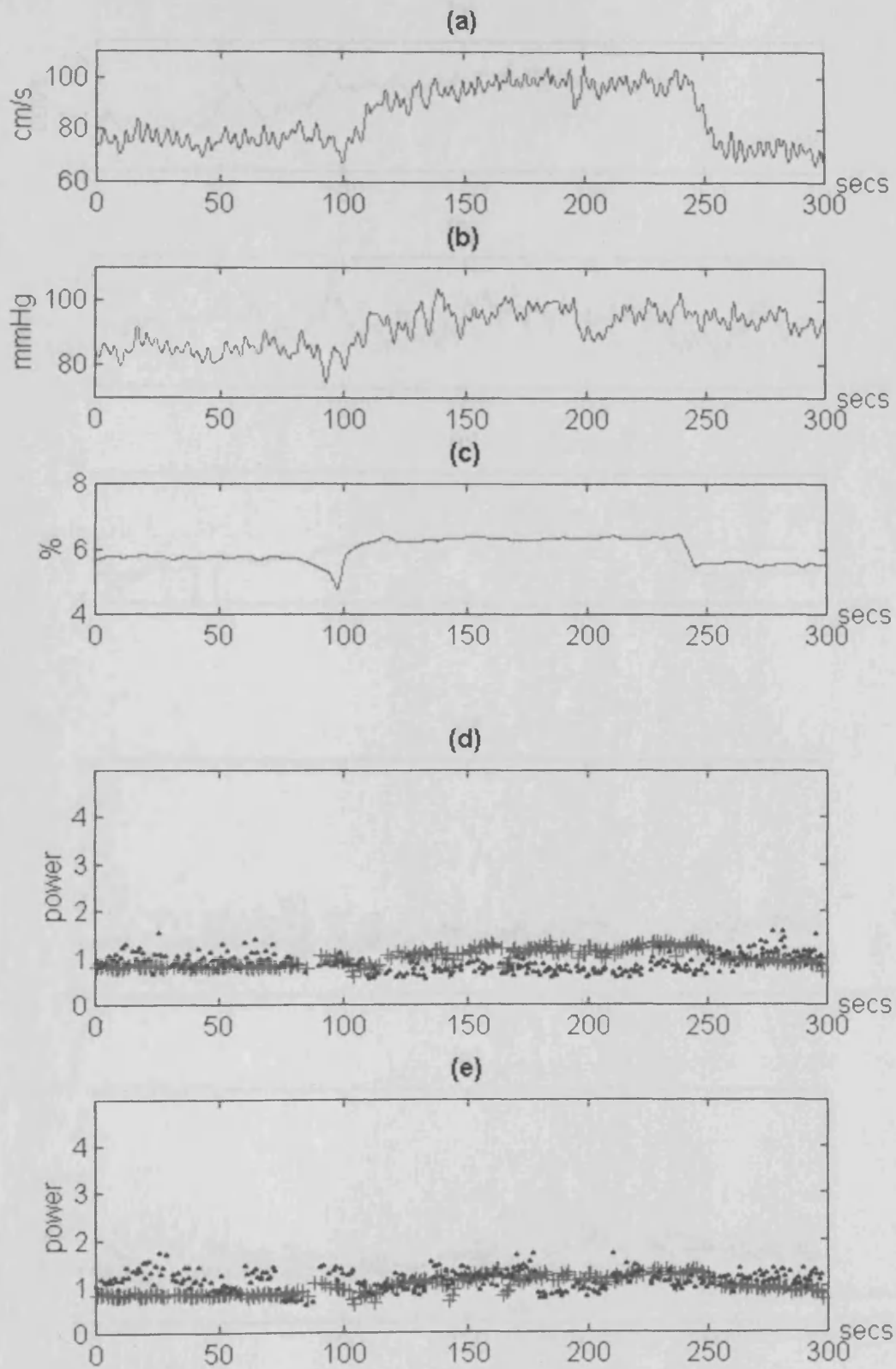


Figure 8.5 CO₂ reactivity data for subject 3, showing (a) maximum blood flow velocity (b) arterial blood pressure (c) end tidal CO₂ (d) raw (+) and corrected (•) power values derived from the unfiltered Doppler sonogram (e) raw (+) and corrected (•) power values derived from the filtered Doppler sonogram

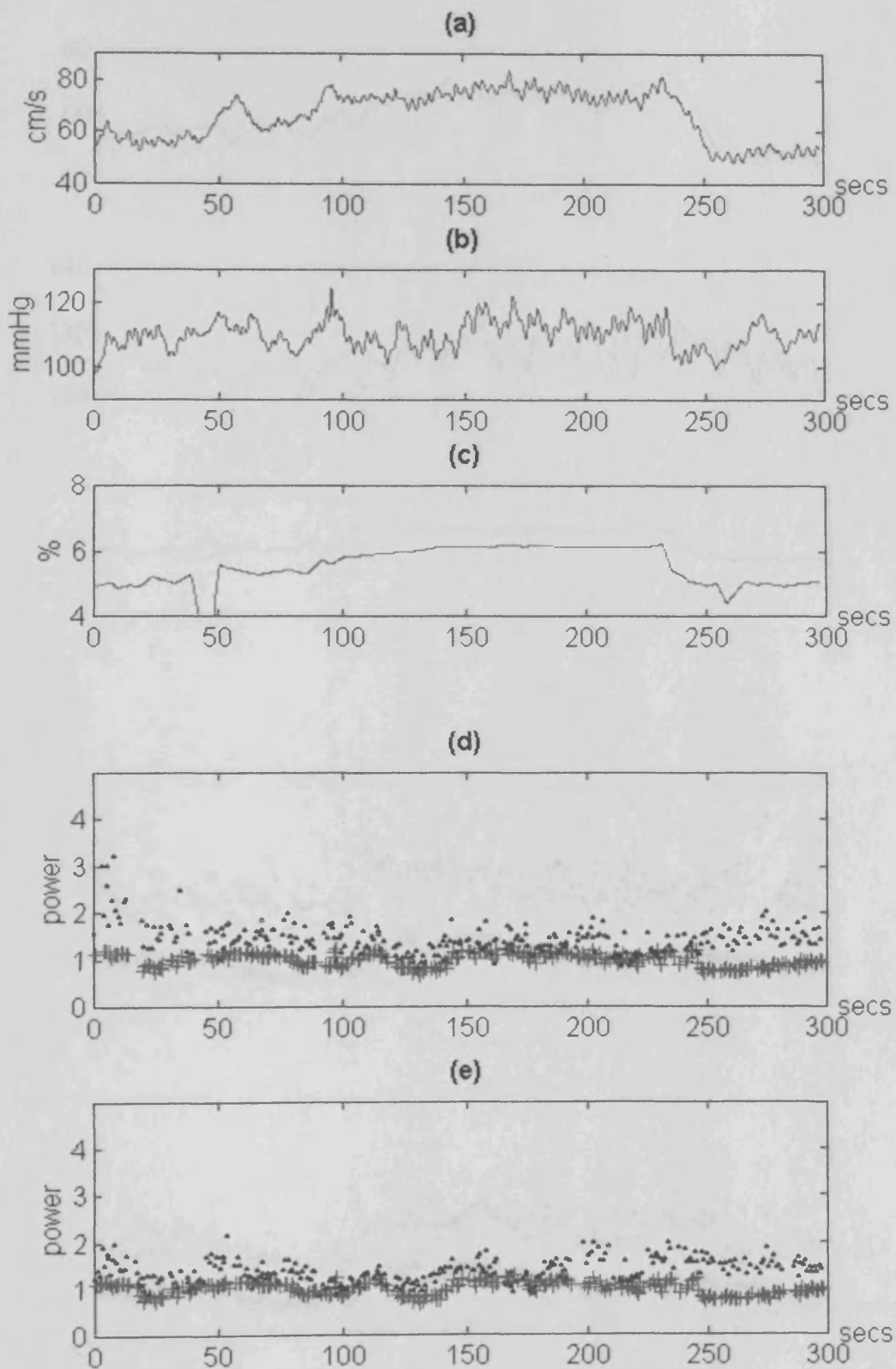


Figure 8.6 CO₂ reactivity data for subject 4, showing (a) maximum blood flow velocity (b) arterial blood pressure (c) end tidal CO₂ (d) raw (+) and corrected (•) power values derived from the unfiltered Doppler sonogram (e) raw (+) and corrected (•) power values derived from the filtered Doppler sonogram

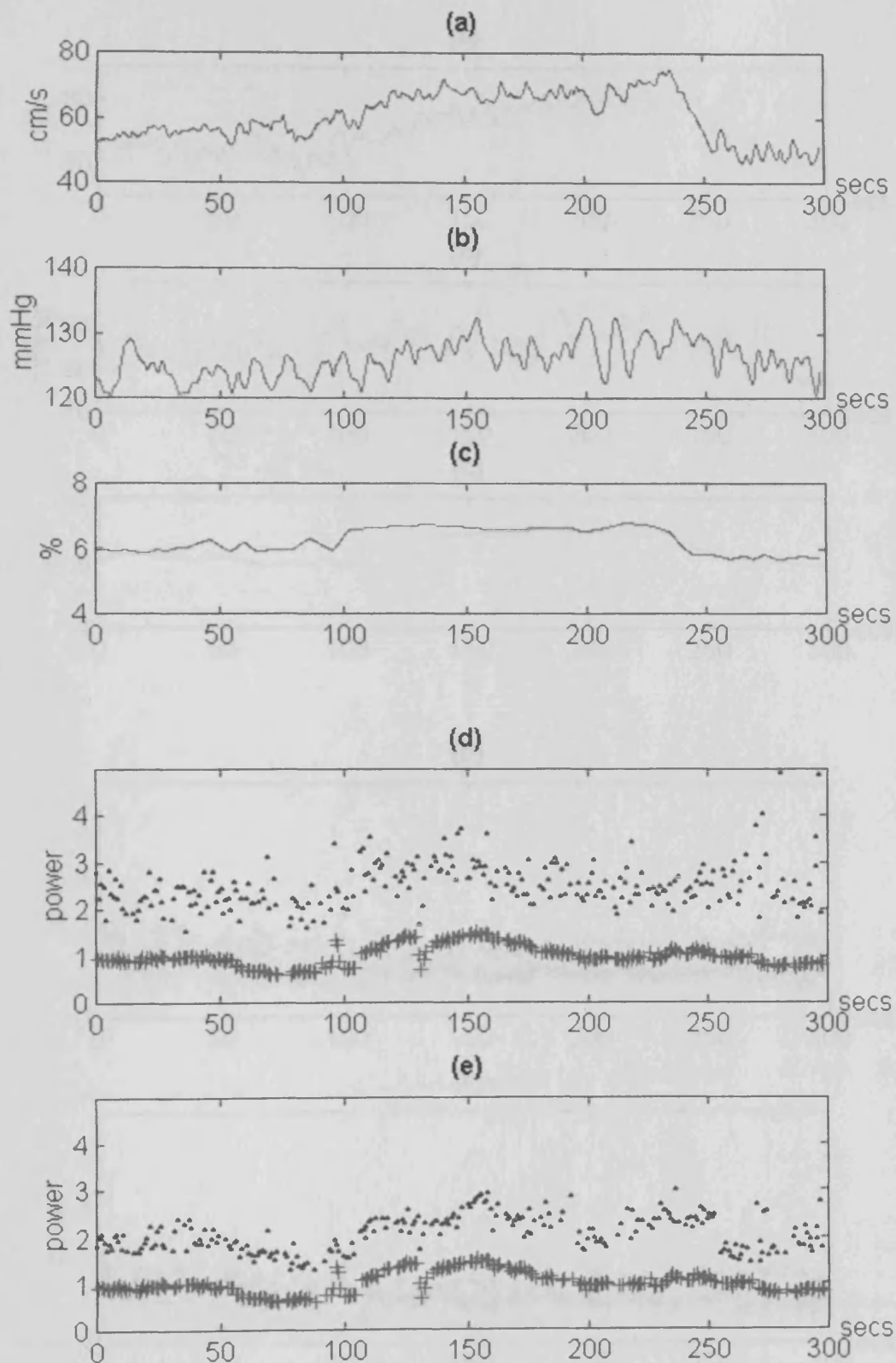


Figure 8.7 CO₂ reactivity data for subject 5, showing (a) maximum blood flow velocity (b) arterial blood pressure (c) end tidal CO₂ (d) raw (+) and corrected (•) power values derived from the unfiltered Doppler sonogram (e) raw (+) and corrected (•) power values derived from the filtered Doppler sonogram

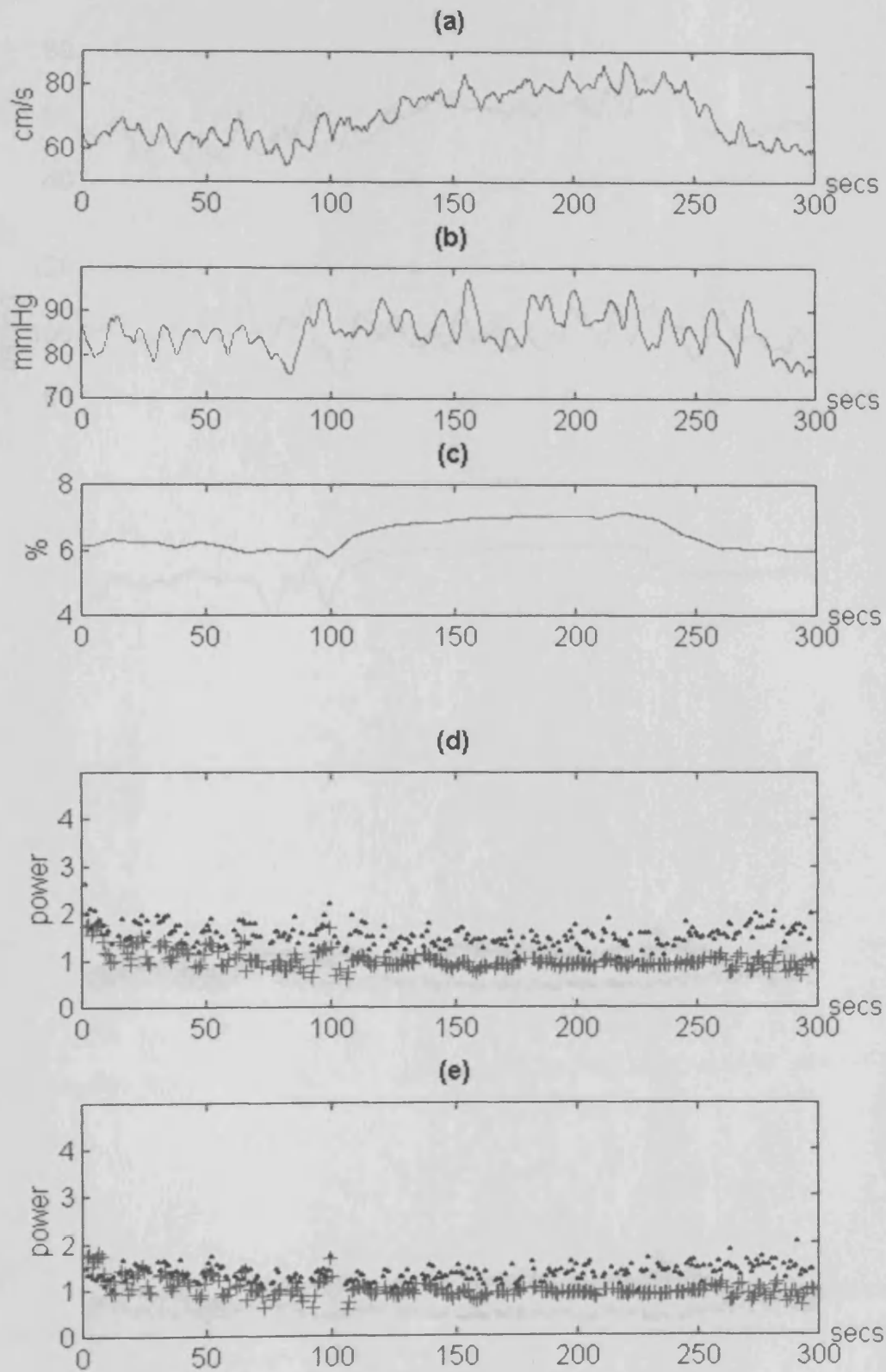


Figure 8.8 CO₂ reactivity data for subject 6, showing (a) maximum blood flow velocity (b) arterial blood pressure (c) end tidal CO₂ (d) raw (+) and corrected (•) power values derived from the unfiltered Doppler sonogram (e) raw (+) and corrected (•) power values derived from the filtered Doppler sonogram

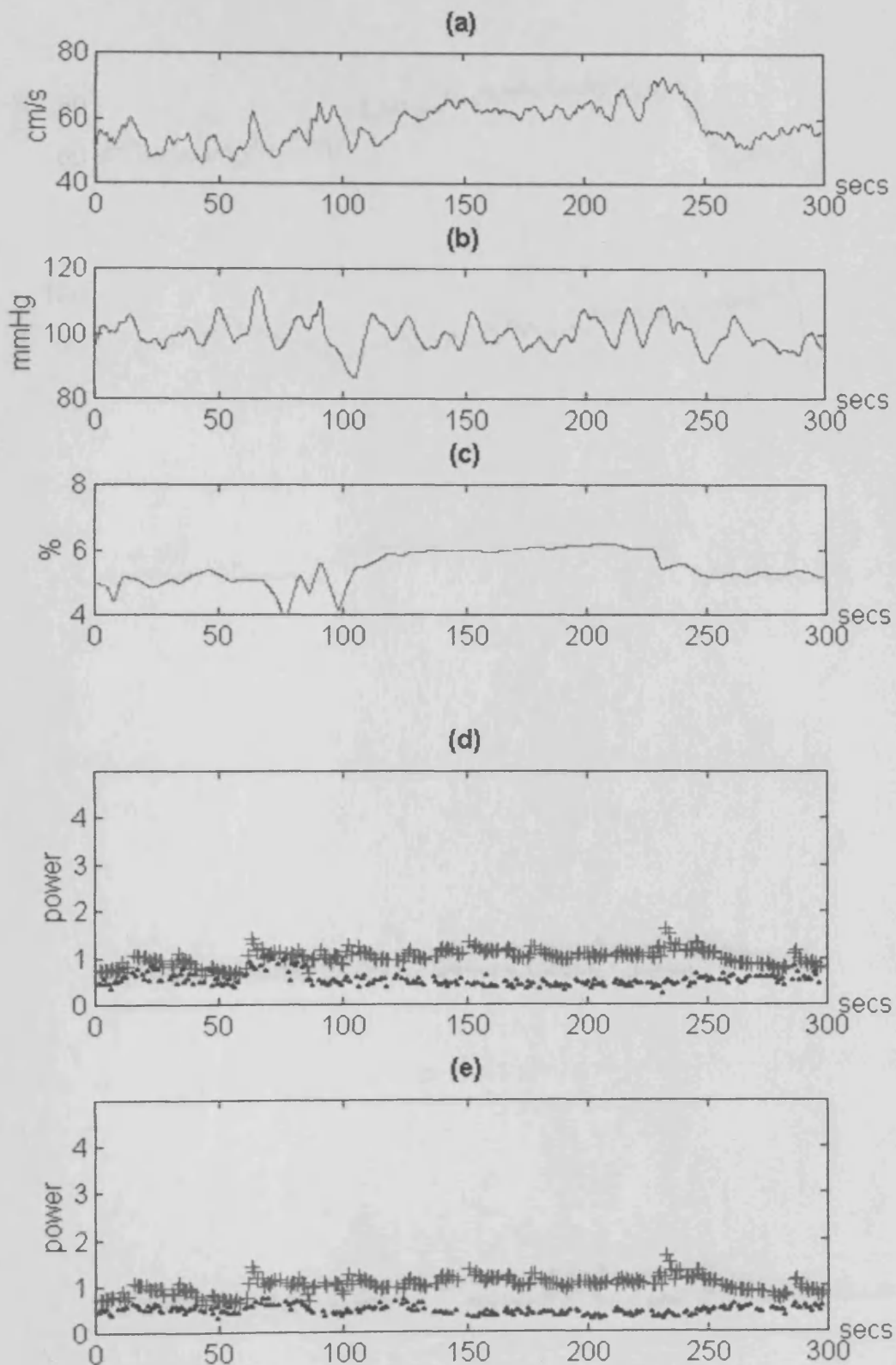


Figure 8.9 CO₂ reactivity data for subject 7, showing (a) maximum blood flow velocity (b) arterial blood pressure (c) end tidal CO₂ (d) raw (+) and corrected (•) power values derived from the unfiltered Doppler sonogram (e) raw (+) and corrected (•) power values derived from the filtered Doppler sonogram

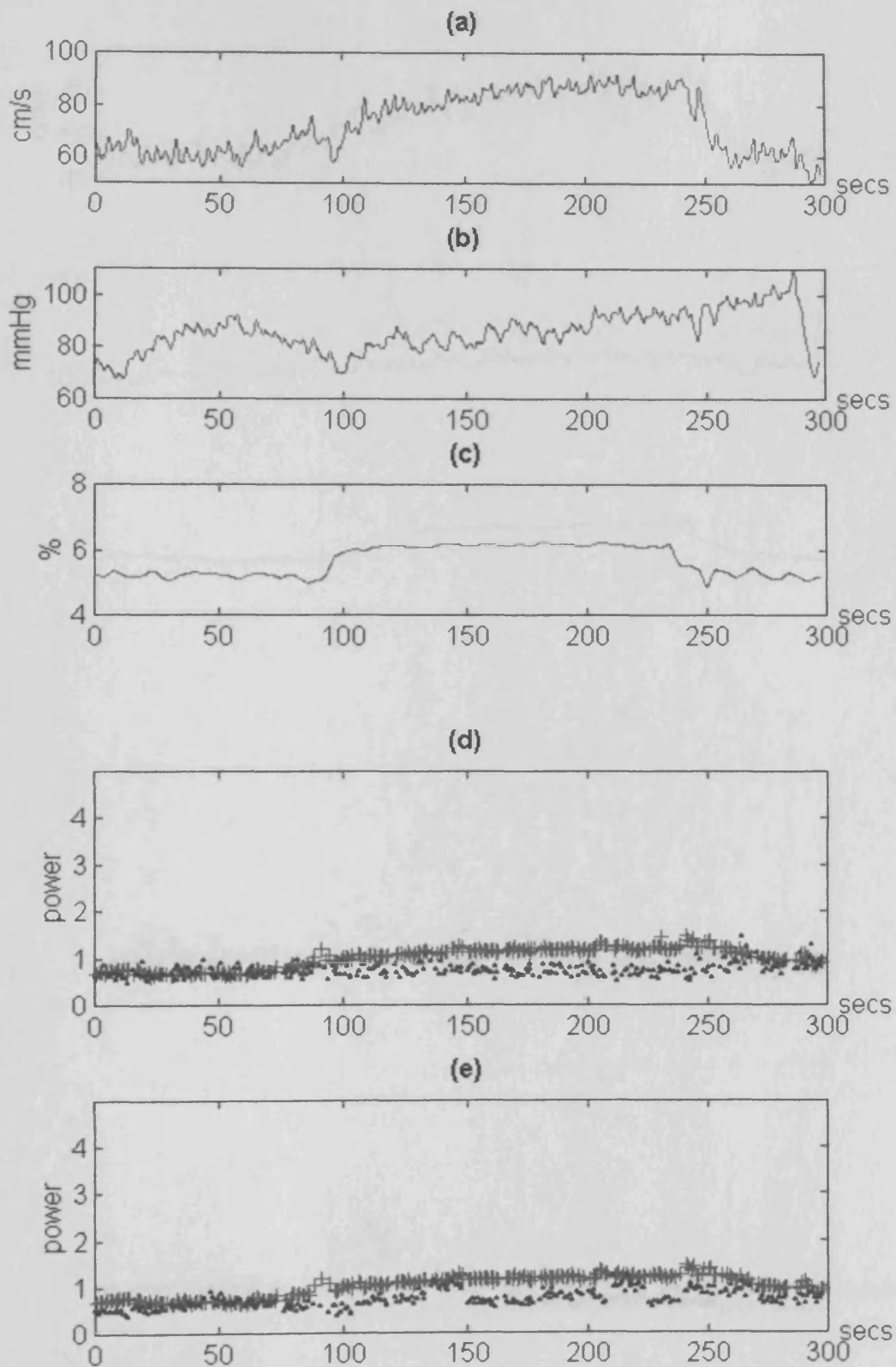


Figure 8.10 CO₂ reactivity data for subject 8, showing (a) maximum blood flow velocity (b) arterial blood pressure (c) end tidal CO₂ (d) raw (+) and corrected (•) power values derived from the unfiltered Doppler sonogram (e) raw (+) and corrected (•) power values derived from the filtered Doppler sonogram

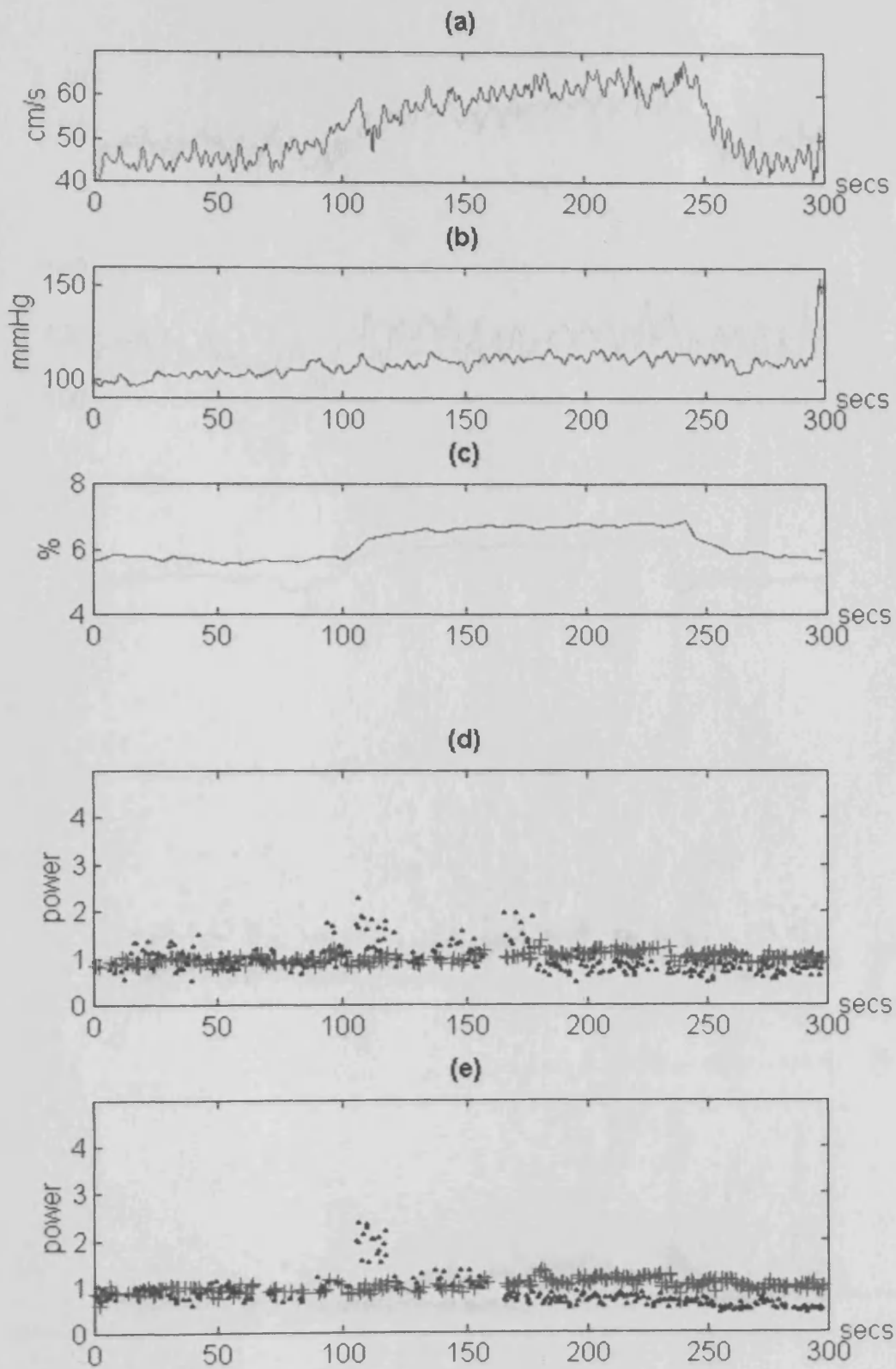


Figure 8.11 CO₂ reactivity data for subject 9, showing (a) maximum blood flow velocity (b) arterial blood pressure (c) end tidal CO₂ (d) raw (+) and corrected (•) power values derived from the unfiltered Doppler sonogram (e) raw (+) and corrected (•) power values derived from the filtered Doppler sonogram

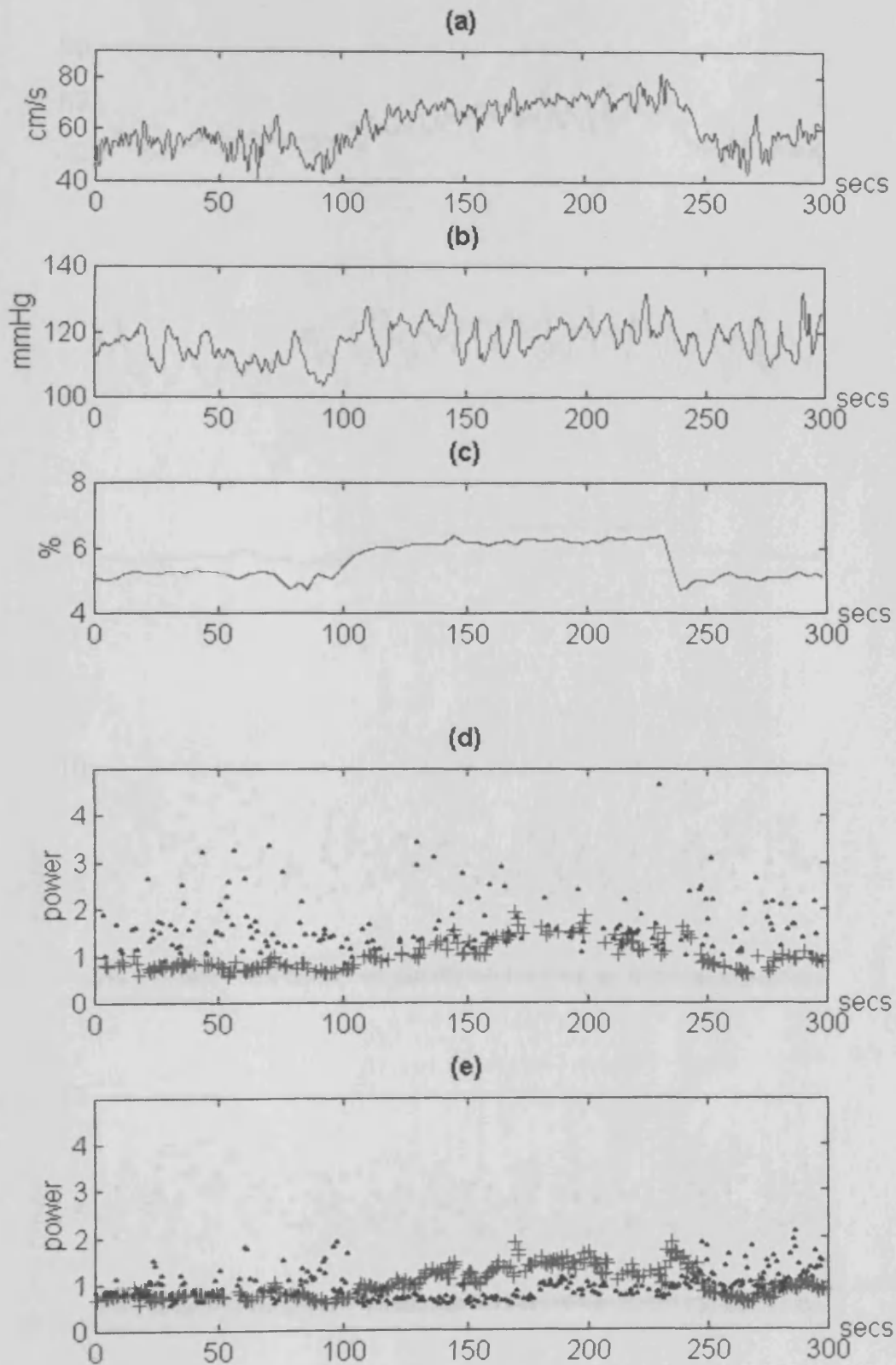


Figure 8.12 CO₂ reactivity data for subject 10, showing (a) maximum blood flow velocity (b) arterial blood pressure (c) end tidal CO₂ (d) raw (+) and corrected (•) power values derived from the unfiltered Doppler sonogram (e) raw (+) and corrected (•) power values derived from the filtered Doppler sonogram

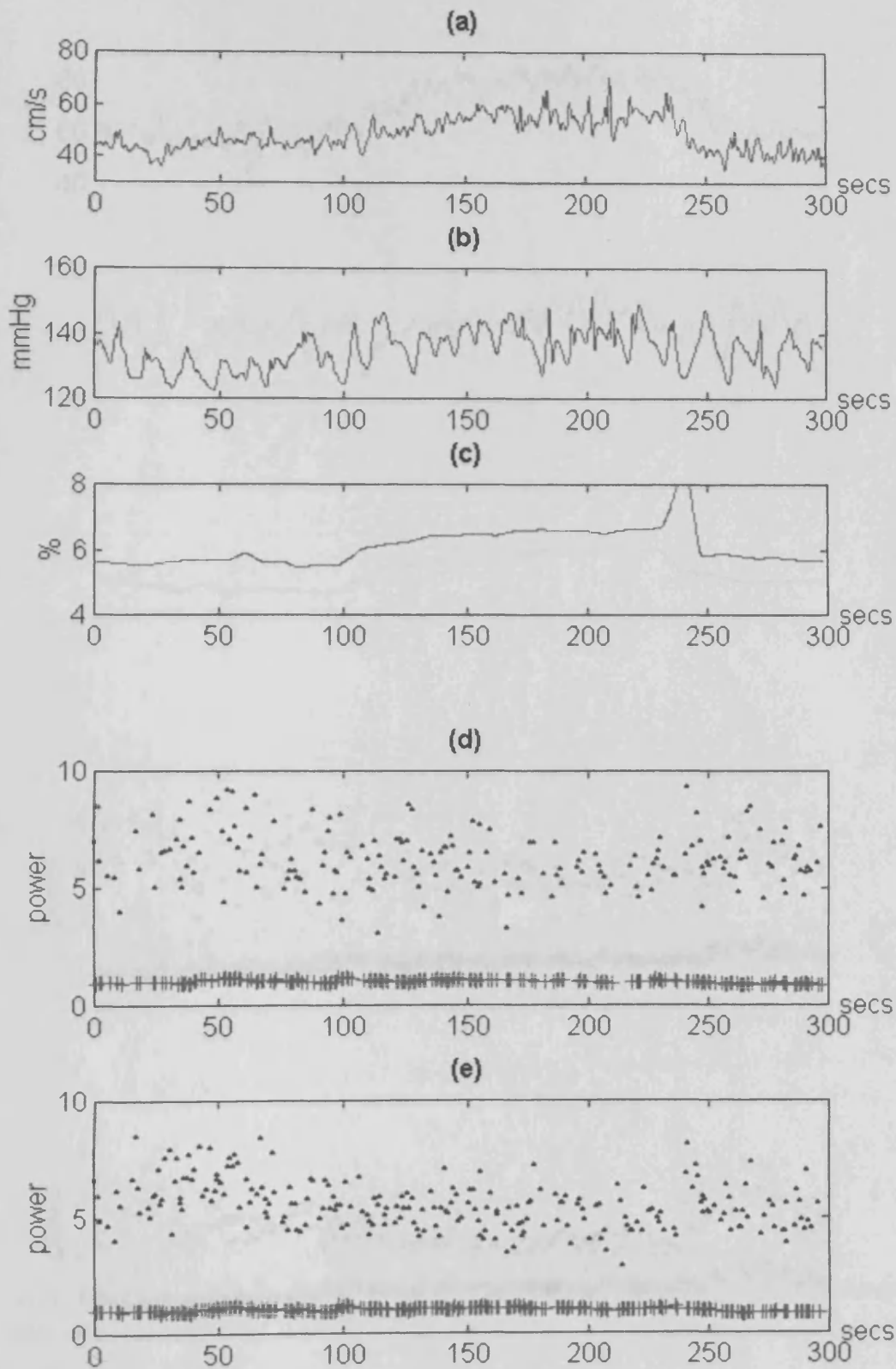


Figure 8.13 CO₂ reactivity data for subject 11, showing (a) maximum blood flow velocity (b) arterial blood pressure (c) end tidal CO₂ (d) raw (+) and corrected (•) power values derived from the unfiltered Doppler sonogram (e) raw (+) and corrected (•) power values derived from the filtered Doppler sonogram

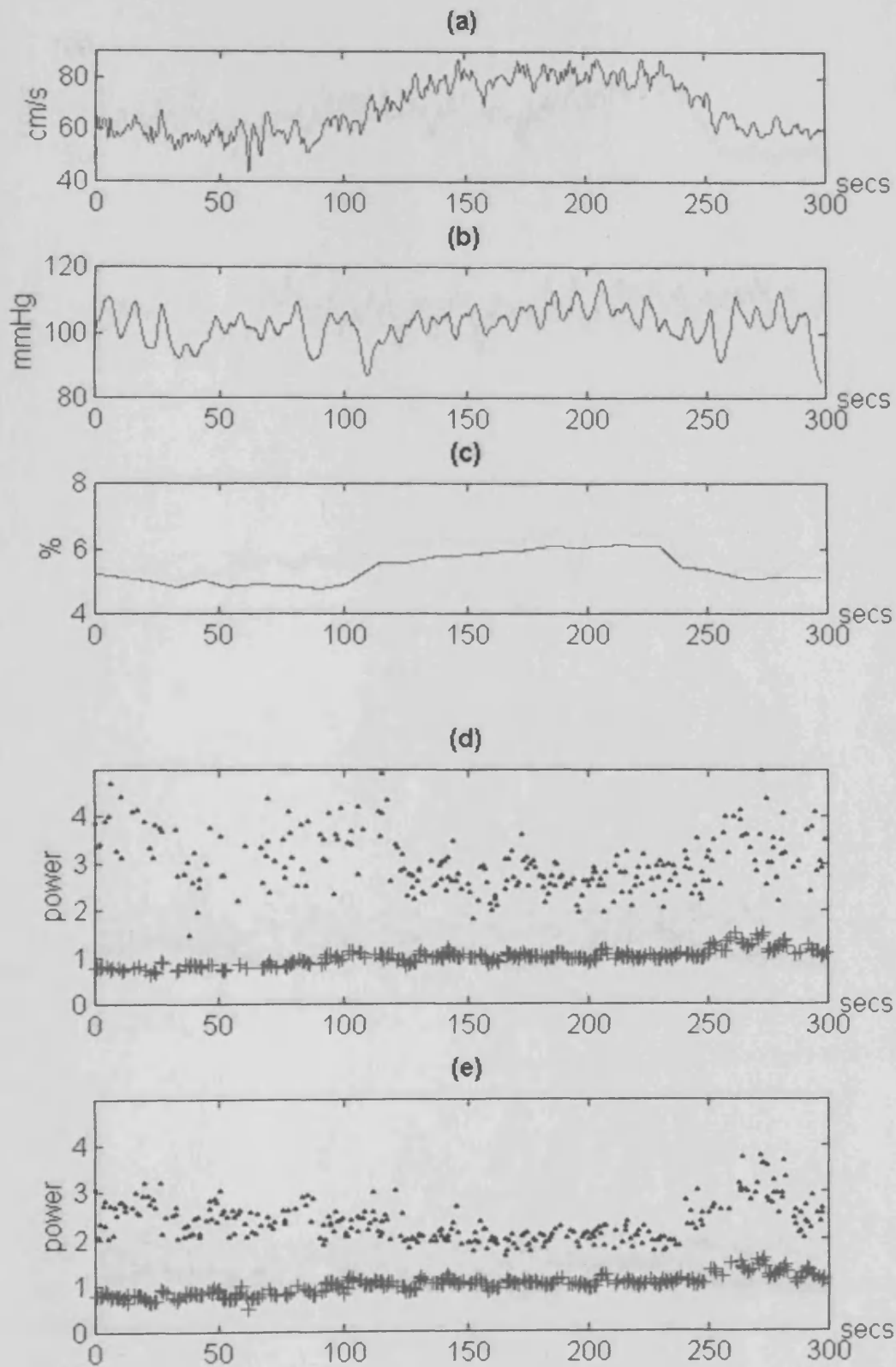


Figure 8.14 CO₂ reactivity data for subject 12, showing (a) maximum blood flow velocity (b) arterial blood pressure (c) end tidal CO₂ (d) raw (+) and corrected (•) power values derived from the unfiltered Doppler sonogram (e) raw (+) and corrected (•) power values derived from the filtered Doppler sonogram

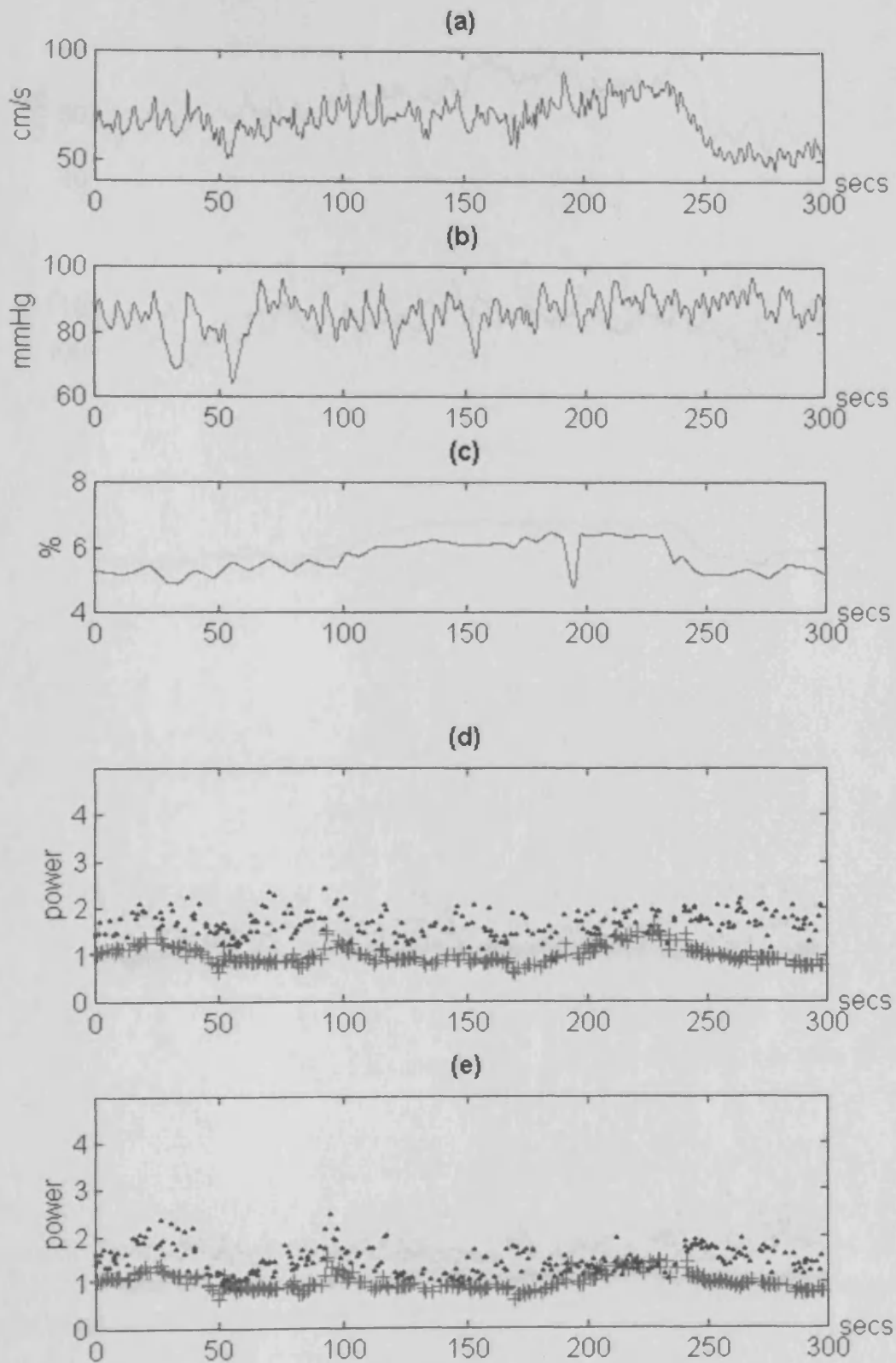


Figure 8.15 CO₂ reactivity data for subject 13, showing (a) maximum blood flow velocity (b) arterial blood pressure (c) end tidal CO₂ (d) raw (+) and corrected (•) power values derived from the unfiltered Doppler sonogram (e) raw (+) and corrected (•) power values derived from the filtered Doppler sonogram

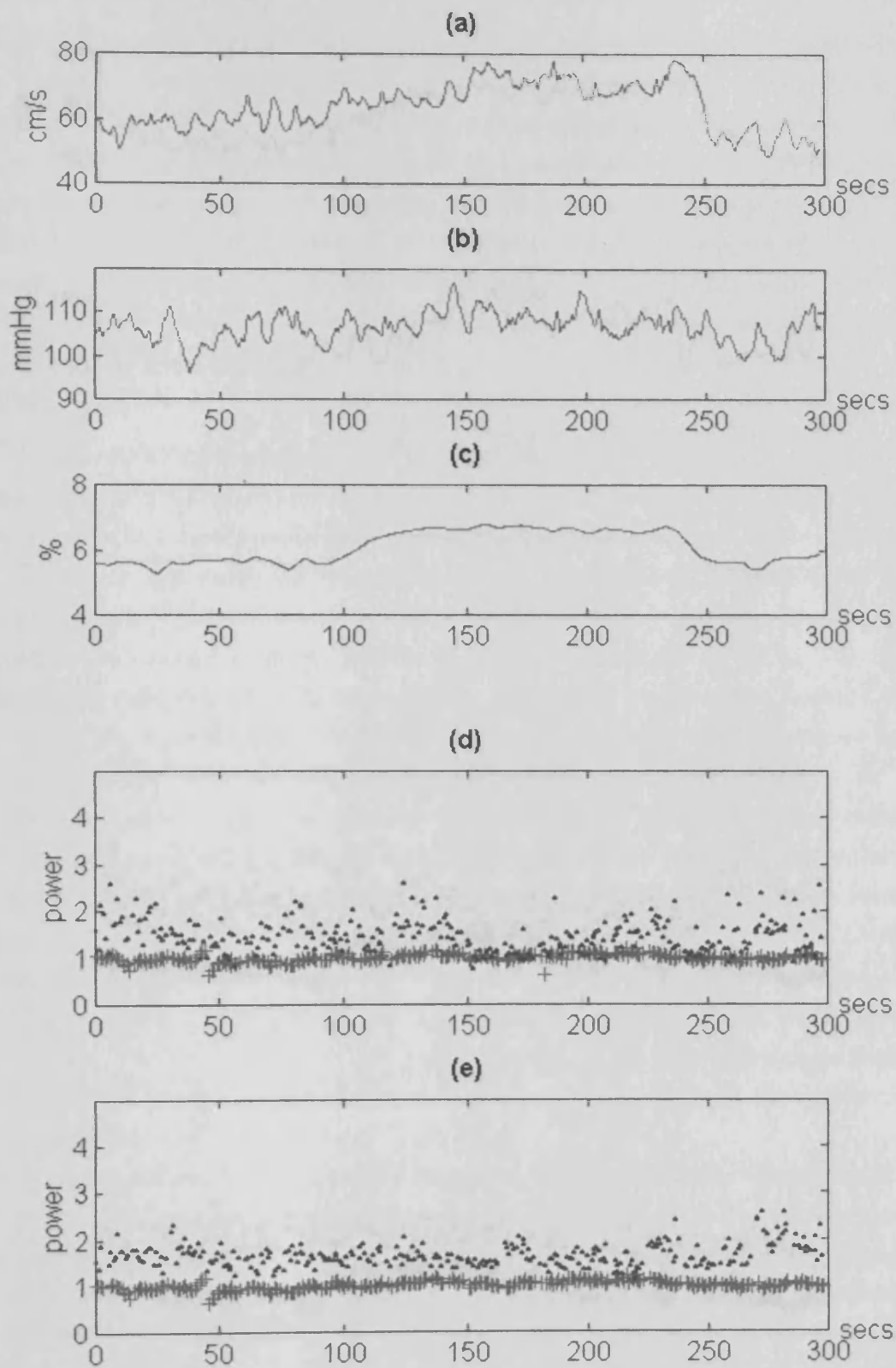


Figure 8.16 CO₂ reactivity data for subject 14, showing (a) maximum blood flow velocity (b) arterial blood pressure (c) end tidal CO₂ (d) raw (+) and corrected (•) power values derived from the unfiltered Doppler sonogram (e) raw (+) and corrected (•) power values derived from the filtered Doppler sonogram

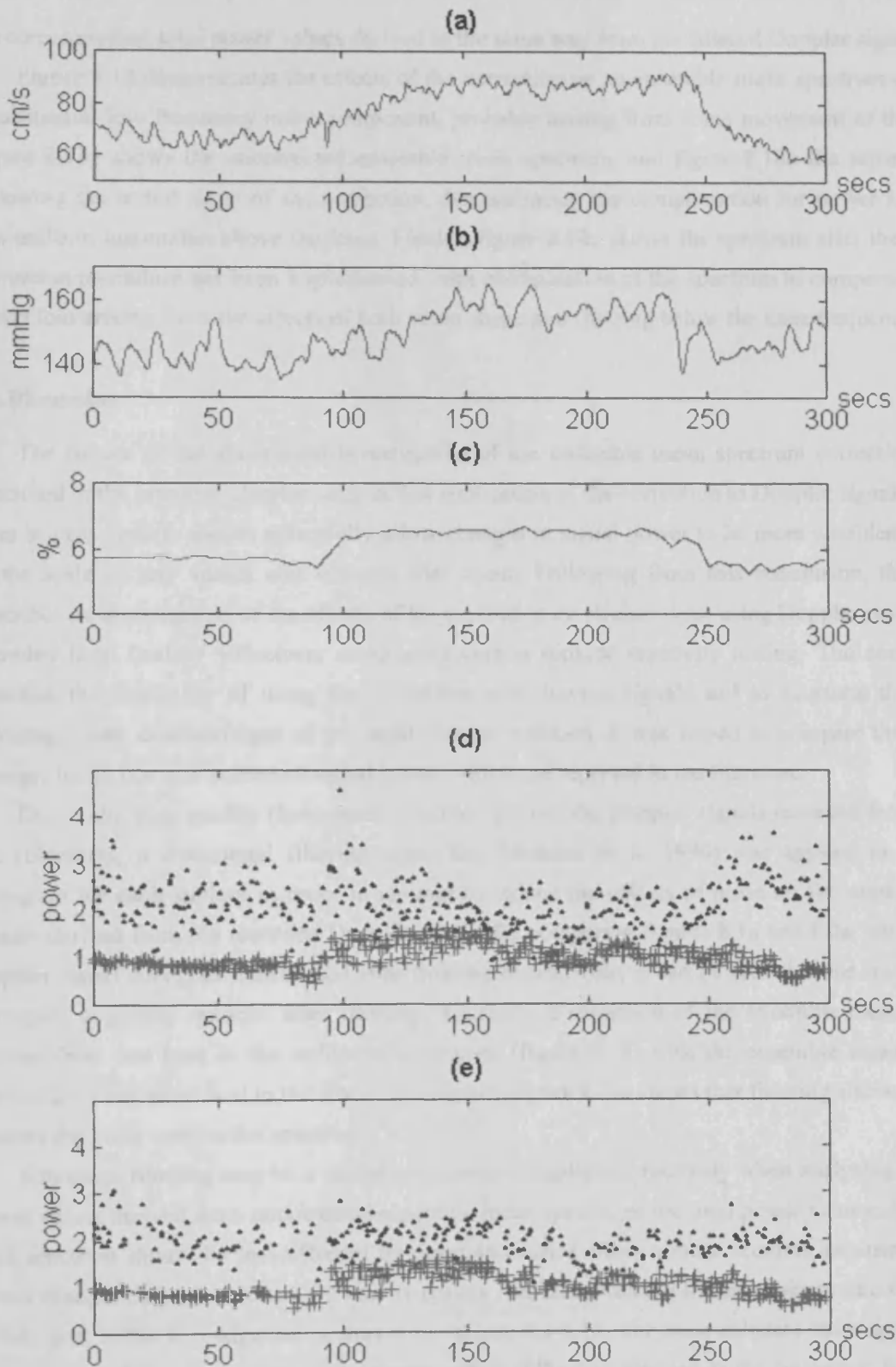


Figure 8.17 CO₂ reactivity data for subject 15, showing (a) maximum blood flow velocity (b) arterial blood pressure (c) end tidal CO₂ (d) raw (+) and corrected (•) power values derived from the unfiltered Doppler sonogram (e) raw (+) and corrected (•) power values derived from the filtered Doppler sonogram

the corresponding total power values derived in the same way from the filtered Doppler signal.

Figure 8.18 demonstrates the effects of the correction on an ensemble mean spectrum containing a substantial low frequency noise component, probably arising from some movement of the subject. Figure 8.18a shows the uncorrected ensemble mean spectrum, and figure 8.18b the same spectrum following the initial stage of the correction, demonstrating the compensation for power loss due to non-uniform insonation above the knee. Finally, figure 8.18c shows the spectrum after the complete correction procedure has been implemented, with extrapolation of the spectrum to compensate for the power loss arising from the effects of both beam shape and filtering below the knee frequency.

8.6 Discussion

The results of the theoretical investigation of the ensemble mean spectrum correction method described in the previous chapter suggest that application of the correction to Doppler signals recorded from in-vivo vessels should potentially allow changes in signal power to be more confidently related to the scale of any vessel size changes that occur. Following from this conclusion, this chapter describes an investigation of the effects of the correction on clinical data, using Doppler power signals recorded from healthy volunteers undergoing carbon dioxide reactivity testing. The aims were to establish the feasibility of using the correction with in-vivo signals and to illustrate the possible advantages and disadvantages of the technique. In addition, it was hoped to compare the observed changes in the raw and corrected signal power with those reported in the literature.

Due to the poor quality (low signal-to-noise ratio) of the Doppler signals recorded from some of the volunteers, a directional filtering algorithm (Hoskins et al. 1990) was applied to the signal sonogram for each subject in order to attempt to reduce the effects of noise on the ensemble mean spectra derived from the recorded Doppler signal. By comparing figures 8.1a and 8.2a, which show a Doppler signal sonogram before and after filtering respectively, it can be seen that the speckle in the sonogram is greatly reduced after filtering. Similarly, comparison of the ensemble mean spectrum derived from one beat in the unfiltered sonogram (figure 8.1b) with the ensemble mean spectrum derived from the same beat in the filtered sonogram (figure 8.2b) shows that filtering also successfully reduces the noise seen in the spectrum.

Sonogram filtering may be a useful procedure to implement routinely when analysing raw signal power values derived from uncorrected ensemble mean spectra, as the total power value calculated for each spectrum should be less affected by noise and hence allow a more accurate assessment of any power changes that occur. The CO₂ reactivity data recorded from the fifteen subjects who volunteered to take part in the investigation is shown in figures 8.3-8.17. For most subjects there appears to be little obvious change in the raw signal power values following filtering of the sonogram, but on close inspection it is possible to identify at least one example where filtering results in a slightly reduced spread of values (figure 8.17). Although the effects are not apparent in many cases, the potential for improvement in only a few might make the use of a filtering procedure worthwhile when analysing Doppler power data.

A more obvious benefit of filtering the Doppler sonogram occurs when applying the ensemble mean spectrum correction to clinical signals. Filtering the sonogram has two main effects on the

correction, being a multiple of the average envelope is indicated, which allows the derivation of more accurate values for the knee and maximum frequency of the envelope's mean spectrum. It is usually a judgement for the choice of noise on the envelope mean spectrum which used in the correction. Figure 8.18(a) shows that for the unfiltered signal power values, the correction tends to increase the dispersion over a low frequency range, but only to the extent that the uncorrected total power value.

However, this dispersion is not as large as for the power values derived from the filtered signal (Figure 8.18(b)). The correction of the power values at low frequencies is not as large as for the uncorrected power values, and following the application of the correction, the dispersion over a low frequency range is also likely to increase. The correction of the power values is also likely to increase the dispersion over a low frequency range that are required by the correction.

The effect of the correction on the dispersion of the power values is also likely to increase the dispersion over a low frequency range that are required by the correction. The correction of the power values is also likely to increase the dispersion over a low frequency range that are required by the correction.

and very little dispersion. The correction of the power values is also likely to increase the dispersion over a low frequency range that are required by the correction. The correction of the power values is also likely to increase the dispersion over a low frequency range that are required by the correction.

of the spectrum. The correction of the power values is also likely to increase the dispersion over a low frequency range that are required by the correction. The correction of the power values is also likely to increase the dispersion over a low frequency range that are required by the correction.

frequency. The correction of the power values is also likely to increase the dispersion over a low frequency range that are required by the correction. The correction of the power values is also likely to increase the dispersion over a low frequency range that are required by the correction.

signal on the spectrum. The correction of the power values is also likely to increase the dispersion over a low frequency range that are required by the correction. The correction of the power values is also likely to increase the dispersion over a low frequency range that are required by the correction.

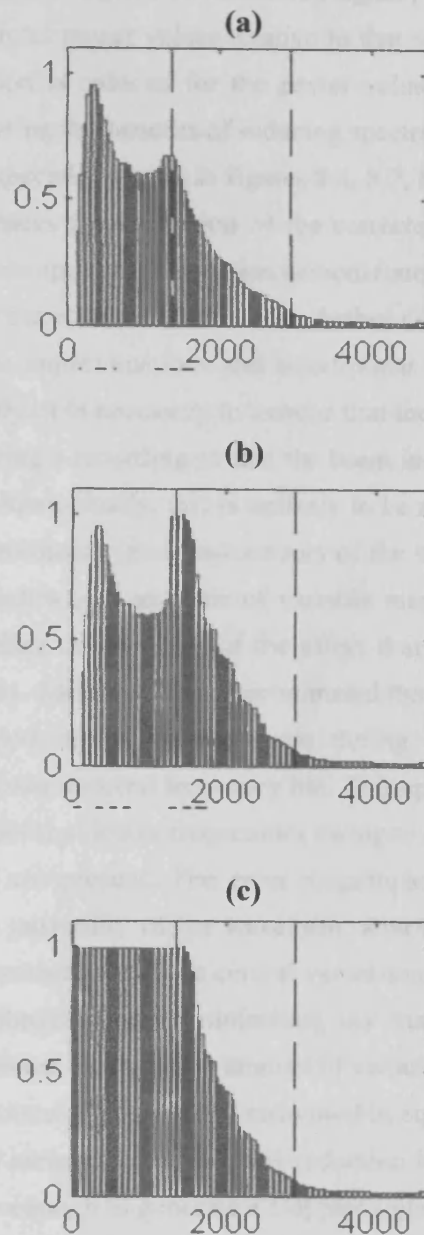


Figure 8.18 The effects of correction on an ensemble mean spectrum exhibiting a low frequency noise peak. **(a)** shows the raw spectrum, **(b)** the spectrum after the initial stage of the correction and **(c)** the spectrum after extrapolation of the power value at the knee frequency to cover the frequencies below this.

...the magnitude of the individual errors for any one flow will depend on the relative conditions at that time, the level of noise in the corrected power values will also vary with flow, indicating the dispersion over the flow, being to the fact that it is not possible to correct...

correction; firstly it enables a cleaner sonogram envelope to be derived, which allows the derivation of more accurate values for the knee and maximum frequencies of the ensemble mean spectra, and secondly it minimises the influence of noise on the ensemble mean spectrum values used in the correction. Figures 8.3d-8.17d show that for the unfiltered signal power values, the correction tends to increase the dispersion of the total power values relative to that seen for the uncorrected total power values. However, this dispersion is reduced for the power values derived from the filtered signals (figures 8.3e-8.17e), demonstrating the benefits of reducing spectral noise. The reduction of the power value dispersion can be seen especially clearly in figures 8.4, 8.7, 8.12, 8.14, 8.16 and 8.17.

The fact that filtering reduces the dispersion of the corrected power values seen following the application of the ensemble mean spectrum correction demonstrates that spectral noise is one source of the spread in values caused by the correction. However, further dispersion of the power values is also likely to arise from the various approximations and assumptions that are required by the correction theory (see section 7.4.3). Firstly, it is necessary to assume that the relative positions of the transducer and vessel remain constant during a recording so that the beam intensity covering the central annulus of the vessel does not change. Realistically, this is unlikely to be achievable for the duration of an in-vivo recording owing to unpreventable small movements of the subject and of the transducer (these are discussed in more detail below), so an error of variable magnitude might be introduced to the corrected power values depending on the scale of the effect that any movements have on the beam shape across the central annulus. Secondly, it is approximated that the maximum blood flow velocity remains constant for the period in the cardiac cycle during which the flow contains velocity components relevant to a particular spectral frequency bin. This approximation is good for the highest frequency bins, but becomes poorer at lower frequencies owing to the increasing periods for which the relevant velocity components are present. The error magnitude introduced from this source will depend on the variation in the pulsatility of the waveform, with highly pulsatile flow producing the greatest errors. Finally, the allocated size of the central vessel annulus is required to remain constant, but this criteria can only be approximated by minimising any changes in the annulus size that result from changes in the vessel diameter. Because the amount of variation in the size of the central annulus is proportional to the selected value of the velocity ratio used in equation 7.23, it can be minimised by reducing the size of the central annulus. However, any reduction in size is limited by the need for the central annulus to remain large enough to generate a Doppler signal of an adequate magnitude to give an accurate measure of the relevant volume of blood. The error introduced in this case will therefore depend on the velocity ratio value and the scale of any vessel size changes that occur.

The magnitude of the total error introduced by the above sources to the corrected power value calculated for each beat in a signal will depend on the individual error from each that arises on a beat-to-beat basis. For example, a large total error might be expected if a shift in the position of the vessel in the beam occurs simultaneously to a change in vessel size at a time when the blood flow is exhibiting increased pulsatility over the cardiac cycle and the recorded Doppler signal has a low signal-to-noise ratio. Because the magnitude of the individual errors for any one beat will depend on the relevant conditions at that time, the total error present in the corrected power values will also vary with time, producing the dispersion seen in the data. Owing to the fact that it is not possible to control

either the pulsatility of the blood flow waveform or the size of any changes in vessel size that occur, the only ways of minimising the dispersion in power values caused by the correction are to optimise the signal-to-noise ratio, filter the Doppler signals to reduce noise, and attempt to keep the vessel position stationary in the beam.

The recording of the Doppler signals during the CO₂ reactivity tests highlighted the difficulties encountered when attempting to obtain Doppler signal power data that can confidently be considered to represent changes in vessel size. It was observed that even very small involuntary movements of a subject could cause changes in the signal power that were unrelated to changes in vessel size, providing the potential for misinterpretation as vessel size changes. Examples of such movements included swallowing, jaw movements, eye movements and speech. Although it was requested that each subject remain as still as possible during the tests, it proved extremely difficult to eliminate all movements which affected the signal power. The fact that this was the case for healthy volunteers with a good understanding of what was required of them suggests that maintaining a stationary transducer position during recordings from patients in poor health may present even greater difficulties.

Observation of the subjects during the CO₂ reactivity study and the subsequent analysis of the recorded signals demonstrated that movement of the subjects could cause changes in power to occur by two processes; firstly by facial movements causing the displacement of the transducer and resulting in an increase or decrease in the total power depending on the change in the beam shape across the MCA, and secondly by noise actions (for example speech and throat clearing) causing the introduction of low frequency noise to the signal. Power changes arising from these sources were further investigated by taking Doppler signal recordings from the MCA of a volunteer placed under the same conditions as used for the CO₂ reactivity tests, but without subjecting them to any form of cerebral blood flow stimulus. Recordings were made while the volunteer carried out a range of actions which were considered to be representative of the type that might occur during a standard clinical Doppler recording taken from a conscious subject - swallowing, moving eyebrows, speaking, clearing throat, small head movements and smiling. The effect of each of these on the Doppler signal power is shown in figures 8.19 and 8.20 respectively. It can be seen that most of the actions causes a noticeable change in the raw signal power, which if observed in a routine clinical recording could erroneously be interpreted as a change in vessel size. Unfortunately, because the recorded signals were of poor quality, a large degree of dispersion is evident in the corrected power values even after filtering of the sonogram, and it is therefore difficult to establish how well the correction has compensated for the change in power caused by each movement. However, it can be predicted that correcting the ensemble mean spectrum is likely to compensate for any power changes arising from low frequency noise because the correction method involves the extrapolation of the power at the knee frequency to replace the spectral values at frequencies below this, hence eliminating any low frequency noise peaks (figure 8.18). Conversely, the correction method is unlikely to completely compensate for any power changes arising from a change in beam shape across the vessel, as the changes to the ensemble mean spectrum are more likely to affect the entire spectral frequency range.

In addition to movement of the subjects causing unwanted changes in power during the CO₂ reactivity tests, further power changes were seen to arise from unprovoked movements of the

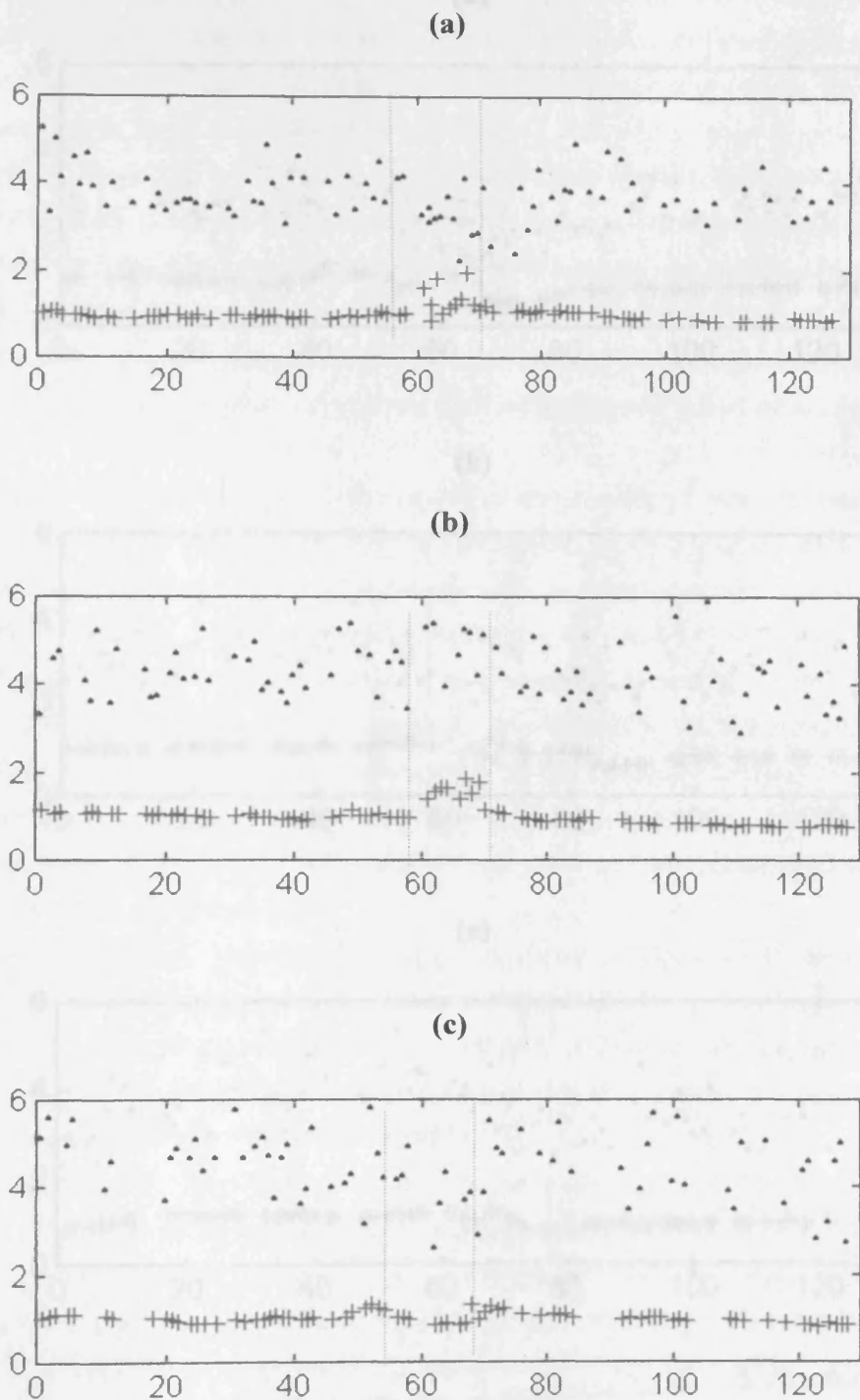
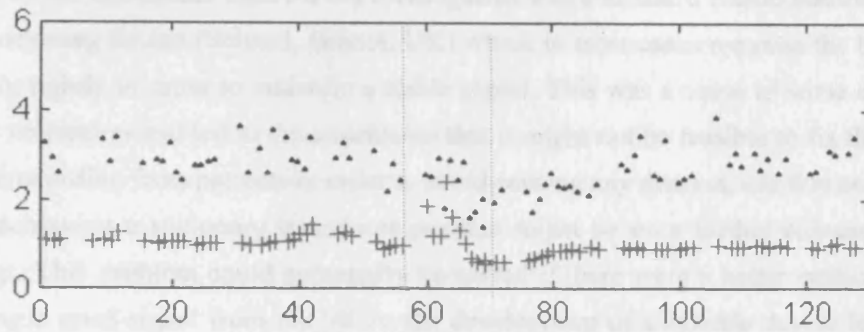


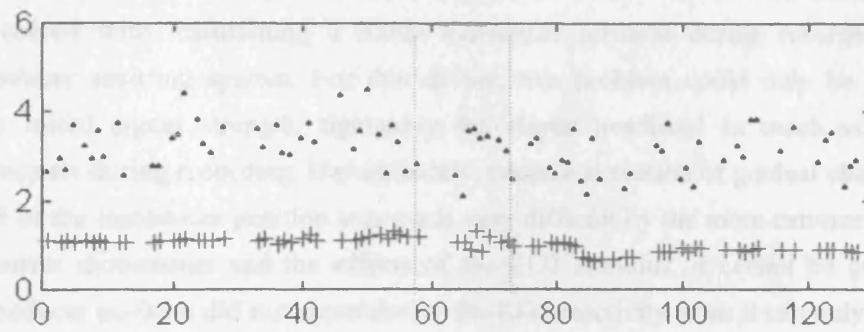
Figure 8.19 Raw (+) and corrected (•) power values derived from filtered sonograms for recordings made from a subject (a) swallowing (b) raising eyebrows (c) speaking, for a period of 10 seconds in each recording as shown by the dashed lines.

...clearing throat ... Data when the subject is engaged in ... a gradual ... (a)



(b)

...nodding head ... The change in power ... (b)



(c)

...smiling ... (c)

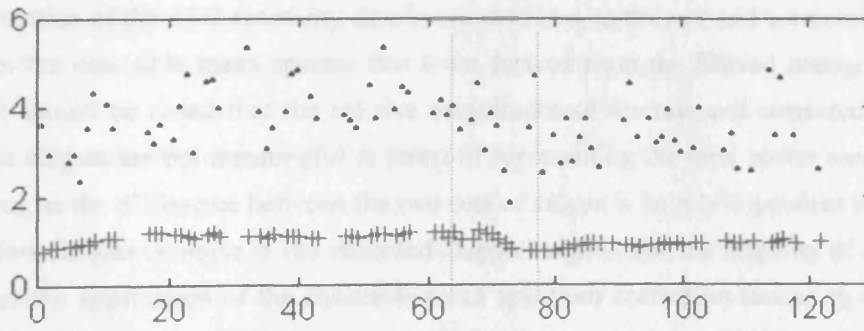


Figure 8.20 Raw (+) and corrected (•) power values derived from filtered sonograms for recordings made from a subject (a) clearing throat (b) nodding head (c) smiling, for a period of 10 seconds in each recording shown by the dashed lines.

...the corrected power ... the total power ... the corrected power ...

transducer during recordings. Even when the subjects remained as motionless as possible, a gradual reduction of signal strength thought to be due to slippage of the transducer holding apparatus was frequently observed. The holder used for the investigation was a standard elastic headband and plastic transducer positioning device (Scimed, Bristol, UK) which in most cases required the headband to be fixed extremely tightly in order to maintain a stable signal. This was a cause of some discomfort to a number of the volunteers and led to the conclusion that it might not be feasible to fix the headband so securely when recording from patients in order to avoid causing any distress, and that consequently the likelihood of achieving a stationary transducer position might be even further reduced for many in-vivo recordings. This problem could potentially be solved if there were a better method of obtaining and maintaining a good signal from the MCA; the development of a suitable device for this purpose would appear to be an important future requirement if robust Doppler power recordings are ever to be made routinely.

The changes in power arising from unprovoked movements of the transducer illustrate the difficulties involved with maintaining a stable transducer position during recordings using the available transducer securing system. For this device, this problem could only be minimised by optimising the initial signal strength, tightening the elastic headband as much as possible and observing the signals during recording. Unfortunately, because detection of gradual changes in power caused by drift of the transducer position was made very difficult by the more extreme influences on power of volunteer movements and the effects of the CO₂ stimulus, it cannot be guaranteed that changes in transducer position did not occur during the CO₂ reactivity tests. It can only be hoped that the steps taken to minimise such movement will have prevented any significant changes in power arising from this unwanted source.

Because of the potential benefits of filtering sonograms to remove unwanted noise (discussed above), interpretation of the CO₂ reactivity data is concentrated on the raw and corrected power values calculated from the ensemble mean spectra that were derived from the filtered sonograms (plot *e* in each figure). It should be noted that the relative magnitudes of the raw and corrected power values plotted for each subject are not meaningful in terms of representing the total power received from the blood in a vessel, as the difference between the two sets of values is largely dependent on the presence or absence of low frequency noise in the recorded Doppler signal. For the majority of the subjects, it can be seen that the application of the ensemble mean spectrum correction causes an increase in the total power. This would be the predicted response if it were assumed that the correction compensates for the losses in spectral power occurring due to beam shape and high-pass filtering. However, in some cases the correction appears to have little effect on the total power, and in others causes a decrease relative to the raw power. This can be explained by the fact that the presence of low frequency noise in the raw ensemble mean spectrum (as seen in figure 8.18a) may potentially produce a substantial increase in the total power value calculated from the uncorrected spectrum, but because the correction eliminates any low frequency noise peaks by the procedure of extrapolating the power at the knee frequency to replace the spectral values at frequencies below this (figures 8.18b and c), the total power in the corrected spectrum may be similar in magnitude to (or even smaller than) the corresponding raw power value.

It can be seen from the power data plotted in figures 8.3e-8.17e that there does not appear to be an obvious trend in the effects of CO₂ on the raw signal power; eight of the subjects exhibit no obvious changes in raw signal power during the period of CO₂ inhalation (figures 8.3, 8.4, 8.6, 8.8, 8.11, 8.13, 8.14, 8.16), while the remaining seven subjects show some evidence of an increase in the raw signal power during this period (figures 8.5, 8.7, 8.9, 8.10, 8.12, 8.15, 8.17). There are a number of basic reasons that could possibly explain this lack of consistency between subjects. Firstly, due to time constraints and the difficulty of obtaining a stable transducer position, a compromise in terms of reduced signal strength was necessary in several cases. Weaker signals have the disadvantage of a lower signal-to-noise ratio, and hence provide a less accurate estimate of total signal power. Secondly, the response to increased CO₂ was poor for some subjects (the level of response was assessed by eye from the resulting increase in blood flow velocity; obvious increases in velocity were assumed to be indicative of a good response). Variations in the level of response might have arisen due to differences in the size of the CO₂ step, and also from natural variations in the physiological effects of CO₂ for different subjects. Poor CO₂ steps might have resulted from incomplete contact between the mask and face, or other leaks in the system, and could mean that there was not an adequate stimulus to cause a change in vessel size large enough to be detected as a change in power. Finally, undetected changes in the relative positions of the transducer and MCA may still occur despite all efforts to obtain a stable transducer position and to prevent movements during recordings, and these may produce power changes that outweigh those originating from vessel size changes. It should especially be noted that the action of inserting the elephant tubing into the facemask at the start of the period of CO₂ inhalation might cause changes in power if the transducer position was inadvertently altered at this time.

In order to attempt to isolate the recordings that are likely to provide the most accurate representation of the effects of CO₂ on MCA size, the subjects with good quality signals were selected (figures 8.4, 8.5, 8.6, 8.7, 8.8, 8.14, 8.16, 8.17). Good quality signals were defined as those with a high signal-to-noise ratio for which a smooth maximum frequency envelope could be derived. Out of these, the subjects with signals containing significant low frequency noise or exhibiting a poor velocity response to the CO₂ step were rejected. This left only four sets of data (figures 8.7, 8.14, 8.16, 8.17). Two of these data sets display obvious increases in power during the period of CO₂ inhalation, and two display no obvious change in power. In terms of the magnitude of the power change observed before and after correction, three of the data sets exhibit no obvious difference, while the dispersion of the corrected power values in the fourth set (figure 8.17) prevents comparison with the uncorrected data. It was not considered worthwhile to calculate the magnitude or the statistical significance of the power changes, owing to the small number of data sets prohibiting any definite conclusions being drawn about the effects of CO₂ on the vessel size, or about the effects of the correction on the magnitude of the power changes that were seen.

The unsatisfactory quality of the data recorded in this study has unfortunately prevented any conclusions being reached regarding changes in MCA size or the effectiveness of the correction method in compensating for the influences of non-uniform insonation and high-pass filtering on signal power. However, on a more positive note, it has usefully highlighted a number of factors which need to be addressed during any future investigations of the Doppler power method and the proposed

correction technique. The results have provided a good illustration of the problems associated with recording Doppler power data of an adequate quality for use in analysing changes in vessel size; it has been shown that the signal power is sensitive to small movements of the subject, with changes in power arising from both changes in transducer position and the introduction of low frequency noise to the spectrum, and that the complete elimination of these spurious changes does not appear to be feasible when using the transducer holding device utilised in this study. This is an important finding with regard to any future routine use of the Doppler power method, as the device is of a standard design utilised for TCD recordings by many vascular ultrasound departments.

The investigation has also given an insight into some of the problems that may be encountered when attempting to correct the Doppler signal power for the effects of beam shape and filtering. The results have illustrated the need for high quality signals if the proposed correction method is to be used successfully, as it has been seen that errors introduced to the corrected power values by spectral noise may cause dispersion of the values which can potentially hide any changes in power that occur. Although it has been shown that the spread of values arising from this source can be reduced by smoothing the Doppler sonogram to minimise noise, additional dispersion arising from other sources can only be minimised by attempting to keep the vessel position stationary in the beam, once again emphasising the need for a better transducer holding device than that used for this study. Unfortunately, the problem of dispersion of the power values after the correction has been applied may eventually prove to be unresolvable, as it may not be possible to adequately minimise the variable errors introduced by the approximations made in the correction method. In particular, unavoidable dispersion is likely to arise because it is necessary for the velocity ratio used in the method to have a value which will allow the correction to remain viable up to the largest potential in-vivo vessel sizes and size changes; consequently it is unlikely that the selected value will be the optimum for the majority of in-vivo cases. However, further investigation is obviously required before a definite conclusion can be reached regarding the feasibility of using this particular correction method with in-vivo signals.

8.7 Conclusions

The study described in this chapter has looked at the effects of the ensemble mean spectrum correction on the Doppler signal power recorded from the MCA of healthy subjects undergoing CO₂ reactivity testing, and has illustrated that the feasibility of using the proposed correction method with in-vivo signals appears to depend primarily on the quality of the recorded Doppler signals. The investigation has highlighted the necessity for an optimum quality signal to be recorded, plus the need for an improved transducer holding device and the requirement that subjects remain as motionless as possible. These criteria can be considered to be vital for all recordings of Doppler signal power, regardless of whether the correction is used or not, if any power changes are to be confidently assumed to originate from changes in vessel size.

Unfortunately, the unsatisfactory quality of the signals recorded in this particular study has prevented any conclusions being reached regarding the scale of any MCA size changes occurring due to increased CO₂ levels, and hence it has not been possible to compare the results with those published

in the literature. For the same reason, it has not been feasible to analyse the differences between the changes observed in the uncorrected and corrected power values, and therefore the assessment of the ability of the correction method to provide an improved measure of vessel size changes has been prevented. These unfulfilled aims can only be achieved after addressing the problems involved with obtaining suitable power signals that have been illustrated by the work in this chapter, and subsequently taking further recordings. However, if it is possible for the dispersion introduced to the power values by the correction to be limited to a level that allows small changes in power to be identified, and if a transducer holding device can be developed that will prevent small patient movements from causing unwanted changes in the signal power, then there does not appear to be any reason why the correction technique will not produce power data that provides a more accurate measure of changes in vessel size, even if only because of the advantage that it offers in terms of removing unwanted low frequency spectral noise.

CHAPTER 9

Summary and Future Work

9.1 Introduction

In order to assess changes in the blood supply to the brain caused by disease, drugs or other physiological stimuli, a robust method of measuring changes in blood flow in the large cerebral vessels is required. Many of the techniques currently available for this purpose, for example radioisotope imaging, MRI and ultrasound imaging, are limited by factors such as safety considerations, expense, image resolution and speed of image acquisition. However, one method that overcomes these limitations is the transcranial Doppler (TCD) technique, which is widely used for detecting flow changes in the MCA. Unfortunately, the accuracy of TCD is potentially limited by the fact that Doppler ultrasound measures only blood velocity and not true volume flow. Consequently, measurements may be subject to error if a vessel undergoes size changes during recordings. Evidence is available to show that the MCA is potentially capable of changing in size, and it is possible that this may be a cause of the inaccuracies that have been observed in some TCD measurements of cerebral blood flow.

Because TCD offers so many advantages over other methods of detecting changes in cerebral blood flow, the ideal solution to the problem would be to measure changes in vessel size simultaneously to TCD measurements of velocity in order that a calculation of the true changes in volume flow could be made from the two recordings. One possible option for detecting changes in cerebral vessel size is the Doppler signal power technique, which offers the major advantage of allowing a calculation of vessel size changes using the same signal from which the TCD velocity is obtained. To date, only limited research has been carried out to investigate the accuracy of the technique for quantifying in-vivo vessel size changes; the aim of this thesis was therefore to provide a comprehensive investigation of the validity of using the Doppler signal power for detecting changes in MCA size.

9.2 Summary of Research

The Doppler signal power technique relies on the theory that the total power of the Doppler signal is proportional to the volume of blood from which the signal originated, and hence that any changes in the size of a vessel will produce a proportional change in signal power. In practice, this theoretical relationship between power and vessel size may be adversely affected by a number of other factors which affect the shape and magnitude of the signal spectrum, for example non-uniform insonation of the blood vessel, attenuation of the signal, intrinsic spectral broadening, electronic filtering, blood haematocrit and flow conditions. Chapter 2 of this thesis provided a description of such factors, enabling the identification in chapters 3 and 4 of those which are likely to be the most important for in-vitro and in-vivo signal power recordings respectively. In both cases it was deduced that any distortion of the theoretically proportional relationship between Doppler signal power and the size of the MCA is likely to arise primarily from beam shape and high pass filtering. Relative to these major

influences, the contribution of the remaining factors can be assumed to be unimportant provided that various criteria are fulfilled during recordings to ensure that their influence is minimised.

At the present time, the theoretical relationship between the Doppler signal power and vessel size has only been investigated using a conventional tubing flow phantom; this design may produce distortion of the power spectra due to the different acoustic properties of the tube walls and the surrounding medium. Furthermore, no allowance has been made for the effects of transducer position on the signal power, a factor that must be considered for flow phantom recordings of signal power due to the movement of the transducer in order to record signals from different sized tubes. The aim of the in-vitro investigation described in chapter 3 was therefore to provide a more robust assessment of the relationship between signal power and vessel size by using a wall-less flow phantom and more rigorously addressing the factors likely to affect the recorded signal power, and consequently enabling a detailed insight into the factors likely to affect the Doppler signal power recorded from in-vivo vessels. The results illustrated a number of previously unreported points regarding in-vitro Doppler signal power measurements. Maximisation of the signal power received from different channels was seen to be necessary in order to ensure that the insonating beam intensity is approximately equal for each channel and that the true relationship between power and channel size is plotted. It was also demonstrated that the relationship between the maximised raw signal power and channel size is not proportional for the wall-less flow phantom case, but that this can be approximately accounted for by considering the influences of filtering and beam shape. Finally, signal power values were shown to vary for different applications of the transducer to the phantom surface, despite careful maximisation of the signal intensity in each case.

The relevance of these in-vitro findings to recordings of Doppler signal power taken from in-vivo vessels was discussed in chapter 4, along with additional factors that could potentially affect the signal power for the in-vivo case. It was concluded that it is essential for a stationary transducer position to be maintained during power recordings in order to prevent variations in power caused by movements of the transducer being misinterpreted as changes in vessel size. In addition, the comparison of power values obtained from non-continuous recordings is prohibited, as there is once again the potential for misinterpretation of power changes due to the transducer having been moved. However, provided that the transducer position remains stationary and that flow conditions and haematocrit are stable during recordings, it can be assumed that the theoretical relationship between Doppler signal power and the size of the MCA will primarily be influenced by beam shape and high pass filtering. The effect of filtering is likely to be less significant than for the in-vitro case due to the higher in-vivo flow velocities, whereas the effects of non-uniform insonation will probably be more pronounced owing to the distortion of beam shape by the temporal bone and the inhomogeneous tissues in the beam path.

The importance of non-uniform insonation of the MCA with regard to the accuracy of the Doppler power method was initially assessed from a study of the beam shape distortion likely to arise in-vivo; details of this are given in chapter 5. The aim of the investigation was to provide information about the range of beam shapes likely to arise for in-vivo recordings of the Doppler signal power from the MCA, and hence to predict the scale of the errors introduced by non-uniform insonation and to potentially enable the derivation of some type of in-vivo correction. The results demonstrated that

there was relatively little variation in the sensitivity patterns for the different commercial transducers that were investigated, and it was therefore inferred that the type of transducer does not substantially influence beam shape across the MCA. In contrast, a high degree of variability was seen in the distortion caused by different samples of temporal bone, and also in the distortion arising from different beam paths through the bone. This suggested that the extent of the effects of beam shape on the relationship between the Doppler signal power and the MCA size may vary both between individuals, and for individual recordings if transducer displacements occur.

The potential scale of the errors introduced by beam shape to Doppler power measurements of vessel size changes was investigated in chapter 6. The objective was to create a model that would predict the percentage change in Doppler signal power arising from a dilation or contraction of a theoretical vessel insonated by various non-uniform beam shapes, and to investigate the effects on the power change of initial vessel size, area changes of varying magnitude, increasing or decreasing vessel size, vessel position in the beam and insonation angle. The investigation of different beam shapes was carried out in order to provide an estimation of in-vivo variability in the errors introduced by non-uniform insonation. The results of the modeling suggested that beam shape could potentially have a substantial influence on the power change detected from an in-vivo change in vessel area. With the transducer positioned to give the maximum signal intensity, errors of between 10% and 75% were derived for the power changes arising from 10% and 20% changes in the areas of vessels with diameters between 2mm and 4mm for a zero degree angle of insonation. These values are likely to represent the maximum error range, as it was found that the discrepancy between a vessel area change and the resulting power change is reduced for increasing angle of insonation. The change in power was shown to be dependent on the beam shape itself, the position of the vessel in the beam, the original size of the vessel, the change in area that occurred and the beam-vessel angle. The fact that many of these variables are unknown in-vivo means that it is difficult to determine the precise error introduced by beam shape to the change in signal power arising from a change in the size of the MCA in an individual.

The variability seen in chapter 6 of the errors derived for different beam shapes, vessel sizes and insonation angles illustrated the need for some form of correction factor for in-vivo signals that would compensate for the effects of beam shape and re-establish a proportional relationship between the Doppler signal power and vessel size. Owing to the unpredictable nature of the beam shape distortion arising from the passage of the ultrasound beam through temporal bone and the unknown size and position of the MCA, specific corrections cannot be derived for individual cases. Consequently, a more universal approach to correcting for non-uniform insonation was proposed, with the aim of at least approximately compensating for both the beam shape and high pass filtering in all cases. Chapter 7 described the theory behind a novel correction technique (the ensemble mean spectrum correction), and used simulated Doppler spectra and signals recorded from the wall-less flow phantom to test the effectiveness of the technique under defined insonation and flow conditions. The results obtained using the simulated Doppler signals demonstrated that an approximately proportional relationship between vessel area and total power was re-established for stationary vessels of between 1.5mm and 3.5mm diameter undergoing size and flow velocity changes under the non-uniform insonation

conditions produced by six different beam shapes. The technique was shown to be viable for very small vessel movements in the beam, and to be independent of the vessel position in the beam. A similar re-establishment of proportionality between power and size was also seen for the flow phantom Doppler signals, and it was therefore concluded that applying the ensemble mean spectrum correction to in-vivo Doppler signals should potentially allow changes in signal power to be more confidently related to the scale of any changes in the size of the MCA.

In chapter 8, Doppler power signals were recorded from healthy volunteers undergoing carbon dioxide reactivity testing with the aim to investigate the effects of the ensemble mean spectrum correction on in-vivo signal power values. A secondary aim of the study was to assess the effects of CO₂ on MCA size by comparing the observed changes in the raw and corrected signal power with those reported in the literature. Despite great effort to obtain good quality power recordings by maintaining a stationary transducer position and minimising movements of the volunteers, the quality of the recorded signals was still unsatisfactory and therefore prevented any conclusions being reached regarding the scale of the MCA size changes occurring due to increased CO₂ levels. Consequently, it was not possible to compare the results with those published in the literature. For the same reason, it was not feasible to analyse the differences between the changes observed in the uncorrected and corrected power values, and therefore an assessment of the ability of the correction method to provide an improved measure of vessel size changes was prevented.

Although the investigation did not provide the level of conclusion originally desired, it did illustrate a number of positive and important points regarding the many problems associated with recording Doppler power signals of an adequate quality for determining changes in vessel size. The importance of taking recordings with a high signal-to-noise ratio was highlighted, as the feasibility of using the correction with in-vivo data appears to depend primarily on the quality of the recorded Doppler signals; errors introduced to the corrected power values by spectral noise cause dispersion of the in-vivo power values relative to that seen for the uncorrected data. In addition, the influence of both transducer and patient movements on the recorded signal power drew attention to the requirement for a more effective transducer holding device. These points can be considered to be vital for any recordings of Doppler signal power, regardless of whether the correction is used or not, if power changes are to be confidently assumed to originate from changes in vessel size.

9.3 Future Work

The research in this thesis provides a robust assessment of the feasibility of using the Doppler power method for measuring vessel size changes. Important findings have included the observation of a non-proportional relationship between power and channel size for in-vitro signals, details regarding the accurate recording of power signals from flow phantoms, an assessment of the nature and variability of beam shape distortion by temporal bone, and an estimation of the errors in signal power changes that are likely to be caused by non-uniform insonation when monitoring power changes from the MCA. Further work is required to establish the effects of the ensemble mean spectrum correction on in-vivo signal power values, and to assess the true effects of CO₂ on MCA size, but this can only

be achieved after addressing the problems involved with obtaining suitable power signals that were illustrated by the work in chapter 8, and subsequently taking further recordings. In particular, a more effective transducer positioning and holding system might enable good quality signals to be obtained and maintained in more cases, and the development of such a device would appear to be a vital future requirement if robust Doppler power recordings are to be made under routine conditions from patients who are less able or willing to remain still than the volunteers taking part in this study. If the problems that were identified in chapter 8 are resolved, then there does not appear to be any reason why the correction technique will not produce power values that give a more accurate measure of changes in in-vivo vessel size than provided by the raw power data, even if only because of the advantage that the correction offers in terms of removing unwanted low frequency spectral noise.

Other future research might include the recording of beam shapes from additional temporal bone samples; by building a library of beam shapes, it may be possible to identify sex or age related trends in the errors introduced to changes in signal power changes. If the error arising from non-uniform insonation can be estimated for an individual, then it will remove the need for correction of Doppler power values and hence eliminate the associated problems. Another alternative might be the development of a method for obtaining an in-vivo measurement of bone thickness across the temporal window, in order that the beam shape could be simulated for an individual and the non-uniform insonation error predicted from this source.

REFERENCES

- Aaslid R (1987) Visually evoked dynamic blood flow response of the human cerebral circulation. *Stroke* 18: 771-775
- Aaslid R, Lindegaard KF, Sorteberg W, Nornes H (1989) Cerebral autoregulation dynamics in humans. *Stroke* 20: 45-52
- Aaslid R, Newell DW, Stoss R, Sorteberg W, Lindegaard KF (1991) Assessment of cerebral autoregulation dynamics from simultaneous arterial and venous transcranial Doppler recordings in humans. *Stroke* 22: 1148-1154
- Angelsen BAJ (1980) A theoretical study of the scattering of ultrasound from blood. *IEEE Trans Biomed Eng BME-27*: 61-67
- Arts MGJ, Roelvros JMIG (1972) On the instantaneous measurement of blood flow by ultrasonic means. *Med & Biol Eng & Comput* 10: 23-34
- Bascom PAJ, Cobbold RSC (1996) Origin of the Doppler ultrasound spectrum from blood. *IEEE Trans Biomed Eng* 43: 562-571
- Bishop CCR, Powell S, Rutt D, Browse NL (1986) Transcranial Doppler measurement of middle cerebral artery blood flow velocity: A validation study. *Stroke* 17: 913-915
- Bissonnette B, Armstrong D, Burrows P (1992) Effects of CO₂ on the size of cerebral vessels measured by cerebral angiography in children. *Stroke* 23: 465 (abstract)
- Brauer P, Kochs E, Werner C, Bloom M, Policare R, Pentheny S, Yonas H, Kofke WA, Esch JSA (1998) Correlation of transcranial Doppler sonography mean flow velocity with cerebral blood flow in patients with intracranial pathology. *J Neurosurg Anesth* 10: 80-85
- Brooks DJ, Redmond S, Mathias CJ, Bannister R, Symon L (1989) The effect of orthostatic hypotension on cerebral blood flow and middle cerebral artery velocity in autonomic failure, with observations on the action of ephedrine. *J Neurol Neurosurg Psychiatry* 52: 962-966
- Clark JM, Skolnick BE, Gelfand R, Farber RE, Stierheim M, Stevens WC, Beck G, Lambertsen C (1996) Relationship of Xe-133 cerebral blood flow to middle cerebral arterial flow velocity in men at rest. *J Cereb Blood Flow & Metab* 16: 1255-1262
- Cloutier G, Shung KK (1993) Cyclic variation of the power of ultrasonic Doppler signals backscattered by polystyrene microspheres and Porcine erythrocyte suspensions. *IEEE Trans Biomed Eng* 40: 953-961
- Cobbold RSC, Veltink PH, Johnston KW (1983) Influence of the beam profile and degree of insonation on the CW Doppler ultrasound spectrum and mean velocity. *IEEE Trans Sonics Ultrason* SU-30: 364-370
- Dacie JV, Lewis SM (1995) *Practical Haematology*, 8th edn. Churchill-Livingstone, Edinburgh

- Dahl A, Russell D, Nyberg-Hansen R, Rootwelt K (1989) Effect of nitroglycerin on cerebral circulation measured by transcranial Doppler and SPECT. *Stroke* 20: 1733-1736
- Dahl A, Lindegaard KF, Russell D, Nyberg-Hansen R, Rootwelt K, Sorteberg W, Nornes H (1992a) A comparison of transcranial Doppler and cerebral blood flow studies to assess cerebral vasoreactivity. *Stroke* 23: 15-19
- Dahl A, Russell D, Nyberg-Hansen R, Rootwelt K (1992b) A comparison of regional cerebral blood flow and middle cerebral artery blood flow velocities - simultaneous measurements in healthy subjects. *J Cereb Blood Flow & Metab* 12: 1049-1054
- Demolis P, Dinh YRT, Giudicelli JF (1996) Relationships between cerebral regional blood flow velocities and volumetric blood flows and their respective reactivities to acetazolamide. *Stroke* 27: 1835-1839
- Djurberg HG, Seed RF, Evans DAP, Brohi FA, Pyper DL, Tjan GT, Al Moutaery KR (1998) Lack of effect of CO₂ on cerebral arterial diameter in man. *J Clin Anesth* 10: 646-651
- Drayton MR, Skidmore R (1987) Vasoactivity of the major intracranial arteries in newborn infants. *Arch Dis Child* 62: 236-240
- Eastham RD, Slade RR (1992) *Clinical Haematology*, 7th ed. Butterworth-Heinemann, Oxford
- Evans DH (1988) A pulse-foot-seeking algorithm for Doppler ultrasound waveforms. *Clin Phys Physiol Meas* 9: 267-271
- Evans DH, Schlindwein FS, Levene MI (1989) An automatic system for capturing and processing ultrasonic Doppler signals and blood pressure signals. *Clin Phys Physiol Meas* 10: 241-245
- Evans DH (1992) Doppler ultrasound and the neonatal cerebral circulation: methodology and pitfalls. *Biol Neonate* 62: 271-279
- Evans DH, McDicken WN (2000) *Doppler ultrasound: physics, instrumentation and signal processing*. John Wiley & sons, Chichester
- Fry FJ, Barger JE (1978) Acoustical properties of the human skull. *J Acoust Soc Am* 63: 1576-1590
- Giller CA, Bowman G, Dyer H, Mootz L, Krippner W (1993) Cerebral arterial diameters during changes in blood pressure and carbon dioxide during craniotomy. *Neurosurgery* 32: 737-742
- Giller C, Hatab M, Giller A (1998) The use of a TCD index to measure oscillations in CBF: are TCD velocities reliable? *Cerebrovasc Dis* 8 (Suppl. 3): 7
- Grocott HP, Amory DW, Lowry E, Croughwell ND, Newman MF (1998) Transcranial Doppler blood flow velocity versus ¹³³Xe clearance cerebral blood flow during mild hypothermic cardiopulmonary bypass. *J Clin Monit Comput* 14: 35-39
- Grolimund P (1986) Transmission of ultrasound through the temporal bone. In: Aaslid R (ed) *Transcranial Doppler Sonography*. Springer-Verlag, Vienna, New York

- Hames TK, Nelligan BJ, Nelson RJ, Gazzard VM, Roberts J (1991) The resolution of transcranial Doppler scanning: a method for in-vitro evaluation. *Clin Phys Physiol Meas* 12: 157-161
- Harer C, Widder B, Klemm P (1995) Influence of various factors on the Doppler flow index measured in a flow model. *J Neuro-Imaging* 5: s86
- Hartmann A, Ries F, Tsuda Y, Lagreze H, Seiler R, Grolimund P (1991) Correlation of regional cerebral blood flow and blood flow velocity in normal volunteers and patients with cerebrovascular disease. *Neurochirurgia* 34: 6-13
- Hatab MR, Giller CA, Clarke GD (1997) Evaluation of cerebral arterial flow with transcranial Doppler ultrasound: theoretical development and phantom studies. *Ultrasound Med Biol* 23: 1025-1031
- Hoskins PR, Loupas T, McDicken WN (1990) A comparison of three different filters for speckle reduction of Doppler spectra *Ultrasound Med Biol* 16: 375-389
- Huber P, Handa J (1967) Effects of contrast material, hypercapnia, hyperventilation, hypertonic glucose and papaverine on the diameter of the cerebral arteries. *Invest Radiol* 2: 17-32
- Kofke WA, Brauer P, Policare R, Penthany S, Barker D, Horton J (1995) Middle cerebral artery blood flow velocity and stable xenon-enhanced computed tomographic blood flow during balloon test occlusion of the internal carotid artery. *Stroke* 26: 1603-1606
- LaFollette PS, Ziskin MC (1986) Geometric and intensity distortion in echography. *Ultrasound Med Biol* 12: 953-963
- Larsen FS, Olsen KS, Hansen BA, Paulson OB, Knudsen GM (1994) Transcranial Doppler is valid for determination of the lower limit of cerebral blood flow autoregulation. *Stroke* 25: 1985-1988
- Lindegaard KF, Lundar T, Wiberg J, Sjoberg D, Aaslid R, Nornes H (1987) Variations in middle cerebral artery blood flow investigated with noninvasive transcranial blood velocity measurements. *Stroke* 18: 1025-1030
- Madsen PL, Sperling BK, Warming T, Schmidt JF, Secher NH, Wildschiodtz G, Holm S, Lassen NA (1993) Middle cerebral artery blood velocity and cerebral blood flow and O₂ uptake during dynamic exercise. *J Appl Physiol* 74: 245-250
- Mahajan RP, Cavill G, Simpson EJ (1998) Reliability of the transient hyperemic response test in detecting changes in cerebral autoregulation induced by the graded variations in end-tidal carbon dioxide. *Neurosurg Anesth* 87: 1-7
- Markwalder TM, Grolimund P, Seiler R, Roth F, Aaslid R (1984) Dependency of blood flow velocity in the middle cerebral artery on end-tidal carbon dioxide partial pressure - a transcranial ultrasound Doppler study. *J Cereb Blood Flow & Metab* 4: 368-372
- Martin PJ, Evans DH, Naylor AR, Bell PRF (1993) Transcranial colour coded sonography as an aid to measurement of blood flow velocity in the basal cerebral arteries. *Ultrasound Med Biol* 19: 711-716

- Martin PJ, Evans DH, Naylor AR (1995) Measurement of blood flow velocity in the basal cerebral circulation: advantages of transcranial colour-coded sonography over conventional transcranial Doppler. *J Clin Ultrasound* 23: 21-26
- McDicken WN (1990) *Diagnostic Ultrasonics: Principles and Use of Instruments*. Churchill Livingstone, Edinburgh.
- Meixensberger J, Bravanski A, Holzschuh M, Danhauser-Leistner I (1992) Blood flow velocity and cerebral blood flow after subarachnoid hemorrhage. *Stroke* 23: 466 (abstract)
- Mo LYL, Kuo I-Y, Shung KK, Ceresne L, Cobbold RSC (1994) Ultrasound scattering from blood with hematocrits up to 100%. *IEEE Trans Biomed Eng* 41: 91-95
- Muller HR, Casty M, Moll R, Zehnder R (1991) Response of middle cerebral artery volume flow to orthostasis. *Cerebrovasc Dis* 1: 82-89
- Muller HR (1994) Flow and velocity during autoregulation testing in humans. *Stroke* 25: 1296-1297
- Muller M, Voges M, Piepgras U, Schimrig K (1995) Assessment of cerebral vasomotor reactivity by transcranial Doppler ultrasound and breath holding: a comparison with Acetazolamide as vasodilatory stimulus. *Stroke* 26: 96-100
- Newell DW, Aaslid R, Lam AM, Mayberg TS, Winn HR (1994) Comparison of flow and velocity during dynamic autoregulation testing in humans. *Stroke* 25: 793-797
- Nuttall GA, Cook DJ, Fulgham JR, Oliver WC, Proper JA (1996) The relationship between cerebral blood flow and transcranial Doppler blood flow velocity during hypothermic cardiopulmonary bypass in adults. *Anesth Analg* 82: 1146-1151
- Poulin MJ, Liang PJ, Robbins PA (1996a) Dynamics of the cerebral blood flow response to step changes in end-tidal pCO₂ and pO₂ in humans. *J Appl Physiol* 81: 1084-1095
- Poulin MJ, Robbins PA (1996b) Indexes of flow and cross-sectional area of the middle cerebral artery using Doppler ultrasound during hypoxia and hypercapnia in humans. *Stroke* 27: 2244-2250
- Ramnarine KV, Nassiri DK, Hoskins PR, Lubbers J (1998) Validation of a new blood-mimicking fluid for use in Doppler flow test objects. *Ultrasound Med Biol* 24: 451-459
- Ramnarine KV, Hoskins PR, Routh HF, Davidson F (1999) Doppler backscatter properties of a blood-mimicking fluid for Doppler performance assessment. *Ultrasound Med Biol* 25: 105-110
- Rickey DW, Picot PA, Christopher DA, Fenster A (1995) A wall-less vessel phantom for Doppler ultrasound studies. *Ultrasound Med Biol* 21: 1163-1176
- Saini VD, Maulik D, Nanda NC, Rosenzweig MS (1983) Computerized evaluation of blood flow measurement indices using Doppler ultrasound. *Ultrasound Med Biol* 9: 657-660

- Schreiber SJ, Gottschalk S, Weih M, Villringer A, Valdueza JM (1999) Assessment of blood flow velocity and diameter of the middle cerebral artery during Acetazolamide-provocation-test using TCD and MRI. 4th meeting of the European Society of Neurosonology and Cerebral Haemodynamics, Venice, Italy: *poster presentation abstract*
- Schregel W, Schaefermeyer H, Sihle-Wissel M, Klein R (1994) Transcranial Doppler sonography during isoflurane / N₂O anaesthesia and surgery: flow velocity, "vessel area" and "volume flow". *Can J Anaesth* 41: 607-612
- Shung KK, Sigelmann RA, Reid JM (1976) Scattering of ultrasound by blood. *IEEE Trans Biomed Eng BME-23*: 460-467
- Shung KK, Yuan YW, Fei DY (1984) Effect of flow disturbance on ultrasonic backscatter from blood. *J Acoust Soc Am* 75: 1265-1272
- Shung KK, Cloutier G, Lim CC (1992) The effects of haematocrit, shear rate and turbulence on ultrasonic Doppler spectrum from blood. *IEEE Trans Biomed Eng* 39: 462-469
- Teirlinck CJPM, Bezemer RA, Kollman C, Lubbers J, Hoskins PR, Fish P, Fredfeldt KE, Schaarschmidt UG, Ramnarine KV (1998) Development of an example flow test object and comparison of five of these test objects, constructed in various laboratories. *Ultrasonics* 36: 653-660
- Thompson RS, Aldis GK, Linnett IW (1990) Doppler ultrasound spectral power density distribution: measurement artefacts in steady flow. *Med & Biol Eng & Comput* 28: 60-66
- Thompson RS, Aldis GK (1996) Effect of a cylindrical refracting interface on ultrasound intensity and the CW Doppler spectrum. *IEEE Trans Biomed Eng* 43: 451-459
- Valdueza JM, Balzer JO, Villringer A, Vogl TJ, Kutter R, Einhaupl KM (1997) Effect of hyperventilation on the diameter and blood flow velocity of the middle cerebral artery: a TCD and MR study. In: Klingelhofer J (ed) *New Trends in Cerebral Haemodynamics and Neurosonology*. Elsevier Science B.V.
- Valdueza JM, Draganski B, Hoffmann O, Dirnagl U, Einhaupl KM (1999) Analysis of CO₂ vasomotor reactivity and vessel diameter changes by simultaneous venous and arterial Doppler recordings. *Stroke* 30: 81-86
- Van der Linden J, Wesslen O, Ekroth R, Tyden H, Vonahn H (1991) Transcranial Doppler-estimated versus thermodilution-estimated cerebral blood flow during cardiac operations - influence of temperature and carbon-dioxide tension. *J Thorac Cardiovasc Surg* 102: 95-102
- Van der Linden J, Hallhagen S, Wesslen O, Ekroth R, Lincoln C (1992) Influence of blood pressure changes on the diameter of the middle cerebral artery in children undergoing cardiac surgery as measured with the Diamove phase-locked echo-tracking technique. *Stroke* 23: 465 (abstract)
- van der Zwan A, Hillen B, Tulleken CAF, Dujovny M (1993) A quantitative investigation of the variability of the major cerebral arterial diameters. *Stroke* 24: 1951-1959

Weyland A, Stephan H, Kazmaier S, Weyland W, Schorn B, Grune F, Sonntag H (1994) Flow velocity measurements as an index of cerebral blood flow - validity of transcranial Doppler sonographic monitoring during cardiac surgery. *Anesthesiology* 81: 1401-1410

White DN, Clark JM, White AW, Campbell JK, Bahuleyan K, Kraus AS, Brinker RA (1969) The deformation of the ultrasonic field in passage across the living and cadaver head. *Med & Biol Eng* 7: 607-618

White DN, Curry GR, Stevenson RJ (1978) The acoustic characteristics of the skull. *Ultrasound Med Biol* 4: 225-252

Widder B (1989) The Doppler CO₂ test to exclude patients not in need of extracranial / intracranial bypass surgery. *J Neurol Neurosurg Psychiatry* 52: 38-42